Preparation of Composite Particles and Application to Medical Fields

Kiyomi Fuchigami

Doctoral Program in Advanced Materials Science and Technology

Science and Technology for Materials

Graduate school of Science and Technology

Niigata University

2008

Le vent se lève, il faut tenter de vivre

Preparation of Composite Particles and Application to Medical Fields

Kiyomi Fuchigami

Doctoral Program in Advanced Materials Science and Technology

Science and Technology for Materials

Graduate school of Science and Technology

Niigata University

2008

Contents

Chapter III

"Preparation of Microcapsules Containing TMBA (1,3,5-trimethylbarbituric acid) by the Drying-in-liquid Method and its application"

Chapter IV

"Preparation of spherical calcium carbonate crystal using anionic surfactant"

Chapter V

"Synthesis of calcium carbonate vaterite crystals and effect of them on stabilization of suspension polymerization of MMA"

Chapter VI

“Spherical silica synthesized by sol-gel method and Application”

Chapter VII

“Preparation of hemispherical hollow silica microcapsules with different affinity surface by using spherical vaterite calcium carbonate as template”

Chapter I

Introduction

I-1. General Introduction

In the last few centuries, there has been impressive development in the fields of science and technology, especially in the field of engineering. i.e. the discoveries of X-ray, elemental particles, synthetic macromolecule such as nylon, electrically-conductive polymers, semiconductor materials, superconducting materials and so on. These discoveries had been separately accepted by society without being fused with other fields of science and technology. Today, however, such individual acceptances are not ethically allowed any more: newly invented scientific technologies should be utilized in conjunction with other fields of technologies in order to better contribute to society and make our lives easier. CT (Computerized tomography), MRS (Magnetic resonance scanner) and TOF-MS (Time-of-flight mass spectrometer) are some typical examples that successfully integrate multiple technologies for use, crossing over the boundaries of scientific fields. In particular, today, a fusion between medical sciences and engineering technologies is essential. Among them, it seems to be useful to fuse the microcapsule technologies with medical sciences for the drug delivery system and adhesion system to biological hard tissue.

I-2. Review of previous works

It is now well recognized that radical polymerization initiators play an important role in bonding adhesive resins to biological hard tissue and several artificial materials used in the fields of dentistry and orthopedics. Masuhara ***et al*** [1]. found that the tri-n-butyl borane

(TBB)-initiated methyl methacrylate (MMA) resin successfully adhere to moist ground ivory, a model adherent of dentin substrate[1], in spite of polymerization shrinkage (21 vol% for MMA shrinkage) occurring at the bonding interface [2]. This success was a milestone for the field of adhesive science and brought new vistas for dentistry and orthopedics. Accordingly, since the creative work [1] by Masuhara ***et al***, numerous studies [3-10] have attempted to develop advanced radical polymerization initiators. Since the study [3] by Bredereck ***et al***, much attention has been focused on the use of barbituric acid derivatives for initiating dental and orthopedics resins, and ternary polymerization initiator systems comprising 5-monosubstituted barbituric acid (5-MSBA) (**Figure I-1**) were developed [7-10]. An adhesive resin containing an initiator system comprising 5-MSBA, organic peroxide, and aromatic tertiary amine, together with adhesive monomers of 4-acryloxyethyltrimellitic acid (4-AET) and its acid anhydride (4-AETA) showed good bonding performance to biological hard tissue and its curing time was favorable [10]. Another ternary initiator system comprising 5-MSBA, aromatic sulfinate amide (ASA), and tert-butyl peroxymaleic acid (*t*-BPMA) also exhibited good polymerization initiating ability [10]. These polymerization initiators, however, tend to prematurely interact with one another or with acidic adhesive monomers, which leads to phenomena such as a formation of a charge-transfer (C-T) complex [10-11], giving a problematic stability to the systems. To prevent such undesirable difficulties, there is a need to have a means so that these polymerization initiators and

adhesive monomers can stably coexist within the adhesive formulation.

Microcapsule technologies have been receiving considerable attention for their interesting characteristics in terms of physical chemistry and polymer science. They, thus, have been widely applied in various fields such as information recording, cosmetics, paintings, medicine, agriculture, food and so on [12], and active researches and developments have been performed to prepare various microcapsules [13]. One potential application of microcapsule technologies is to prepare one-liquid, biological hard tissue-adhesive materials, which are conventionally two-liquid type materials. In this case, the reactive compound, such as polymerization initiator (BPO, TMBA, etc.), is microencapsulated to be contained in the matrix agent, and a proper stimulus is given to break the microcapsules for reaction. Inevitably for such adhesive biomaterials, microcapsules contained therein have to be biocompatible, and thus it is necessary to investigate whether it is possible to design microcapsules using biocompatible materials. Although microcapsule technologies have been well-studied in various fields, little attention has been paid to their application to biological hard tissue-adhesive materials, and consequently little is known about the behaviors of microencapsulated polymerization initiators formulated in such materials. Therefore, in order to develop biological hard tissue adhesive materials, the research strategy in this study focused on the microencapsulation of polymerization initiators (BPO and TMBA).

As the next stage of the study, microenpsulation used for drug delivery systems (DDSs) was investigated. It is well known that DDS plays an important role in the field of pharmaceuticals. DDS is a technology to deliver and release a necessary dose of drugs to an affected site in the body for an appropriate period of time. It is comprised of a drug controlled release technology, drug targeting technology and drug absorption controlling technology. The drug controlled release technology, also known as “effective releasing technology”, involves two technologies: releasing a drug gradually in the body to retain the effect of the drug for a long period of time and modifying a hydrophobic drug into a hydrophilic one for easy adsorption in the affected body cells. The drug targeting technology involves two technologies: “active targeting technology” to deliver a drug using accepters and antibodies of body cells and “passive targeting technology” to prolong the drug retention time to accumulate the effects against the cancer cells. The drug absorption controlling technology involves two technologies: “drug infusion technology” to absorb a drug via skin and “gene transmittance technology” to transmit a gene into a cell. Among these technologies, the drug controlled release technology is mainly employed for microencapsulation. The most famous, commercially-available drug (microencapsulated DDS) is “Leuprorelin (Lupron depot)” [**Figure I-2**]. This drug contains acetic acid-glycolic acid copolymer as a biodegradable wall material. The core material, i.e. Leuprorelin LHRH ligand is gradually released at the hypodermis (subcutaneous

tissue) by using the biodegradability of acetic acid-glycolic acid copolymer. As stated above, this microencapsuled DDS does not have directivity to the affected area (affected cells), which suggests that the drug also permeates the healthy cells in the body. To resolve this undesirable drug diffusing mechanism, active researches and developments have been performed to synthesize microcapsules that detect the affected area (e.g. cancer cells) [14-24]. These microcapsules developed are, however, in spherical form: such a shape of the microcapsule limits the area of contact with the affected cells. Generally, most of the microcapsules synthesized for DDS today have the vapor-liquid or liquid-liquid interface, and thus are generally in spherical form. Although some studies attempted the surface modification on these spherical microcapsules, all of them resulted in modifying the whole surface. To date, no studies have reported the synthesis of hemispherical hollow microcapsules having a polarity between its base and rounded surface. It is expected that these hemispherical microcapsules will increase the level of drug-releasing efficiency since the flat surface of hemispherical microcapsules comes in contact with affected cells more efficiently. Additionally, their bipolar nature allows for various surface modification: a molecular chain having high affinity (binding property) for affected cells can be grafted on the contact surface, while an antithrombotic polymer can be grafted on the noncontact surface. The **Scheme I-1** was prepared for explaining this conception briefly. The red tube is expressive of capillary blood vessel, the red particles are expressive of anticancer

drug, the blue prominences are expressive of blood platelet, respectively. Furthermore, the both side of blackened indeterminate form is expressive of tumor cell. Here, the rightward large particles which exist in capillary blood vessel are expressive of conventional drug delivery system. It is easy to get the idea from this figure, the conventional drug delivery system can contact with only restricted area at the inner of capillary blood vessel. Thus, the releasing dose of anticancer drug to tumor cell is confined. Furthermore, a great deal of anticancer drug is spring a leak to capillary blood vessel. These anticancer drugs may give huge damages to individual organism by circulating the body. In addition, like this spherical drug delivery system is hard to make a surface modification. Therefore, it will be expected that the conventional drug delivery system may encounter an attack from blood platelet by recognition as inert matter. As a result of this, it is thought of the generation of thrombus. On the other hand, the leftward hemi spherical microcapsules which exsist in capillary blood vessel are expressive of newly developed drug delivery system by this study. It is easy to get the idea from this figure, the newly developed drug delivery system which has flat surface with chemical modification, contact selectively on the inner of capillary blood vessel which fend for tumor cell. It is easy to understand from this figure, the contact area is wider in comparison to the conventional spherical drug delivery system. As a result of this, huge amount of anticancer drug is released effectively to the tumor cell via capillary blood vessel. Furthermore, it is possible to provide bipolarity to the drug delivery

system, accordingly, it can modify by grafting antithrombotic polymer materials. Hence, it can be expected to prevent the thrombus by blood platelet. Correspondingly, it can be expected the less side effect by the anticancer drug circulating in the individual organism in comparison to the conventional drug delivery system.

I-3. Scope of this thesis

Microencapsulation technology is indispensable in today's general industrial field: its various applications include information equipment, cosmetics, food products, agricultural chemicals, drug deliveries, etc. This paper summarizes a study on microcapsules applicable in the medical and dental fields.

This paper consists of the following 8 chapters:

Chapter I is an introduction, where the background of the present study and a summary of the past studies were described to clarify the current problems existing in the medical and dental fields as well as the importance of solving those problems, and based on such clarification the objectives of the present study were specified.

Chapter II "**Preparation of microcapsules containing reactive compound by the drying-in-liquid method using calcium carbonate as stabilizer**" examined microencapsulation of benzoyl peroxide (BPO), a polymerization initiator heavily used in the fields of orthopedics and dentistry for polymerizing polymethyl

methacrylate (PMMA)/methyl methacrylate (MMA), using the drying-in-liquid method, and also investigated the effect of calcium carbonate (types of crystal system, particle size, etc.) used as a dispersion stabilizer. Consequently, unlike the conventional (non-encapsulated) BPO-added system, the addition of the obtained BPO microcapsules enabled, for the first time, the development of a significantly stable composition adhesive to biological hard tissue.

In Chapter III **"Preparation of Microcapsules Containing TMBA (1,3,5-trimethylbarbituric acid) by the Drying-in-liquid Method and its application"**, experimented on microencapsulation of TMBA (1,3,5-trimethylbarbituric acid), a polymerization coinitiator heavily used in the fields of orthopedics and dentistry for polymerizing polymethyl methacrylate (PMMA)/methyl methacrylate (MMA), using the drying-in-liquid method. Additionally, the obtained TMBA microcapsules were used for preparing a biological hard tissue-adhesive material and validated for the microencapsulation effects. The results showed that the microencapsulated systems had excellent bonding properties and high storing stability.

In *Chapter IV* "**Preparation of spherical calcium carbonate crystals using anionic surfactant**", the synthesis of calcium carbonate was carried out under various conditions (reaction mole concentration, reaction temperature, and anionic surfactant concentration). There are many published reports on preparation of calcium carbonate, especially the spherical vaterite crystals, however,

these studies used dilute solutions for calcium carbonate synthesis, which are not industrially applicable due to the low yields. This chapter described the method of efficiently and sufficiently producing spherical calcium carbonate vaterite crystals with less than 3 μm of diameter, which has not been achieved by the conventional preparation methods.

In *Chapter V* "Synthesis of calcium carbonate vaterite crystals and their effect of stabilization on suspension polymerization of MMA", metastable spherical calcium carbonate vaterite crystals and DBS were used as a stabilizer for suspension polymerization of MMA, and the effect of stabilization was examined. The following findings were obtained: 1) spherical calcium carbonate vaterite crystals exhibited the effect similar to that of the conventional calcium carbonate crystal systems such as stable aragonite and calcite crystals used as inorganic suspension stabilizer, and 2) the obtained complex polymer was unique in form, where the spherical calcium carbonate microparticles were hemispherically embedded into the spherical mother particle (PMMA), i.e. metastable vaterite calcium carbonate was stabilized by being embedded into PMMA polymer without undergoing a phase transition into aragonite or calcite even in the severe polymerization conditions of 343K-3H. Since there have been no previous reports on the synthesis of such a complex polymer with spherical calcium carbonate vaterite crystals embedded on its surface, this is considered a novel complex, and can be expected for various applications, including templates for preparing microcapsules

as described in ***Chapter VII***. The spherical form of vaterite crystals gives the resulting complex a repose angle greatly different from that in the case of the use of other forms of calcium carbonate crystals, which is also considered to offer the potential of wider use.

Chapter VI "**Spherical silica synthesized by sol-gel method and its application**" describes the synthesis of spherical silica using the sol-gel method by hydrolyzing tetraethyl orthosilicate (TEOS) with an alkali catalyst. There are only a few previous reports focusing on the dropping rate of the hydrolysis catalyst. In the present study, a systematical investigation was conducted on the synthesis conditions including the reaction temperature, concentration and dropping rate of the hydrolysis catalyst, and also the synthesized silica was doped with sodium fluoride to measure its ion release ability. The findings are as follows. The slower the dropping rate of the hydrolysis catalyst was, the smaller mean particle size was obtained, whereas the faster the dropping rate was, the smaller the specific surface area became. Thus, the dropping rate should be slower to obtain a porous particle structure. It was suggested that the particle porosity and size were fully controllable by manipulating the dropping rate of the catalyst and reaction temperature during the silica synthesis. In other words, the controlling of the dropping rate of catalyst, a simple and inexpensive operation method, allowed the synthesis of silica particles in various sizes and porosity levels. This method was applied to develop a drug-release control means. As one example of such an application, two groups of silica particles with the same size and different surface

area values were doped with fluoride to measure their fluoride release ability. The results showed that the fluoride retaining ability was proportional to the surface area value of the particles, and that the fluoride ion release was equilibrated at approx. 5 minutes for both groups.

Chapter VII "**Preparation of hemispherical hollow silica microcapsules with different affinity surface using spherical vaterite calcium carbonate as template**" describes the development of completely novel microcapsules based on the findings indicated in ***Chapters IV*** to ***VI***, i.e. hemispherical hollow silica microcapsules with a diameter of approx. 5 μm, having a polarity between its base and rounded surface. As noted above, a lot of attention is being focused on microcapsules used as a drug-delivery material. Most of the microcapsules synthesized today, however, have the vapor-liquid or liquid-liquid interface, and thus are generally in spherical form, which limit the area of contact with affected cells when applied to a drug delivery system. Although some studies attempted the surface modification on these spherical microcapsules, all of them resulted in modifying the whole surface. With these issues in mind, the present study was pursued to develop a new method to synthesize hemispherical microcapsules. It is expected that these hemispherical microcapsules will increase the level of drug-releasing efficiency since the flat surface comes in contact with affected cells more efficiently. Additionally, their bipolar nature allows for various surface modification: a molecular chain having high affinity (binding

property) for affected cells can be grafted on the contact surface, while an antithrombotic polymer can be grafted on the noncontact surface.

Chapter VIII “**Concluding remarks**” is a summary of the findings obtained by the present study.

REFERENCES

[1] Masuhara E, Kojima K, Hirasawa T, Tarumi N, Kimura T. Studies on dental self-curing 3. Effects of alkylboran on the adhesive force to ivory and tooth surface. Rep Inst Dent Mater Tokyo Med Dent Univ 1963; **2**: 457-456

[2] Lai JH, Johnson AE. Measuring polymerization shrinkage of photo-activated restorative materials by water-filled dilatometer. Dent Mater 1993; **16**: 139-143

[3] Bredereck VH, Fölisch B, Franz R. Über CH-aktive polymerisation-initiation XIII. Mit polymerisationen und polymerisation initiatoren. Makromol Chem 1966; **92**: 70-90

[4] Yamauchi J. Study on dental adhesive resin containing phosphoric acid methacrylate monomer, J Jpn Dent Mater 1989; **5** (1): 144-154

[5] Kadoma Y, Imai Y. Visible-light initiator system using thiobarbituric acid derivatives with methyl substituent. J Jpn Dent Mater 1990; **9** (5): 747-753

[6] Kadoma Y, Imai Y. Studies on initiator system for cold curing resin using thiobarbituric acid derivatives. J Jpn Dent Mater 1991; **10** (5): 692-698

[7] Ikemura K, Nakamura S, Urabe S. Dental restorative compositions, Japanese Patent Open No. Toku-Kai-Hei-02-175412, 1987. (Shofu Inc.).

[8] Ikemura K, Nakamura S, Urabe S. Dental restorative compositions, Japanese Patent No. Toku-Kou-Hei-05-88683, 1993. (Shofu Inc.)

[9] Urabe S, Ikemura K, Nakamura S. Dental restorative compositions, Japanese Patent No. Toku-Kou-Hei-06-19164, 1994. (Shofu Inc.).

[10] Ikemura K, Endo T. Effect on adhesion of new polymerization initiator systems comprising 5-monosubstituted barbituric acids, aromatic sulfinate amides and *tert*-butylperoxymaleic acid in dental adhesive. J Appl Polym Sci 1999; **72**: 1655-1668

[11] Bowen RL, Cobb EN, Rapson JE. Adhesive bonding of various materials to hard tooth tissues: Improvement in bond strength to dentin. J Dent Res 1982; **61** (9): 1070-1076

[12] Kondo T, Koishi M. Microcapsule, Sankyo Shuppan, Tokyo, Japan, 1989

[13] Omi S, Koishi M. Nano/microcapsule technology. Kogyo Zairyo 2004; **52**(6): 18-70

[14] Yamaguchi T. et. al., Journal of the American chemical society 1999, **121**, 4078-4079

[15] Ito T. et. al., Journal of the American chemical society 2002, **124**, 7840-7846

[16] Chu, L-Y. et. al., Adv. Mater. 2002, **14**, 386-387

[17] Chu, L-Y. et. al., AIChEJ. 2003, 49, 896-909

[18] Kataoka K. et. al., Journal of the American chemical society **120**, 12694(1998)

[19] Shiono et. al., Biomaterials **15**, 121(1994)

[20] LY Chu et. al., Langmuir **18**, 1856(2002)

[21]Ito T. et. al., Journal of the American chemical society **124**, 7840(2002)

[22] Yanagioka M. et. al., Ind. Eng. Chem. Res. **42**, 380(2003)

[23] I. Koguma et. al., Biotechnol. Prog. **16**, 456-461(2000)

[24] K. Saito et. al., Rad. Phys. Chem. **54**, 517-525(1999)

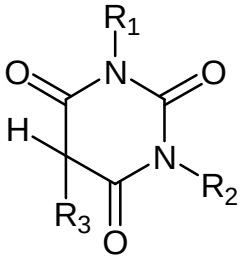

General formula of 5-MSBA

Abbr.	R_1	R_2	R_3	mp(K)
BBA	—H	—H	—C_4H_9	478.0
CEBA	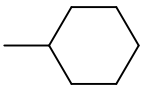	—H	—C_2H_5	389.3
BPBA	—H_2C— 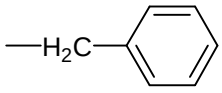	—H	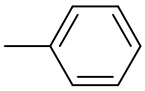	430.8
TMBA	—CH_3	—CH_3	—CH_3	424.8

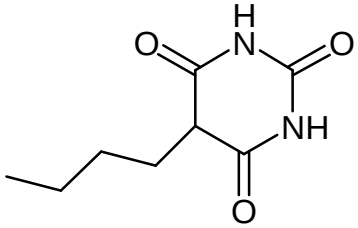

5-butylpyrimidine-2,4,6(1H,3H,5H)-trione
[BBA : 5-butylbarbituric acid]

Figure I-1. Structural formulas of
5-monosubstitute barbituric acids

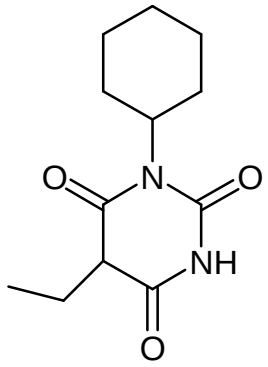

1-cyclohexyl-5-ethylpyrimidine-2,4,6(1H,3H,5H)-trione
[CEBA: 1-cycrohexyl-5-ethylbarbituric acid]

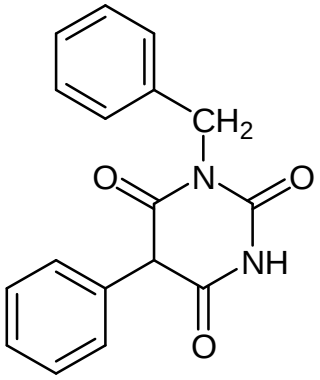

1-benzyl-5-phenylpyrimidine-2,4,6(1H,3H,5H)-trione
[BPBA : 1-benzyl-5-phenylbarbituric acid]

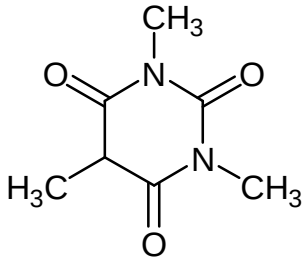

1,3,5-trimethylpyrimidine-2,4,6(1H,3H,5H)-trione
[TMBA : 1,2,3-trimethylbarbituric acid]

Figure I-1. Structural formulas of
5-monosubstitute barbituric acids

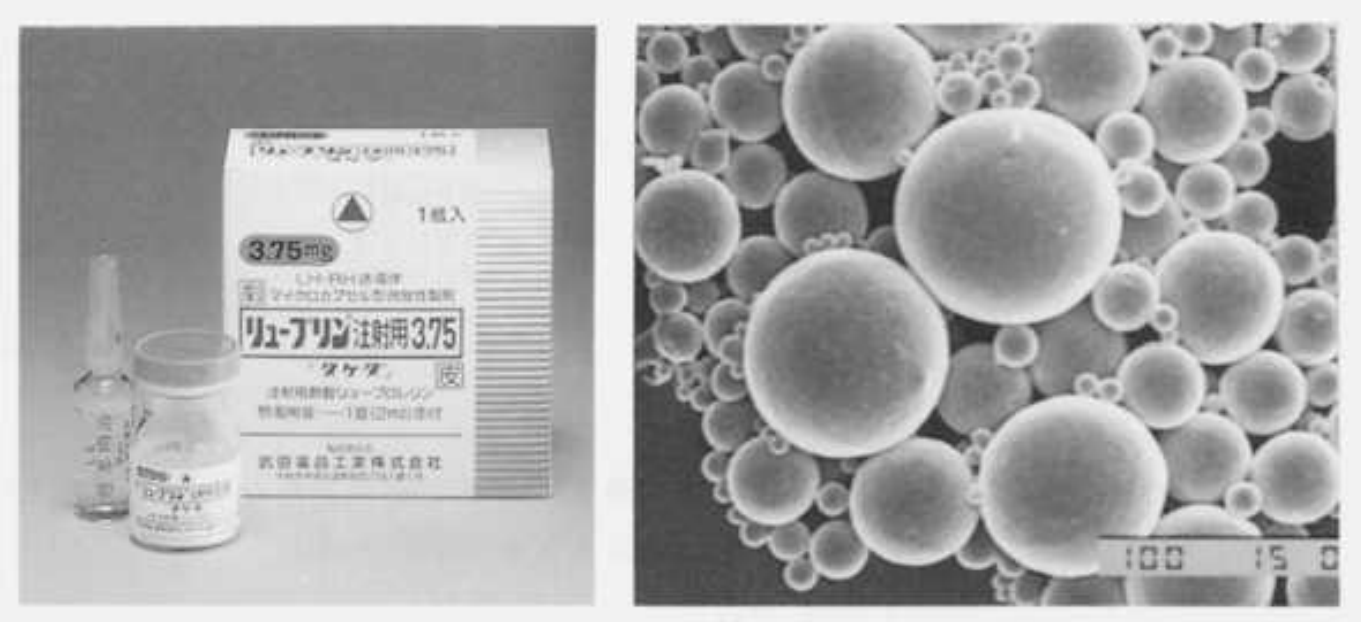

Figure I-2. Leuprorelin : commercially available anticancer drug

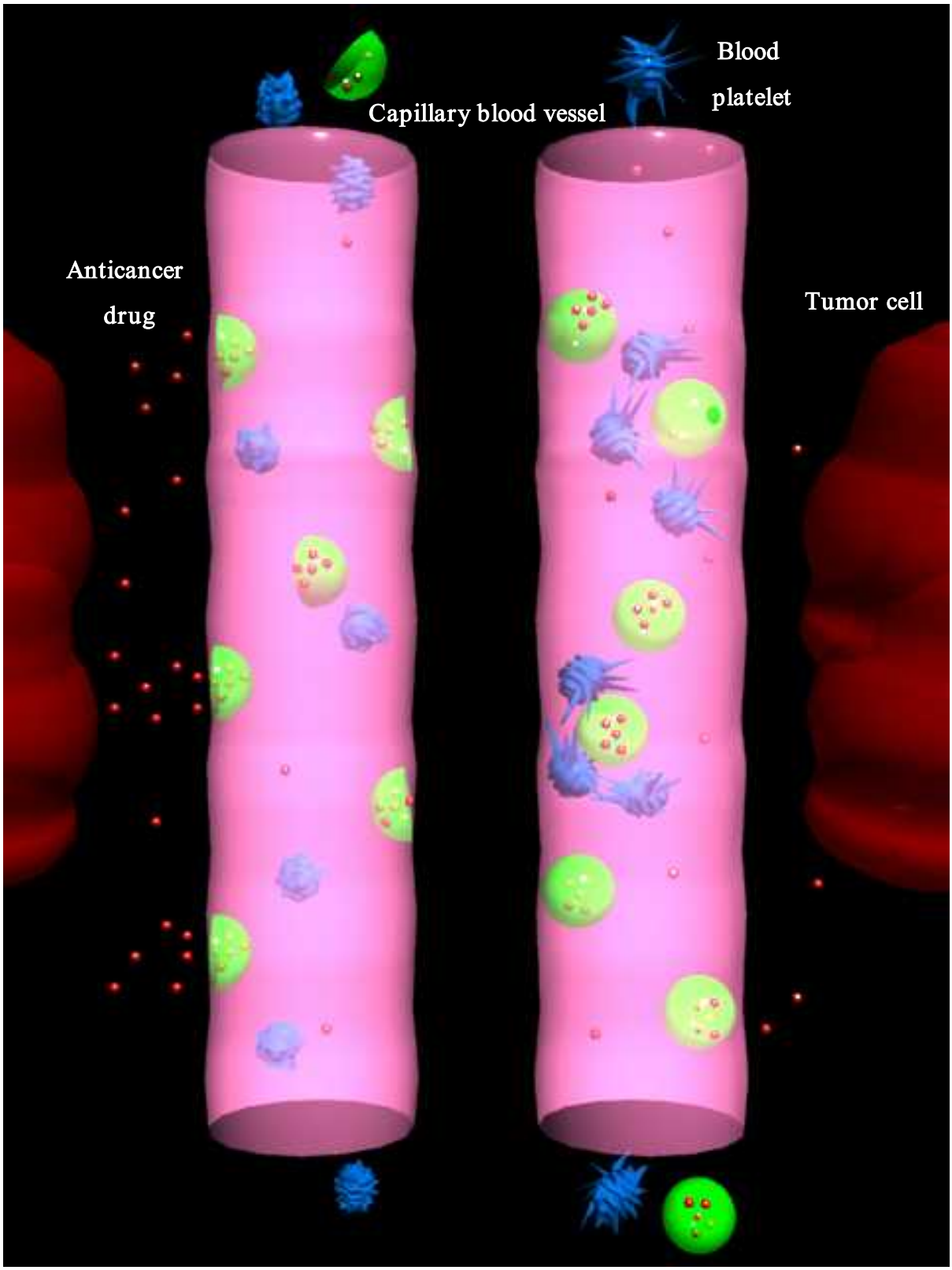

Scheme I-1. The expected effect of newly conceptual DDS

Chapter II

Preparation of Microcapsules Containing Reactive Compound by the Drying-in-liquid Method using Calcium Carbonate as Stabilizer

II-1. Abstract

Benzoyl peroxide (BPO) was microencapsulated with polyethyl methacrylate (PEMA) by the drying-in-liquid method using calcium carbonate as stabilizer. Methyl methacrylate (MMA) was used as solvent for PEMA in consideration of biosafety. Microcapsules prepared were characterized for medical applications. It was found that adhesive biomaterials prepared using microcapsules had sufficient ability for initiating radical polymerization even after one and two month storage at 313K and relative humidity of 75 %.

II-2. Introduction

Microcapsules have been applied in various fields such as information recording, cosmetics, paintings, medicine, agriculture, food and so on (Kondo and Koishi, 1989). Moreover, active researches and developments have been performed to prepare microcapsules with various functions (Omi, Koishi *et al*, 2004). Among the applications of microcapsules, there is the modification of the two liquid types of adhesive into the one liquid type. In this case, the hardening agent microencapsulated has been mixed in the matrix agent beforehand and then, microcapsules are broken with the proper stimulus. If microcapsules as stated just above will be applied in the field of adhesive biomaterials, it is naturally that microcapsules have to be prepared by using biocompatible materials (Ikemura and Endo, 1998). Accordingly, it is necessary to investigate whether microcapsules are able to be prepared or not by using designed biocompatible materials. In this study, in order to apply microcapsules into the artificial bone, it was tried to microencapsulated benzoyl

peroxide (BPO) as core material with polyethyl methacrylate (PEMA) as wall material by the drying in liquid method. In this microencapsulation process, in order to make the dispersion stable and to remove stabilizer as perfectly as possible, two types of calcium carbonate powders, needle and square type were used as stabilizer. The purpose of this study is to investigate whether microcapsules containing BPO powder are able to be prepared by the drying-in-liquid method or not and to evaluate the performance of microcapsules as adhesive biocompatible materials.

II-3. Experimental

II-3-1. Materials

Polyethyl methacrylate (PEMA ; MW= 80000, Negami Chemical Industrial Co., Tokyo Japan) was used as the microcapsule shell polymer. Methyl methacrylate monomer (MMA ; Mitsubishi Rayon Co., Ltd.) was used as the solvent for PEMA. Benzoyl peroxide (BPO ; Kawaguchi Chemical Co., Ltd.) powder with the mean diameter of 44 μm was used as the core material. Two types of calcium carbonate with the different crystal shape as shown in **Table II-1** (CC ; Komesho Sekkai Kogyo Co., Osaka, Japan), namely needle type and square type, were used as stabilizer. Sodium dodecyl sulfonate (DBS ; Daiichi Kogyo Seiyaku Co., Ltd.) was used as co-stabilizer.

II-3-2. Preparation of microcapsules

Microcapsules were prepared as follows. Experimental conditions are shown in **Table II-2**. The given amounts of PEMA and BPO were added into MMA of the given volume. This mixture was kneaded for

5min at the revolution speed of 16.7s^{-1} with the Thinky Non-bubbling Kneader to prepare the primary suspension (solid in oil; S/O), which was the dispersed phase. This dispersed phase was pored into the continuous water phase, in which the given amounts of DBS and CC were added. This dispersion, (S/O)/W), was irradiated by ultrasound at the condition of 150 W-35 kHz for 3min and then, was mixed at the revolution speed of 83.3s^{-1} for 5 min with the rotary homogenizer (IUCHI Co., Ltd.). The (S/O)/W dispersion was transferred to the separable flask with the effective volume of $5.0\times10^{-4}m^3$ and four teflon baffle plates of width of 1.0×10^{-2}m and then, MMA of the solvent was removed for 3h at 313K under reduced pressure of 700 mHg and the revolution speed of 5s^{-1} using EYELA UNITRAP VT-2000 (Tokyo Rikakikai Co.,Ltd.). Microcapsules prepared were separated by centrifugal separator for 1h under the conditions of temperature of 278K and the acceleration gravity of $134.3\times10^3m/s^2$. The separated microcapsules were thoroughly washed with ion-exchanged water and freeze-dried for seven days. Next, the freeze-dried microcapsules of given amount (10×10^{-3} kg) were suspended in ion-exchanged water of $1.0\times10^{-4}m^3$, and hydrochloric acid solution of the concentration of 1 N was added to remove calcium carbonate under magnetic agitation (2s^{-1}). Then, this suspension was filtered under reduced pressure and microcapsules were thoroughly washed with ion-exchanged water and then, freeze-dried. These freeze-dried microcapsules of given amount (3.0×10^{-3} kg) were suspended in n-hexane of $30\times10^{-4}m^3$ for 1h to remove unmicroencapsulated BPO under the room temperature and magnetic agitation (2s^{-1}) and then, filtered. After one more washing with n-hexane, microcapsules were then dried at the room temperature for

1 h under reduced pressure of 350mmHg, and dried again at 303K for 1h under high vacuum of 0.05 Torr.

II-3-3. Preparation of adhesive biomaterials

Materials adherable to living hard tissues, often applied in the field of orthopedics, were prepared by using microcapsules prepared in this study and others as follows. Standard powdery adhesive materials (SPAM) was prepared with BPO of 1×10^{-4} kg according to the previous works (Ikemura and Endo, 1998, 1999). Fundamental recipe for preparing SPAM and powdery adhesive materials (PAM) containing BPO-microcapsules is shown in **Table II-3**. Each element in **Table II-3** was mixed with blender (1.0 s^{-1}) to prepare SPAM and PAM. Fundamental recipe for preparing liquid adhesive materials containing polymerizable monomer is shown **Table II-4** (Ikemura and Endo, 1998, 1999). Each element was dissolved in the beaker with magnetic agitation ($2s^{-1}$). An efficacy of the microcapsules was estimated by mixing SPAM or PAM and liquid adhesive materials.

II-3-4. Characterization

II-3-4-1. Observation of microcapsules

The whole, the surface and the cross section morphologies of microcapsules were observed by scanning electron microscopy (SEM). The cross section was observed as follows. Microcapsules were embedded, hardened in epoxy resin and polished with #1200 water–proof adhesive paper on pouring water. The exposed cross section surface was washed again with n-hexane to remove BPO.

II-3-4-2. Diameter distribution and mean diameter

The diameter distributions and mean diameters of microcapsules were measured from the photographs of about five hundreds of microcapsules taken by the optical microscope. The mean diameter was the Sauter mean diameter.

II-3-4-3. Microencapsulation efficiency

Microencapsulation efficiency of BPO was measured by using a high performance liquid chromatography (HPLC) as follows. Microcapsules of 10 mg were dissolved into 10ml of acetone. This solution was filtered through the 0.45 μm membrane filter and used as a test solution. Standard solutions were prepared to make the calibration curve by dissolving the given weight of BPO in acetone of 10 ml. Microencapsulation efficiency was estimated by comparing the value obtained for the test solution with one for the calibration curve. Measuring conditions of HPLC were as follows.

HPLC: SHIMADZU LC-4A, LC-10Avp
Eluent: CH_3CN 70 vol%/H_2O 30 vol%
Flow rate: 0.5 ml/min
Column temp: 323K
Detector: UV-210 nm
Injection amount: 5 μl

II-3-4-4. Curing time and adhesive strength

In order to estimate the effect of microencapsulation of BPO, the curing times of PAM and SPAM were measured to obtain a thermal curve representing degradation levels as follows. SPAM or PAM of

5.0×10^{-3} kg was added into a silicon cup and liquid adhesive materials of 2.5×10^{-3} kg was poured into this cup. These materials were mixed for 10 s using a spatula. Thermocouples were embedded into these materials, and the time (curing time) required for the temperature to rise to the highest was measured immediately after mixing both adhesive materials. Operation of measuring temperature like this was performed for PAM and SPAM just after prepared and after stored for one and two months at the conditions of 313K and relative humidity of 75%, respectively. Adhesion strength was measured as follows. The surface of a SUS rod with 5 mm diameter was sandblasted with alumina under pressure of 5 kgf/cm^2. Gold alloy of a Type 4 medical devise was polished pouring water by use of a #600 waterproof abrasive paper and sandblasted with alumina under pressure of 5 kgf/cm^2. Then, the sandblasted SUS rod and gold alloy were ultrasonically cleaned and dried at the room temperature. A mixture of PAM and liquid adhesion materials was set between the SUS rod and the gold alloy. Then, load of 200 gf was applied on the SUS rod for the curing time previously measured plus additional 1min. After removing the load, the test sample composed of the SUS rod and the gold alloy was immersed in water at 310K for 24 h. The shear bond strength (F) of the test sample was measured using INSTRON-5543 (INSTRON Co., Ltd.) at a cross head speed of 1.0 mm/min.

II-4. Results and Discussion

II-4-1. Morphological observation

Figures II-1 and **II-2** show typical SEM photographs of the whole and surface of microcapsules prepared by adding CC of 5.4×10^{-3} kg. From these photographs, the following results were obtained.

Microcapsules are almost spherical. The surface became rougher in case of needle shape than in case of square shape calcium carbonate and rougher with the size of needle shape calcium carbonate. Furthermore, a number of fine pores on the surface of microcapsule decreased with decrease in the size of calcium carbonate. From these results, it is considered that the surface morphology was made by the traces of calcium carbonate adhered on the surface of microcapsule. **Figure II-3** shows the SEM photographs of the cross section of microcapsules. The traces of BPO crystals can be seen in all the photographs, but no difference in the inner structure of microcapsule due to the shape and size of calcium carbonate is observed. From these results, BPO as core material was found to be microencapsulated well.

II-4-2. Diameter distribution and mean diameter of microcapsules

Generally, the mean diameters of droplets in the liquid-liquid dispersion decreased with the concentration of solid powder and the diameter distributions became narrower with decrease in the size of powder particle (Tanaka and Hayashi, 1989; Taguchi and Tanaka, 1998, 1999). Here, the effect of added amount of CC on the mean diameter of microcapsules was investigated. **Figure II-4** shows the dependence of the mean diameter (dp) on the amount adhered (W) per unit surface area of microcapsule, in which the amount adhered per unit surface area was calculated by assuming that CC added entirely adhered on the surface of microcapsules. From this figure, it is found that the mean diameters strongly depend on the amount adhered per unit surface area and their dependences are different due to the shape of CC. As the adhesion layer of CC with the smaller size may become

more minute and the stabilizing effect for the emulsion may be higher, the dependence for square shape CC may become saturated by smaller amount and be smaller than that for needle shape CC.

II-4-3. Microencapsulation efficiency

Figure II-5 shows the dependence of the microencapsulation efficiency on the concentration of CC. It is found that the microencapsulation efficiencies were above 0.9 at all the conditions and were slightly higher in case of square type CC. These results may be attributable to the facts that the dispersion stability could be established by an addition of CC powder as stabilizer and became higher with square type than with needle type CC as shown in **Figure II-4**.

II-4-4. Performance test of microcapsules

Performance of microcapsules prepared here was estimated by measuring the curing times for PAM and SPAM. **Figure II-6** shows thermal curves obtained by conducting polymerization with PAM and SPAM, respectively. From this figure, the following things are obtained. Almost the same curing time (tc=304s) was obtained in the case of conducting polymerization just after preparation of PAM and SPAM. However, the curing times for PAM were tc=500 s and tc=980 s after one month storage and two month storage at 313K and a relative humidity of 70 %, respectively, whereas the curing time for SPAM was tc=1222s after one month storage and could not be measured after two month storage, namely BPO was substantially deactivated. From these results, microcapsules prepared in this study were found to have the ability for initiating polymerization after two

months storage and to be able to apply to pharmaceutical products and medical devices. **Figure II-7** shows the measured adhesive strength. Adhesive strength (F) for SPAM was found to significantly decrease with the storage period and to be completely lost after two month storage at 313K and a relative humidity of 75 %. Meanwhile, adhesive strength (F) for PAM was found to slightly decrease after one month storage and to retain adhesive strength of about 12% even after two month storage. These results confirmed that microcapsules exhibited the function controlling activation adequately enough for use in adhesive biomaterials.

II-5. Conclusion

In the present study, BPO was microencapsulated with polyethyl methacrylate by the drying-in-liquid method using calcium carbonate with different crystal shape and size as an inorganic stabilizer. We evaluated the surface morphology, the particle diameter distributions, the microencapsulation efficiency together with their possibility for use in adhesive biomaterials. The results obtained are as follows.

(1) Microcapsules containing BPO were able to be prepared by using polyethyl methacrylate as shell material, calcium carbonate powder as stabilizer and MMA monomer as volatile solvent.

(2) The mean diameters of microcapsules strongly depended on the amount of calcium carbonate adhered on the surface of microcapsule.

(3) The surface of microcapsule became smoother with decrease in the

size of calcium carbonate.

(4) Microencapsulation efficiencies of BPO were above 0.90 under all the experimental conditions adopted here.

(5) Microcapsules had the ability for initiating polymerization after two month storage at 313K and relative humidity of 70%

REFERENCES

1) Ikemura, K and T. Endo; “Effect of a New 4 acryloxyethyl trimellitic Acid in a Visible Light Cured Dental Adhesive on Adhesion and Polymerization Reactivity”, J. Appl. Polym. Sci., **69**, 1057-1069 (1998)

2) Ikemura, K and T. Endo; “Effect on Adhesion of New Polymerization Initiator Systems Comprising 5-Monosubstituted Barbituric Acids, Aromatics Sulfinate Amides and Tert-Butyl Peroxymallic Acid in Dental Adhesive Resin,” J. Appl. Polym. Sci.; **72**, 1655-1668 (1999)

3) Kondo, T. and M. Koishi; Microcapsule, Sankyo Shuppan, Tokyo, Japan (1989) Omi, S., M, Koishi *et al*.; “Nano/Microcapsule Technology,” Kogyo Zairyo, **52**, 18-70 (2004)

4) Tanaka, M. and K, Hagashi; “Preparation of Polystyrene Particles Coated with Ferrite Powder by Suspension Polymerization,” Kagaku Kogaku Ronbunshu, **15**, 1144-1152 (1989)

5) Taguchi, Y. and M. Tanaka; “Effect of Solid Powders as Stabilizers on Polymer Particles Sizes in Suspension Polymerization” Kagaku Kogaku Ronbunshu, **24**, 603-608 (1998)

6) Taguchi, Y., K. Hosogai and M. Tanaka; “Effect of Fine Solid Powders as Stabilizers on Distributions of Polymer Particle Diameters in Suspension Polymerization”, Kagaku Kogaku Ronbunshu, **25**, 758-763 (1999)

Figure Captions

Table Captions

Table II-1. Calcium carbonate used

Table II-2. Experimental conditions for microcapsule synthesis

Table II-3. Fundamental recipe for preparing standard powdery adhesive materials and powdery adhesive materials

Table II-4. Fundamental recipe for preparing liquid adhesive material

Table II-1. Calcium carbonate used

Shape of crystal	Particle size [μ m]		
Needle	1.00	2.00	5.00
Square	0.04	0.15	0.80

Table II-2. Experimental conditions for microcapsule synthesis

Continuos phase	Deionized water [ml]	270
	Amount of CC [g]	2.70, 5.4 0, 8.10
	Concentration [wt%]	0.9, 1.8, 2.6
	DBS [g]	2.70×10^{-2}
Dispersed phase	PEMA [g]	7.00
	MMA [g]	28.0
	BPO or TMBA [g]	7.00
Hold up		0.1
Stirring speed		$5\ s^{-1}$
Drying condition		313K, 3h, 700 mHg

Note: CC: calcium carbonate, DBS: sodium dodecyl sufonate, PEMA: poly(ethylmethacrylate), MMA: methylmethacrylate, BPO: benzoyl peroxide, TMBA: 1,3,5-trimethylbarituric acid

Table II-3. Fundamental recipe for preparing standard powdery adhesive materials [a)] and powdery adhesive materials [b)]

PMMA	40×10^{-3}Kg
PMMA-PEMA	45×10^{-3}Kg
PEMA	15×10^{-3}Kg
SiO2 powder	10.5×10^{-3}Kg
4-AET	2.3×10^{-3}Kg
4-AETA	0.8×10^{-3}Kg
BPO	0.3×10^{-3}Kg
BPO-microcapsule	0.63×10^{-3}Kg
TMBA	1.0×10^{-3}Kg

PMMA: Polymethyl methacrylate
PEMA: Polyethyl methacrylate
4-AET: 4-acryloxyethyl trimellitic acid
4-AETA: 4-acryloxyethyl trimellitate anhydride
TMBA: 1,3,5-trimethyl barbiturate

Table II-4. Fundamental recipe for preparing liquid adhesive material

MMA	50×10^{-3}Kg
DEPT	0.6×10^{-3}Kg
2-HEMA	2.9×10^{-3}Kg
p-MeHQ	2.0×10^{-6}Kg
EGDMA	1.0×10^{-3}Kg
BHT	1.5×10^{-4}Kg

DEPT: N,N-di(hydroxyethyl)-p-toluidine
2-HEMA: 2-hydroxyethyl methacrylate
p-MeHQ: p-Methoxyphenol
EGDMA: Ethylene glycol dimethacrylate
BHT: 2,6-di-t-butyl-4methylphenol

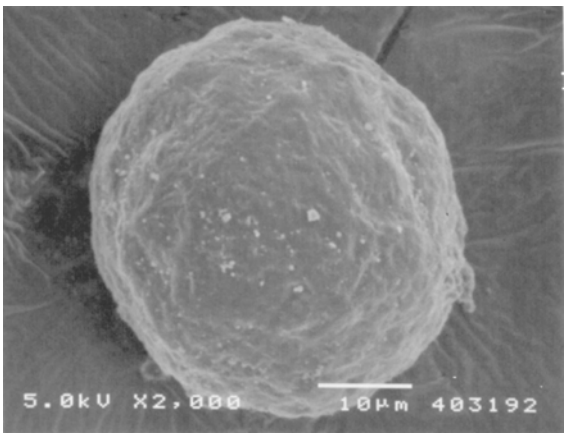

1.0 μ m-Needle shape crystal

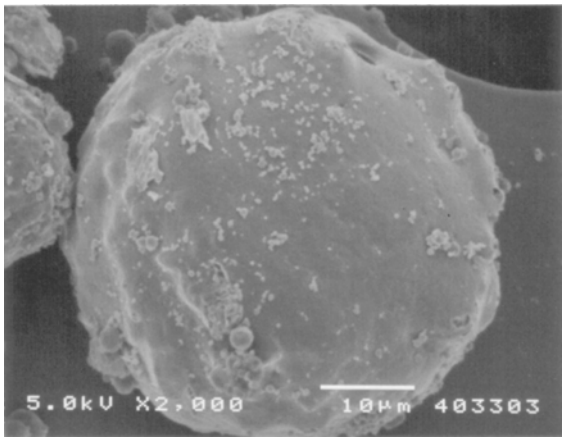

0.04 μ m-Cubic shape crystal

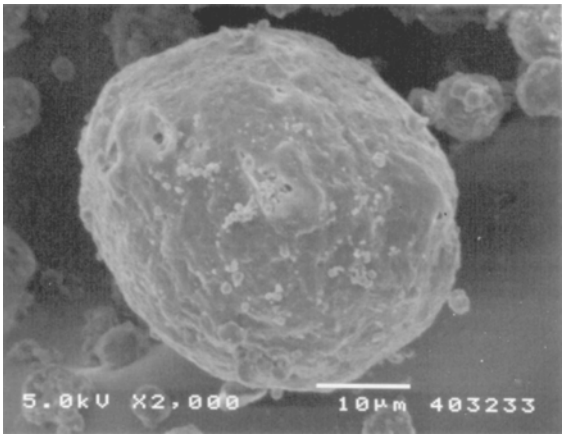

2.0 μ m-Needle shape crystal

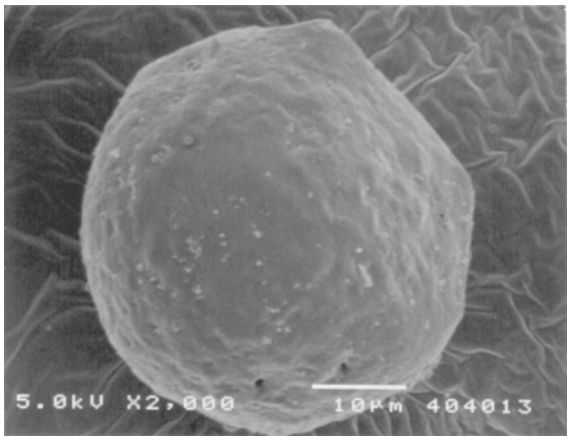

0.15 μ m-Cubic shape crystal

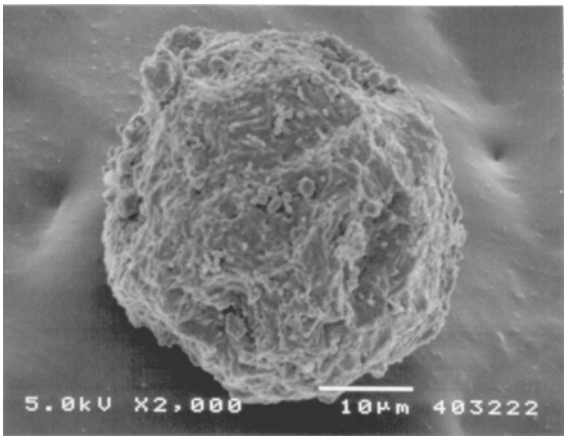

5.0 μ m-Needle shape crystal

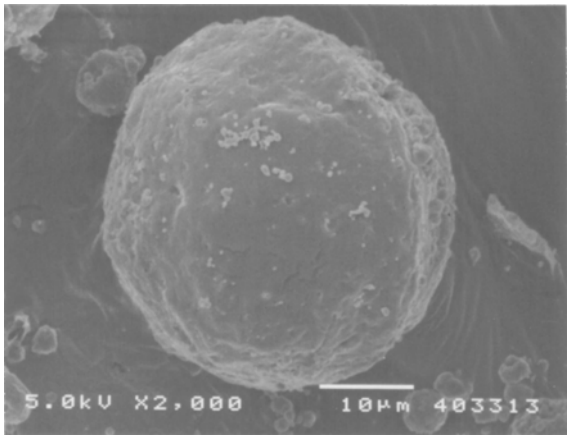

0.80 μ m-Cubic shape crystal

Fig.II-1. SEM photographs of whole of microcapsules

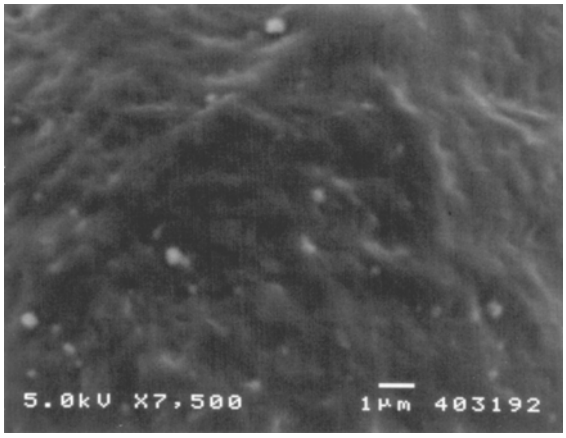

1.0 μ m-Needle shape crystal

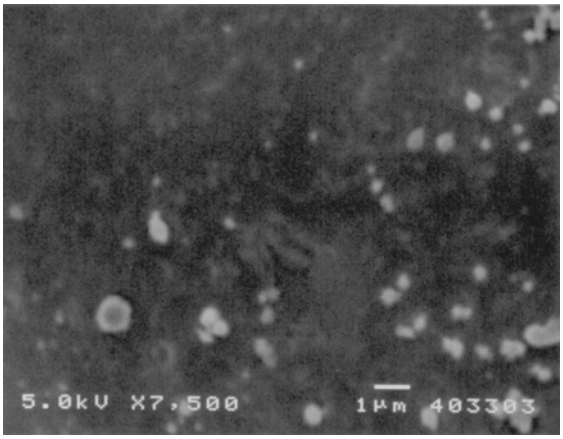

0.04 μ m-Cubic shape crystal

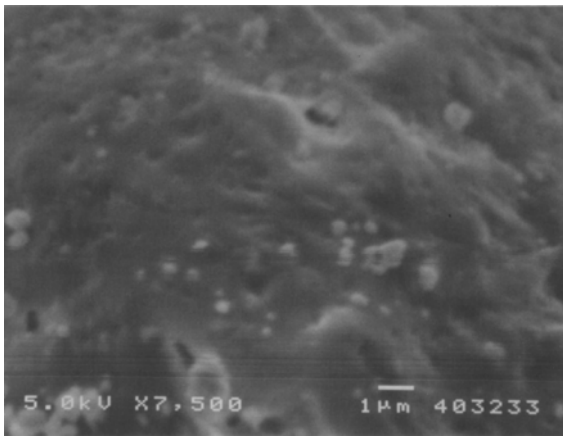

2.0 μ m-Needle shape crystal

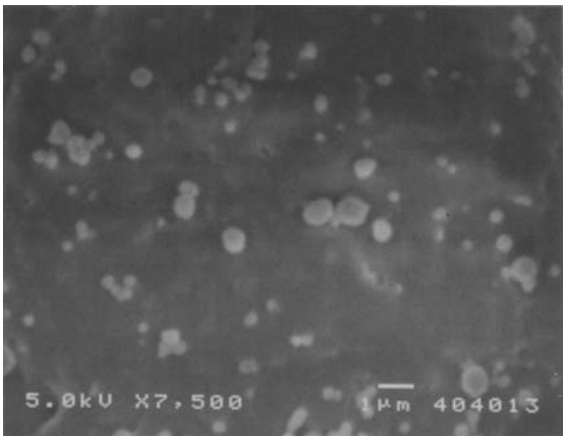

0.15 μ m-Cubic shape crystal

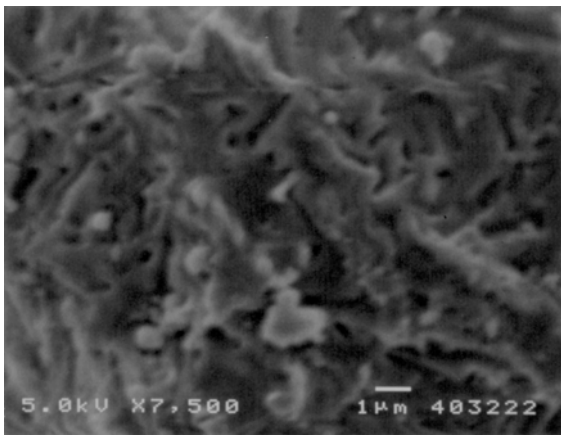

5.0 μ m-Needle shape crystal

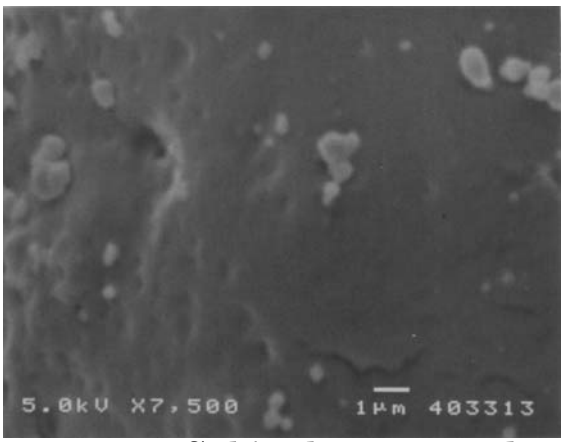

0.80 μ m-Cubic shape crystal

Fig.II-2. SEM photographs of surface of microcapsules

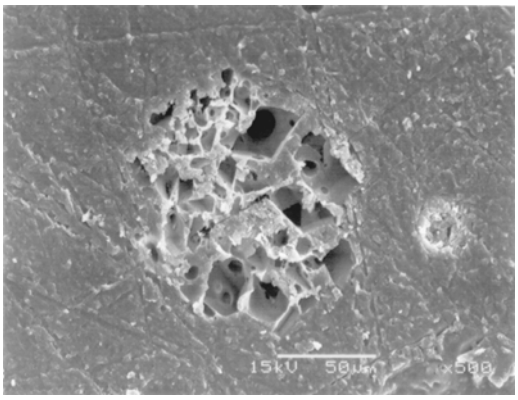

1.0 μ m-Needle shape crystal

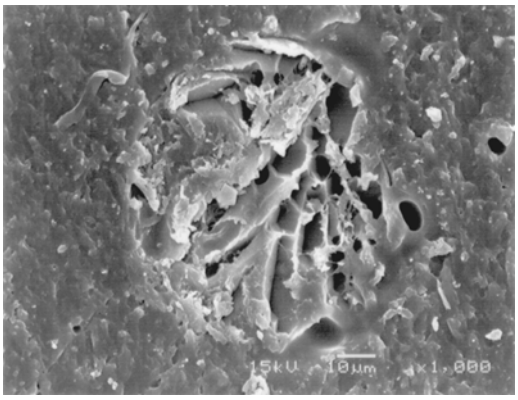

0.04 μ m-Cubic shape crystal

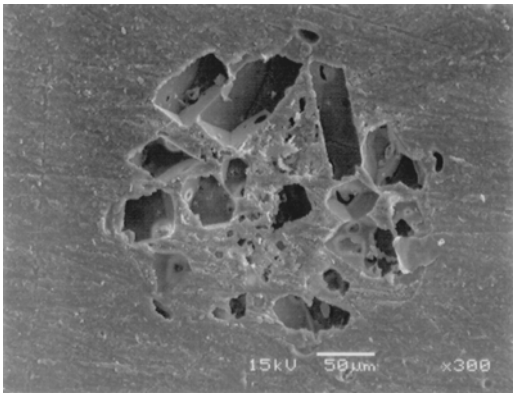

2.0 μ m-Needle shape crystal

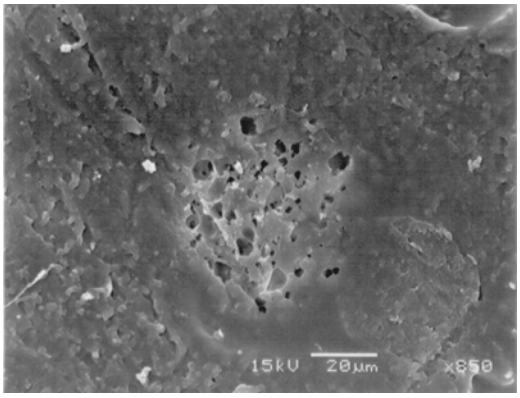

0.15 μ m-Cubic shape crystal

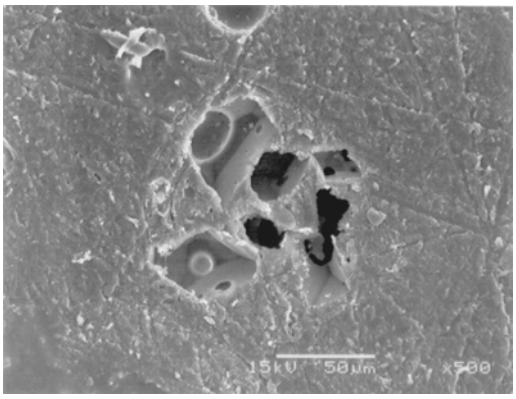

5.0 μ m-Needle shape crystal

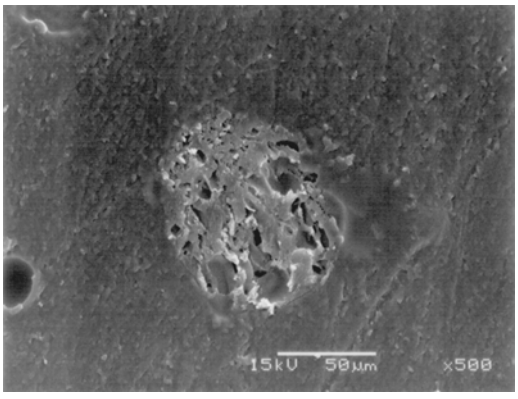

0.80 μ m-Cubic shape crystal

Fig.II-3. SEM photographs of cross section of microcapsules

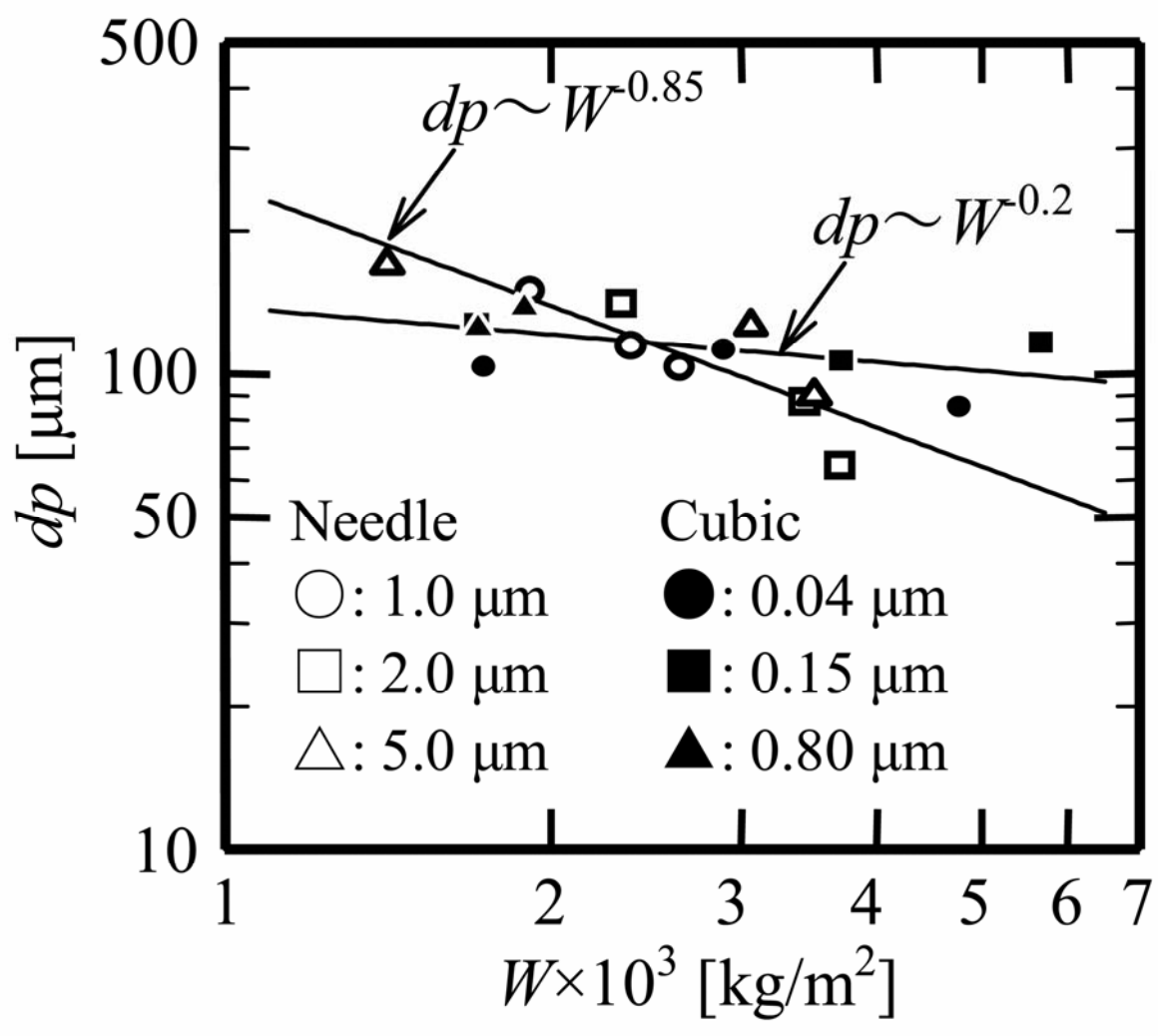

Fig.II-4. Dependence of mean diameter on amount adhered per unit surface area

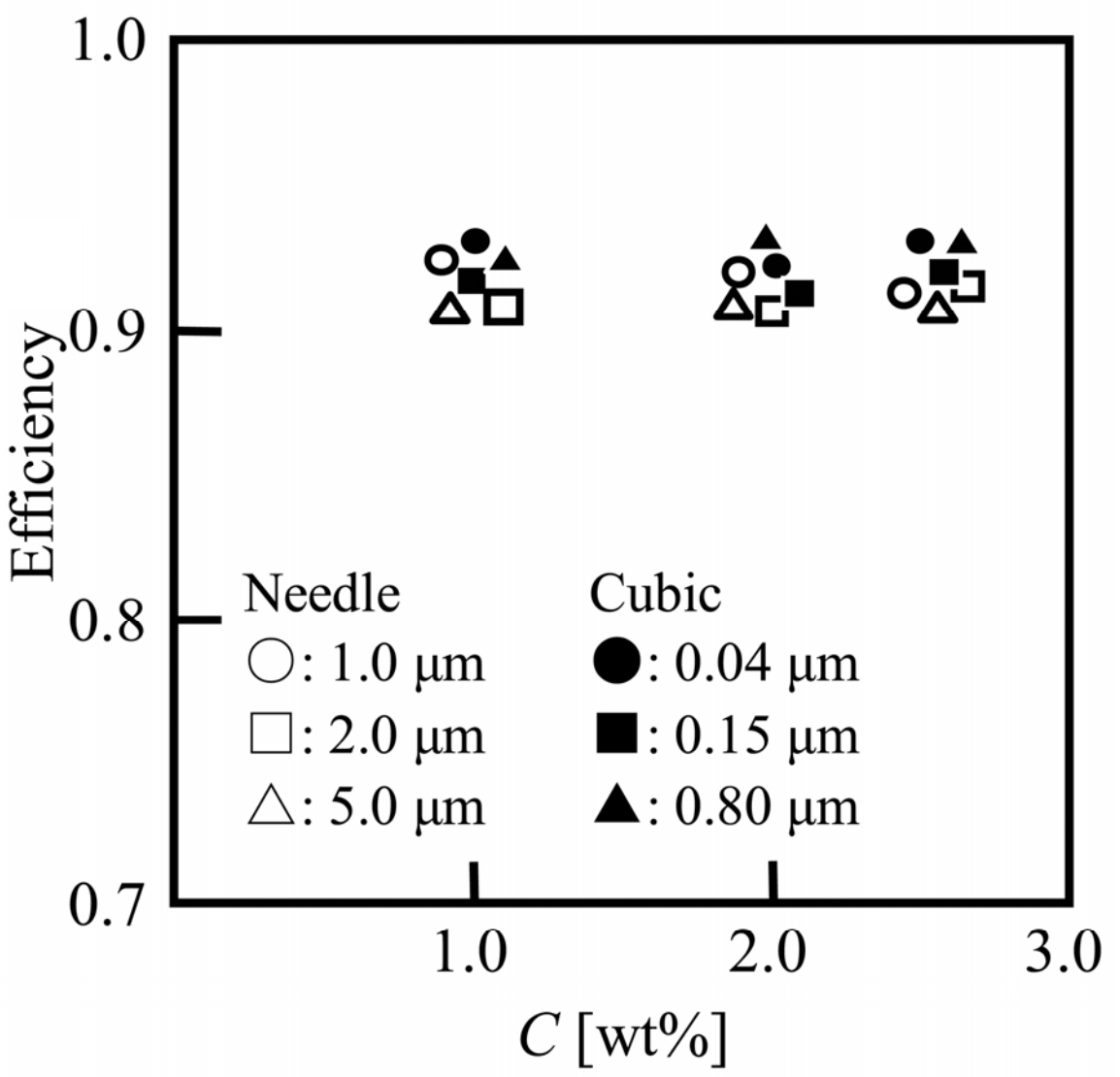

Fig.II-5. Dependence of microencapsulation efficiency on concentration of CC

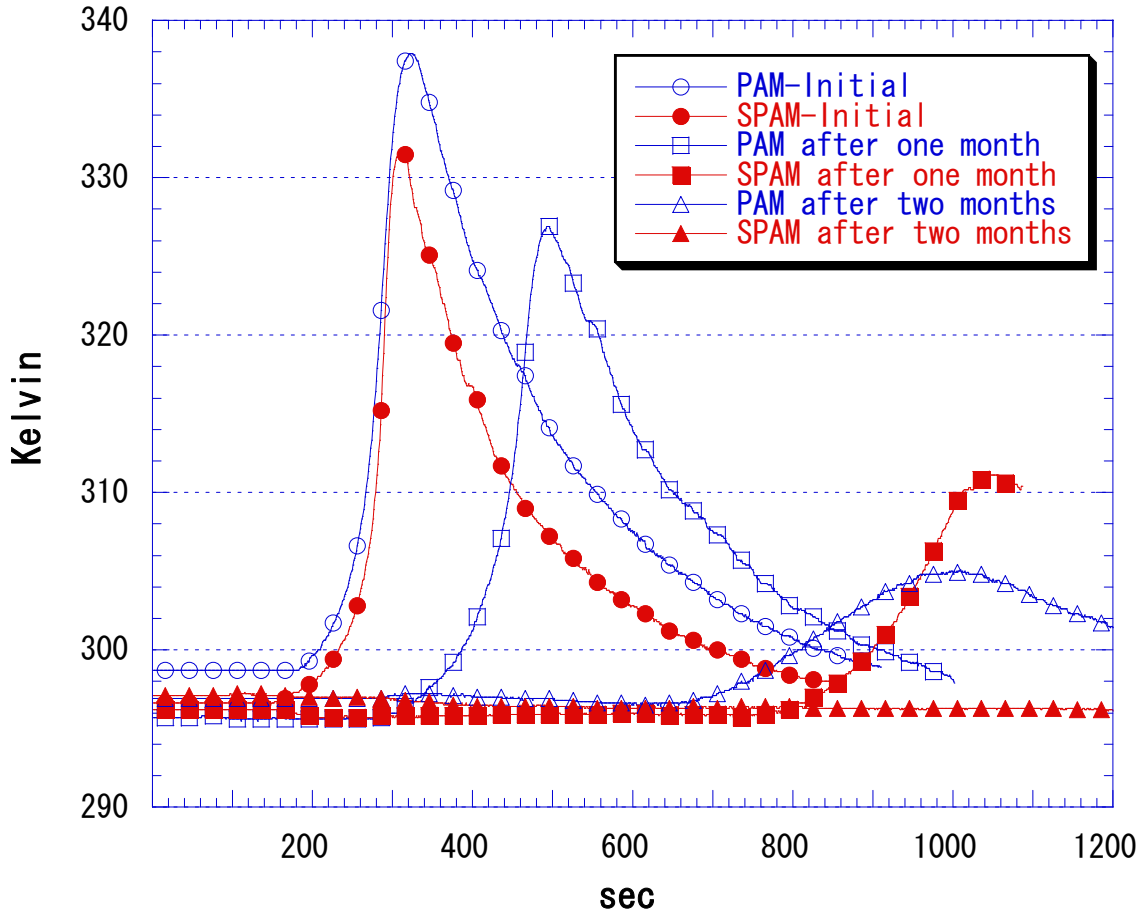

Fig.II-6. Thermal curves for SPAM and PAM

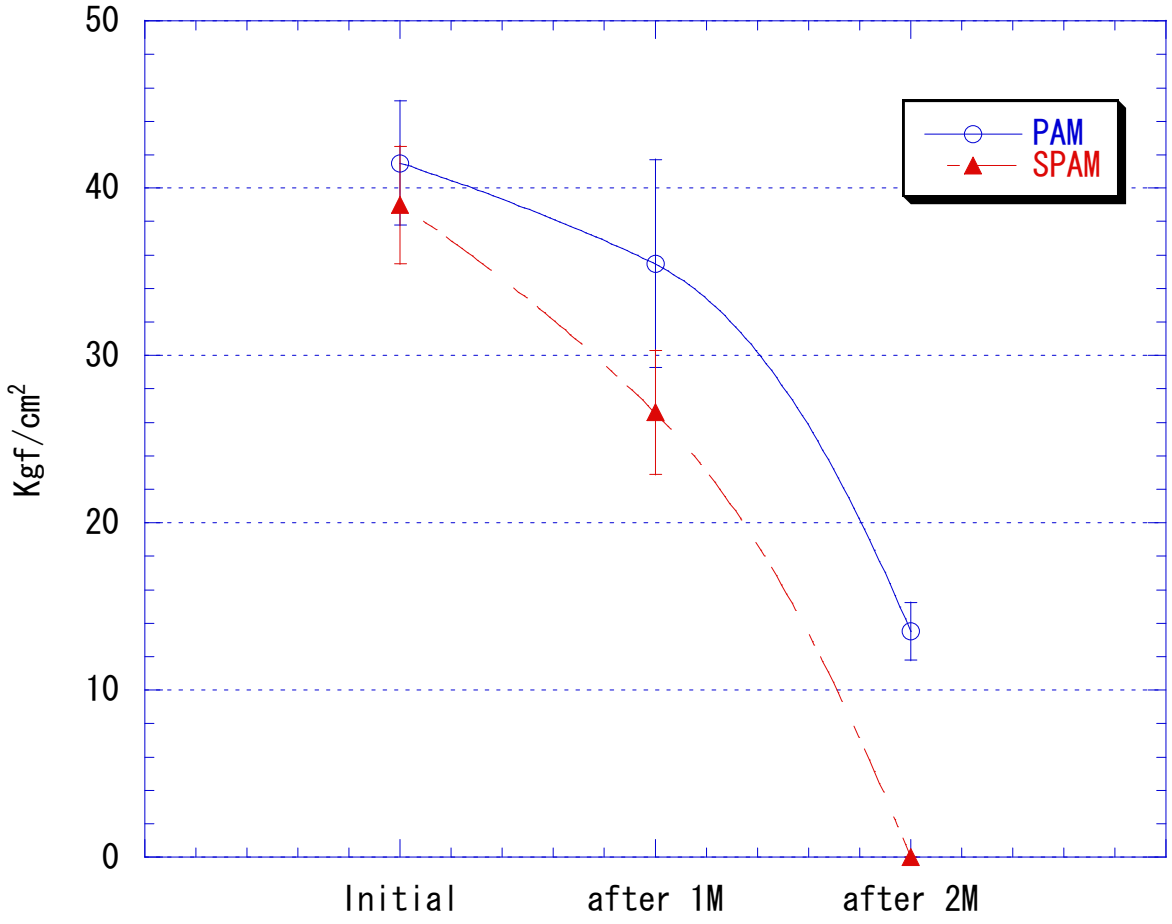

Fig.II-7. Adhesive strength of test materials

Chapter III

Preparation of Microcapsules Containing TMBA (1,3,5-trimethylbarbituric acid) by the Drying-in-liquid Method and its application

III-1. Abstract

Microencapsulation was carried out on 1,3,5-trimethylbarbituric acid (TMBA), a hydrosoluble material used widely for redox catalysts such as organic peroxide, aromatic tertiary amine, and anhydride, by the drying-in-liquid method with the use of PEMA as a wall material. Experimental conditions were made by setting 4 levels of the amount of TMBA added for preventing osmotically-induced leakage of the core material into the continuous phase (PVA solution), and also 3 levels of the disperse phase/continuous phase ratio (hold-up). The results indicated that the microencapsulation efficiency increased with the increase of the amount of TMBA added to the continuous phase, although the efficiency remained 36% at the highest even with the saturated level of TMBA (7wt% TMBA-PMA soln.). No effect was observed on the particle size. As for the systems with different levels of hold-up, the microencapsulation efficiency decreased with the increase of the disperse phase/continuous phase ratio, and no effect on the mean particle diameter was observed in any levels of hold-up. It is generally considered here that as the hold-up level increases, it takes longer for droplets in the disperse phase to reach an equilibrium state following several cycles of break-up and coalescence. It was thus suggested that the systems which went through droplet break-up more frequently, i.e. the systems with a higher level of hold-up, were more likely to have the core material of TMBA leaked in a crystalline state without dissolution. Additionally, the obtained TMBA microcapsules were used for

preparing a biological hard tissue-adhesive material and validated for the microencapsulation effects. The results showed that the microencapsulated systems had excellent bonding properties and high storing stability.

III-2. Introduction

In recent years, bone fillers and bone cements used in the medical and dental fields have evolved remarkably. It's not an exaggeration to say that they are indeed the achievement of many studies carried out on biological hard tissue-adhesive monomers and radical polymerization catalysts (redox catalysts especially). In general, a polymerization initiator used commonly in the medical and dental sectors is BPO; it is a heat-sensitive compound that rapidly breaks down to generate free radicals when heated. BPO also breaks down without heat; for instance when it comes in contact with aromatic tertiary amine, it quickly breaks down at room temperature and generates free radicals. These two ways of radical-generating mechanism in BPO are being applied for bone fillers and bone cements used in the medical and dental fields. The former mechanism requires heat: the half life of BPO is 13 hours at 343K and decreases to 2.2 hours at the higher temperature of 358K. BPO, when it breaks down, generates benzoyloxy radical as shown in **Scheme III-1-1**. A part of benzoyloxy radical further breaks down into phenyl radical. Both of free radicals have an activity capable of polymerizing polymerizable monomers. In the latter radical-generating mechanism, the most typically used amine is *N*,*N*-dihydroxymethyl-*p*-toluidine

(DMPT), which is usually dissolved in liquid acrylic resin monomer. When BPO-containing polymer comes in contact with liquid monomer during mixing, it reacts as shown in **Scheme III-1-2** to generate benzoyloxy radical. More recently, *N*,*N*-dihydroxyethyl-*p*-toluidine (DEPT), which is more reactive and less discolouring than DMPT, have come into use. There is also a technique to react TMBA with copper ions and chloride ions to generate free radical for polymerizing polymerizable monomers.[1-15] Here, TMBA is naturally oxidized to generate hydroperoxide having polymerization initiating-ability. When TMBA is affected by copper ions and chloride ions, it generates free radical according to the reactions indicated in **Scheme III-1-3**.[16-30] Such a polymerization initiator generates highly-concentrated free radical and thus accelerates the polymerization process.[31-40] TMBA, a useful radical source, however, has a major drawback in terms of storing stability due to its highly oxidizable nature as described above. Furthermore, when TMBA is used to prepare a biological hard tissue-adhesive material, the deliquescence of TMBA induces agglomeration and coalescence of coexisting components such as polymer beads, leading to a significant decrease in the handling properties. In order to avoid such problems, microencapsulation of TMBA has been anticipated. With these issues in mind, the present study attempted to microencapsulate hydrosoluble TMBA by the drying-in-liquid method. It has been known that the microencapsulation efficiency of hydrosoluble materials in this method is extremely low since, understandably, a hydrosoluble

material (core material) leaks to the outer phase water during the process. In the present study this leakage issue was addressed by controlling the osmotic pressure to improve the microencapsulation efficiency. The study also investigated the physical effects of a biological hard tissue-adhesive material prepared using the obtained TMBA microcapsules.

III-3. Experimental

III-3-1. Materials

Materials used were: a 100% PEMA polymer (D2528MELL, Mw=80000, manufactured by Negami Chemical Industrial Co., Ltd.) used as a microcapsule wall polymer; MMA (MeHQ3ppm, manufactured by Mitsubishi Rayon Co., Ltd.) used as a low-boiling polymer solvent; TMBA (manufactured by Nagase ChemteX Corporation) used as a core material; and polyvinyl alcohol (polymerization degree: 500, saponification value: 86.5–89.0 mol%, manufactured by Nacalai Tesque, Inc.) used as a surfactant.

Adhesive monomers of 4-AET and 4-AETA were purchased from Wako Pure Chemical Industries, Ltd. (Tokyo, Japan). BPO was purchased from Kawaguchi Chemical Co. Ltd. (Tokyo, Japan). PEMA, PMMA (Mitsubishi Rayon Co., Ltd., Tokyo, Japan), PMMA-PEMA copolymer (Negami Chemical Industrial Co., Tokyo, Japan) and Si-treated silica fillers (mean particle size: 1.5 μm), which were prepared by treating γ-methacryloxypropyl trimethoxysilane (KBM-503, Shinetsu Chemical Co. Ltd., Niigata, Japan), were used as components of powdery adhesives. MMA (Mitsubishi Rayon Co., Ltd.,

Tokyo, Japan), 2-hydroxyethyl methacrylate (HEMA) (Mitsubishi Rayon Co., Ltd., Tokyo, Japan), and ethyleneglycol dimethacrylate (EGDMA) (Shin Nakamura Chemicals, Co. Ltd., Wakayama, Japan) were used as component of liquid adhesive. Methoxy hydroquinone (MEHQ), butylated hydroxytoluene (= 2,6-di-*t*-butyl-4-methylphenol) (BHT), *N*,*N*-dihydroxyethyl-*p*-toluidine (DEPT) were purchased from Wako Pure Chemical Industries, Ltd. (Tokyo, Japan) and used without further purification.

III-3-2. Preparation of TMBA microcapsules

The following is a preparation method of TMBA microcapsules. The test conditions are shown in **Table III-1**. More specifically, the given amount of MMA solution with 30wt% of D2528MELL dissolved was placed into a 150mL PP beaker (inside diameter: 55 mm, height: 70 mm), and TMBA in the specified amounts was added to the solution. The mixture was stirred for approx. 5 min. using a PP spatula to undergo a primary dispersion. Next, for preparation of a continuous phase, 300.0-322.5g of outer phase water containing 4.0wt% PVA (surfactant) and TMBA in the given amounts was prepared in a 500 mL beaker. The outer phase water 300.0-322.5g was then transferred to a SIBATA 500mL flange-type separable flask having 4 stainless baffle plates (size: 1.0×10^{-2}m) inside the flask, and stirred at 313K-200rpm using SIBATA PROMIX PR-1200 having a 6-blade disk turbine (55 mm ϕ) until the temperature of the outer phase water became constant. The primary dispersion liquid of PEMA-MMA solution containing TMBA was then injected all at once into the outer

phase water at 313K-200rpm using a 50mL disposable syringe, and the mixture was desolvated for 2-4 hr at the stirring rate of 200rpm under reduced pressure of 313K-700mmHg. Generated vapor was trapped at 173K using EYELA UNITRAP UT-2000. The turbine used was being placed at one-third of the liquid depth from the bottom of the tank. After desolvation, the obtained microcapsules were filtrated under reduced pressure to be separated from the continuous phase. The separated microcapsules were thoroughly washed with 1L of ion-exchanged water, and freeze-dried for 3 days. After freeze-drying, microencapsulation efficiency was calculated by the subtraction method. SEM observation of the microcapsules, followed by particle size measurement at low magnification were also carried out.

III-3-3. Preparation of adhesive resins

Two experimental powder/liquid, PMMA-type adhesive resins were prepared in the composition listed in **Table III-3**. The powder adhesive (Adhesive-MC) was formulated using PMMA, PEMA, PMMA-PEMA, Si-treated fillers, adhesive monomers of 4-AET and 4-AETA, BPO and MC-TMBA. Control adhesive resin (Adhesive-BR) comprising non-capsulated polymerization initiators (Bare-TMBA) that were displaced with MC-TMBA in Adhesive-MC were prepared. The liquid of adhesive was composed of DEPT in MMA monomer that was used as a solvent for PEMA of microcapsule in consideration of biosafety. The liquid was used to mix with powders of Adhesive-MC and BR. The prepared adhesive resins were placed in 278K, 296K, and 313K (75% relative humidity) in air for 2

months, respectively, and their bonding performance were then examined.

III-3-4. Shear bond strength measurement

III-3-4-1. Preparation of adherents

Freshly extracted bovine incisors were used as substitutes for human specimens[41], due to the large number of teeth required in this study. The bovine teeth cut off the root were embedded in epoxy resin, then ground into enamel or dentin using 600-grit SiC abrasive paper under running water, and then air-dried (ground enamel or dentin). A dental gold alloy (Shofu Super Gold Type 4, Shofu Inc., Kyoto, Japan) was cast with a casting machine (Shofu Argon Caster, Shofu Inc., Kyoto, Japan), and a gold alloy rod (6.0± 0.1 mm in diameter, 3.0 mm in height) were prepared. The gold alloy was embedded in an epoxy resin. Commercially pure titanium (CP Ti) was purchased from Daido Steel Co. Ltd., (Nagoya, Aichi, Japan). Adhesive surfaces of the SUS 303 rod (5.0 ± 0.1 mm in diameter, 6.0 ± 0.1 mm in height), the gold alloy and titanium (4.0 ± 0.1 mm in diameter, 6.0 ± 0.1 mm in height) were flat-ground using 600-grit SiC abrasive paper; and then sandblasted with aluminum oxide (40-50 μm) (Shofu Hi-alumina, Shofu Inc., Kyoto, Japan) under pressure of 5 kgf/cm^2. Then, the sandblasted SUS rod, gold alloy and titanium metal were cleaned ultra-sonically and dried at the room temperature to prepare metal adherends (sandblasted SUS rod, gold alloy and titanium metal).

III-3-4-2. Shear bond testing

The prepared adherends were treated with surface-treating agents before adhesion. The adhesive surface of metal, *i.e.*, the sandblasted SUS rod, titanium and gold ally, was treated with Metal-Link Primer (Shofu Inc., Kyoto, Japan) that is a metal primer for adhesion to precious and non-precious metals. The SUS rod or gold alloy without Metal Link Primer treatment was also used as a control. The adhesive surface of ground enamel or ground dentin was treated with/or without ResiCem Primer (Shofu Inc, Kyoto, Japan) that is a self-etching primer for adhesion to enamel and dentin. The mixed Adhesive-MC or Adhesive-BR and liquid listed in **Table III-3** by brush on technique was placed on the adherends, and made to bond between (1) the titanium and ground enamel or ground dentin treated with/or without surface-treating agents, and (2) the SUS rod and the gold alloy. Load of 200 g was then applied on the titanium rod or SUS rod for the curing time previously measured plus additional 1 min. After 30 min, the test specimens (n = 10) were immersed in distilled water at 310K for 24 h. The Shear bond strength was measured using a mechanical testing machine (Instron-5543, Instron Co., USA) at a crosshead speed of 1 mm/min. All tests were conducted at 296 ± 1K. Fractured surfaces of specimens were examined in a microscope, and adhesive failure, cohesive failure and mixed failure were recorded. The mean and standard deviation for the load at failure were calculated and the results were subjected to a one-way analysis of variance (ANOVA), followed by the Newman-Keuls multiple comparison test.

III-4. Results and Discussion

III-4-1. Morphological observation of TMBA microcapsule, diameter distribution measurement

SEM images of the obtained microcapsules are shown in **Figures III-1-1**, **III-1-2**, and **III-1-3**. It was observed that, although not visible in the lower-magnification photographs (x50 and x200), crater-like pores on the surface of the microcapsules tended to appear more significantly as the amount of TMBA added to the outer phase water increased. Typically, when such pores are observed in the SEM images, encapsulation efficiency decreases with the increase of surface roughness, and thus these pores are considered as the sign that the core material had been leaked out. In the present study, however, as is evident from **Figure III-2-1**, the encapsulation efficiency increased, by contrast, due to the osmotic adjustment achieved by the addition of TMBA to the outer phase water, which suggests that the pores observed in the photographs are not the trace of core material leakage. It is speculated so far that the main factor of this phenomenon is TMBA, which is hydrophilic/phobic, added to the outer phase water. More specifically, in order for MMA, a hydrophobic high-boiling solvent, to be mixed in the outer phase water and volatilized at the air/liquid interface, sufficient force is required to go over the interface energy existing between the dispersed oil droplets containing MMA and the outer phase water, but the hydrophilicity/phobicity of TMBA contained in the outer phase water may have decreased the potential interface energy to activate the evaporation of MMA. Thus it may be considered that the pores observed resulted from MMA, which was in

a bumping state of a sort, being rapidly separated from the dispersion phase.

The graph in **Figure III-2-1** shows the relationship between microencapsulation efficiency and the concentrations of TMBA (core material) added to the outer phase water for osmotic adjustment. The saturated concentration of TMBA in 4wt% PVA solution is approx. 7wt%. Since dissolution beyond a saturation point is chemically impossible, 35% in encapsulation efficiency with the addition of 7wt% TMBA implies a collapse of TMBA, which is physically a core material. In order to obtain a higher encapsulation efficiency, factors other than osmotic pressure, e.g. affinity between the dispersion phase and continuous phase, needed to be controlled. The relationship between the disperse phase/continuous phase ratio (hold-up) and microencapsulation efficiency was plotted in **Figure III-2-2**, which shows that the efficiency decreased with the increase of hold-up. It is generally considered here that as the hold-up level increases, it takes longer for droplets in the disperse phase to reach an equilibrium state following several cycles of breakup and coalescence. It was thus suggested that the system which went through droplet breakup more frequently, i.e. the system with a higher level of hold-up, was more likely to have the core material of TMBA leaked in a crystalline state without dissolution. The relationship between the mean particle diameter and each factor (hold-up and TMBA concentration) was plotted in **Figures III-2-3** and **III-2-4**. No effect of these factors was observed on the mean particle diameter. The mean diameter and microencapsulation efficiency of the obtained microcapsules prepared

with various TMBA concentrations were plotted in **Figure III-2-5**. The graph shows that there is no correlation between the mean diameter and microencapsulation efficiency.

III-4-2. Shear bond strength measurement and polymerization initiating activity

Based on the characterization of microcapsules, the MC-TMBA was used for the formulation of PMMA-type adhesive resin (Adhesive-MC) in this study. **Figure III-3-1** presents the shear bond strength of experimental Adhesive-MC comprising microencapsulated initiators (MC-TMBA) or Adhesive-BR comprising bare initiators (Bare-TMBA) between the sandblasted titanium and unetched ground enamel or unetched ground dentin with/or without surface-treating agent. The statistical analysis (ANOVA) indicated that there were no significant differences between Adhesive-MC and Adhesive-BR in the bond strengths to unetched ground enamel (15.2~16.6 MPa) treated with/or without surface-treating agents ($p<0.05$). While it was indicated that there was no significant difference between Adhesive-MC and Adhesive-BR in the bond strengths to unetched ground dentin treated with surface-treating agents and that to unetched ground dentin without surface-treating agents ($p<0.05$), there were significant differences between the bond strength to unetched ground dentin treated with surface-treating agent (17.5~18.7 MPa) and that without surface-treating agent (3.8~4.0 MPa) ($p<0.05$). **Figure III-3-2** represents the shear bond strengths of Adhesive-MC or Adhesive-BR

between the sandblasted SUS rod and sandblasted gold alloy that was treated with Metal-Link Primer after the storage periods of starting, 1-month and 2-months at 278K, 296K and 313K in a relative humidity of 75 %, respectively. The statistical analysis (ANOVA) indicated that the bond strengths of Adhesive-MC to gold alloy maintained [starting: 42.5 (3.7) MPa] after 2-months storage period at 278K [41.8 (4.8) MPa] and 296K [39.5 (8.1) MPa], 1-month storage period at 313K [31.0 (9.8) MPa], and 100% mixed failure (M) of adhesive resin was observed on the fractured surfaces, respectively ($p<0.05$). To the contrary, the bond strength of Adhesive-BR to gold alloy after 2-months storage period at 296K [12.8 (6.4) MPa] was significantly decreased with 90% adhesive failure (A) ($p<0.05$), and the bond strength using the Adhesive-BR stored for 1-month and 2-months period at 313K could not be tested (CNT). While there were no significant difference between Adhesive-MC and Adhesive-BR in the bond strengths after 2-months storage period at 278K and 1-month storage 296K, respectively, there were significant difference between both adhesive resins in the bond strengths after 2-months storage period at 296K, 313K, respectively ($p<0.05$). Powder property of Adhesive-BC was not significantly changed during 2-months storage period with good mobile handling property, such as brush on technique. In the contrast, Adhesive-BR was markedly changed during 1-month storage at 313K caused by agglomeration of powder adhesive (**Fig. III-4-1**), which was adverse handling property, especially brush on technique of PMMA-type adhesive resin.

III-5. Conclusion

In the present study, TMBA was microencapsulated with polyethyl methacrylate by the drying-in-liquid method using PVA as an organic surfactant. We evaluated the surface morphology, the particle diameter distributions, the microencapsulation efficiency together with their possibility for use in adhesive biomaterials. The results obtained are as follows.

(1) Microcapsules containing TMBA were able to be prepared by using polyethyl methacrylate as shell material, PVA as an organic surfactant and MMA monomer as volatile solvent.

(2) The maximum microencapsulation efficiency of TMBA was around 0.36 under the experimental conditions adopted here.

(3) The higher hold up conditions gave the lower microencapsulation efficiencies.

(4) Microcapsules had the ability for initiating polymerization after two months storage at 313K and relative humidity of 70%

REFERENCES

[1] XII. Mitt.: H. Bredereck, K. Posselt, A. Wagner und G. Wurster, Makromolekulare Chem. **69**(1963)154.

[2] H. Bredereck und E. Bader, Chem. Ber. **87**(1954)129.

[3] E. Bader und H. D. Hermann, Chem.Ber. **88**(1955)41.

[4] H. Bredereck, E. Bader, W. Nubling und A. Wohnhas, fur W. C. Heraeus GmbH. Und DEGSSA vormals ROESSLER ; Amer. P. 2776952v. 8. 1. 57, C. A. **51**(1957)6

[5] H. Bredereck, E. Bader, W. Nubling und A. Wohnhas, Makromolekulare Chem. **18/19**(1955)431.

[6] H. Bredereck, A. Wagner, K. Posselt und A. Fohmann, Makromolekularer Chem. **36**(1959)67.

[7] H. Bredereck, A. Wagner und K. Posselt, Chem. Ber. **93**(1960)1284.

[8] F. Rochlitz, Dissertation Techn. Hochschule Stuttgart 1954.

[9] D.B.P. 861156v. 9. 9. 1944, Farbwerke Hoechst ; C. 1953, 8219.

[10] F. Patat, zitiert bei W. Kern, Makromolekulare Chem. **1**(1947)249.

[11] G. V. Schultz und F. Blaschke, Z. Elektrochem. Angew. Physik. Chem. **47**(1941)749.

[12] H.Hopff und E.Kleiner, Chimia [Zurich] 16(1962)130; 19(1965)99, Uber Keto-Enol-Tautomerie als Polymerisationsinitiatoren, "Vortrag beim 3. Symposium uber makromolekulare Stoffe am 16./17. 10. 1964 ETH Zurich.

[13] Ch. J. Eby und Ch. R. Hauser, J. Amer. Chem. Soc. **79**(1957)723.

[14] R.L.Shriner und R.C.Fuson, The Systematic Identification of Organic Compounds, J. Wiley and Sons, New York 1948, S. 97.

[15] U.S.P. 2446503 v. 3. 8. 1948, Hoffmann-La Roche, Inc. Nutley, N. J., Erf.: W. Wenner; C. A. **42**(1948)8820.

[16] W. Wirths, Diplomarbeit Techn. Hochschule Stuttgart 1965.

[17] H.Bredereck, B. Fohlisch, R. Franz, Makromol. Chem. 92, 70(1966).

[18] H.Bredereck, B. Fohlisch, R. Franz, D. Tagoe, K. Diebel, B.

Kramer, Macromol. Chem. 99, 96(1966)

[19] H.Bredereck, R. Franz, G. Bauer, Angew. Chem. 80, 319(1968)

[20] R. Schaefer, Dissertation, Universitat Stuttgart, 1970

[21] D. Tagoe, Dissertation, Universitat Stuttgart, 1968

[22] H. C. Carrington, J. Chem. Soc. 1944, 124

[23] H. R. Henze, P. E. Smith, J. Amer. Chem. Soc. **65**, 1090(1943)

[24] D. J. Brown, "The Pyrimidines", Interscience Publ., New York 1962, p. 251

[25] A. J. Vazakas, W. Walden Benetts Jr., J. Med. Chem. **7**, 342(1964)

[26] Japan. 6807949(1968), Takeda Chem. Industries Ltd., Erf.: S.senda, H. Fujimura, H. Izumi; C. A. 70, 11714g(1969)

[27] A. C. Cope, D. Heil, D. Peck, C. Eide, A. Arroyo, J. Amer. Chem. Soc. **63**, 356(1941)

[28] E. Miller, J. C. Munch, F. S. Crossley, W. H. Hartung, J. Amer. Chem. Soc. **58**, 1090(1936)

[29] C. O. Wilson, J. H. Boothe, J. Amer. Chem. Soc. **68**, 449(1946)

[30] U.S. 2386026(1945), regents of the university of Minnesota, Erf.: C. O. Wilson, J. H. Boothe; C. A. 40, 1973(1946)

[31] C. O. Wilson, J. H. Boothe, J. M. Dille, Science 104, 100(1946)

[32] J. Seemann, Dissertation, Universitat Stuttgart, 1968

[33] B. Kramer, Dissertation, Universitat Stuttgart, 1967

[34] R. Dorrler, Dissertation, Universitat Stuttgart, 1970

[35] J. D. Dutcher, J. R. Johnson, W. F. Bruce, J. Amer. Chem. Soc. 67, 1736(1945)

[36] H. Blitz, H. Wittek, Ber. Deut. Chem. Ges. **54**, 1035(1921)

[37] E. Hope, W. H. Perkin Jr., J.Chem. Soc. **95**, 1363(1909)

[38] G. V. Schulz, F. Blaschke, Z. Elektrochem. **47**, 749(1941)

[39] Gerwalt Grahe, P. Petranyi, K. Posselt, H. Sigel, E. Tag und W. Wirths, Die Makromolekulare Chem., **92**(1966)70-90

[40] V. Hellmut Bredereck, P. Menzel, R. Argosino und W. Bihlmaier, Die Makromolekulare Chem., **176**(1975)1713-1723

[41] Schilke R, Bauss O, Lisson JA, Geurtsen W. Bovine dentin as a substitute for human dentin in shear bond strength measurements. Am J Dent 1999; 12: 92-96.

Figure Captions

Fig. III-3-2. Shear bond strength of experimental adhesive resin between SUS rod and gold alloy

Fig. III-4-1. A photo of the Powdery adhesive of bare BPO/Amine initiator after 1-month storage at 313K (75% relative humidity)

Table Captions

Table III-1. Experimental conditions for microcapsule synthesis

		Dispersed phase		Continuous phase	
No.	Hold up	TMBA (g)	Polymer soln. [1] (g)	TMBA (g)	PVA soln. [2] (g)
1	1.0	5.50	16.5	None	300
2	1.0	5.50	16.5	5.6	↑
3	1.0	5.50	16.5	11.3	↑
4	1.0	5.50	16.5	22.5	↑
5	1.5	8.25	24.8	22.5	↑
6	2.0	11.0	33.0	22.5	↑

[1] Polyethyl methacrylate (D2528MELL, MW= 80000, Negami Chemical Industrial Co., Tokyo Japan) 30wt%-MMA solution

[2] Poly vinyl alcohol (n:500, S.V. 86.5-89.0mol% Nacalai tesque, INC, Kyoto, Japan) 4wt% aqu. solution

Table III-2. Experimental results of mean diameter and encapsulation efficiency

No.	Encapsulation efficiency (%)	Mean diameter (μ m) M.V (S.D) N
1	0	97.3(142)146
2	3.09	114.6(164)126
3	7.82	74.8(103)134
4	36.7	77.4(96)219
5	29.2	61.8(76)202
6	26.6	118.7(120)138

Table III-3. Composition of experimental PMMA-type adhesive resin

Powdery adhesive	PMMA	PMMA-PEMA	PEMA	SiO_2-powder	4-AET	4-AETA	BPO	TMBA
Adhesive-MC [g]	40.0	45.0	15.0	15.0	2.3	0.8	0.3	MC * 2.05 (1.0)
Adhesive-BR [g]	40.0	45.0	15.0	15.0	2.3	0.8	0.3	Bare 1.0

	MMA	HEMA	EGDMA	DEPT	MEHQ	BHT
Liquid adhesive [g]	100.0	5.0	2.0	1.2	0.004	0.3

Note: PMMA: poly(methyl methacrylate), PMMA-PEMA: copolymer of poly(methyl methacrylate) and poly(ethyl methacrylate), PEMA: poly(ethyl methacrylate), 4-AET: 4-acryloxyethyltrimellitic acid, 4-AETA: 4-acryloxyethyltrimellitic anhydride, SiO_2 powder (= Si-treated silica): particle size 1.5 μm, BPO: benzoyl peroxide, TMBA: 1,3,5-trimethylbarbituric acid, MMA: methylmethacrylate: HEMA: 2-hydroxyethyl methacrylate, EGDMA: ethyleneglycol dimethacrylate, DEPT: *N*,*N*-dihydroxyethyl-*p*-toluidine, MEHQ: methoxy hydroquinone, BHT: butylated hydroxytoluene, *: Figures in parentheses indicate the amount of TMBA in microcapsule, wherein the content of TMBA in MC is 48.8%.

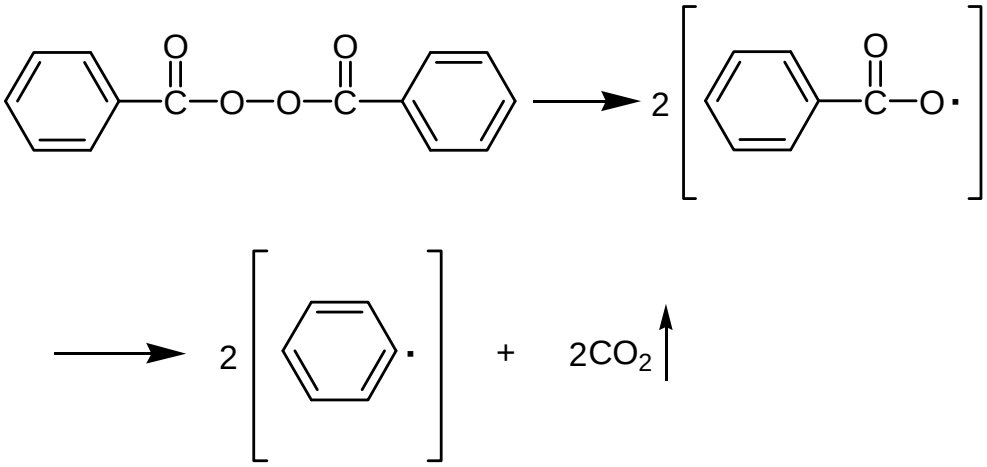

Scheme III-1-1

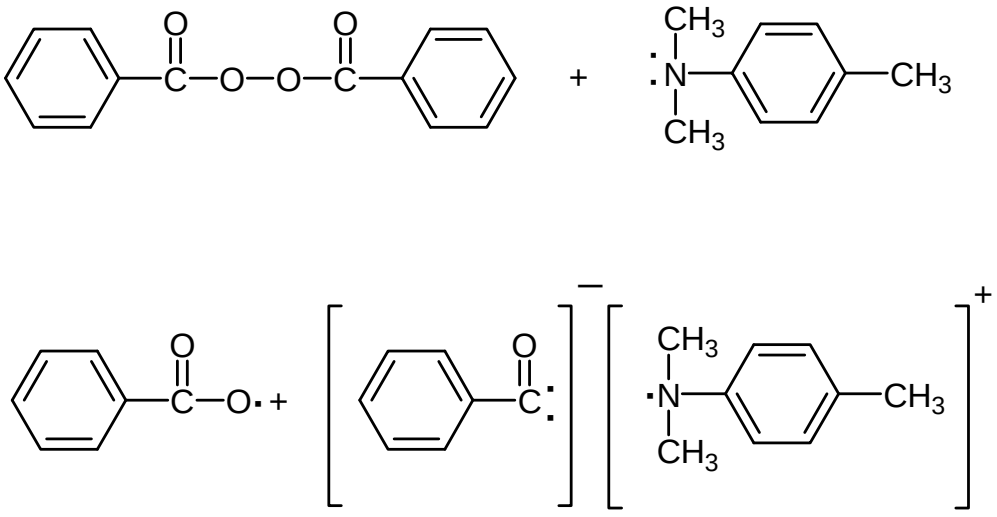

Scheme III-1-2

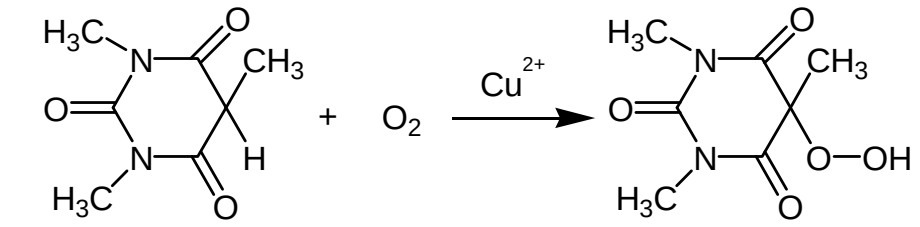

1,3,5-trimethylpyrimidine-2,4,6(1*H*,3*H*,5*H*)-trione

5-hydroperoxy-1,3,5-trimethylpyrimidine-2,4,6(1*H*,3*H*,5*H*)-trione

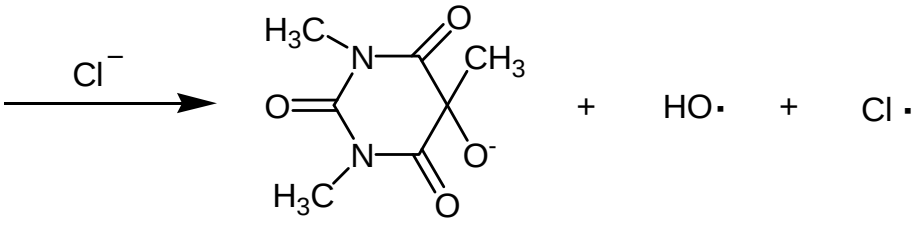

1,3,5-trimethyl-2,4,6-trioxo-hexahydropyrimidin-5-olate

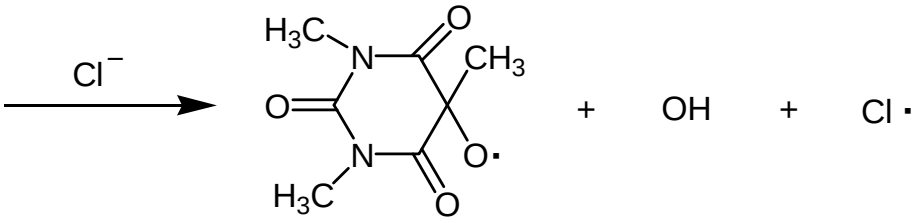

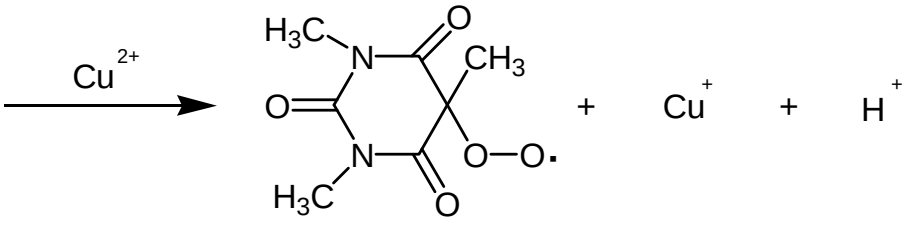

Scheme III-1-3

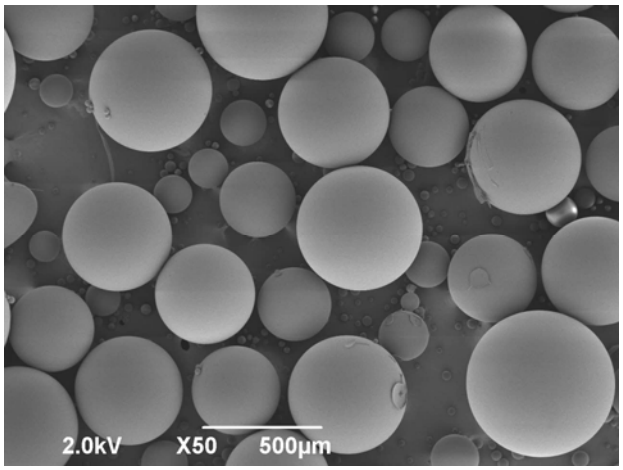

TMBA 0.0g / hold up 1

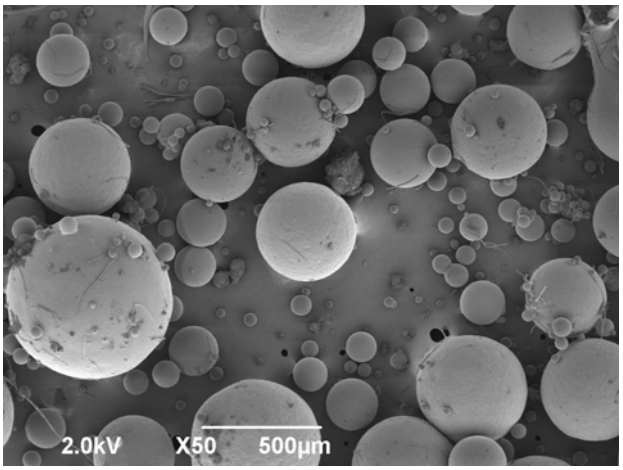

TMBA 22.5g / hold up 1

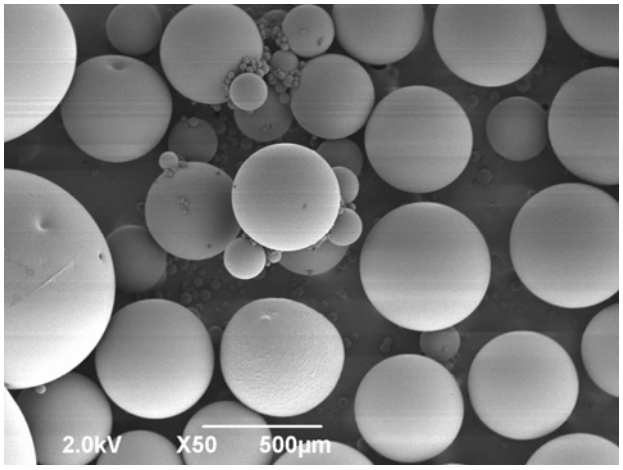

TMBA 5.6g / hold up 1

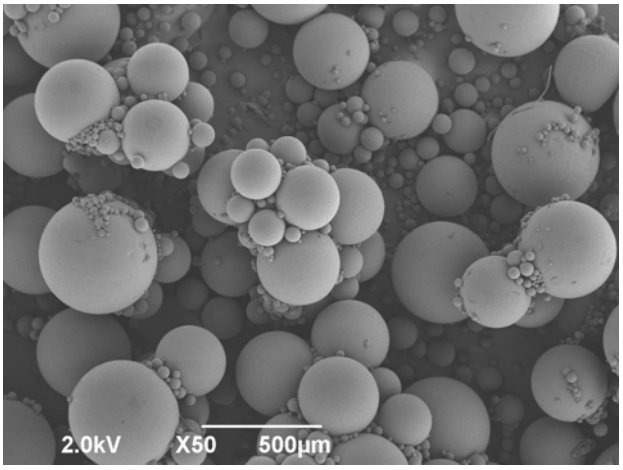

TMBA 22.5g / hold up 1.5

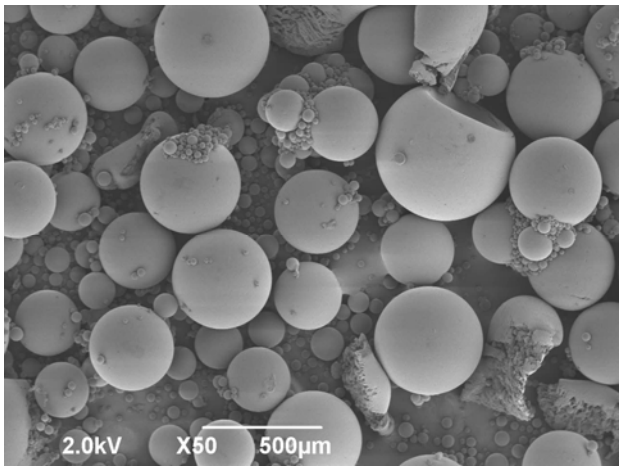

TMBA 11.3g / hold up 1

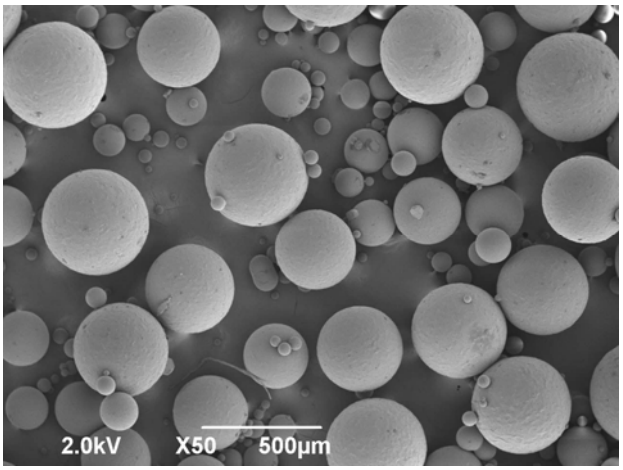

TMBA 22.5g / hold up 2

Fig. III-1-1. SEM photographs of whole of microcapsules(× 50)

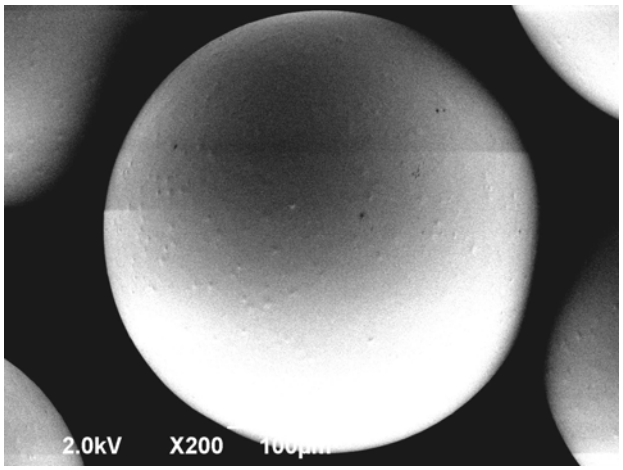

TMBA 0.0g / hold up 1

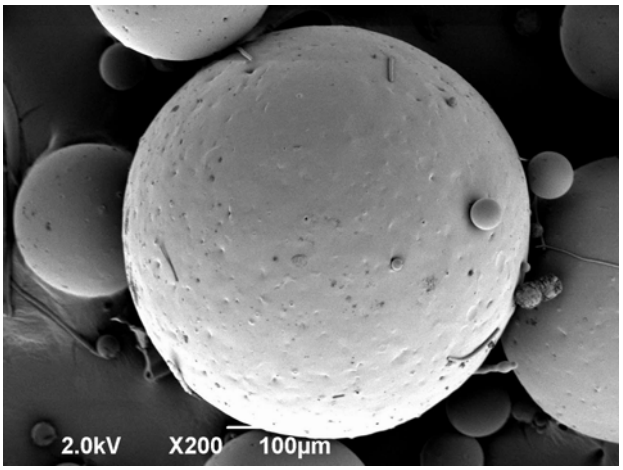

TMBA 22.5g / hold up 1

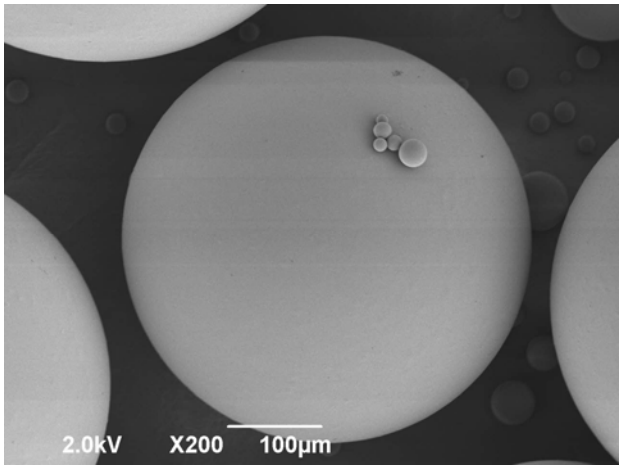

TMBA 5.6g / hold up 1

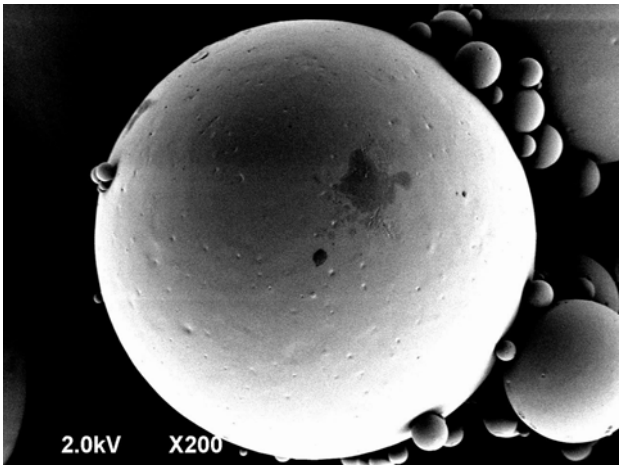

TMBA 22.5g / hold up 1.5

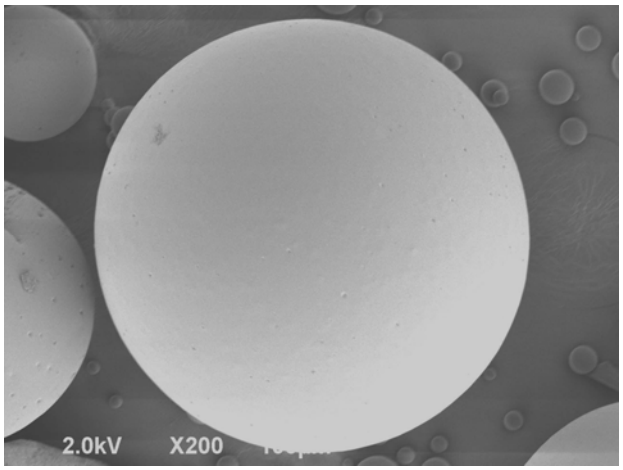

TMBA 11.3g / hold up 1

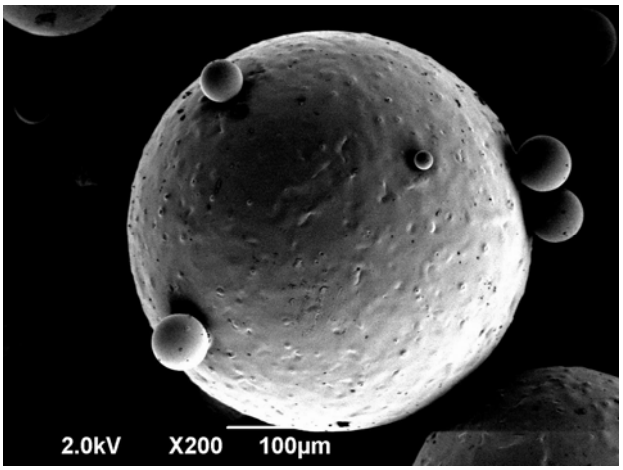

TMBA 22.5g / hold up 2

Fig. III-1-2. SEM photographs of whole of microcapsules(× 200)

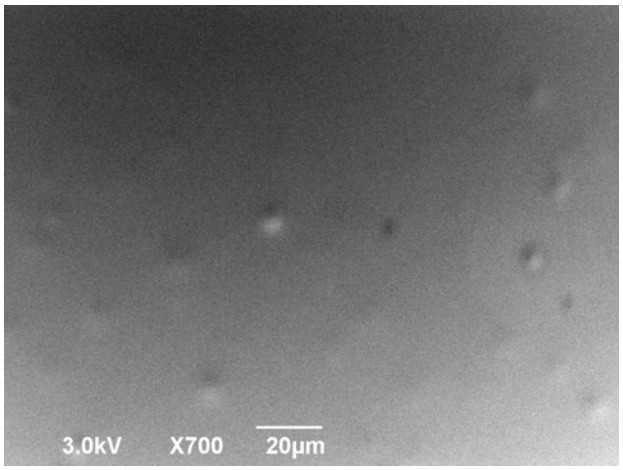

TMBA 0.0g / hold up 1

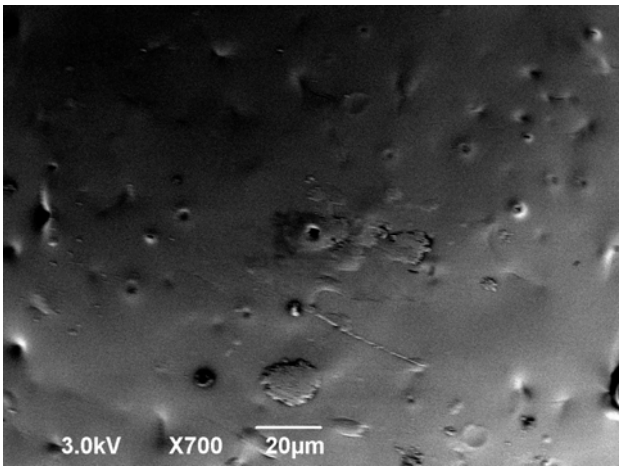

TMBA 22.5g / hold up 1

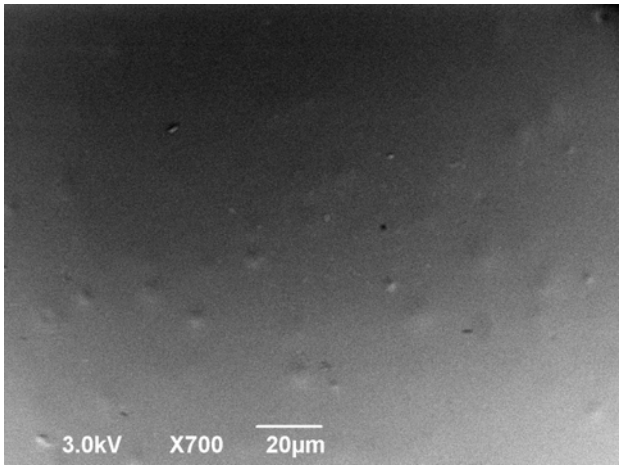

TMBA 5.6g / hold up 1

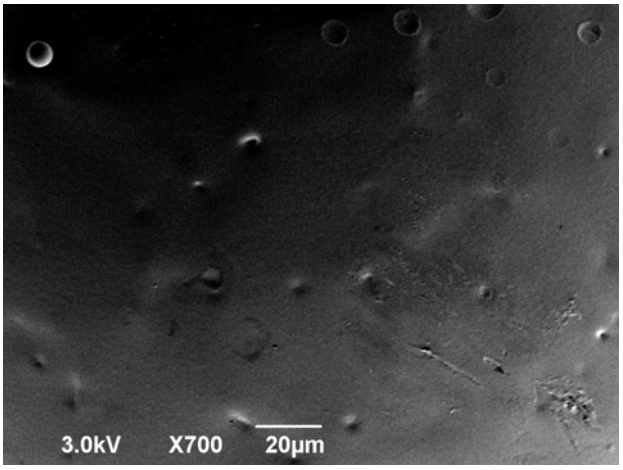

TMBA 22.5g / hold up 1.5

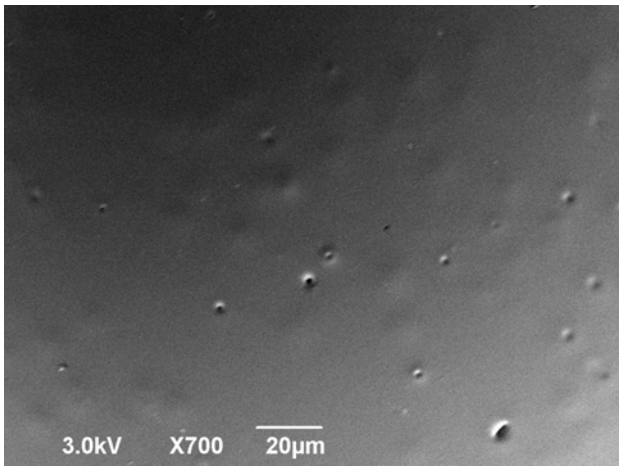

TMBA 11.3g / hold up 1

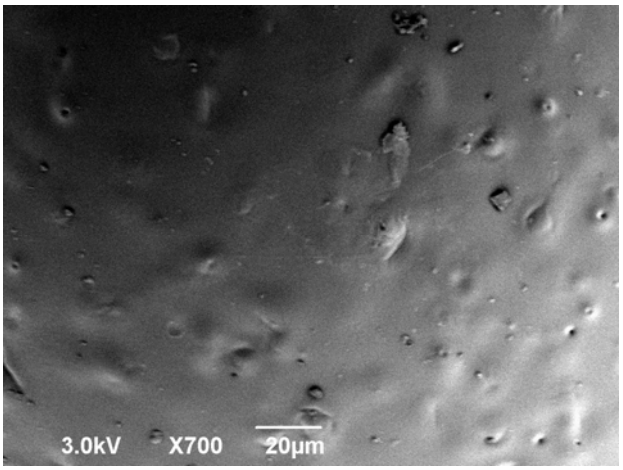

TMBA 22.5g / hold up 2

Fig. III-1-3. SEM photographs of surface of microcapsules(× 700)

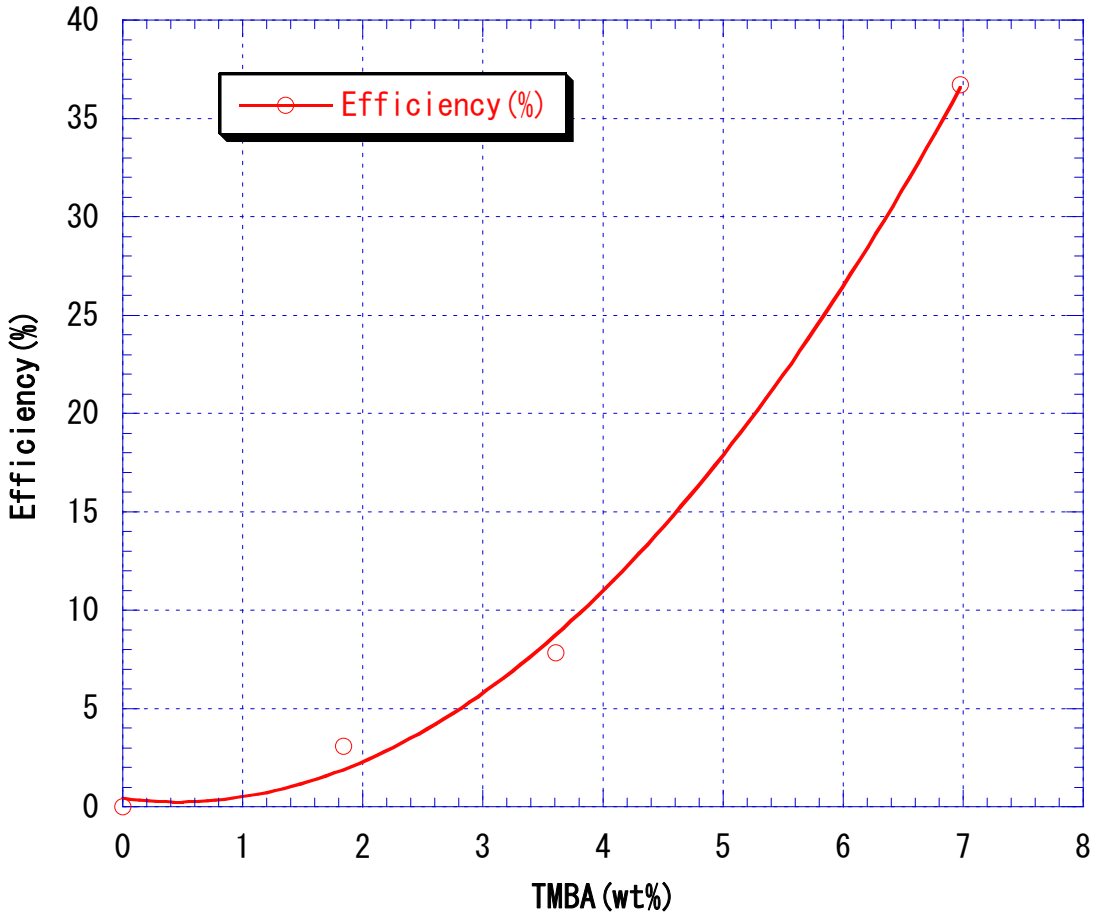

Fig. III-2-1. Dependence of microencapsulation efficiency on the TMBA concentration in continuous phase

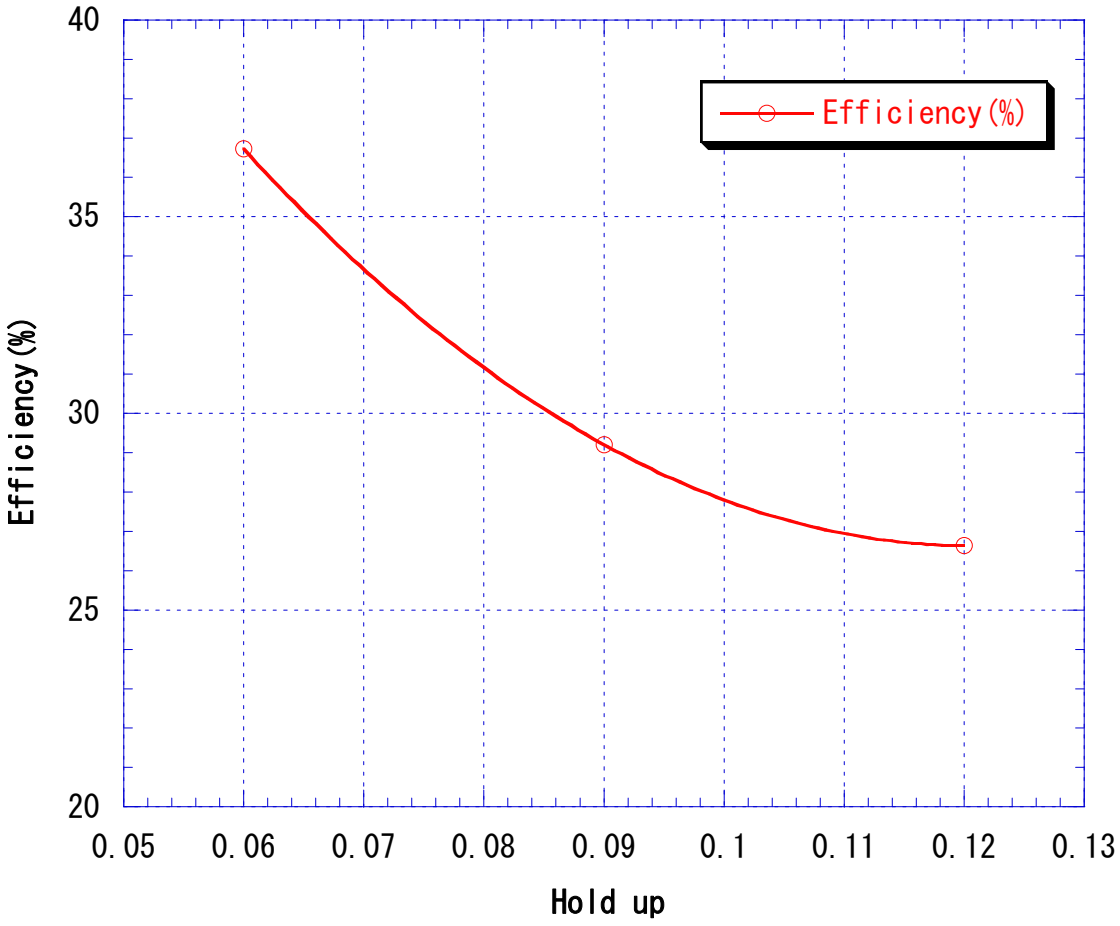

Fig. III-2-2. Dependence of microencapsulation efficiency on the hold up

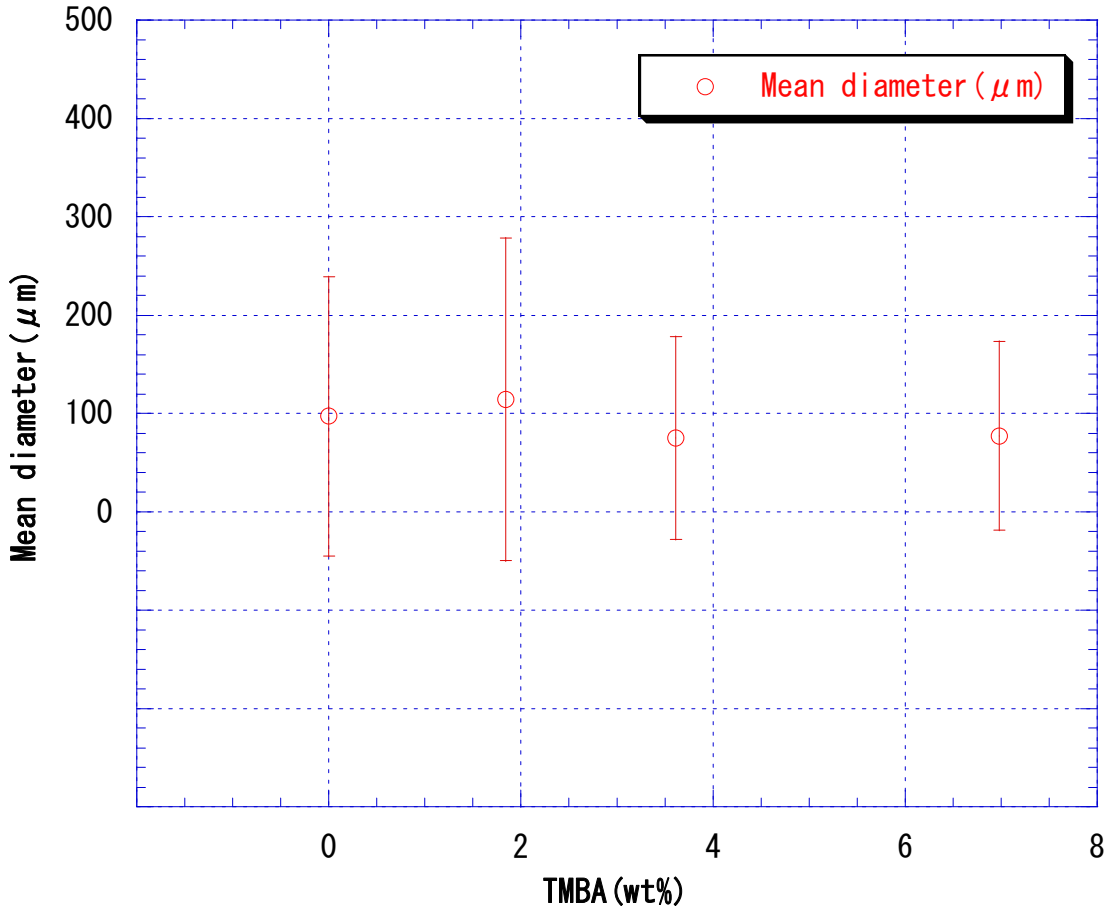

Fig. III-2-3. Dependence of mean diameters on the TMBA concentration

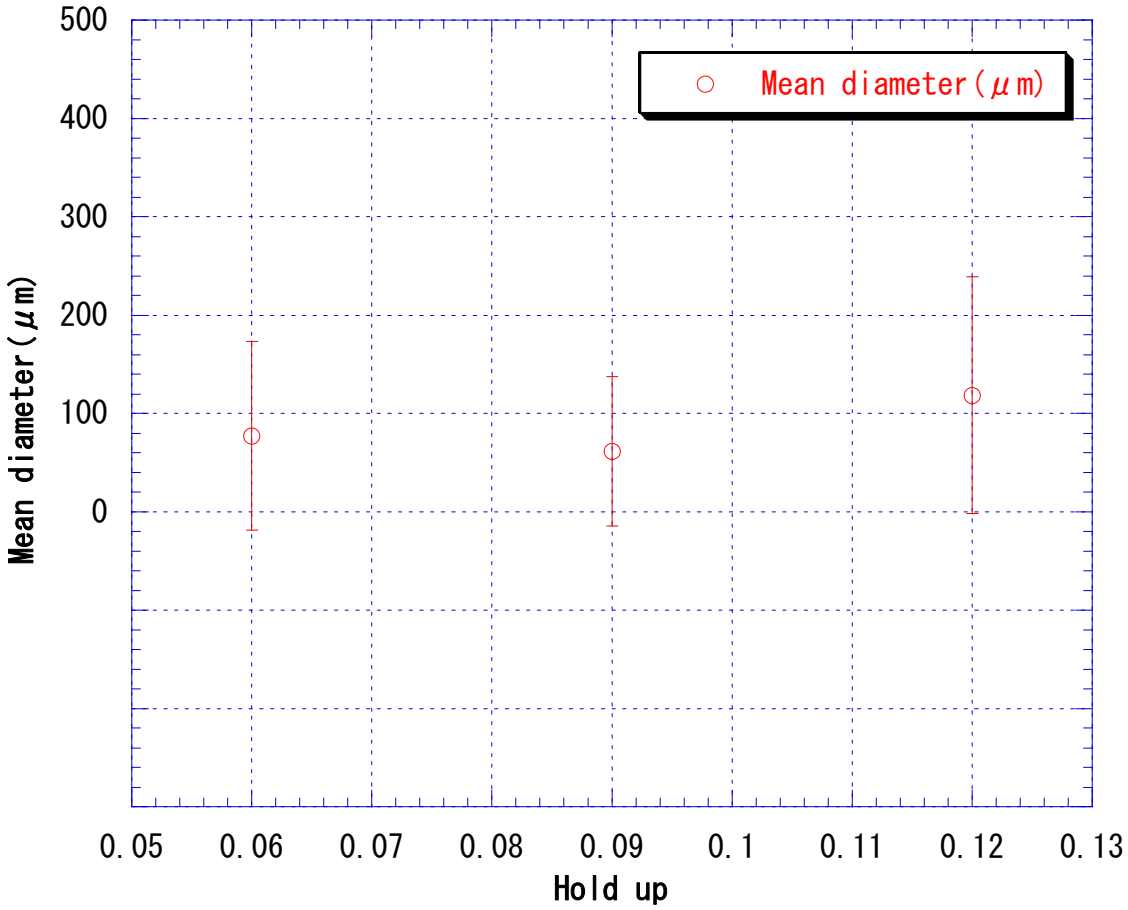

Fig. III-2-4. Dependence of mean diameters on the hold up

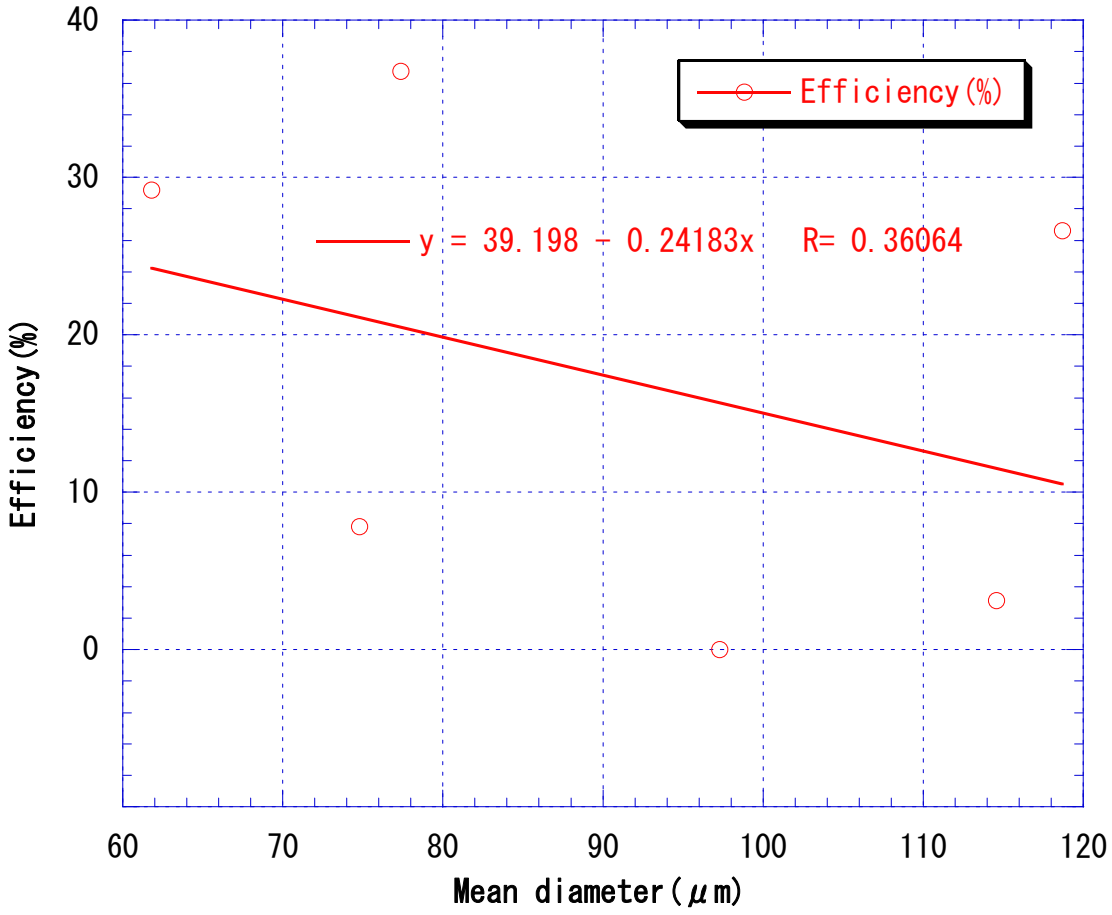

Fig. III-2-5. Correlation between mean diameters and the microencapsulation efficiency

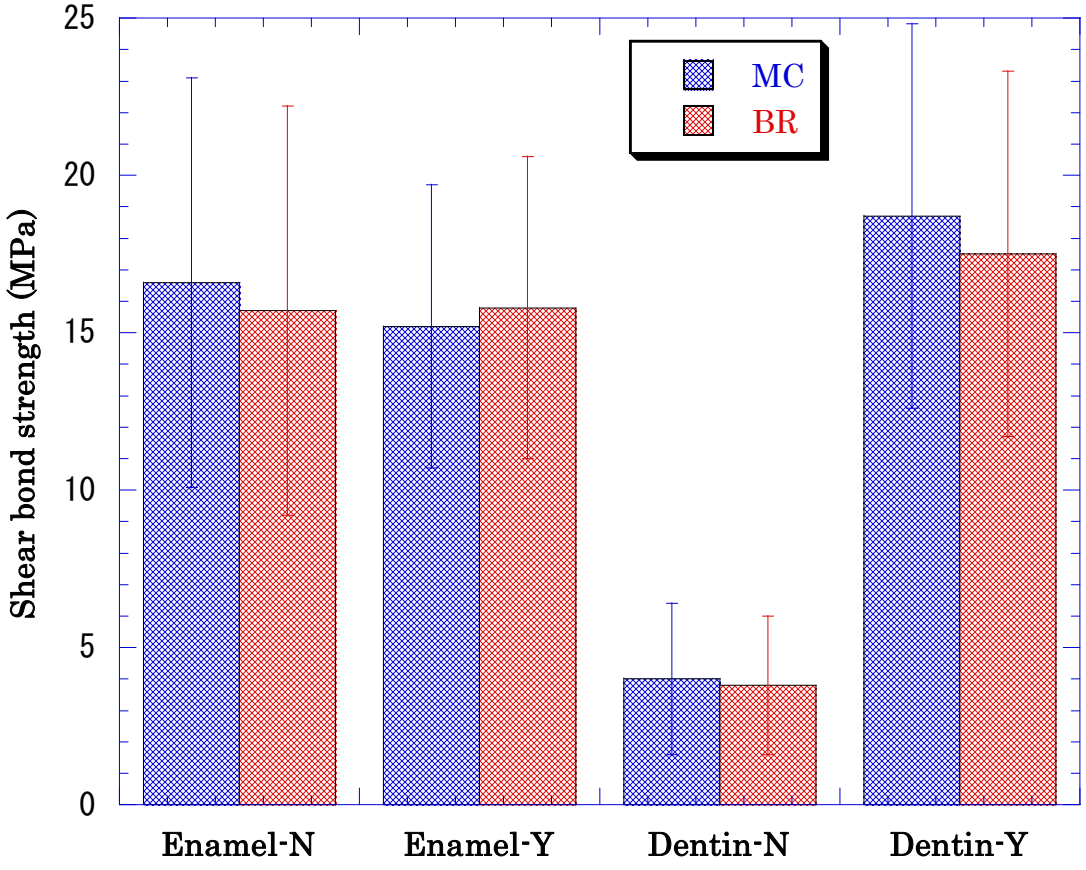

Fig. III-3-1. Shear bond strength of experimental adhesive resin between titanium and unetched ground enamel or unetched ground dentin

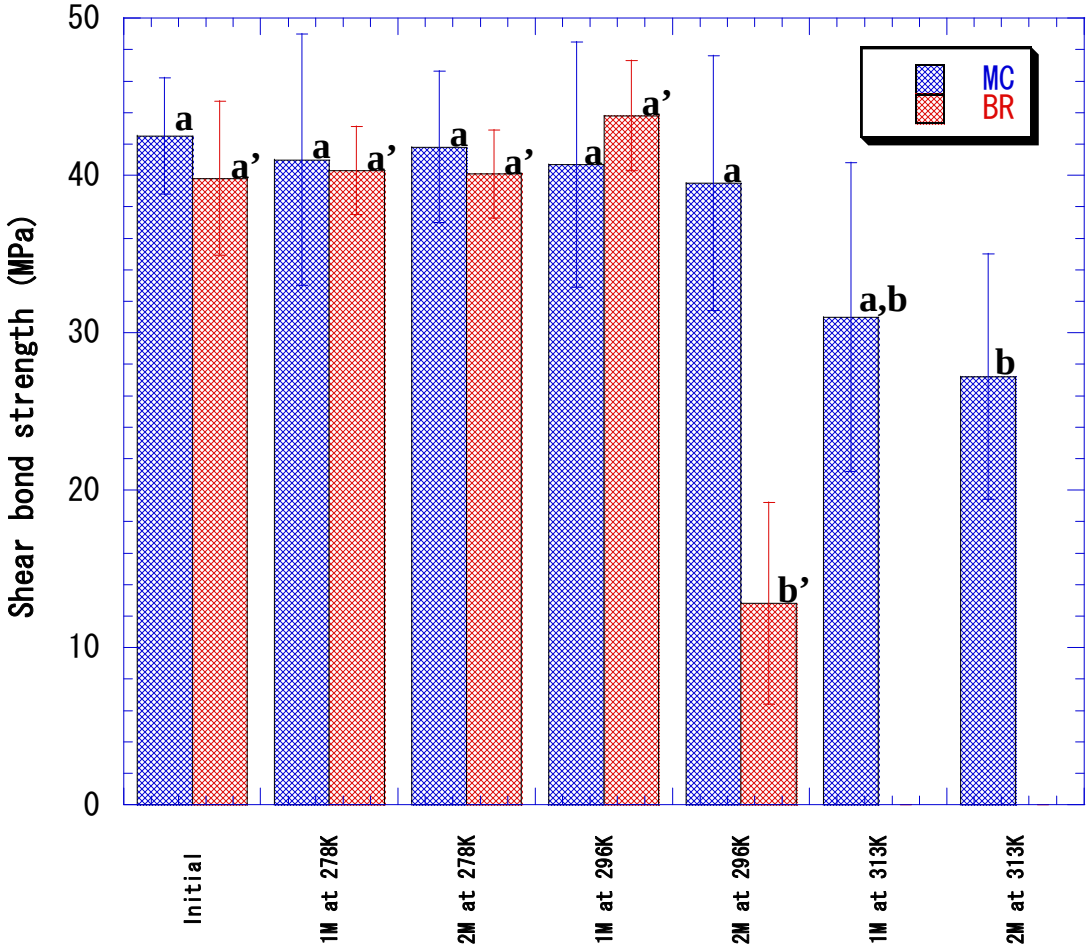

Fig. III-3-2. Shear bond strength of experimental adhesive resin between SUS rod and gold alloy

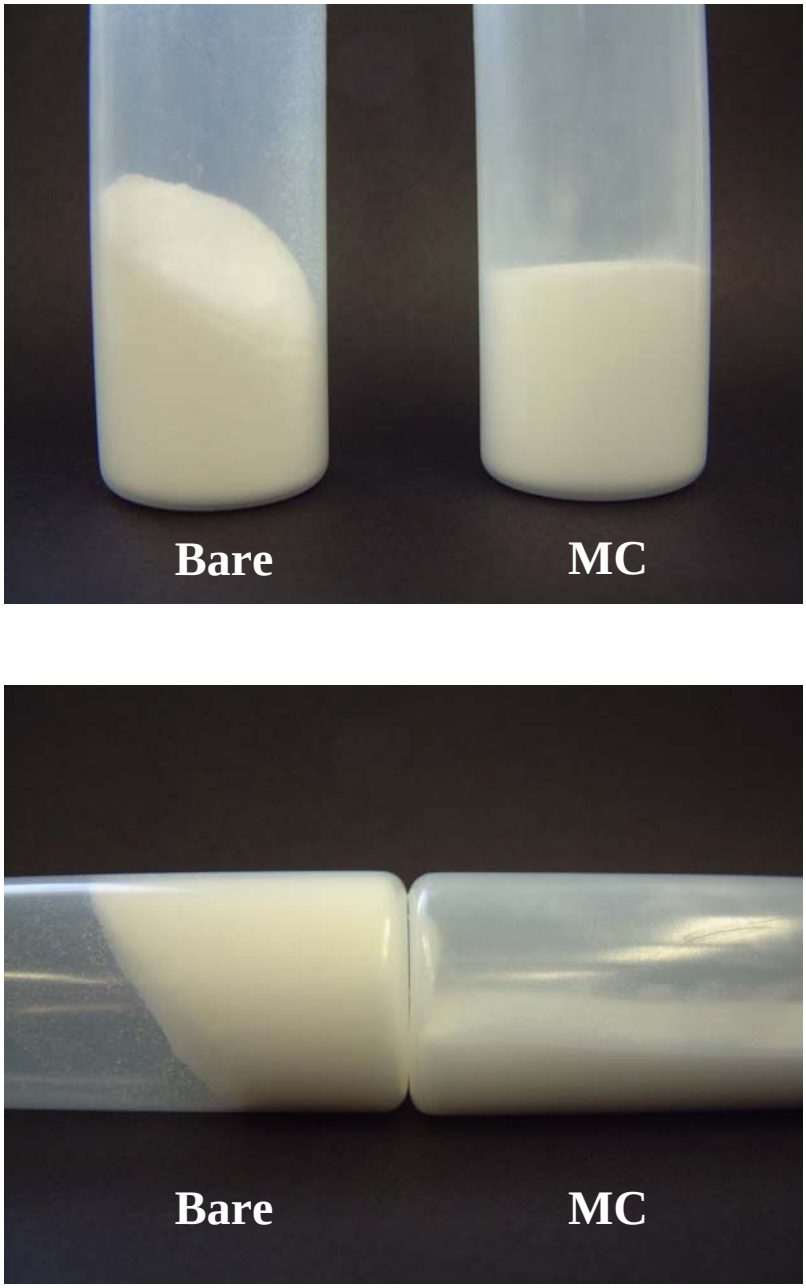

Fig. III-4-1. A photo of the Powdery adhesive of bare BPO/Amine initiator after 1-month storage at 313K (75% relative humidity). It is markedly changed during 1-month storage caused by agglomeration, which is adverse handling property, especially brush on technique of PMMA-type adhesive resin for medical use.

Chapter IV

Preparation of spherical calcium carbonate crystal using anionic surfactant

IV-1. Abstract

The several calcium carbonate crystals were synthesized by changing the reaction conditions. Namely, as factors, the number of reaction moles, reaction temperature for the sodium carbonate/calcium chloride solutions, and the concentration of anionic surfactant may influence the resultant crystal system were chosen. As the results of that, the high-yield synthesis conditions of spherical vaterite-type calcium carbonate crystals with a particle size of less than 3μm could be procured by an addition of anionic surfactant (0.1%) at a high reaction temperature (333K).

IV-2. Introduction

Calcium carbonate, which commonly exists in nature as biomineral, is widely applied for industrial use, including fillers and pigments. There are 4 types of calcium carbonate crystal systems: amorphous crystal, vaterite, calcite, and aragonite[1]. Among these types, vaterite is in spherical form which does not naturally occur. This vaterite crystal has been attracting a lot of attention because it is in metastable crystal structure with high surface activity, unlike the other types. More specifically, surface modification on calcium carbonate is generally difficult due to its significantly low surface activity, and therefore chemical bonding in use of filler to polymer can be hardly achieved. However, a certain level of surface modification for vaterite crystal is possible, chemical bonding can be expected. As many studies have reported unique attempts regarding vaterite crystal preparation[2-19]. For example, prepared by the homogeneous

precipitation method involving urea hydrolysis as well as using urease enzyme and another investigation ureolysis was conducted in the presence of various surfactants[20-23]. Although these studies are academically interesting, they are not industrially applicable because of very low from 20% to 30% reaction yield vaterite crystals prepared thus. In our experiment with the pilot scale apparatus, we unexpectedly found that vaterite calcium carbonate can be efficiently obtained in a yield of almost 100% by homogenizing a mixture of sodium carbonate and calcium chloride solutions at a low temperature as instantaneously as possible to form clusters, and that the particle size of resultant vaterite can be controlled by adjusting the concentration of these solutions, i.e. the higher the concentration of sodium carbonate/calcium chloride solutions, the finer the particle size. There was, however, a limit to the particle size control since significant gelation occurred during mixing of the solutions over the concentration of 0.5mol/L. To solve this problem, the viscosity of the mixture should be reduced by raising the reaction temperature. However, as described above, vaterite with a metastable crystal structure cannot be synthesized at a high reaction temperature. Taking this result into consideration, the present study conducted a systematic experiment to evaluate how the number of reaction moles, the reaction temperature for the sodium carbonate/calcium chloride solutions and the concentration of anionic surfactant influence the resultant crystal system.

IV-3. Experimental

IV-3-1. Materials

Sodium carbonate and calcium chloride (both are special-grade, manufactured by Wako Pure Chemical Industries, Ltd.) were used without refining. As for a surfactant, polyoxyethylene alkyl ether sodium sulfate (325SM, manufactured by Daiichi Kogyo Seiyaku Co., Ltd.) was used as received. Ion exchanged water used was pretreated with an Organo filter to have less than 2μS of electric conductivity.

IV-3-2. Preparation of calcium carbonate vaterite crystal

As shown in **Table IV-1**, the sodium carbonate solution with the given mole concentrations was added within 5s to the calcium chloride solution of 150ml containing polyoxyethylene alkyl ether sodium sulfate with the given concentration under the conditions of the agitation speed of 150rpm and a constant temperature of 293K or 333K. Then, the mixture was agitated. The mixture was sampled immediately after the addition, at 30 min and at completion of reaction (at 60 min.) and morphologically examined under optical microscope (OLYMPUS BX51). After completion of reaction, the mixture was filtrated under reduced pressure and washed to thoroughly remove by-product salt and surfactant, and then freeze-dried. After completion of freeze-drying, crystal types were identified by X-ray diffraction and IR absorption analyses. Based on these results, the mixture proportion of each crystal type obtained was determined.

IV-3-3. Characterization

IV-3-3-1. Optical microscopic observation of calcium carbonate crystal

After completion of reaction, the suspensions of typical calcium carbonate crystal were observed with the optical microscope.

IV-3-3-2. SEM observation of calcium carbonate crystal

After freeze-drying, calcium carbonate crystal was morphologically examined using SEM (JEOL JSM-6390LA).

IV-3-3-3. IR and XRD analyses

Infrared absorption spectrum and X-ray diffraction of carbonate vaterite crystal prepared were measured (FT-IR: SHIMADZU IR Prestige-21; XRD: RIGAKU DENKI) to identify the crystal types and determine the degree of crystallinity.

IV-4. Results and Discussion

IV-4-1. Morphological observation by optical microscope and SEM

Typical optical micrographs of calcium carbonate crystal after completion of reaction were shown in **Figures IV-1-1, IV-1-2, IV-2-1** and **IV-2-2**. All the micron bars in the lower-right corner of the micrographs indicate 50μm. Ratios of the crystal systems obtained are also evaluated based on the XRD results. It is observed that the addition of mere 0.1wt% surfactant had a significant influence on the resultant crystal systems morphologically. The micrograph in **Figure**

IV-1-2 is particularly interesting, because even under the high-temperature of 333K, the added surfactant initiated dislocation of calcium carbonate crystal, which resulted in a morphological change of the crystal from aragonite to vaterite. Also interesting is that the resultant particles in **Figure IV-1-2** are somewhat elliptical in shape, unlike the ones in perfectly spherical form as shown in **Figure IV-1-1**. These results suggest that the growth of the crystals was greatly affected by surfactant. **Figures IV-3-1-1** to **IV-3-3-2** are the SEM photographs of calcium carbonate. The last digit "**-1**" in the Fig numbers indicates a lower magnification, whereas "**-2**" represents a higher magnification of SEM. As seen in these SEM images, the obtained crystals are various in form and size depending on the preparation conditions. With these images, the particle size of approx. 500 particles per sample was measured using WinROOF image analysis software (Mitsutani Corporation). For cubic and spherical particles, their diameters were measured, while for needle-like crystals, a longer side was measured. The measurement results are shown in **Table IV-2** and are plotted in **Figures IV-4-1-1** to **IV-4-2-3**. First of all, the systems prepared at the reaction temperature of 293K show a decrease in mean diameter regardless of the mole concentrations with the surfactant concentration. The effect of surfactant is especially remarkable for the 0.1 mol reaction system. As for the systems without surfactant, the particle size becomes smaller with the mole number. This tendency, however, becomes less prominent with the surfactant concentration. This may be considered to be due to the fact that the surfactant adsorbed on the synthesized cluster inhibits the

growth of the crystals and as a result the particle size is small. Secondly, as for the systems prepared at 333K, it is found that the influence of the surfactant is less than in the case of the 293K systems, and that the number of reaction moles do not affect the particle size for the systems without the surfactant. This may be thought due to the quick completion of crystal growth at a high reaction temperature where the crystal ripening period becomes shorter.

IV-4-2. X-ray diffraction measurement results

Table IV-3 shows the mixture ratios of each crystal type obtained from the XRD analysis. **Figure IV-5-1** is a XRD chart for vaterite, aragonite, and calcite. **Figures IV-5-2-1** to **IV-5-2-6** are XRD charts based on the surfactant concentration. **Figures IV-5-3-1** to **IV-5-3-9** are XRD charts based on the reaction temperature. As seen from **Figure IV-5-1**, the diffraction peaks are at 2θ:33º (vaterite), 2θ:27º (aragonite), and 2θ:29º (calcite). With these values, diffraction intensity per unit area is calculated to obtain the mixture ratio of each crystal system. As for the systems without any surfactant, a mixture of calcite and vaterite types is observed at the reaction temperature of 293K and as the mole concentration increases, the ratio of vaterite rises up to 85%. In this case, the particle size of vaterite is about 20μm at the low mole concentration, but it is reduced to a few μm in the high mole concentration range. On the other hand, the system treated at 333K without any surfactant results in 100% aragonite in dendrimer form in the low mole concentration range, and as the mole concentration increases, the calcite type crystals are also observed, but

no vaterite is detected. As for the systems prepared at 293K with 0.1wt% surfactant, only the calcite-type crystals are obtained when the mole concentration is low, whereas in the high mole concentration range, both vaterite and calcite are observed, but the ratio of vaterite stayed around 40%. In contrast, the systems prepared at 333K with 0.1wt% surfactant show a significant difference: vaterite crystals in a metastable structure are normally difficult to be obtained at such a high temperature, but the addition of mere 0.1wt% of surfactant to the low mole concentration system enables to synthesize the uniform particles of over 95% of vaterite with a size of a few μm. When the mole concentration is high, the ratio of vaterite crystals is 40%. It is considered that this considerable difference is due to the surfactant deficiency compared to the number of initially formed clusters and that high-yield synthesis of only vaterite crystals can be made possible by controlling the surfactant concentration. In conclusion, only vaterite and calcite crystals are produced at any systems prepared at 293K, and the addition of surfactant tends to inhibit vaterite synthesis, whereas at 333K, the resultant crystals are greatly influenced by the addition of surfactant.

IV-4-3. FT-IR measurement results

IR spectrums for each type of calcium carbonate crystals are shown in **Figure IV-6-1**. Shifts in $-CO_3$ absorption spectrum for each crystal type are observed in the 700-750cm^{-1}, 850-875cm^{-1}, and 1400-1475cm^{-1} bands: the absorption shift in the 1400-1475cm^{-1} band is broad and difficult to be recognized because of uneven absorption

intensity, while the infrared absorption in the 700-750cm^{-1} and 850-875cm^{-1} bands shows a low intensity ratio, but is sharp enough to easily identify each crystal system, especially that of aragonite at 700cm^{-1} split into a doublet, which provides easier identification. As a typical example, the infrared absorption plot of the lower chart in **Figure IV-6-2-1** shows 100% calcite for the 0.5% surfactant system, 96% vaterite for the 0.1% surfactant system, and 100% aragonite for the 0% surfactant system. This plot, as well as the rest of the infrared absorption charts, is completely identical with the basic chart in **Figure IV-6-1**, which means that the infrared spectroscopical results are exactly the same as the outcome of the XRD analysis. Therefore, it is suggested that there is no error in identifying the types of synthesized calcium carbonate crystals.

IV-5. Conclusion

The present study conducted a systematic experiment to evaluate how the number of reaction moles, reaction temperature for the sodium carbonate/calcium chloride solutions, and the concentration of anionic surfactant influence the resultant crystal system, and the following findings are obtained:

1. At the reaction temperature of 293K, the systems, regardless of any mol concentrations, showed a decrease in mean diameter of the resultant calcium carbonate crystals with the surfactant concentration. The effect of surfactant was especially remarkable in the 0.1 mol reaction system. As for the systems without

surfactant, the particle size became smaller with the number of reaction moles. This tendency, however, became less prominent as the surfactant concentration became higher. As for the systems prepared at 333K, it was observed that the influence of the surfactant was not as significant as in the case of the 293K systems, and that the number of reaction moles did not affect the particle size for the systems without surfactant.

2. With any systems prepared at 293K, only vaterite and calcite crystals were produced, and the addition of surfactant tended to inhibit vaterite synthesis, whereas at 333K, the resultant crystals were greatly influenced by the addition of surfactant, which means that synthesis of metastable vaterite-type calcium carbonate crystals is achievable under the conditions of the present study.

3. It was found that a high-yield synthesis of vaterite-type calcium carbonate crystals with a particle size of less than 3μm could be obtained by an addition of anionic surfactant (0.1%) at a high reaction temperature (333K).

EFERENCES

[1] Jun Kawanoa, Norimasa Shimobayashia, Masao Kitamuraa, Keiji Shinodab, Nobuyuki Aikawa "Formation process of calcium carbonate from highly supersaturated solution" Journal of Crystal Growth **237–239** (2002) 419–423

[2] C. Shivkumara, Preetam Singh, Asha Gupta, M.S. Hegde "Synthesis of vaterite CaCO3 by direct precipitation using glycine and L-alanine as directing agents" Materials Research Bulletin **41** (2006) 1455–1460

[3] Jiaguo Yua, Xiufeng Zhaoa, Bei Chenga, Qingjie Zhang "Controlled synthesis of calcium carbonate in a mixed aqueous solution of PSMA and CTAB" Journal of Solid State Chemistry **178** (2005) 861–867

[4] Qiu Yu, Huang-Dong Ou, Rui-Qi Song, An-Wu Xu "The effect of polyacrylamide on the crystallization of calcium carbonate Synthesis of aragonite single-crystal nanorods and hollow vatarite hexagons" Journal of Crystal Growth **286** (2006) 178–183

[5] Hao Weia, Qiang Shenb, Ying Zhaoa, Yong Zhoua, Dujin Wanga, Duanfu Xu "Effect of anionic surfactant–polymer complexes on the crystallization of calcium carbonate" Journal of Crystal Growth **264** (2004) 424–429

[6] M. Leia, W.H. Tanga, J.G. Yu "Effect of a new functional double-hydrophilic block copolymer PAAL on the morphology of calcium carbonate particles" Materials Research Bulletin **40** (2005) 656–664

[7] Hao Wei, Qiang Shena, Haihua Wang, Yanyan Gao, Ying Zhao, Duanfu Xu, Dujin Wang "Influence of segmented copolymers on the crystallization and aggregation of calcium carbonate" Journal of Crystal Growth **303** (2007) 537–545

[8] Hirotaka Maeda, Toshihiro Kasuga "Preparation of poly(lactic acid) composite hollow spheres containing calcium carbonates" Acta Biomaterialia **2** (2006) 403–408

[9] Chengyu Wang, Jingzhe Zhao, Xu Zhao, Hari Bala, Zichen Wang "Synthesis of nanosized calcium carbonate (aragonite) via a polyacrylamide inducing process" Powder Technology **163** (2006) 134–138

[10] J.H. Huang a, Z.F. Mao a, M.F. Luo "Effect of anionic surfactant on vaterite $CaCO_3$" Materials Research Bulletin **42** (2007) 2184–2191

[11] An-Jian Xie, Yu-Hua Shen, Chun-Yan Zhang, Zong-Wei Yuan, Xue-Mei Zhu, Yong-Mei Yang "Crystal growth of calcium carbonate with various morphologies in different amino acid systems" Journal of Crystal Growth **285** (2005) 436–443

[12] Sung Hoon Kang, Izumi Hirasawa, Woo-Sik Kim, Chang Kyun Choi "Morphological control of calcium carbonate crystallized in reverse micelle system with anionic surfactants SDS and AOT" Journal of Colloid and Interface Science **288** (2005) 496–502

[13] Hao Wei, Qiang Shen, Ying Zhao, Dujin Wang, Duanfu Xu "Crystallization habit of calcium carbonate in presence of sodium dodecyl sulfate and/or polypyrrolidone" Journal of Crystal Growth **260** (2004) 545–550

[14] Jiaguo Yu, Ming Lei, Bei Cheng, and Xiujian Zhao "Effects of PAA additive and temperature on morphology of calcium carbonate particles" Journal of Solid State Chemistry **177** (2004) 681–689

[15] Qing Li, Yi Ding, Fanqing Li, Bo Xie, Yitai Qian "Solvothermal growth of vaterite in the presence of ethylene glycol, 1,2-propanediol and glycerin" Journal of Crystal Growth **236** (2002) 357–362

[16] Xingfa Zhang, Zhongjie Zhang, Yong Yan "A facile surfactant-assisted approach to the synthesis of urchin-shaped aragonite micropatterns" Journal of Crystal Growth **274** (2005) 550–554

[17] M. Lei, W.H. Tang, L.Z. Cao, P.G. Li, J.G. Yu "Effects of poly (sodium 4-styrene-sulfonate) on morphology of calcium carbonate particles" Journal of Crystal Growth **294** (2006) 358–366

[18] Qiang Shen, Hao Wei, Ying Zhao, Du-Jin Wang, Li-Qiang Zheng, Duan-Fu Xu “Morphological control of calcium carbonate crystals by polyvinylpyrrolidone and sodium dodecyl benzene sulfonate” Colloids and Surfaces A: Physicochem. Eng. Aspects **251** (2004) 87–91

[19] E. Altay, T. Shahwan, M. Tanoğlu “Morphosynthesis of CaCO3 at different reaction temperatures and the effects of PDDA, CTAB, and EDTA on the particle morphology and polymorph stability” Powder Technology **178** (2007) 194–202

[20] Yusaku Takita, Mayumi Eto, Hisao Sugihar, Katsutoshi Nagaoka “Promotion mechanism of co-existing NaCl in the synthesis of $CaCO_3$” Materials Letters **61** (2007) 3083–3085

[21] J. Garcı´a-Carmona, J. Go´mez-Morales, J. Fraile-Sainz, R. Rodrı´guez-Clemente “Morphological characteristics and aggregation of calcite crystals obtained by bubbling CO_2 through a $Ca(OH)_2$ suspension in the presence of additives” Powder Technology **130** (2003) 307– 315

[22] Laifeng Wang, Ivan Sondi, and Egon Matijevic “Preparation of Uniform Needle-Like Aragonite Particles by Homogeneous Precipitation” Journal of Colloid and Interface Science **218**, 545–553 (1999)

[23] M. Faatz, F. Grfhn, G. Wegner “Mineralization of calcium carbonate by controlled release of carbonate in aqueous solution” Materials Science and Engineering C **25** (2005) 153–159

Figure Captions

Table Captions

TableIV-1. Reaction conditions

$CaCO_3/Na_2CO_3$ (mol/L)	0.1	0.3	0.5
Reaction temperature (K)	293	333	
Surfactant conc. (%)	0	0.1	0.5
D.W (dm^{-3})		0.3	

TableIV-2. Results of mean particle size measurement UNIT:μm

	Reaction temperature 293K			Reaction temperature 333K		
	0.1mol	0.3mol	0.5mol	0.1mol	0.3mol	0.5mol
S:0.0%	15.46	8.47	3.51	9.55	8.32	6.91
S:0.1%	7.04	4.94	3.54	2.79	6.55	6.79
S:0.5%	1.77	4.14	1.71	5.30	6.27	5.64

S:Surfactant concentration

Mol:mol/L of $CaCl_2$ and Na_2CO_3

TableIV-3. Results of XRD analysis UNIT:%

mol	kelvin	Surfactant %	Vaterite	Aragonite	Calcite
0.1	293	0.0	50.6	0.0	49.4
0.1	293	0.1	0.0	0.0	100.0
0.1	293	0.5	0.0	0.0	100.0
0.1	333	0.0	0.0	100.0	0.0
0.1	333	0.1	95.5	0.0	4.5
0.1	333	0.5	0.0	0.0	100.0
0.3	293	0.0	55.6	0.0	44.4
0.3	293	0.1	48.4	0.0	51.6
0.3	293	0.5	0.0	0.0	100.0
0.3	333	0.0	0.0	83.5	16.5
0.3	333	0.1	0.0	73.3	26.7
0.3	333	0.5	7.5	37.1	55.4
0.5	293	0.0	85.2	0.0	14.8
0.5	293	0.1	39.5	0.0	60.5
0.5	293	0.5	0.0	0.0	100.0
0.5	333	0.0	0.0	88.9	11.1
0.5	333	0.1	42.5	0.0	57.5
0.5	333	0.5	0.0	34.3	65.7

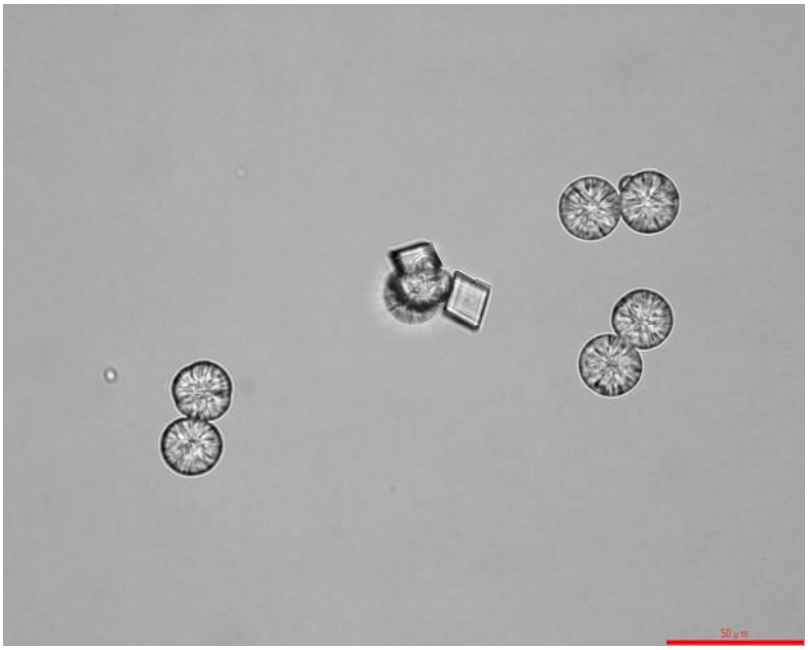

0.1mol/L-293K-325SM 0wt%

Vaterite:50.6%　　Calcite:49.4%

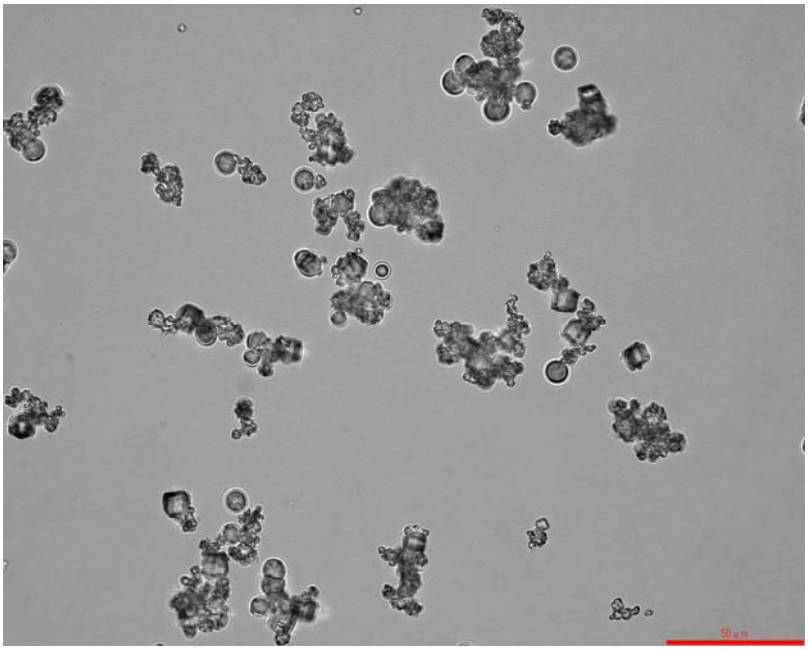

0.1mol/L-293K-325SM 0.1wt%

Calcite:100%

Fig.IV-1-1. Optical micrographs of Calcium carbonate synthesized by 0.1mol/L system

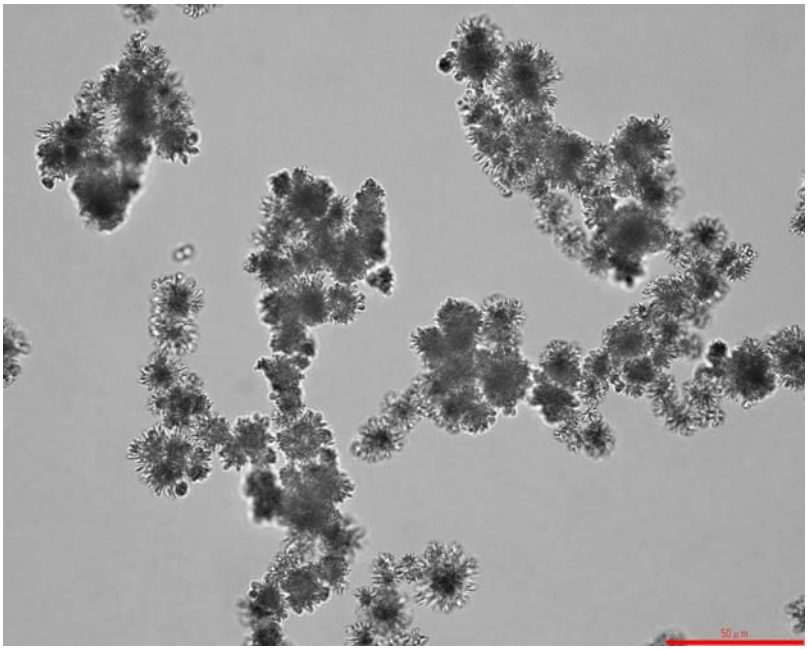

0.1mol/L-333K-325SM 0wt%

Aragonite:100%

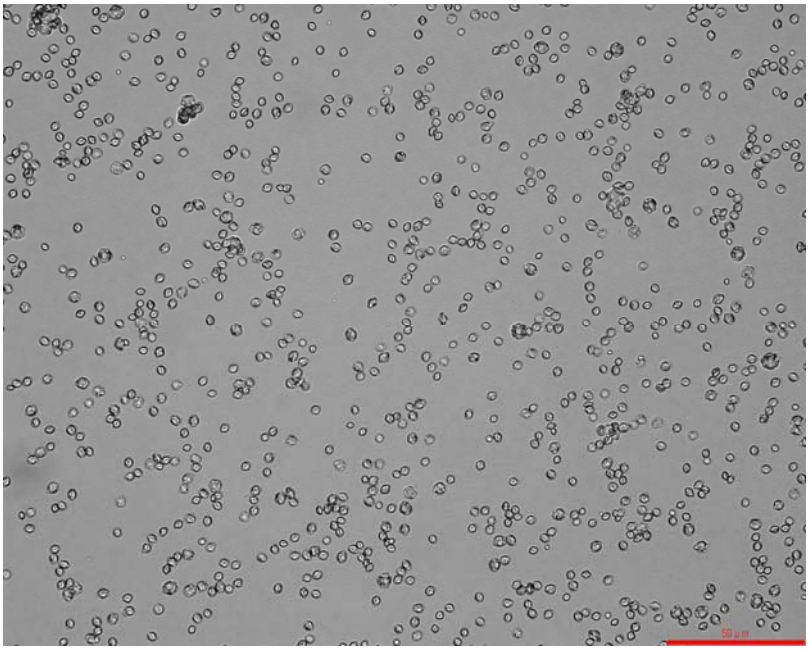

0.1mol/L-333K-325SM 0.1wt%

Vaterite:95.5% Calcite: 4.5%

Fig.IV-1-2. Optical micrographs of Calcium carbonate synthesized by 0.1mol/L system

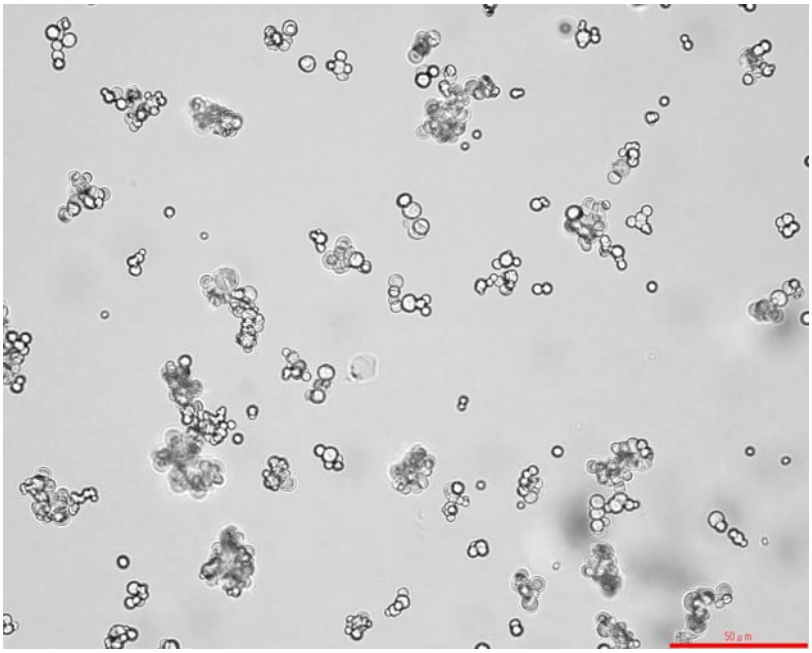

0.5mol/L-293K-325SM 0wt%

Vaterite:85.2% Calcite:14.8%

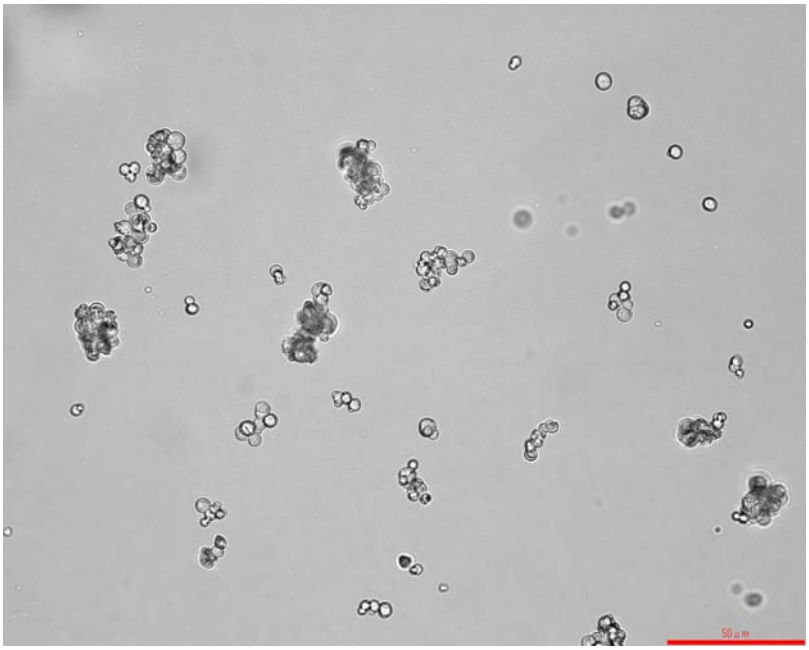

0.5mol/L-293K-325SM 0.1wt%

Vaterite:39.5% Calcite:60.5%

Fig.IV-2-1. Optical micrographs of Calcium carbonate synthesized by 0.5mol/L system

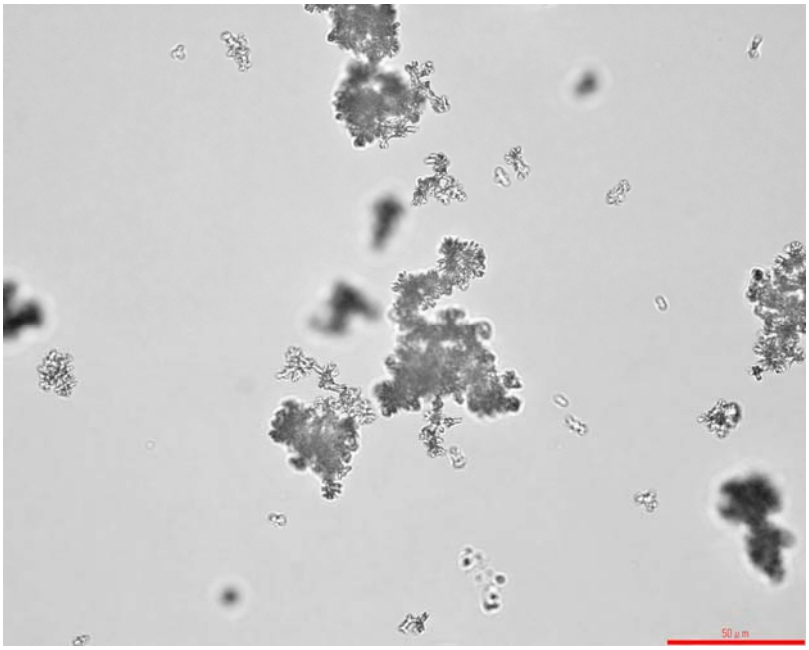

0.5mol/L-333K-325SM 0wt%

Aragonite:88.9% Calcite:11.1%

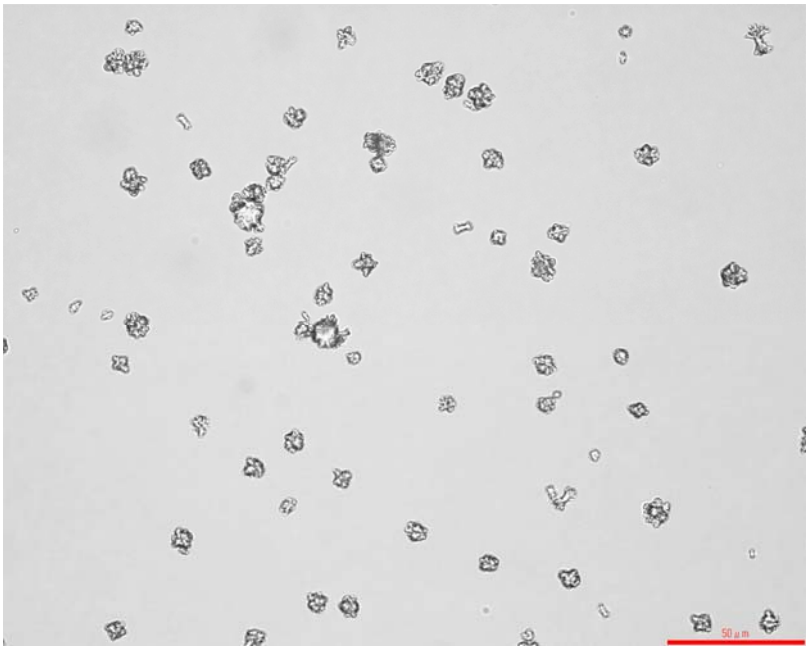

0.5mol/L-333K-325SM 0.1wt%

Vaterite:42.5% Calcite:57.5%

Fig.IV-2-2. Optical micrographs of Calcium carbonate synthesized by 0.5mol/L system

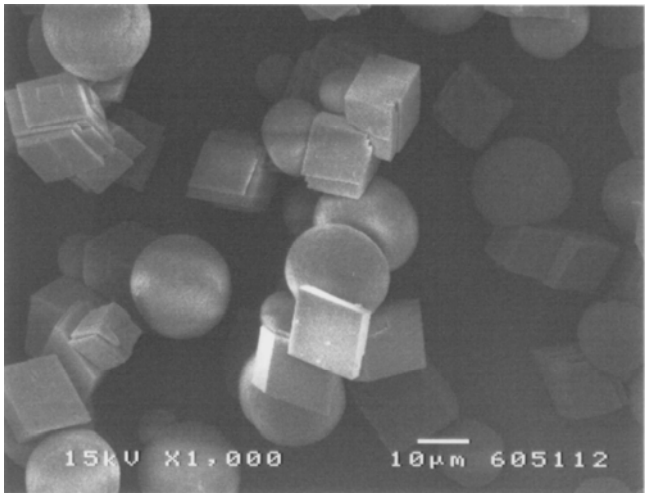

0.1M-293K-325SM 0%

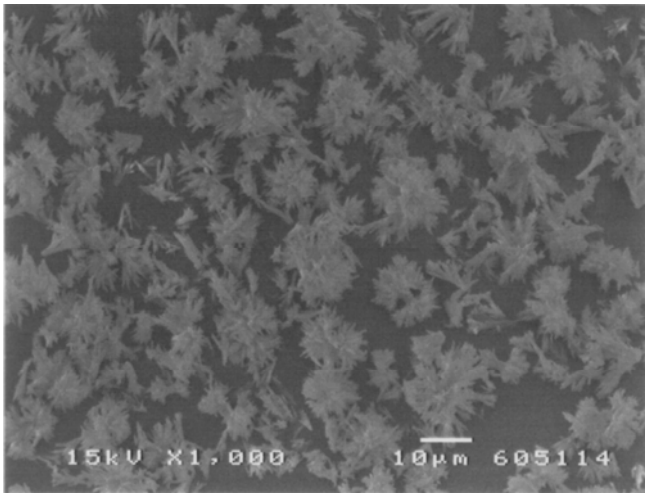

0.1M-333K-325SM 0%

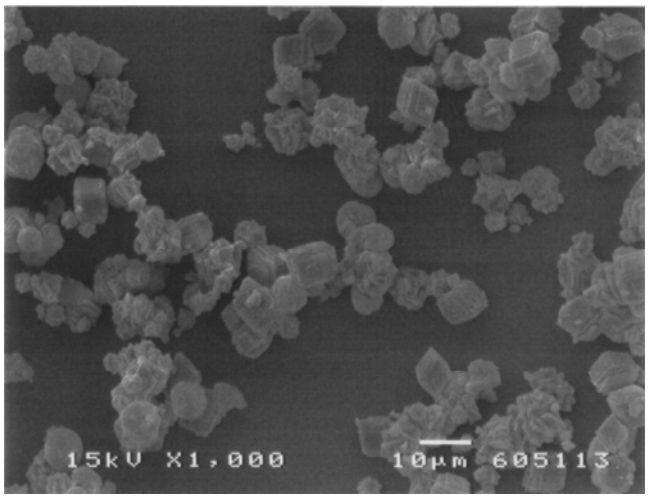

0.1M-293K-325SM 0.1%

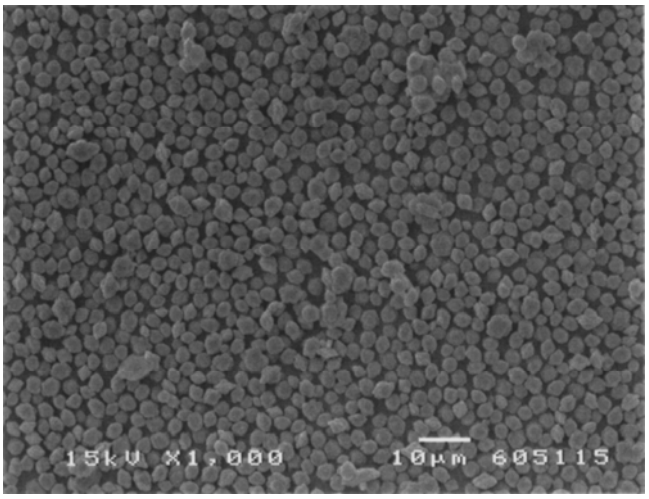

0.1M-333K-325SM 0.1%

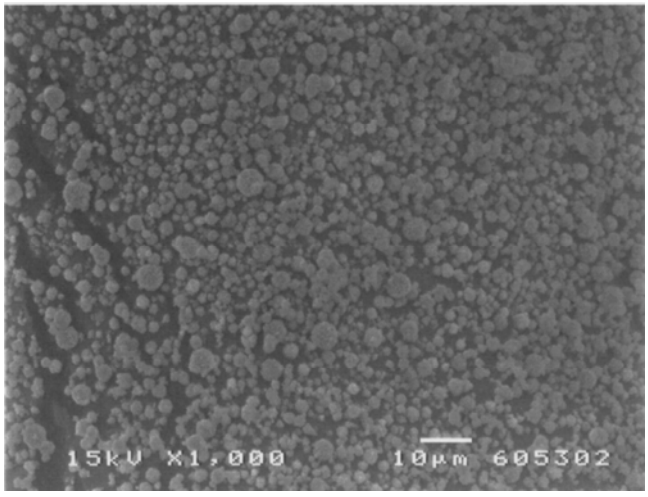

0.1M-293K-325SM 0.5%

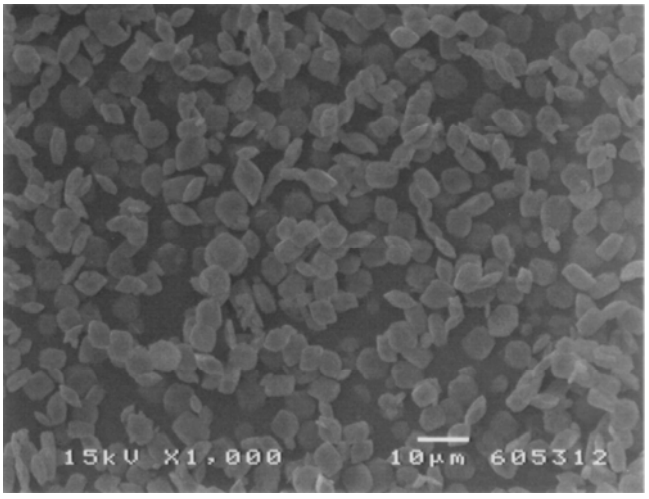

0.1M-333K-325SM 0.5%

Fig.IV-3-1-1. SEM photographs of calcium carbonate

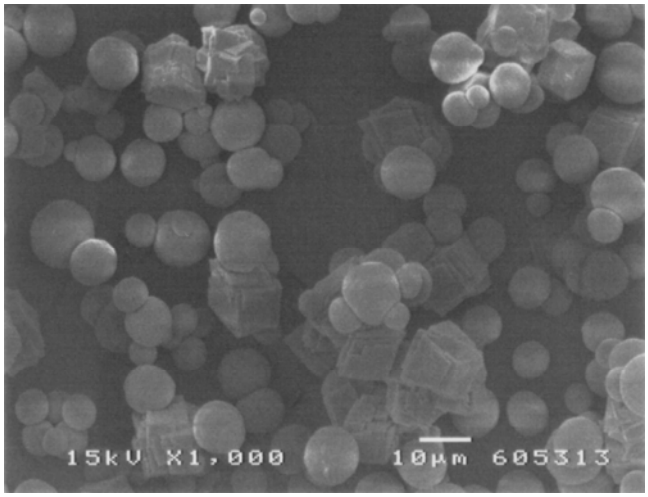

0.3M-293K-325SM 0%

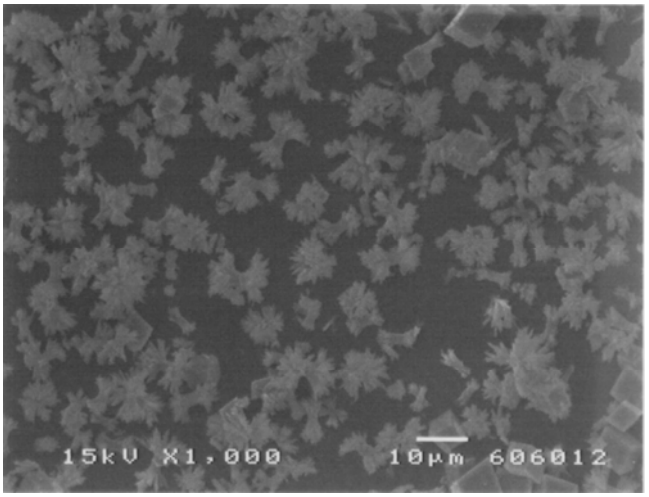

0.3M-333K-325SM 0%

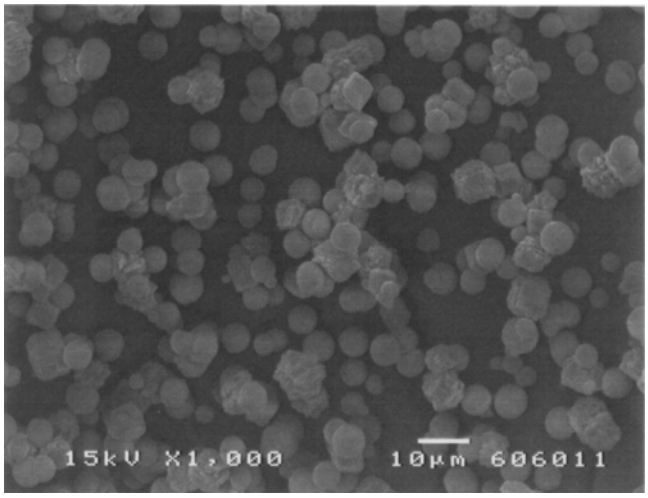

0.3M-293K-325SM 0.1%

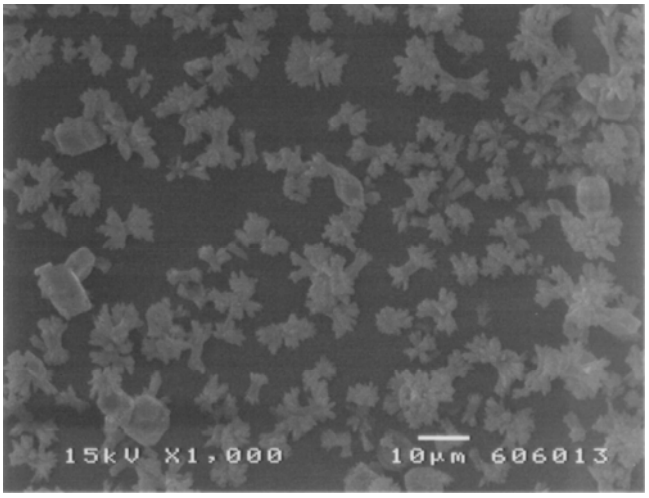

0.3M-333K-325SM 0.1%

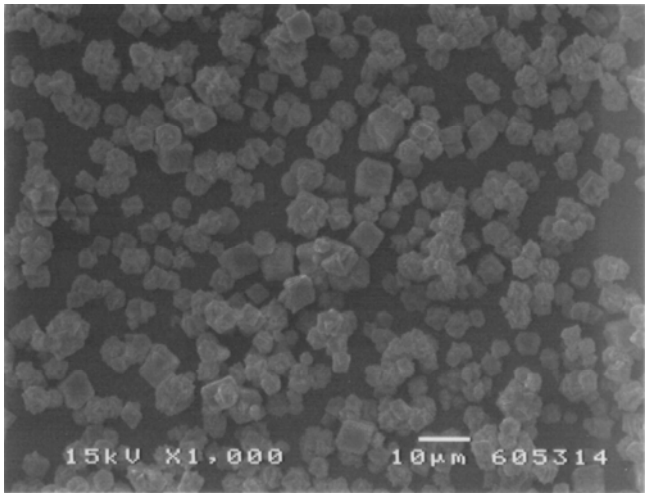

0.3M-293K-325SM 0.5%

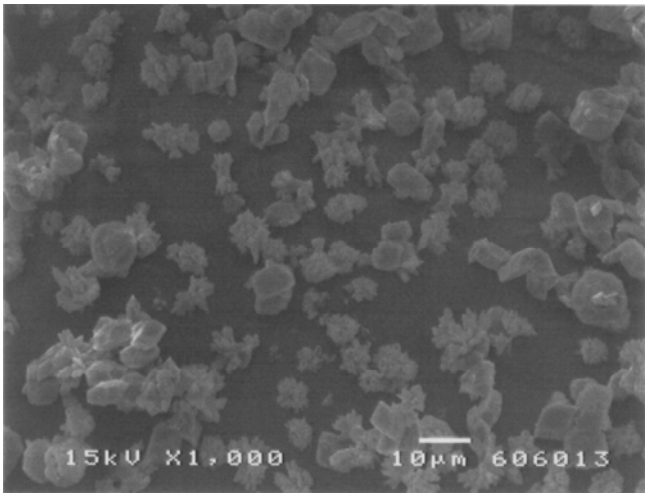

0.3M-333K-325SM 0.5%

Fig.IV-3-2-1. SEM photographs of calcium carbonate

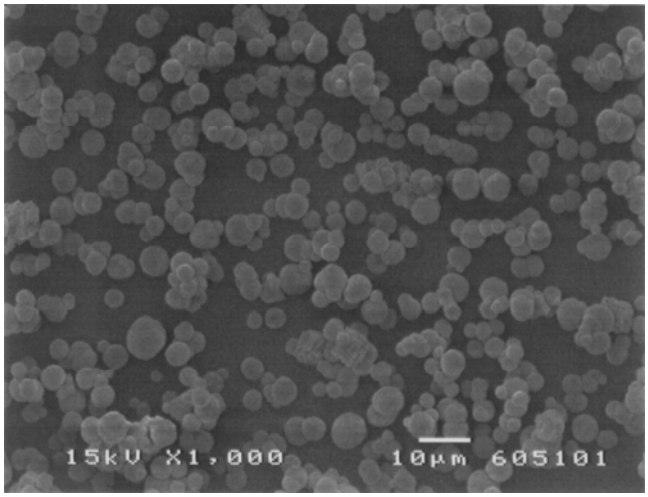

0.5M-293K-325SM 0%

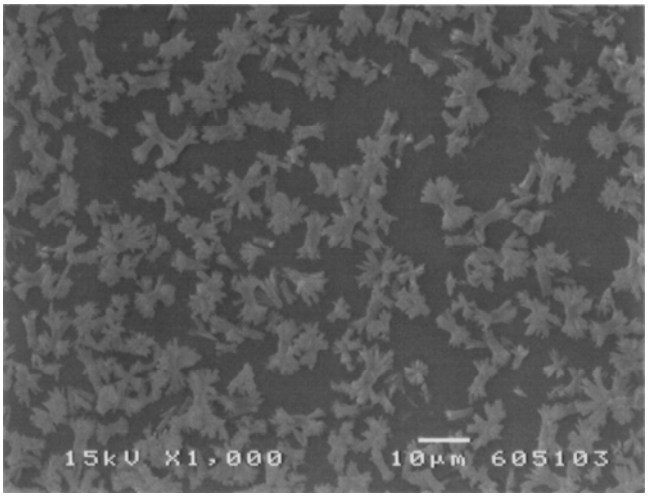

0.5M-333K-325SM 0%

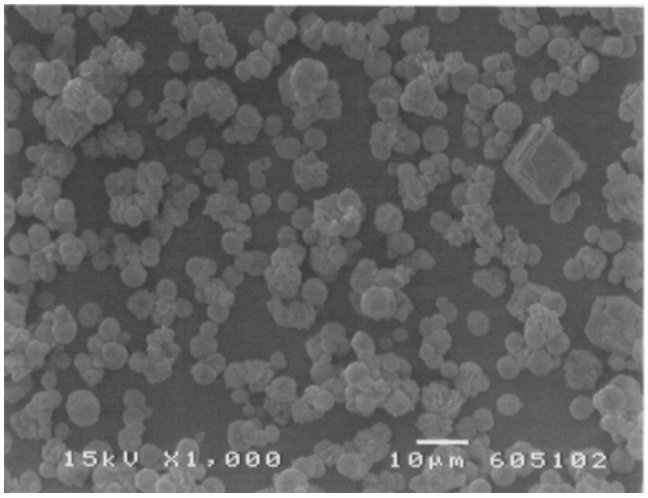

0.5M-293K-325SM 0.1%

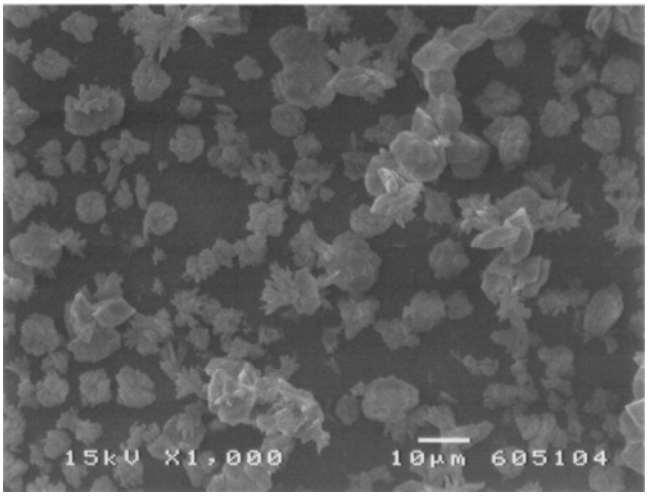

0.5M-333K-325SM 0.1%

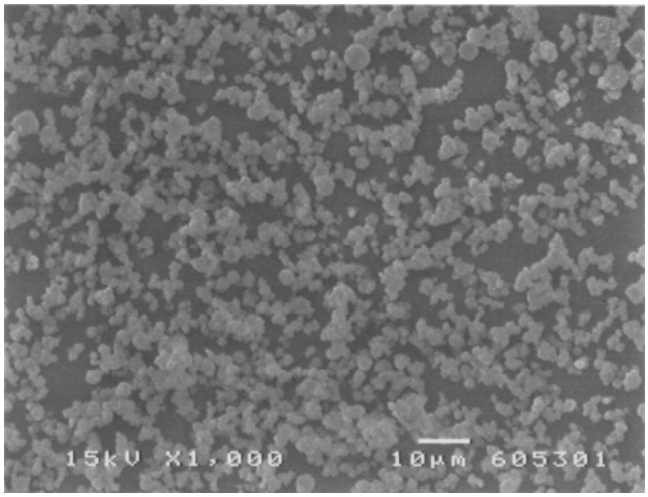

0.5M-293K-325SM 0.5%

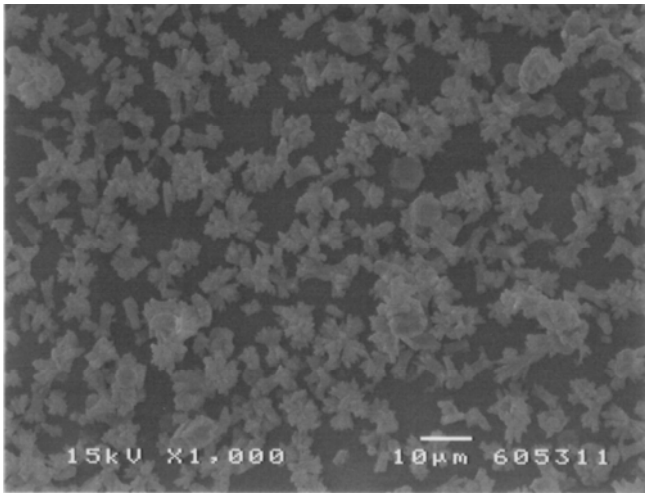

0.5M-333K-325SM 0.5%

Fig.IV-3-3-1. SEM photographs of calcium carbonate

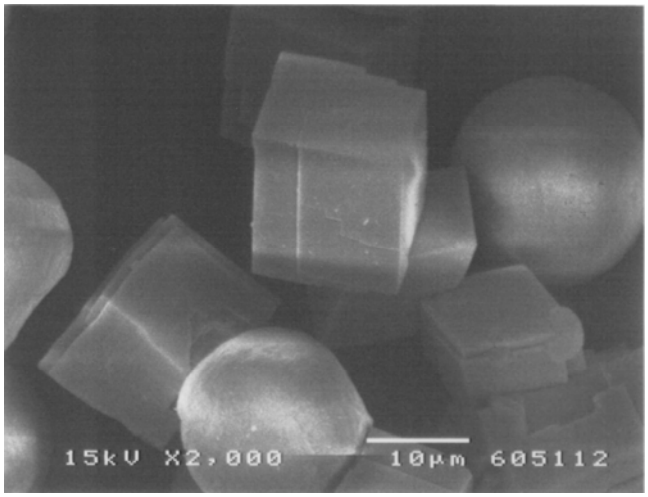

0.1M-293K-325SM 0%

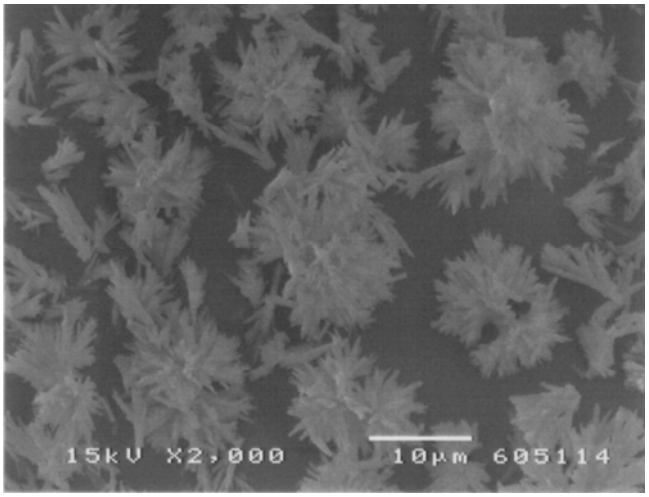

0.1M-333K-325SM 0%

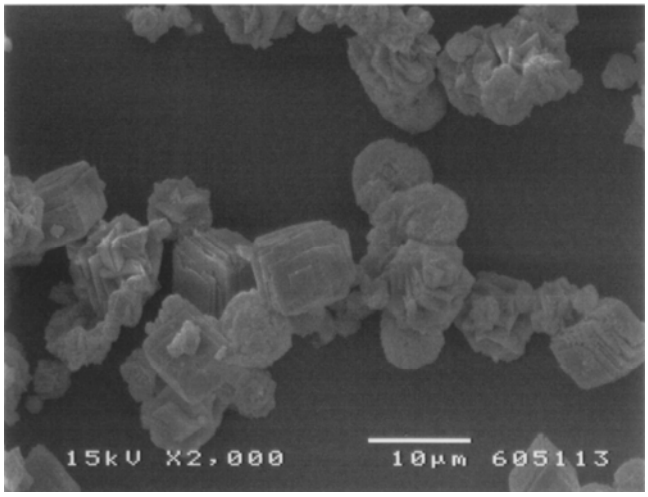

0.1M-293K-325SM 0.1%

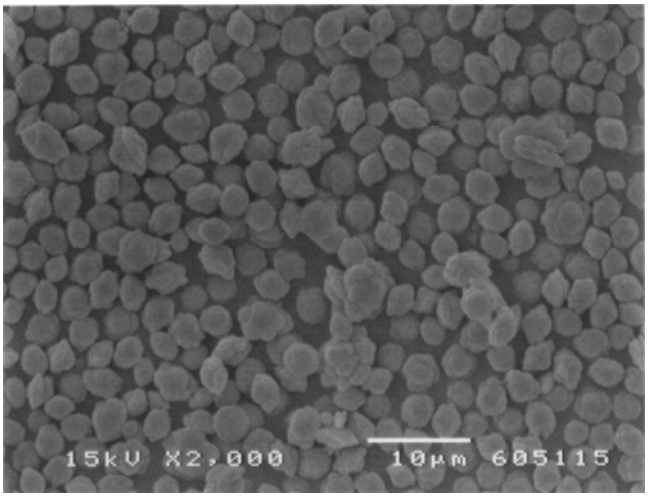

0.1M-333K-325SM 0.1%

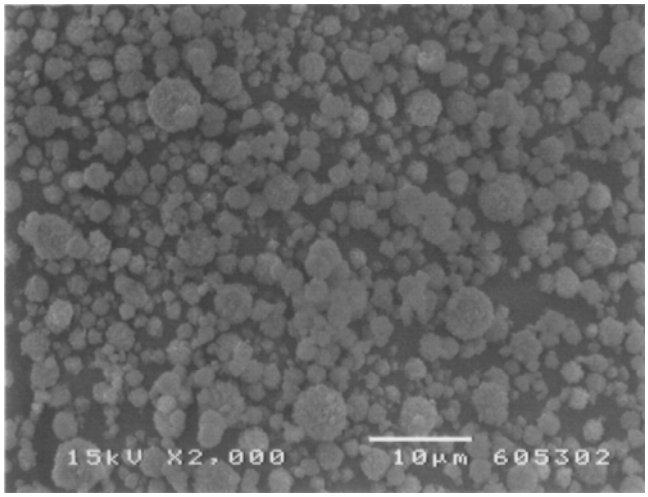

0.1M-293K-325SM 0.5%

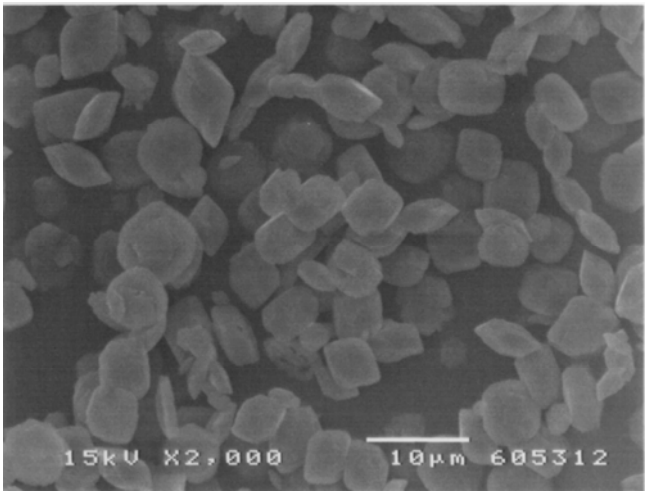

0.1M-333K-325SM 0.5%

Fig.IV-3-1-2. SEM photographs of calcium carbonate

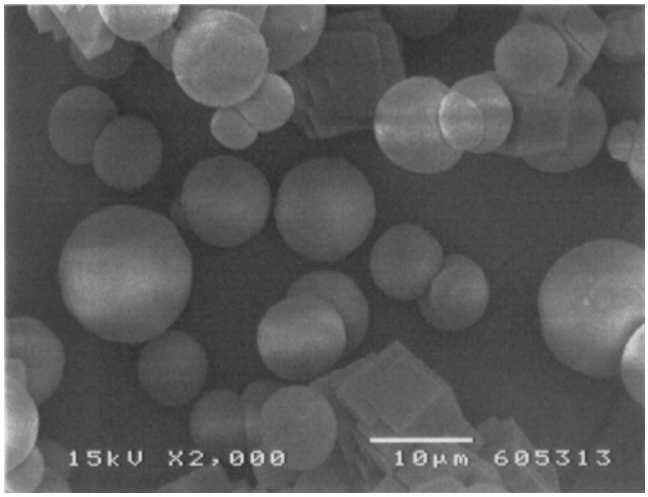

0.3M-293K-325SM 0%

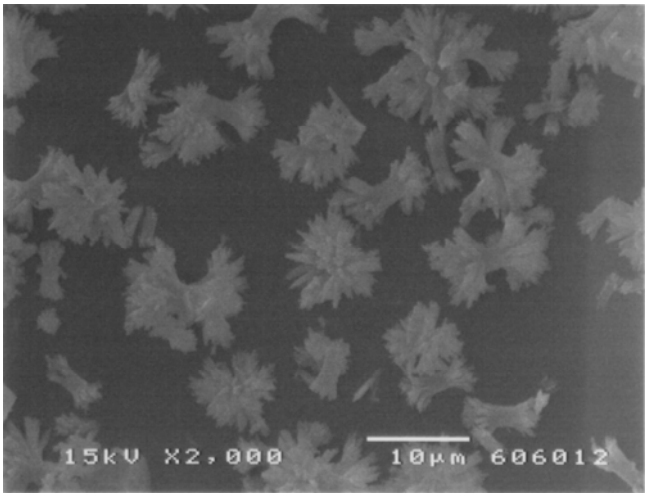

0.3M-333K-325SM 0%

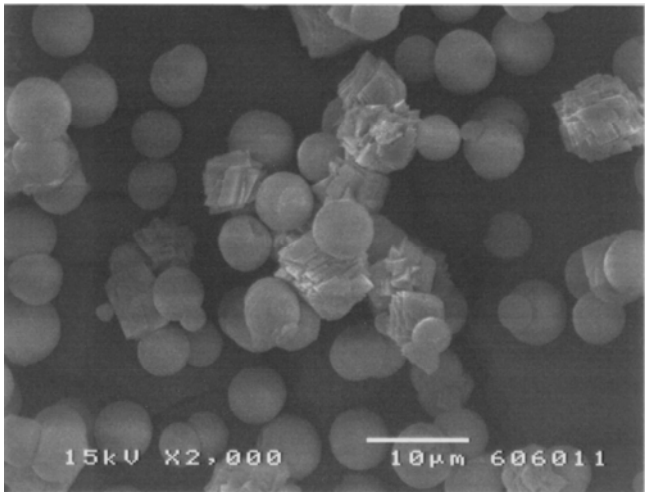

0.3M-293K-325SM 0.1%

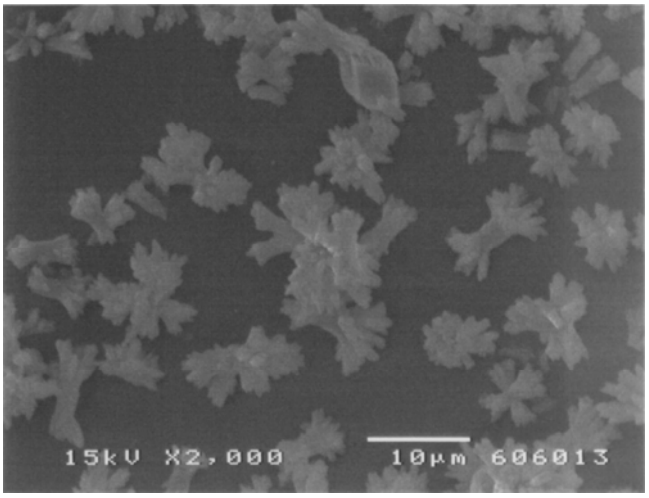

0.3M-333K-325SM 0.1%

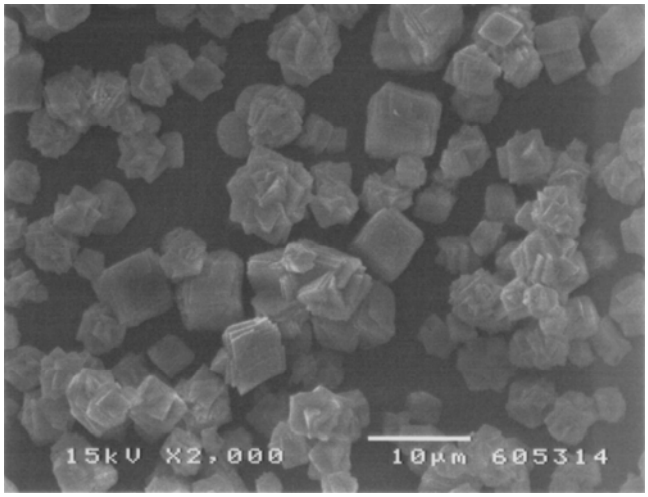

0.3M-293K-325SM 0.5%

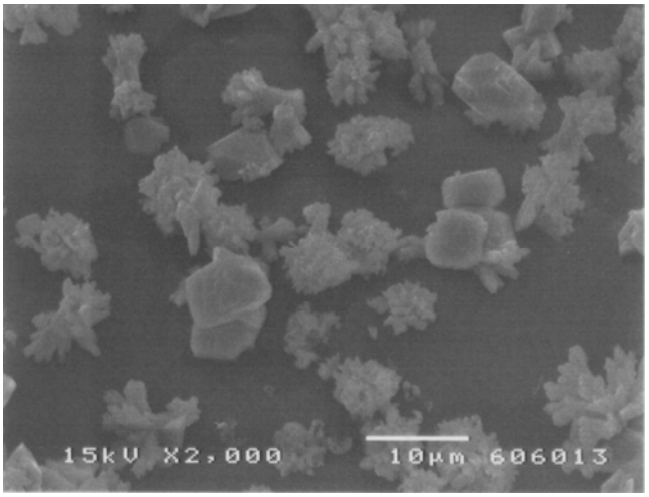

0.3M-333K-325SM 0.5%

Fig.IV-3-2-2. SEM photographs of calcium carbonate

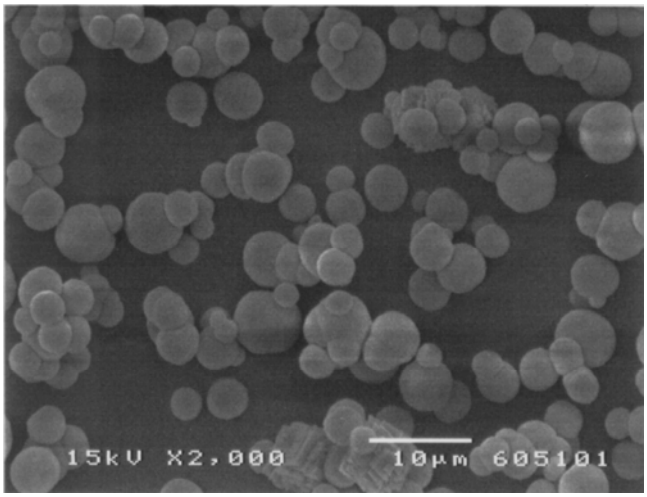

0.5M-293K-325SM 0%

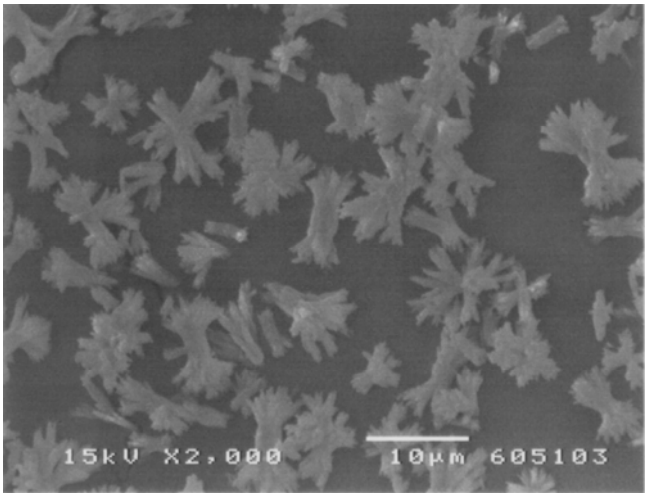

0.5M-333K-325SM 0%

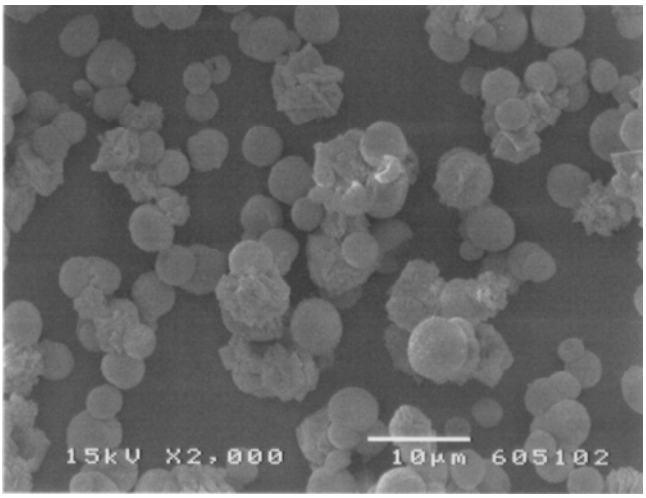

0.5M-293K-325SM 0.1%

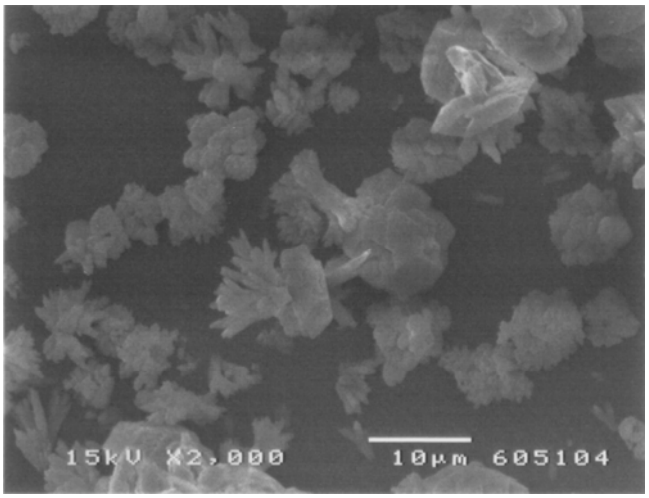

0.5M-333K-325SM 0.1%

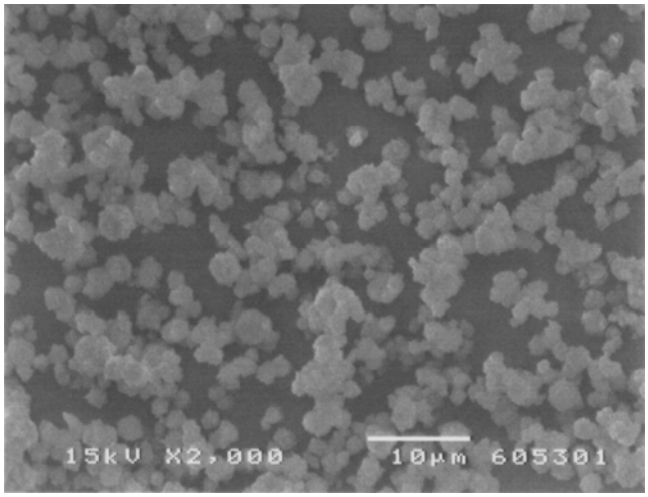

0.5M-293K-325SM 0.5%

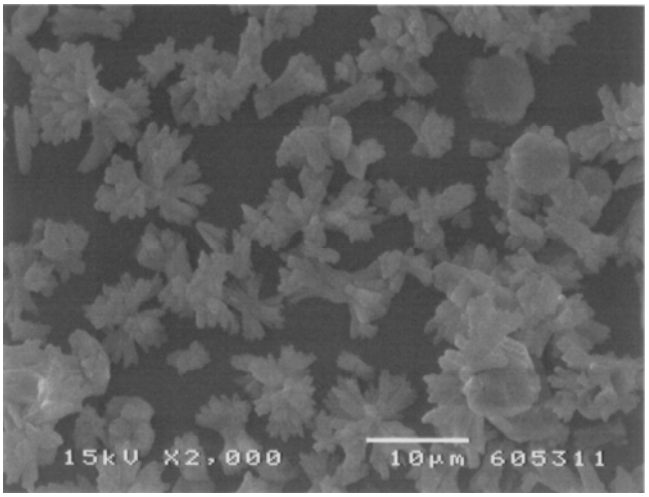

0.5M-333K-325SM 0.5%

Fig.IV-3-3-2. SEM photographs of calcium carbonate

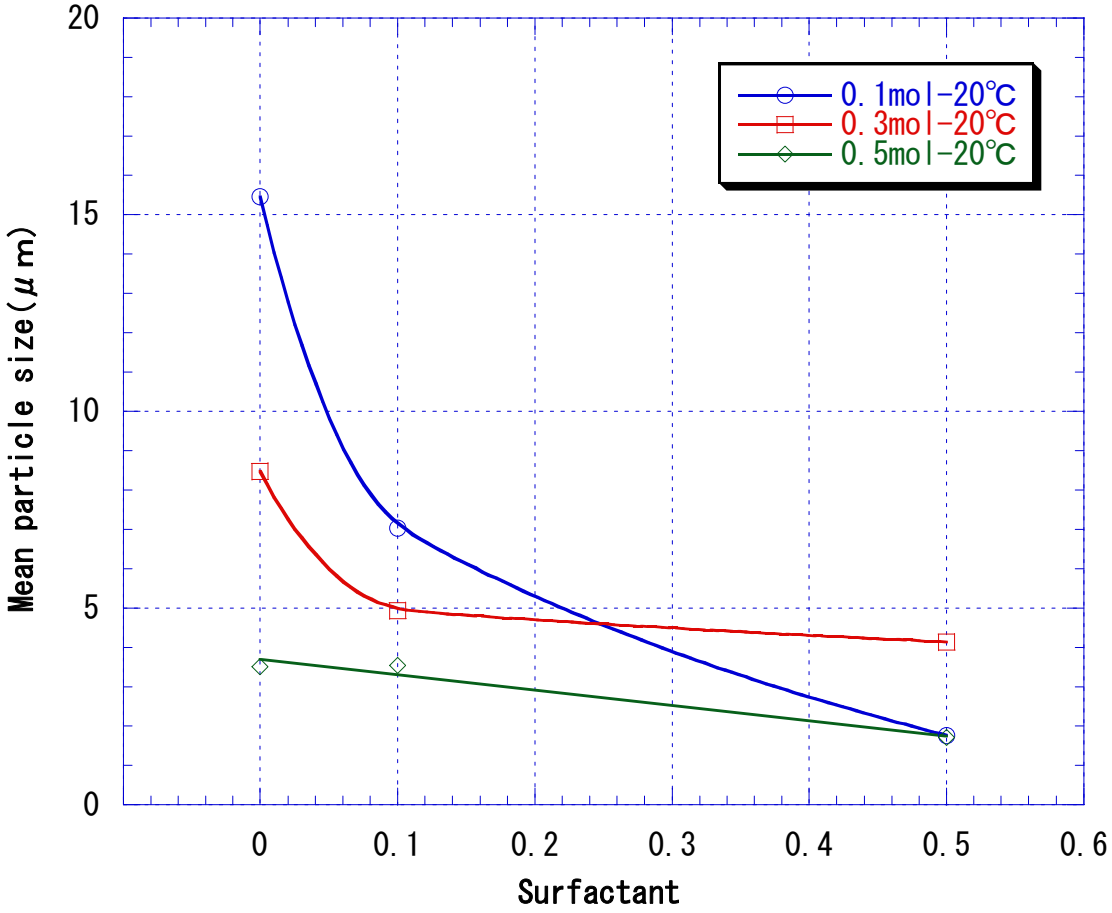

Fig.IV-4-1-1. Particle size distribution on several synthesis conditions

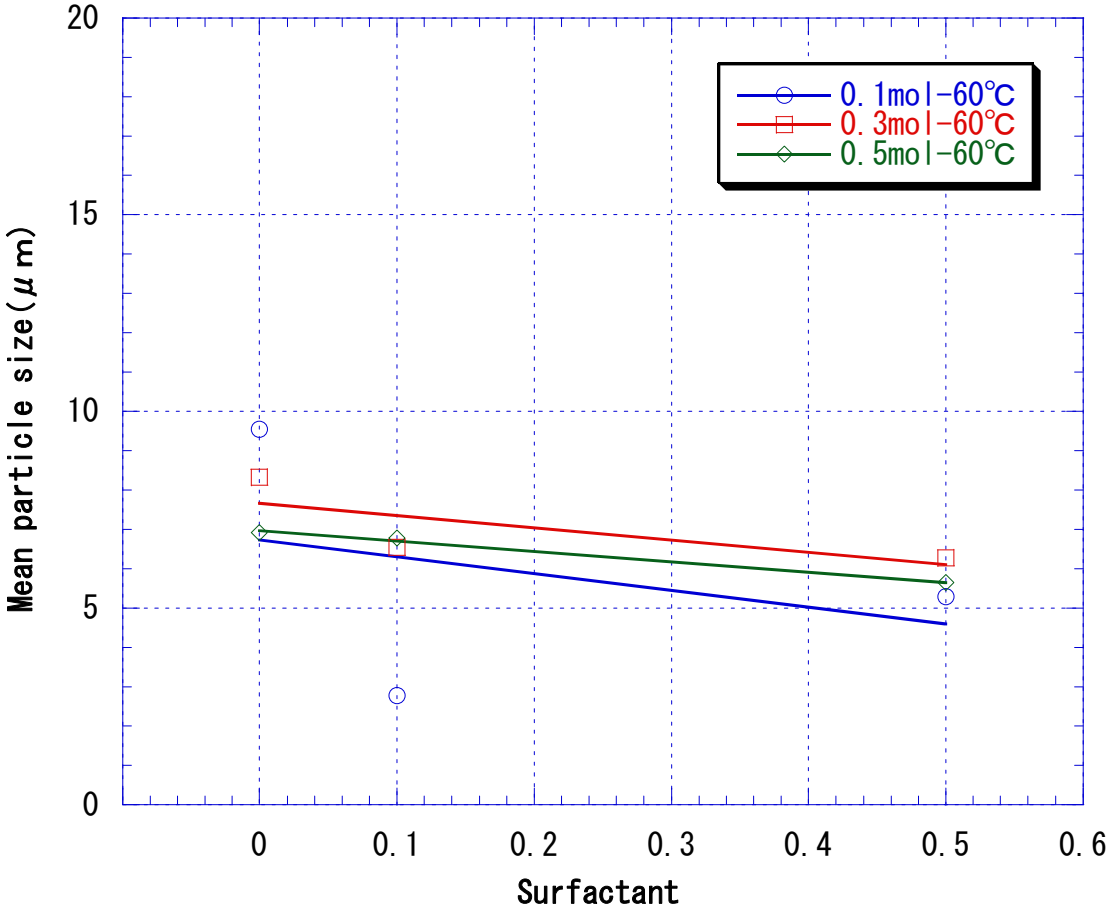

Fig.IV-4-1-2. Particle size distribution on several synthesis conditions

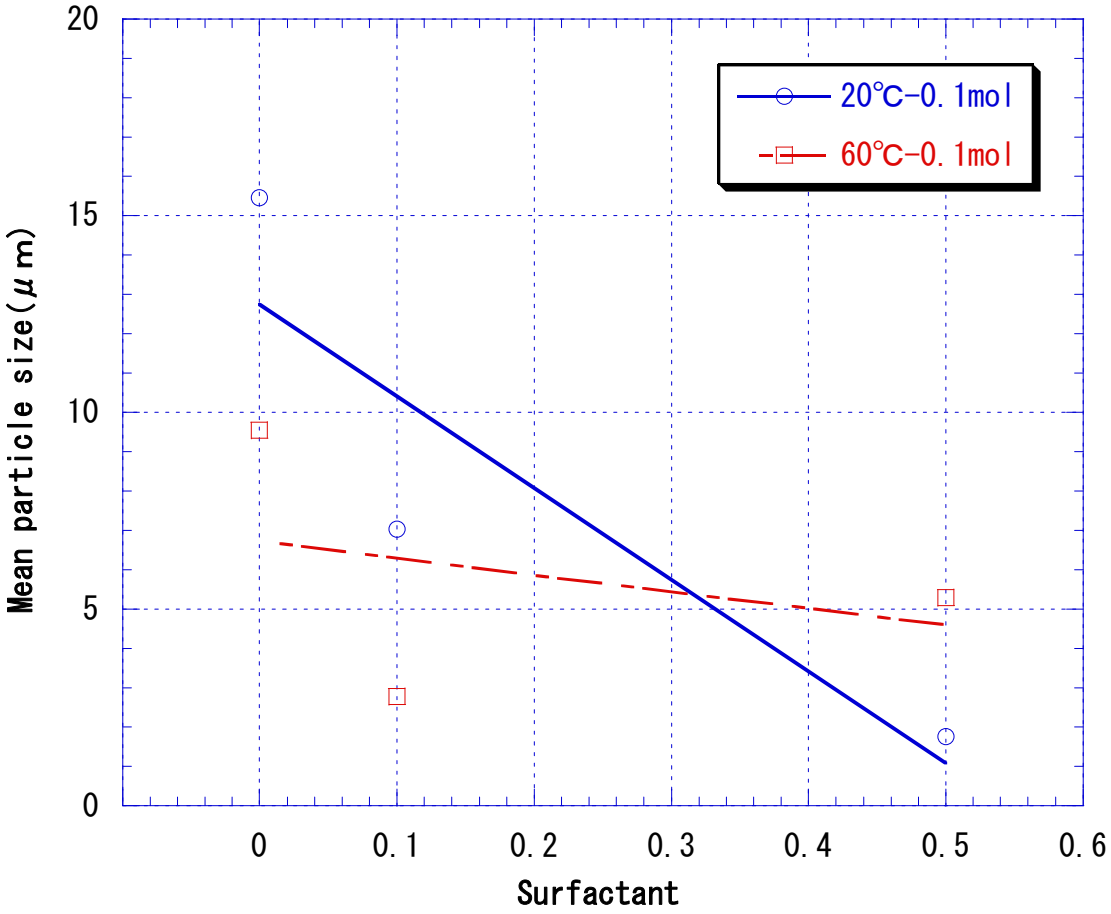

Fig.IV-4-2-1. Particle size distribution on several synthesis conditions

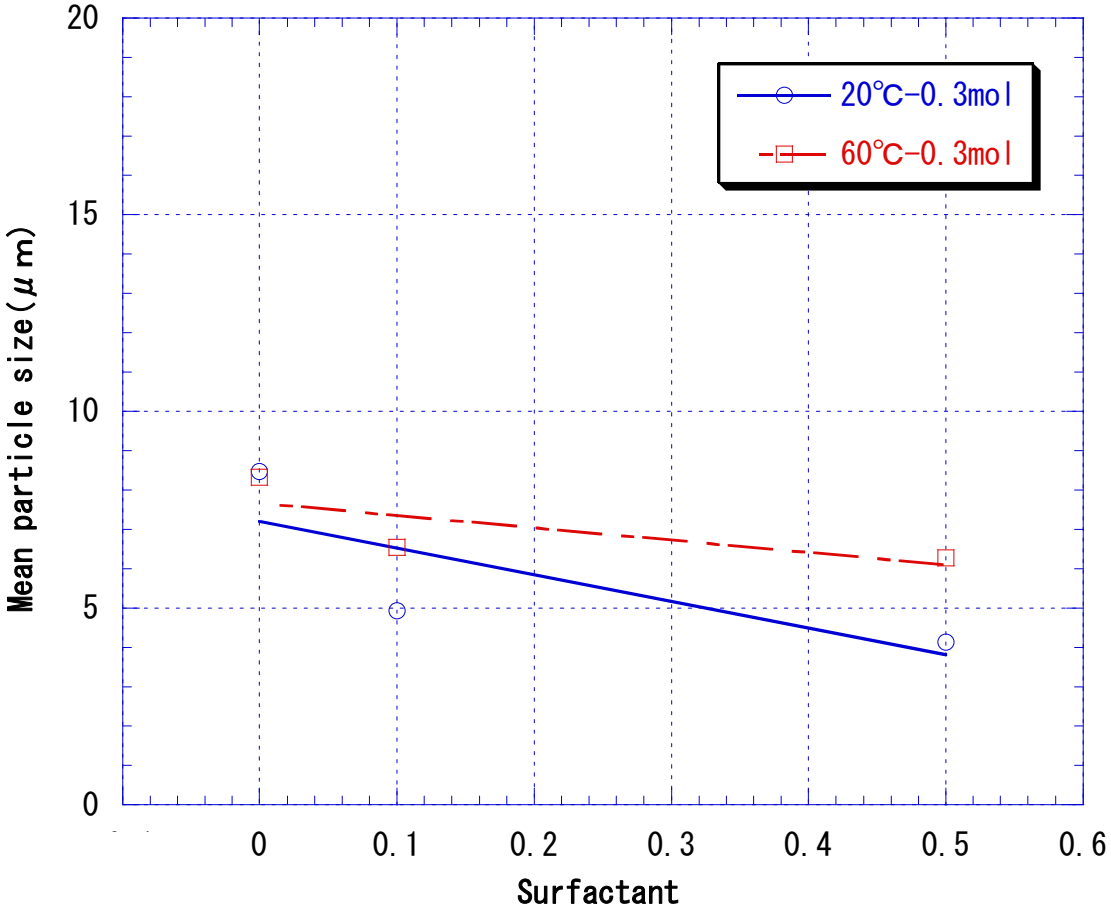

Fig.IV-4-2-2. Particle size distribution on several synthesis conditions

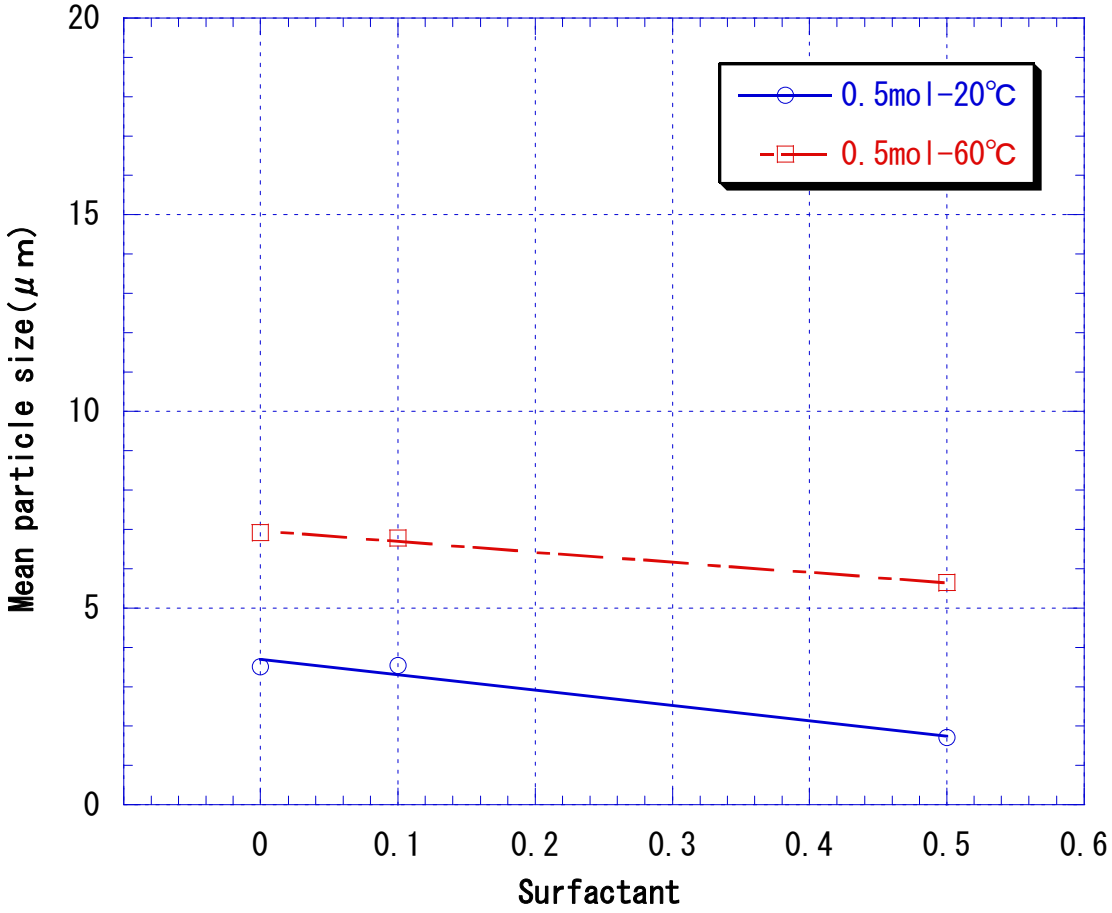

Fig.IV-4-2-3. Particle size distribution on several synthesis conditions

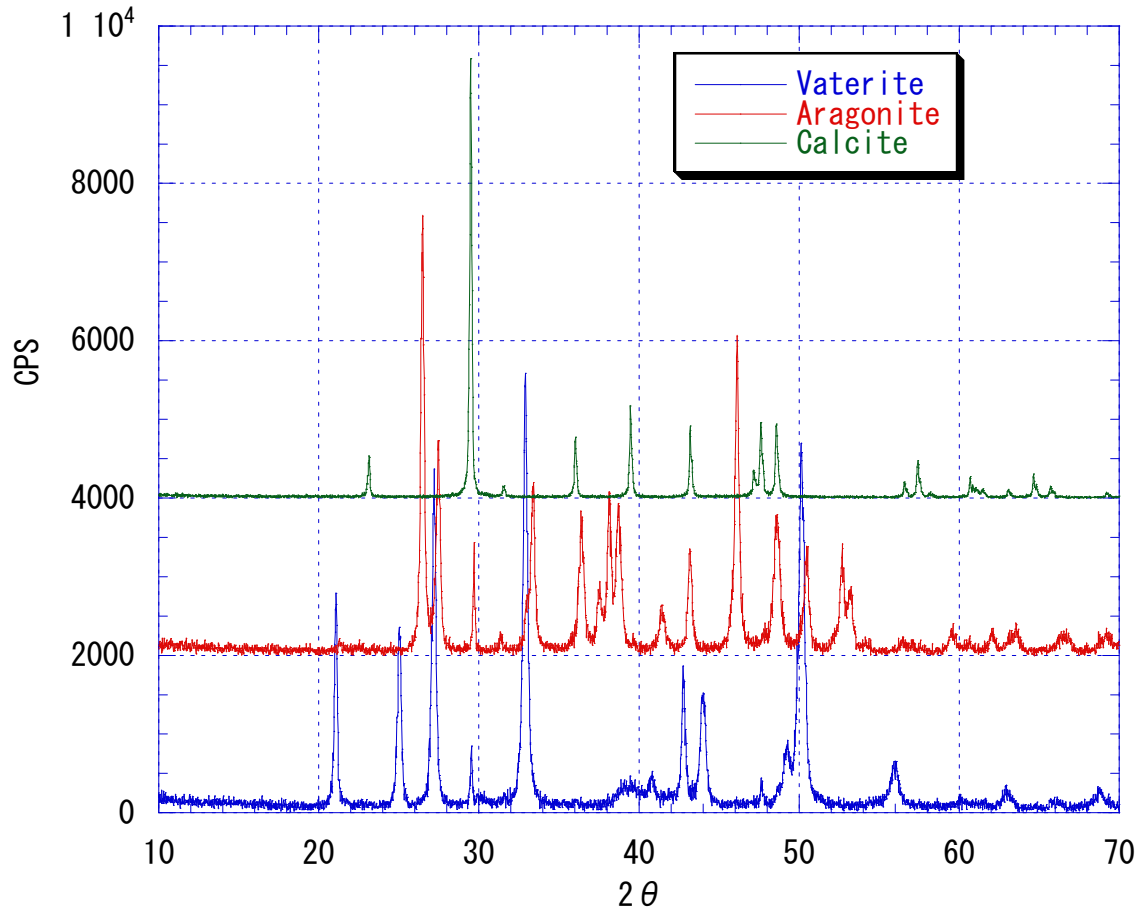

Fig.IV-5-1. XRD spectrum of several crystal type of calcium carbonate

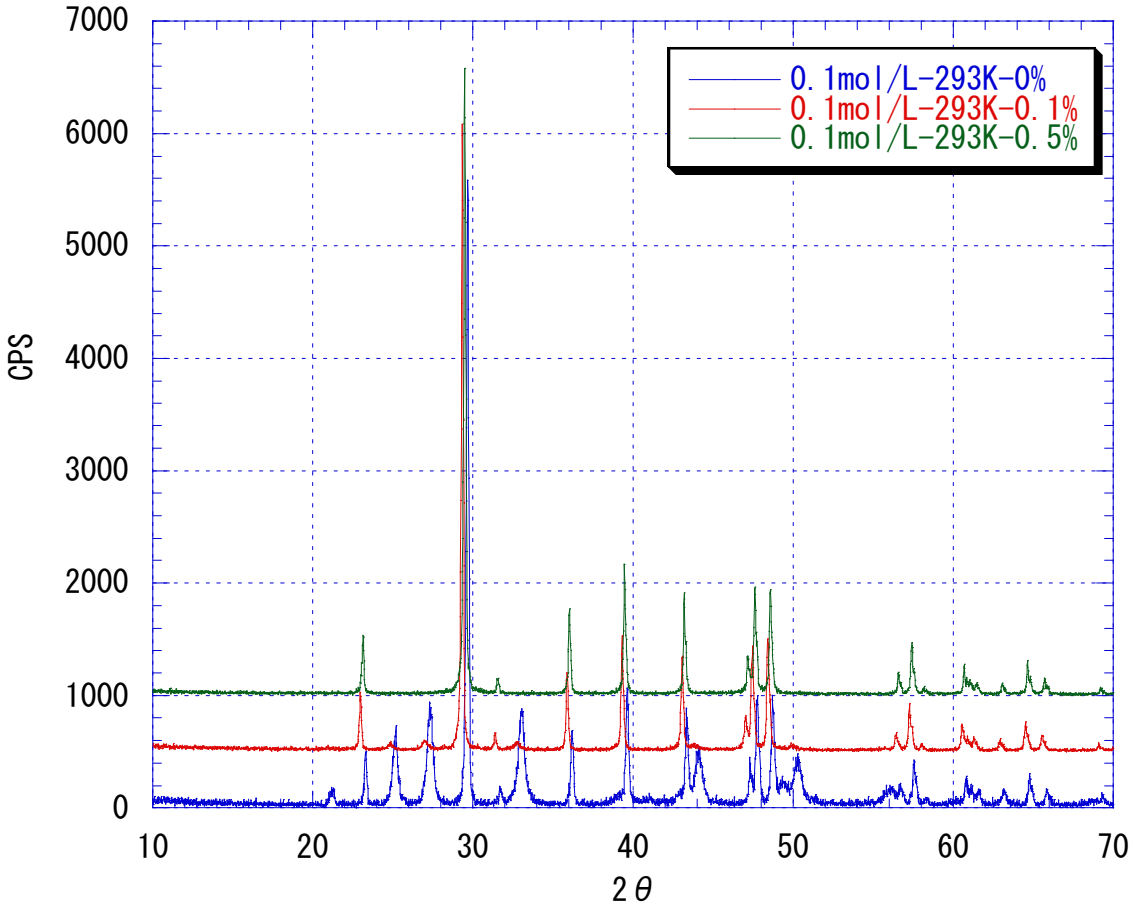

Fig.IV-5-2-1. XRD spectrum of synthesized calcium carbonate

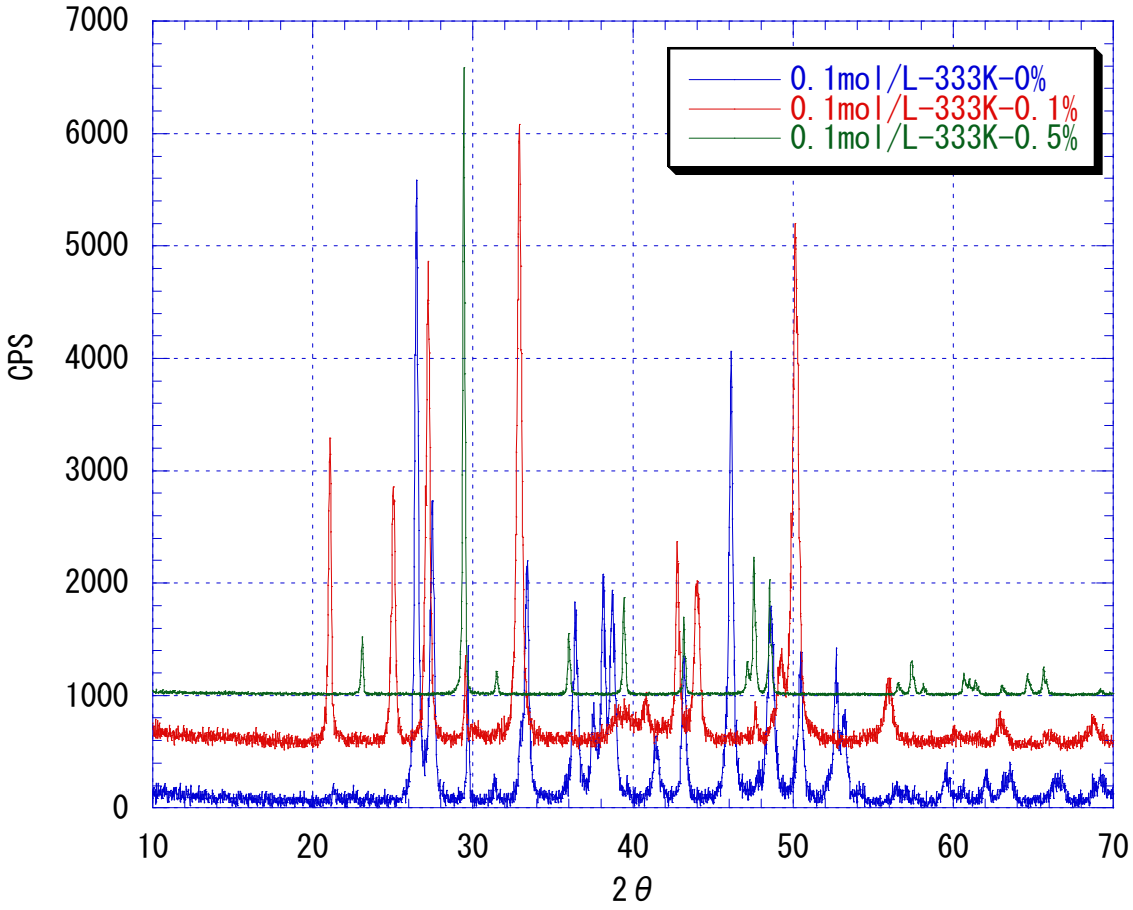

Fig.IV-5-2-2. XRD spectrum of synthesized calcium carbonate

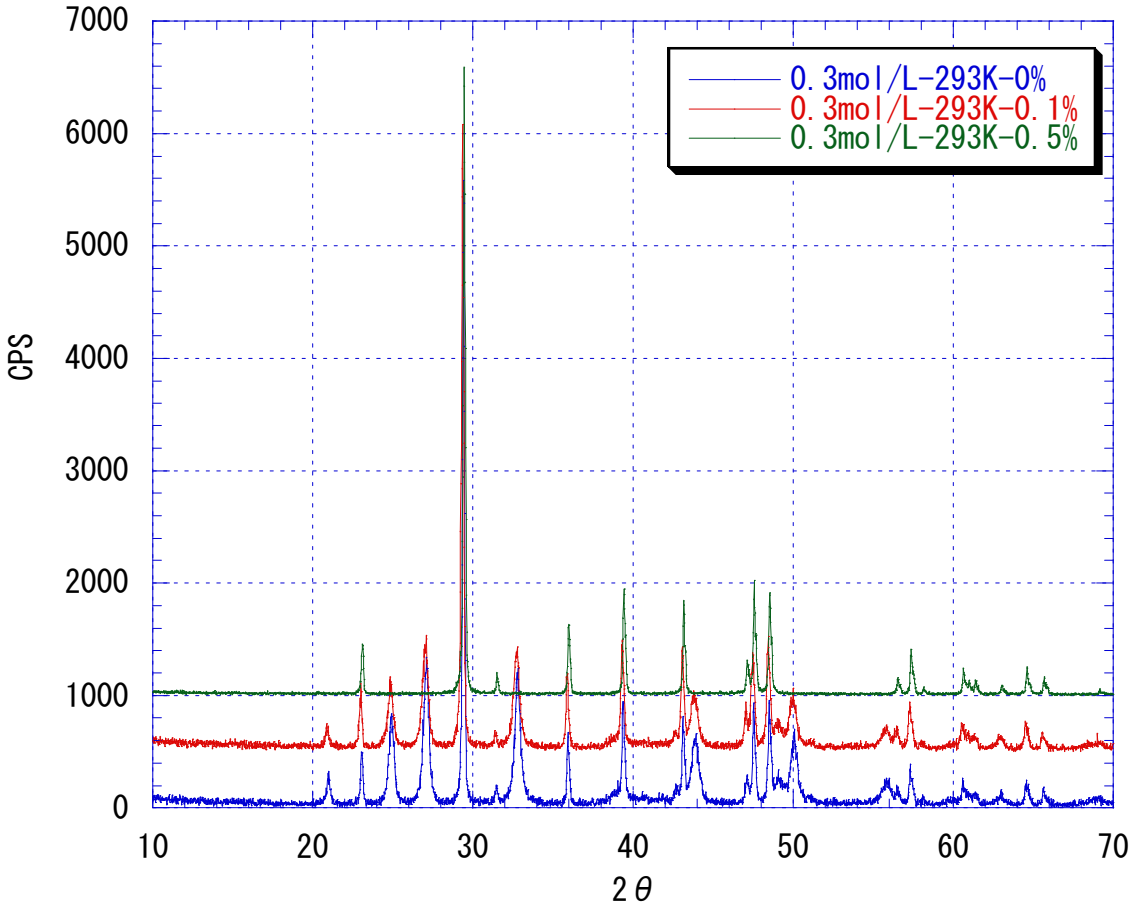

Fig.IV-5-2-3. XRD spectrum of synthesized calcium carbonate

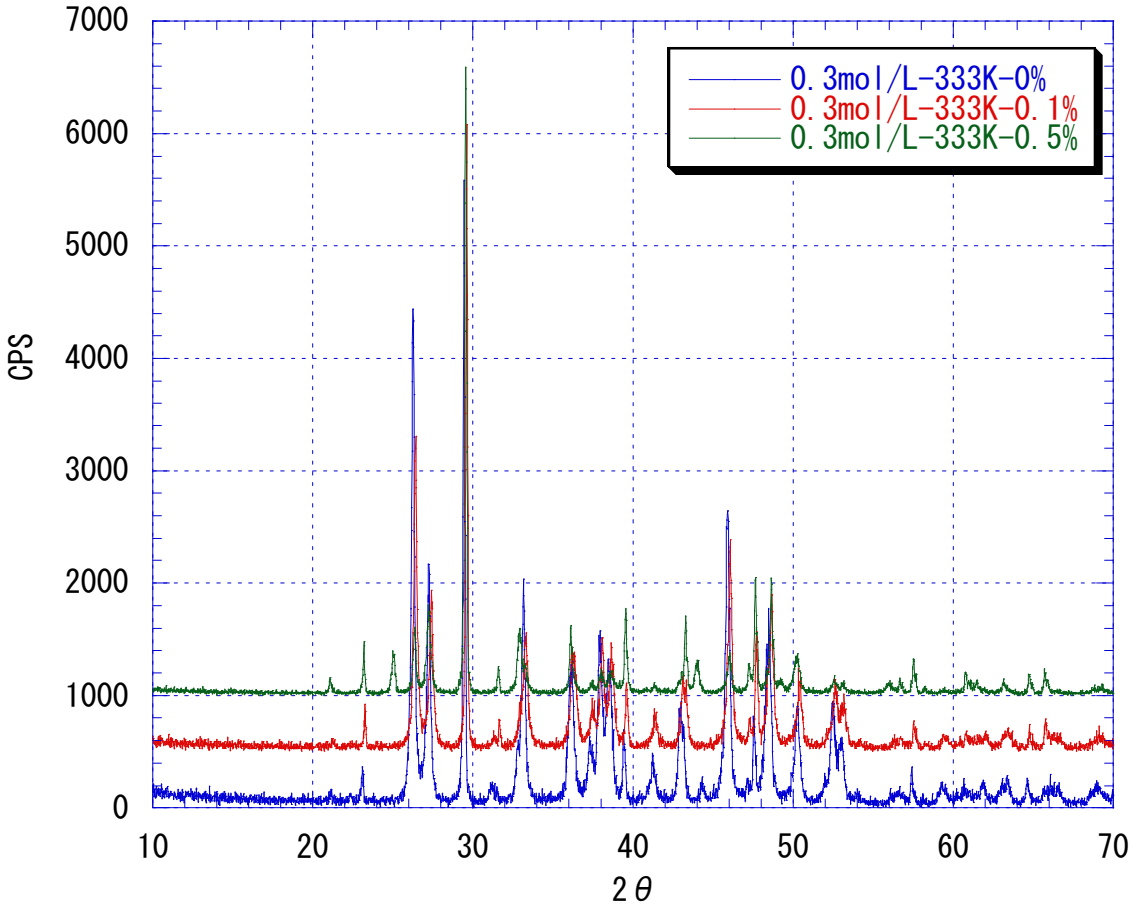

Fig.IV-5-2-4. XRD spectrum of synthesized calcium carbonate

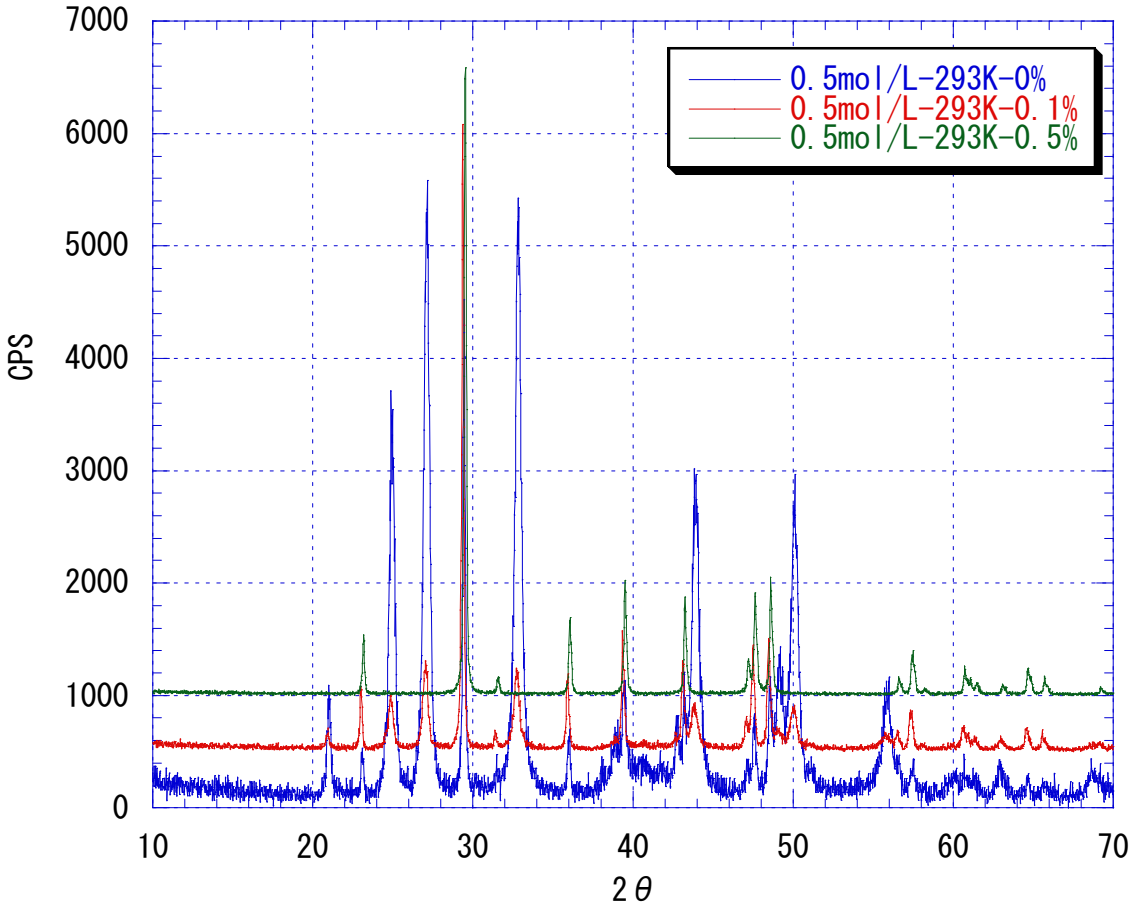

Fig.IV-5-2-5. XRD spectrum of synthesized calcium carbonate

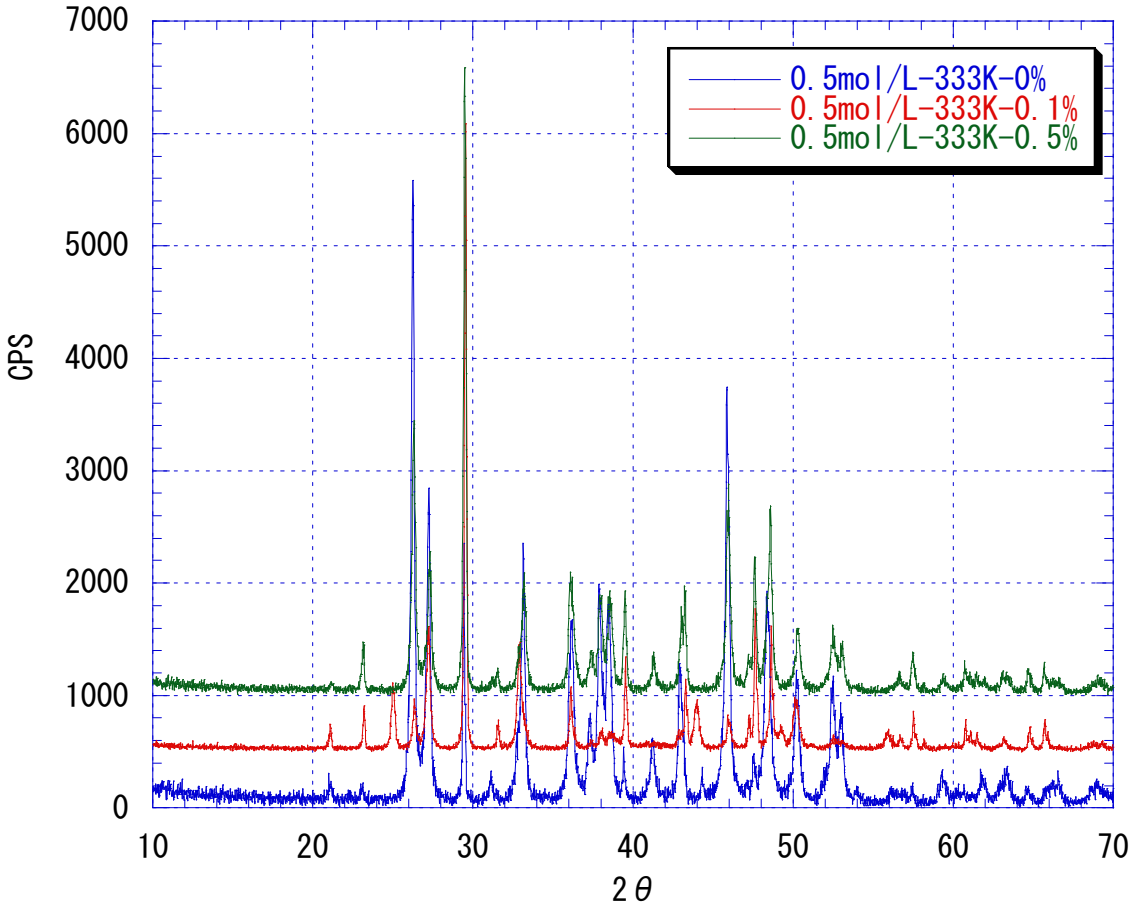

Fig.IV-5-2-6. XRD spectrum of synthesized calcium carbonate

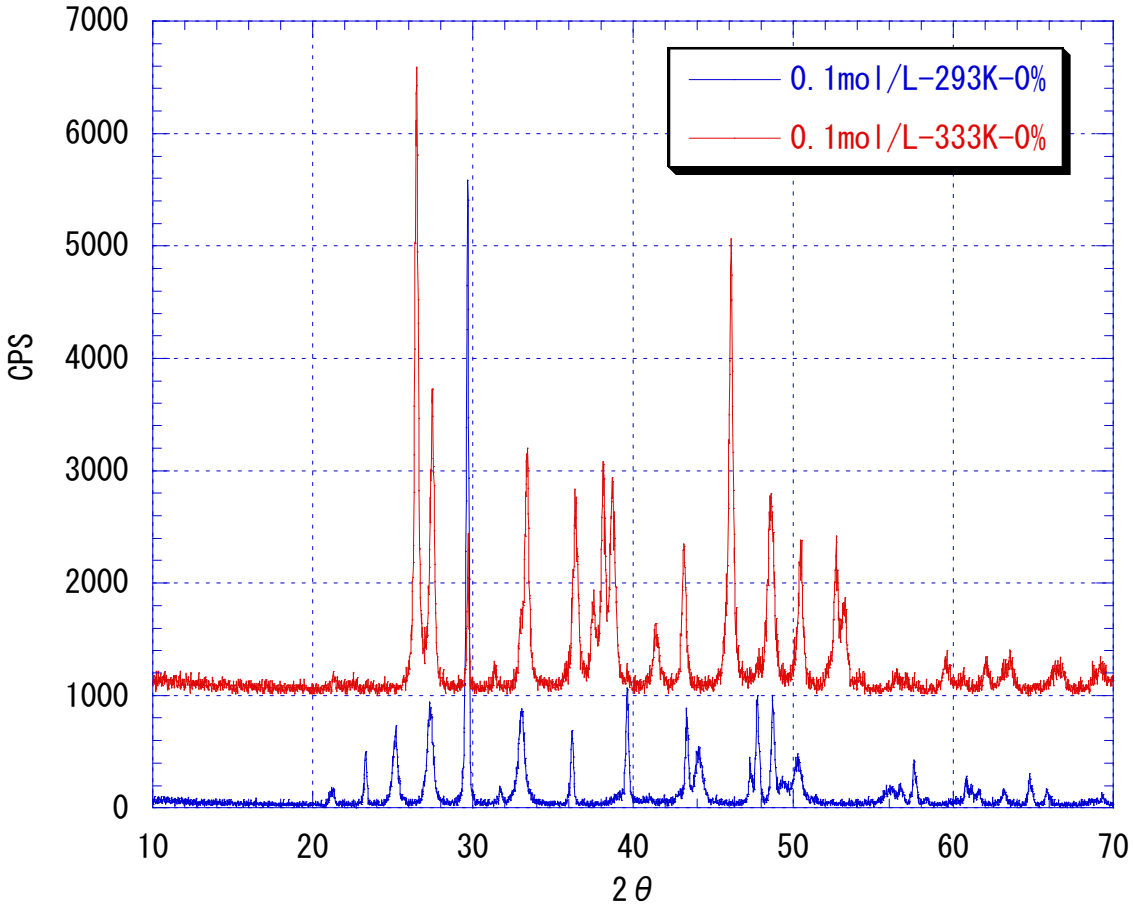

Fig.IV-5-3-1. XRD spectrum of synthesized calcium carbonate

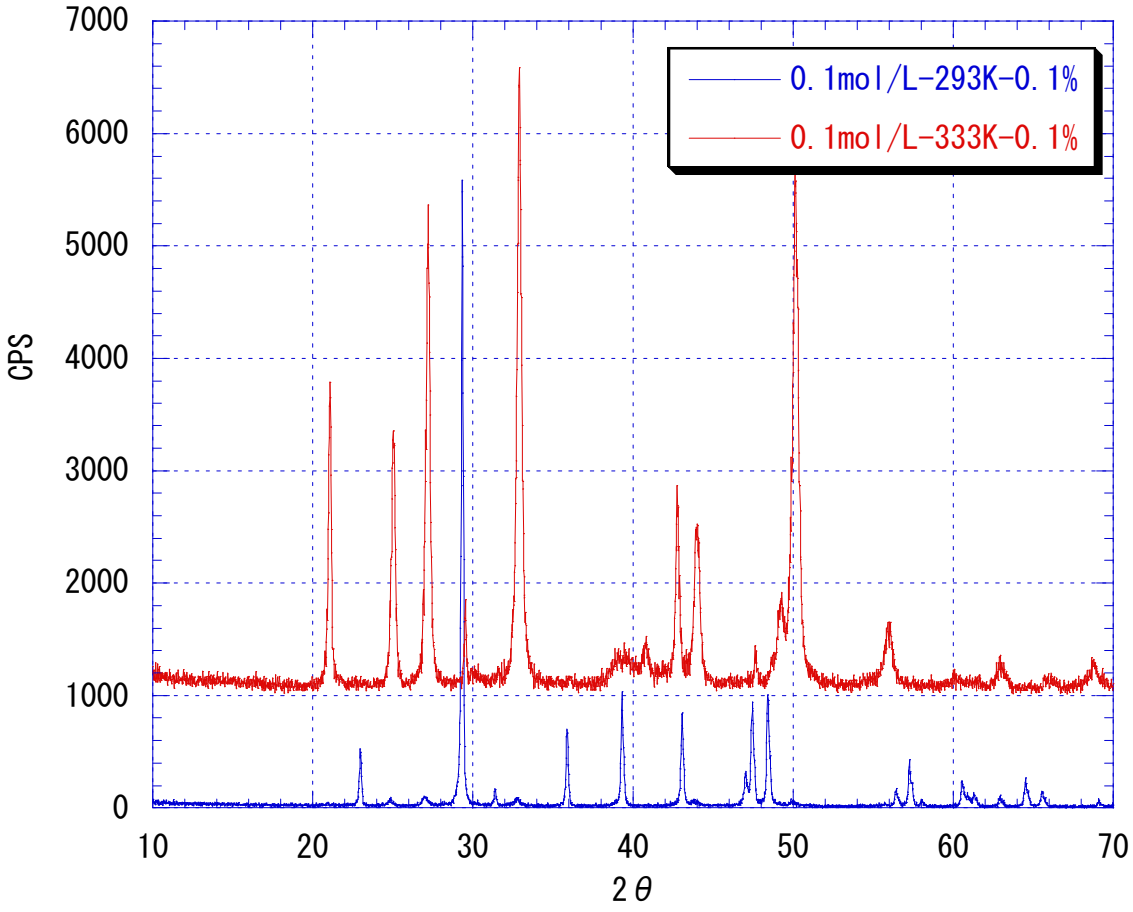

Fig.IV-5-3-2. XRD spectrum of synthesized calcium carbonate

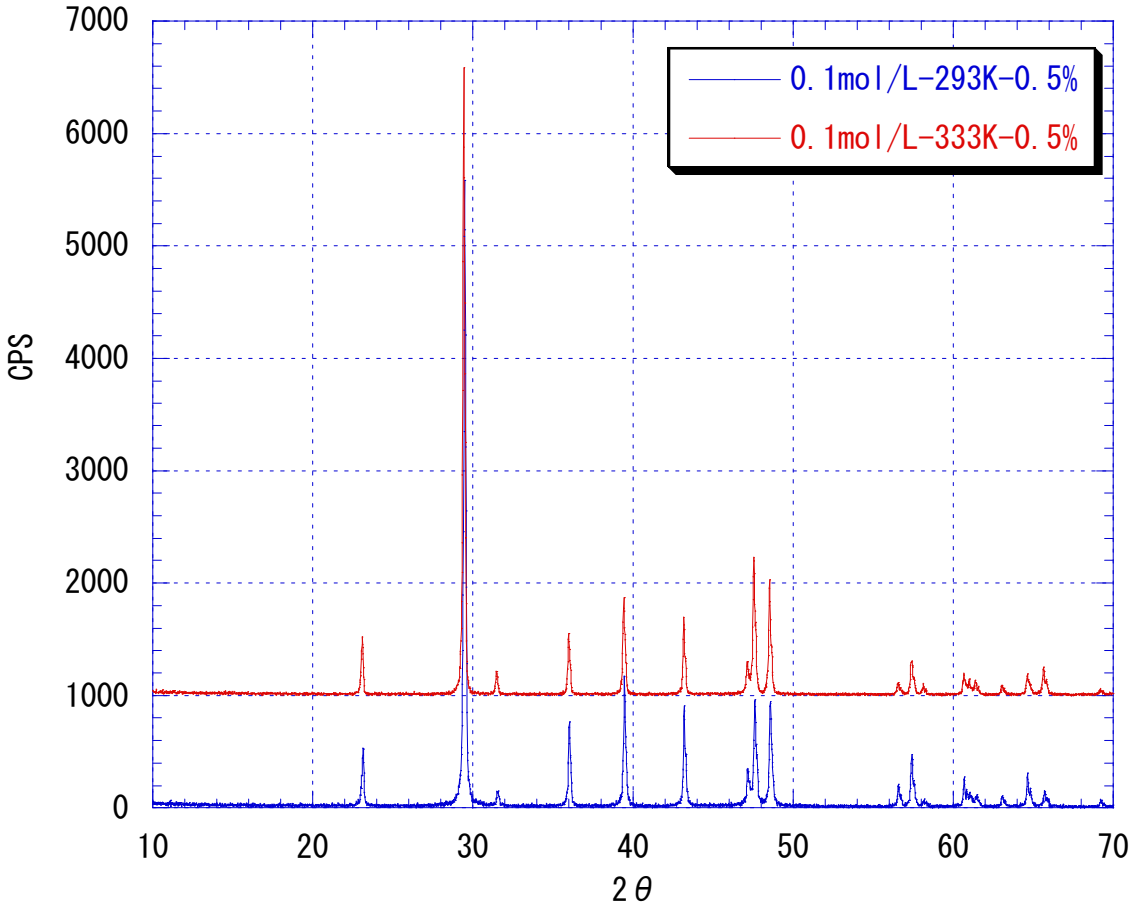

Fig.IV-5-3-3. XRD spectrum of synthesized calcium carbonate

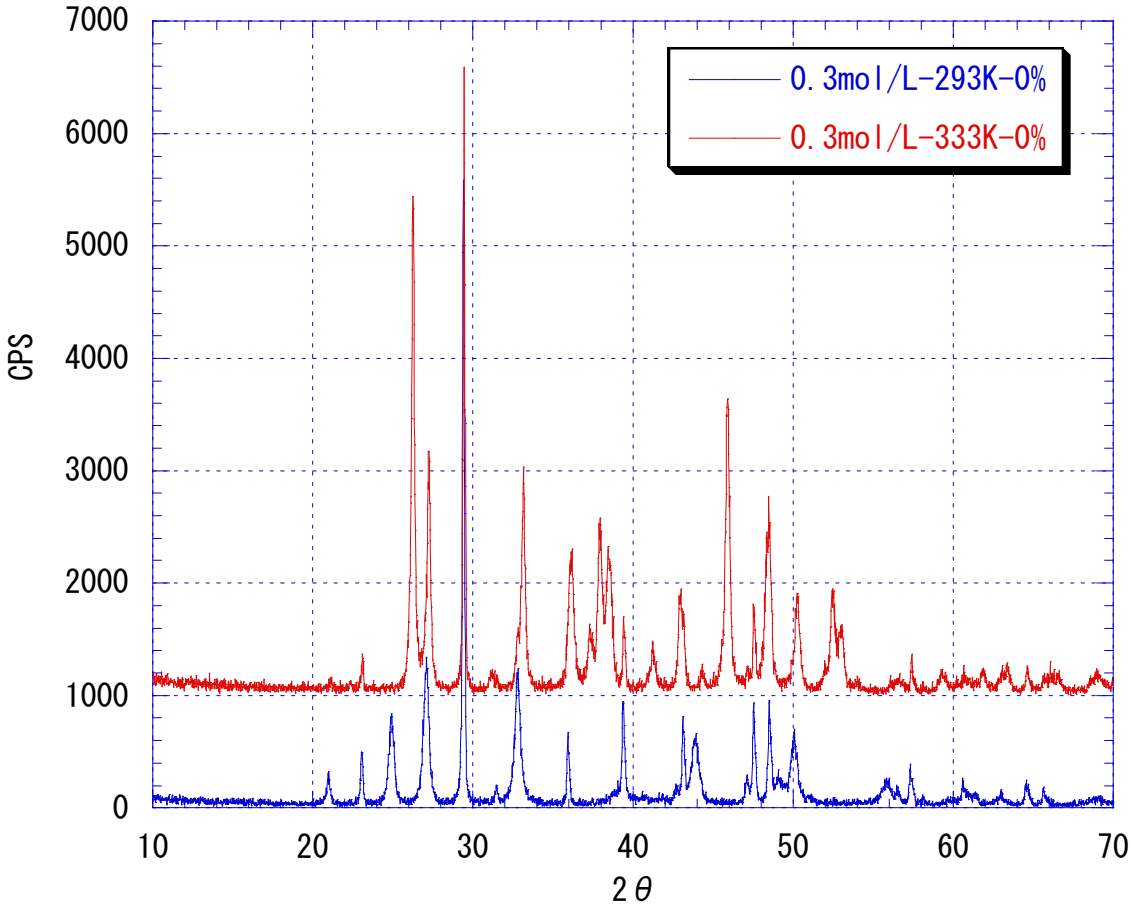

Fig.IV-5-3-4. XRD spectrum of synthesized calcium carbonate

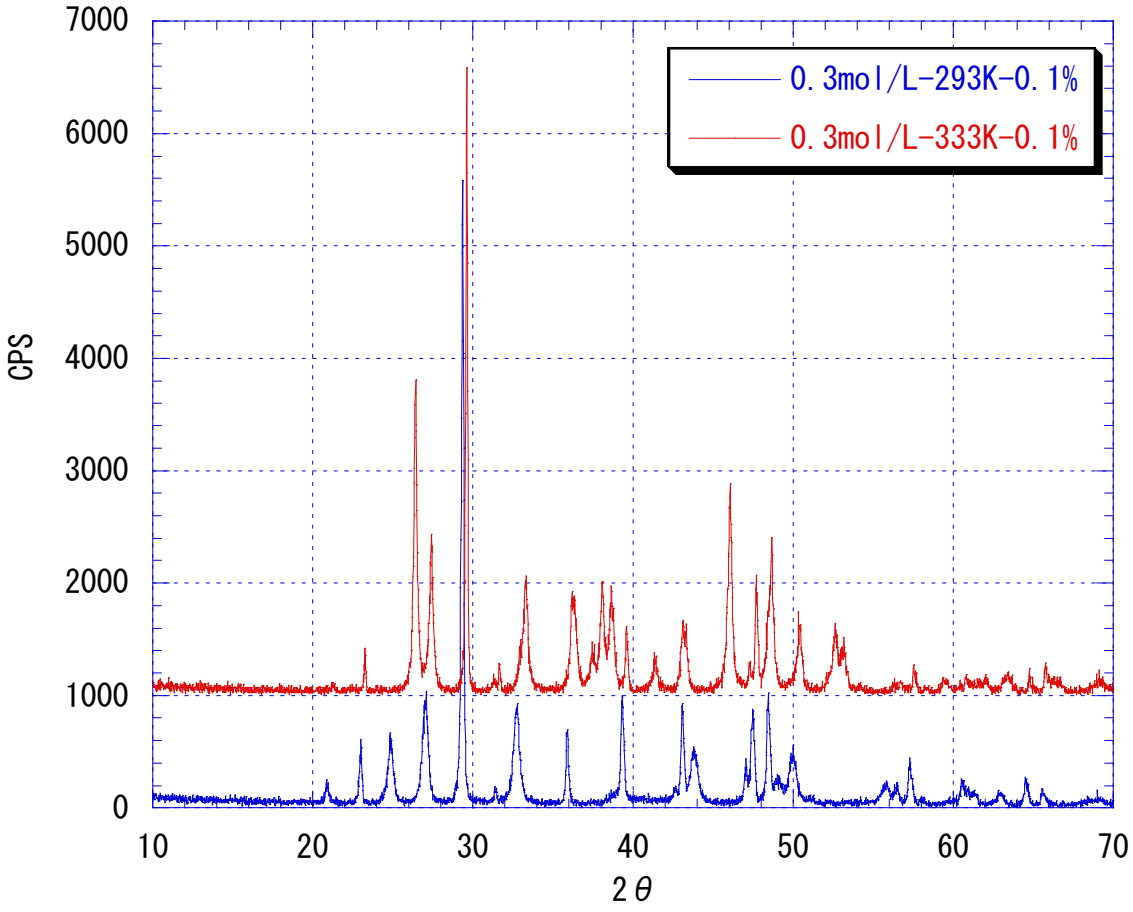

Fig.IV-5-3-5. XRD spectrum of synthesized calcium carbonate

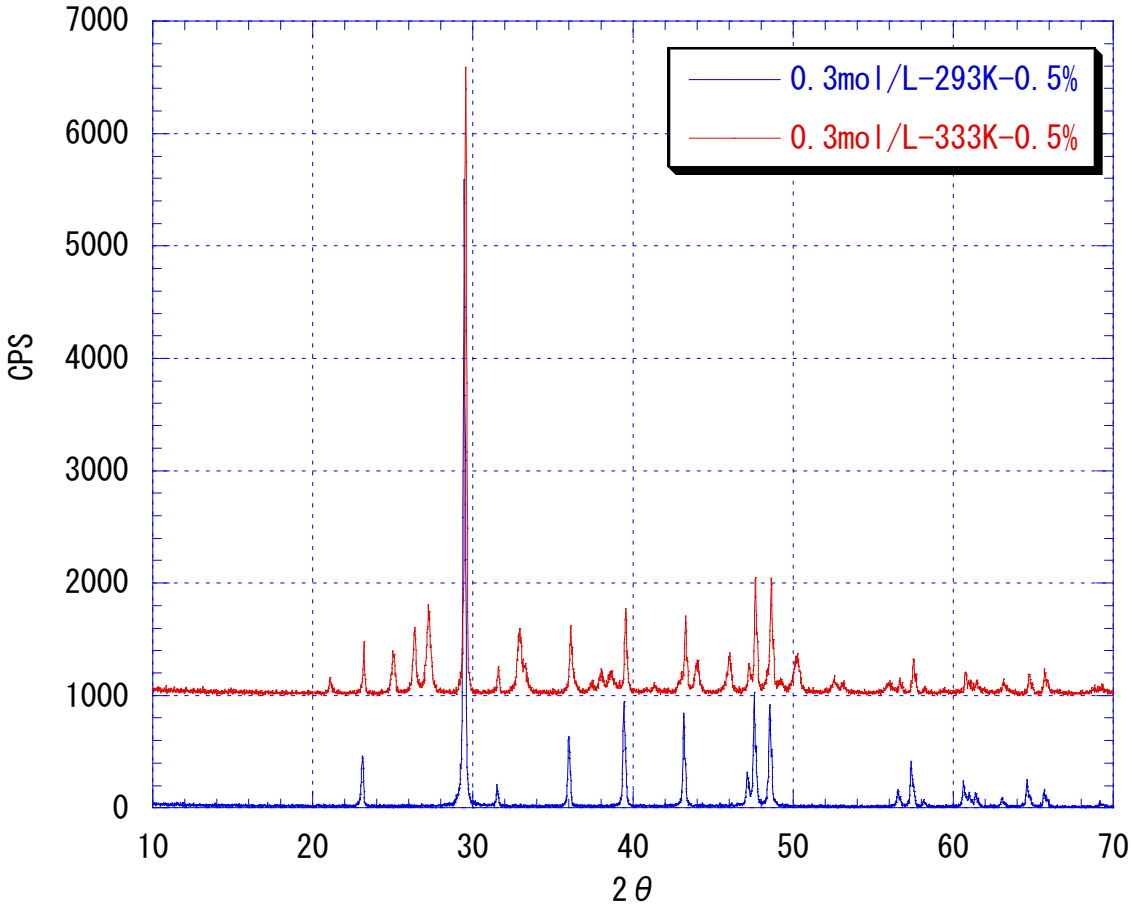

Fig.IV-5-3-6. XRD spectrum of synthesized calcium carbonate

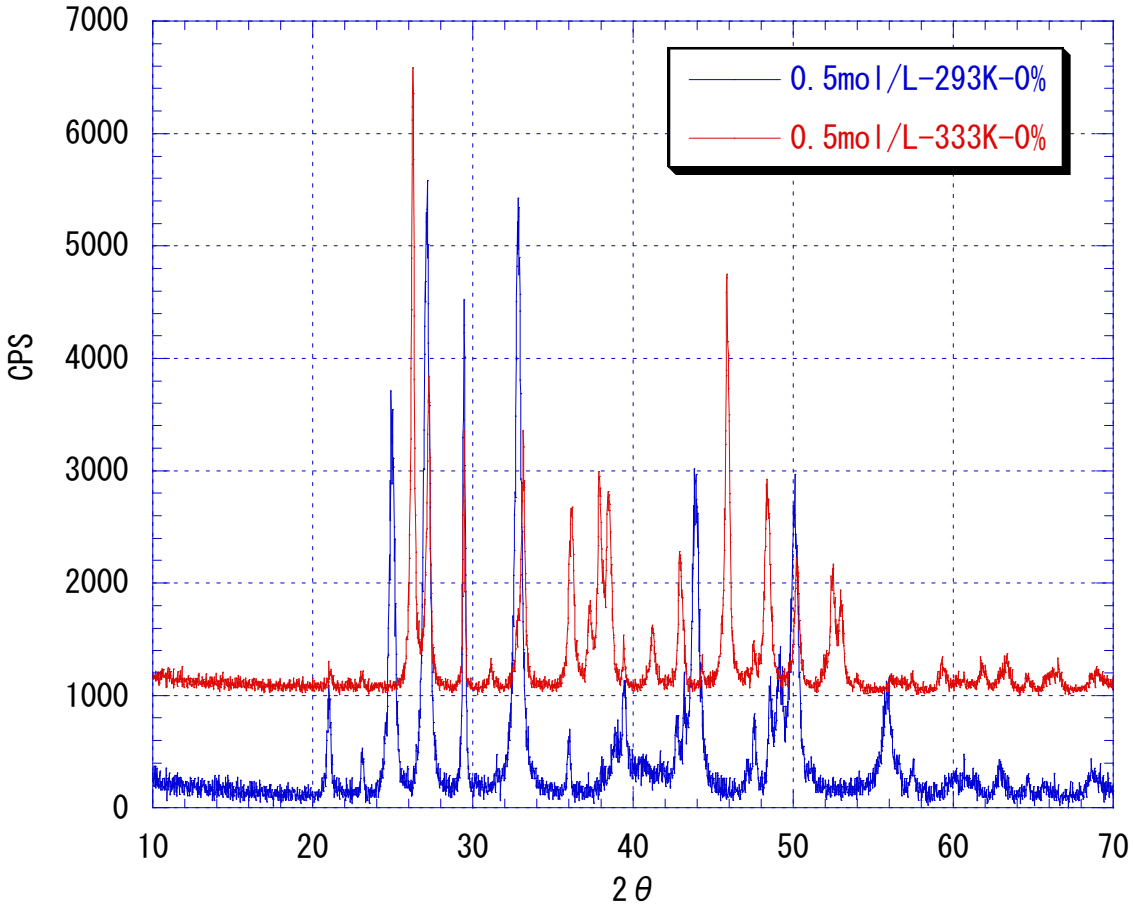

Fig.IV-5-3-7. XRD spectrum of synthesized calcium carbonate

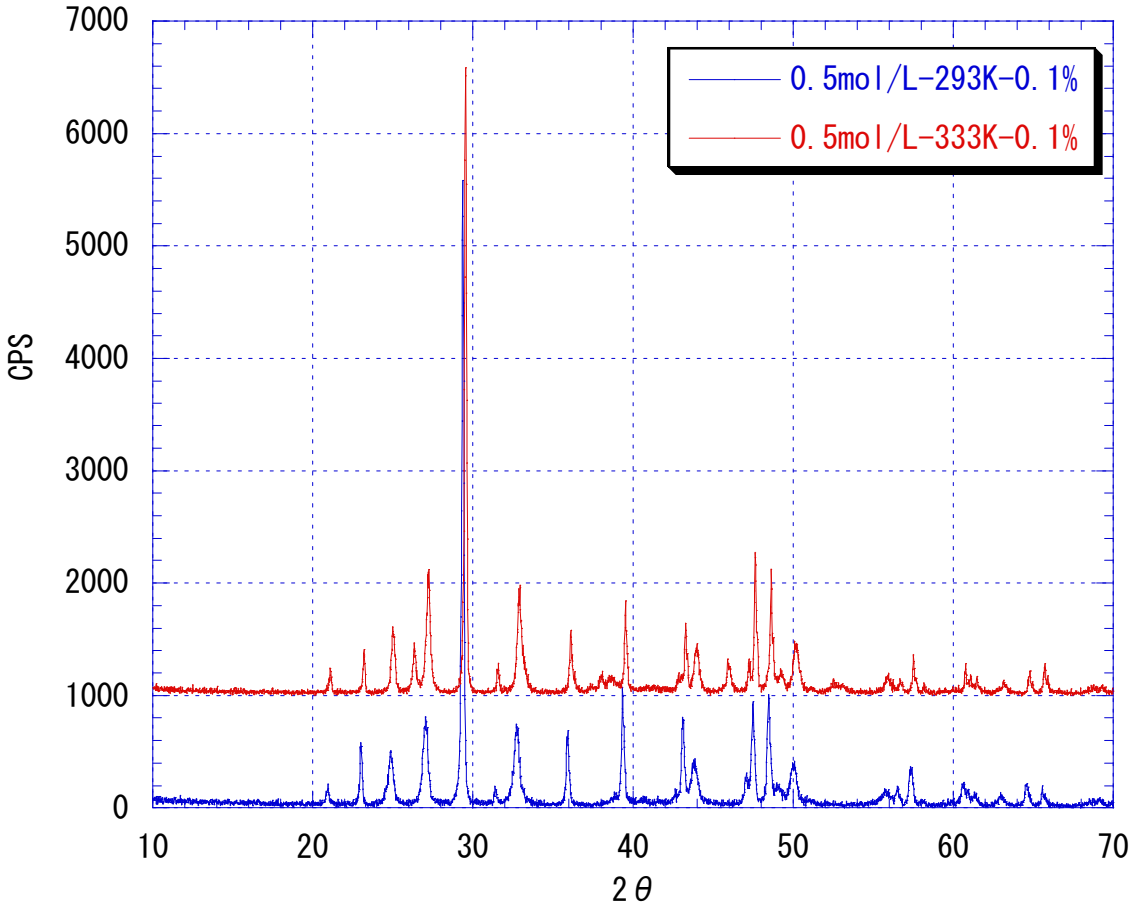

Fig.IV-5-3-8. XRD spectrum of synthesized calcium carbonate

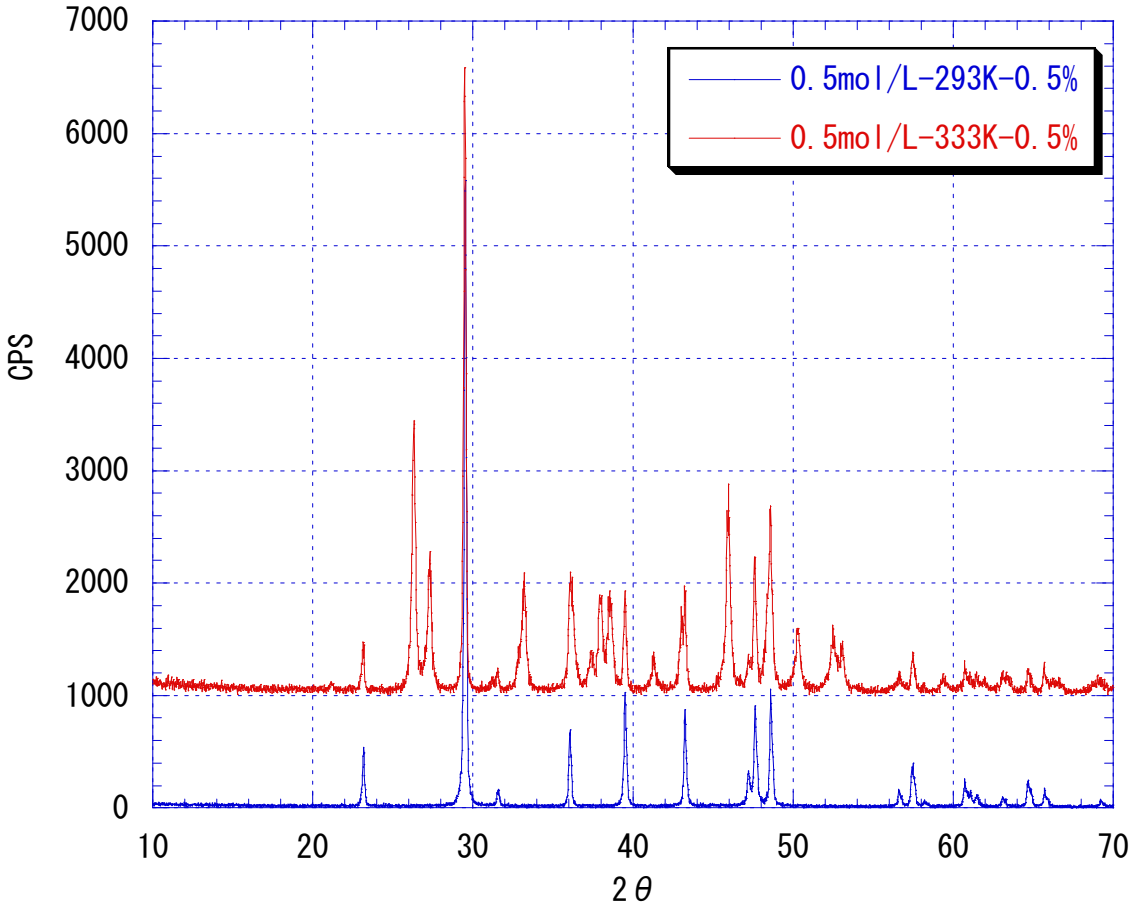

Fig.IV-5-3-9. XRD spectrum of synthesized calcium carbonate

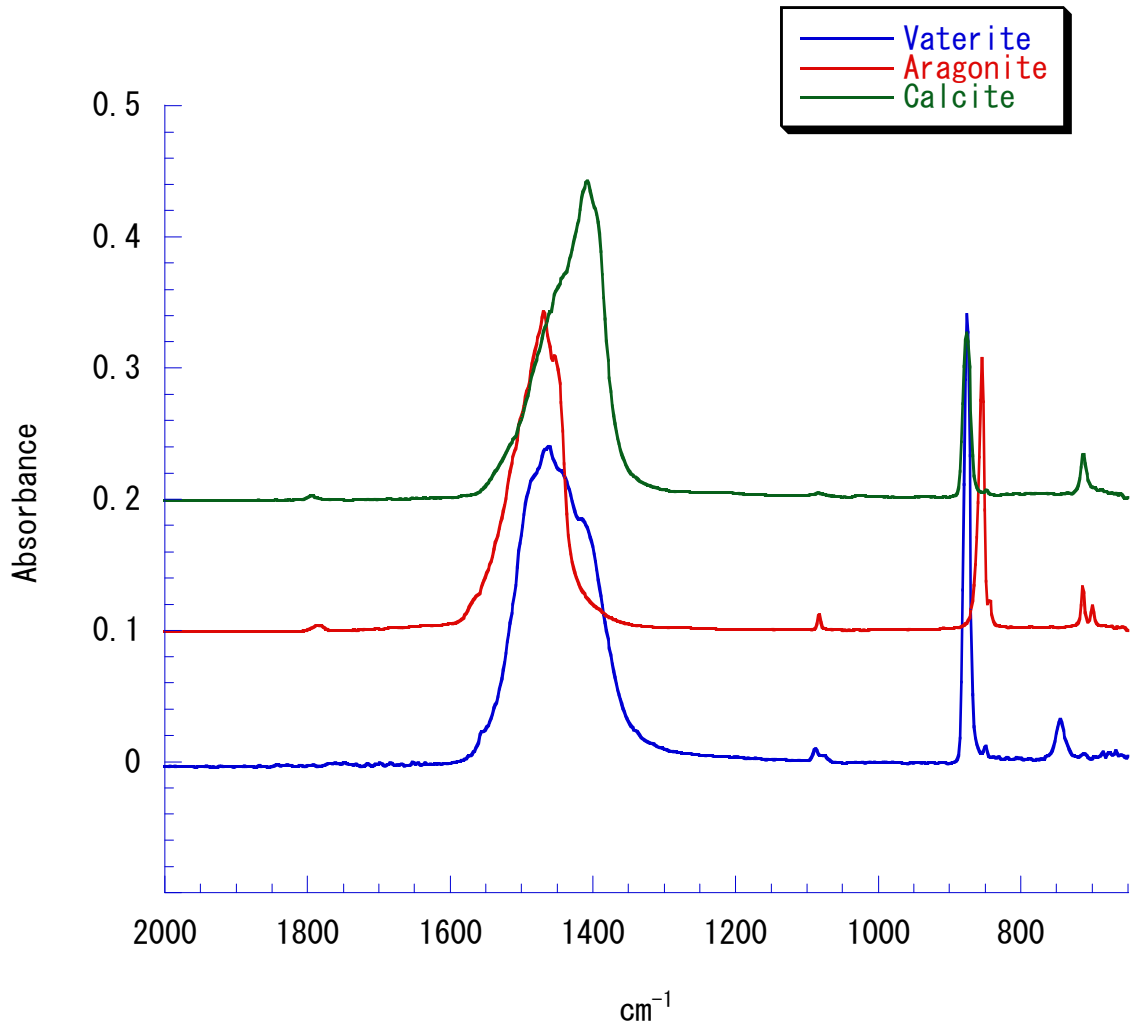

Fig.IV-6-1. IR spectrum of several crystal type of calcium carbonate

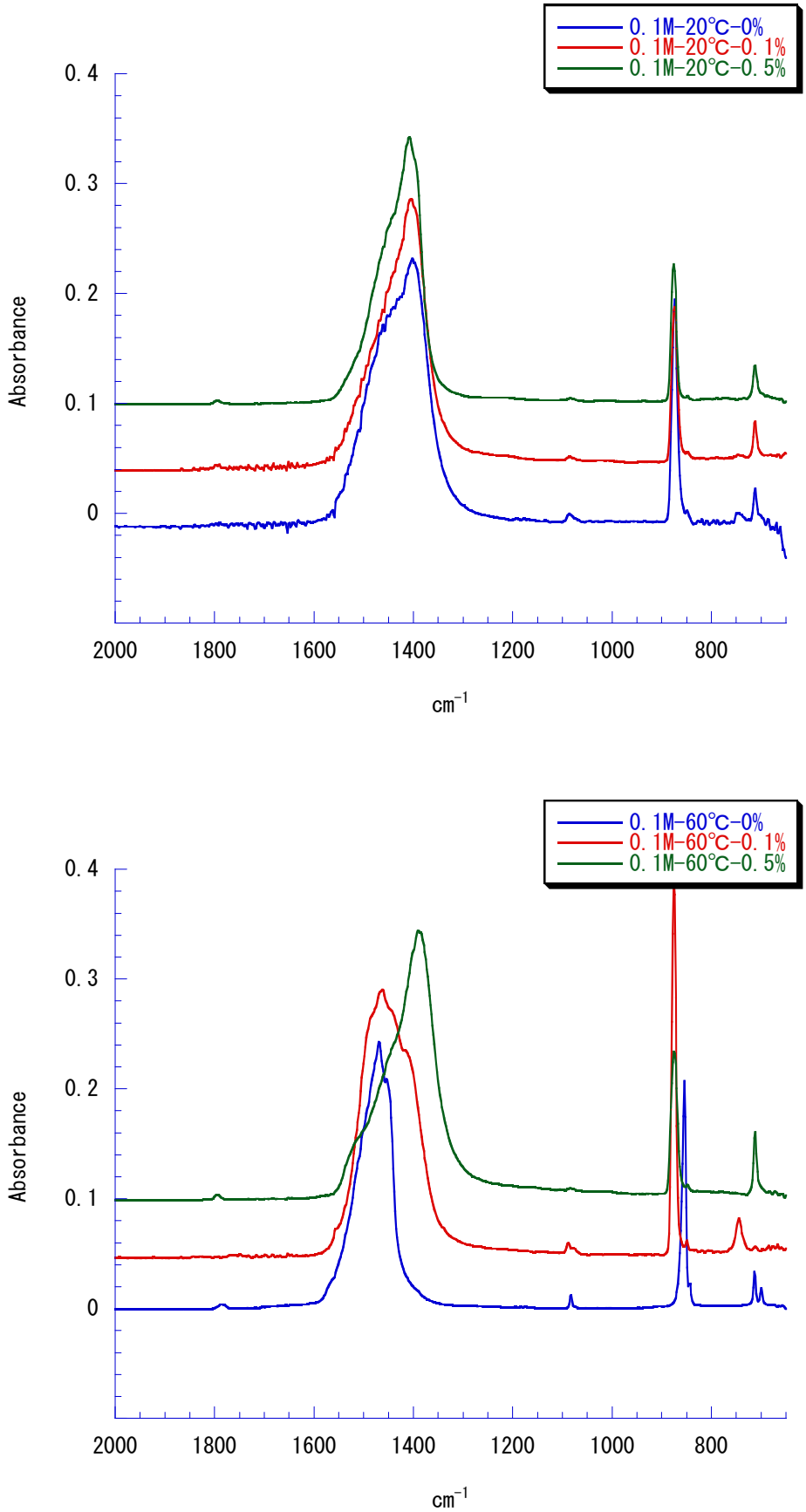

Fig.IV-6-2-1. IR spectrum of synthesized calcium carbonate

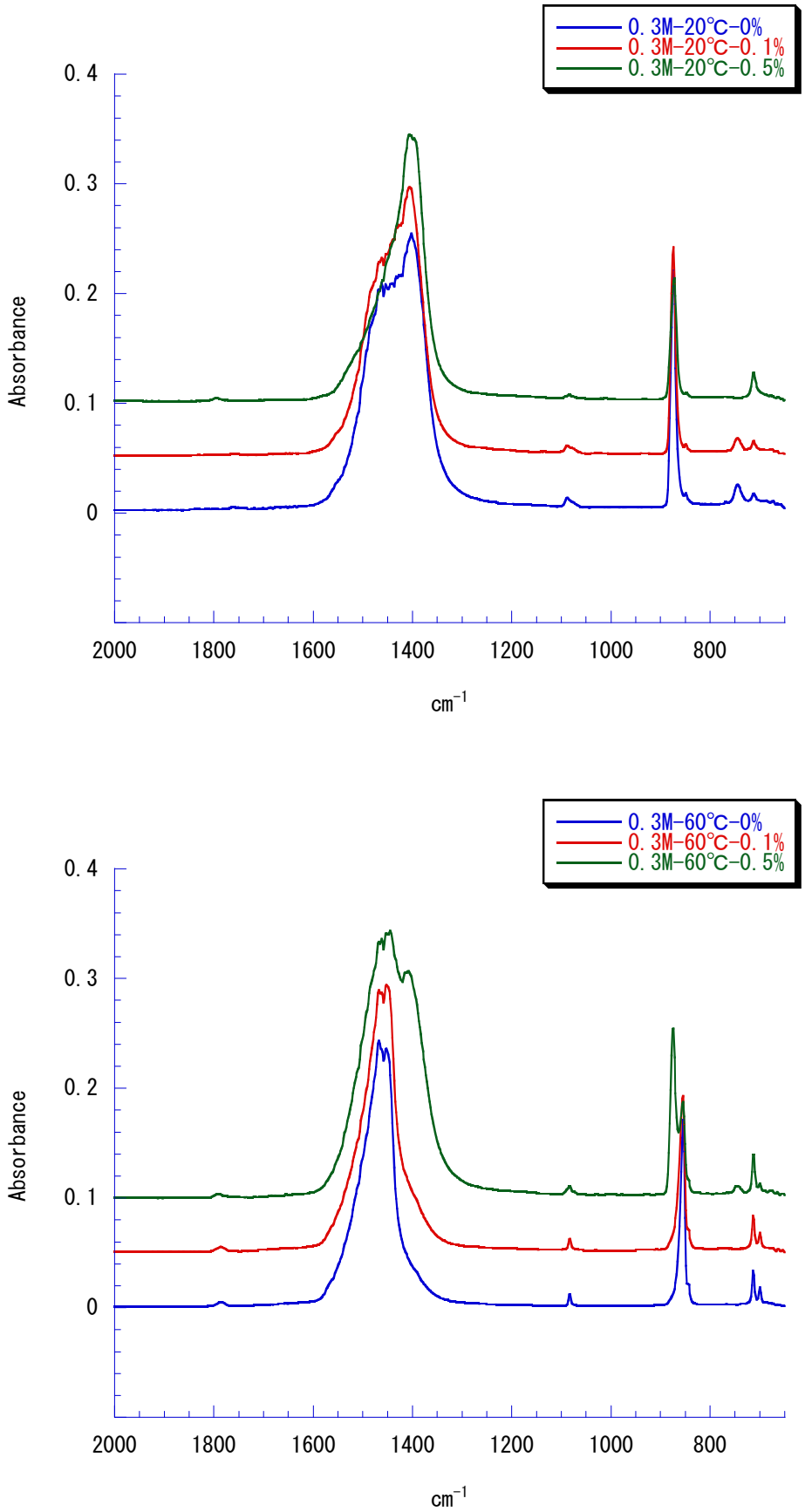

Fig.IV-6-2-2. IR spectrum of synthesized calcium carbonate

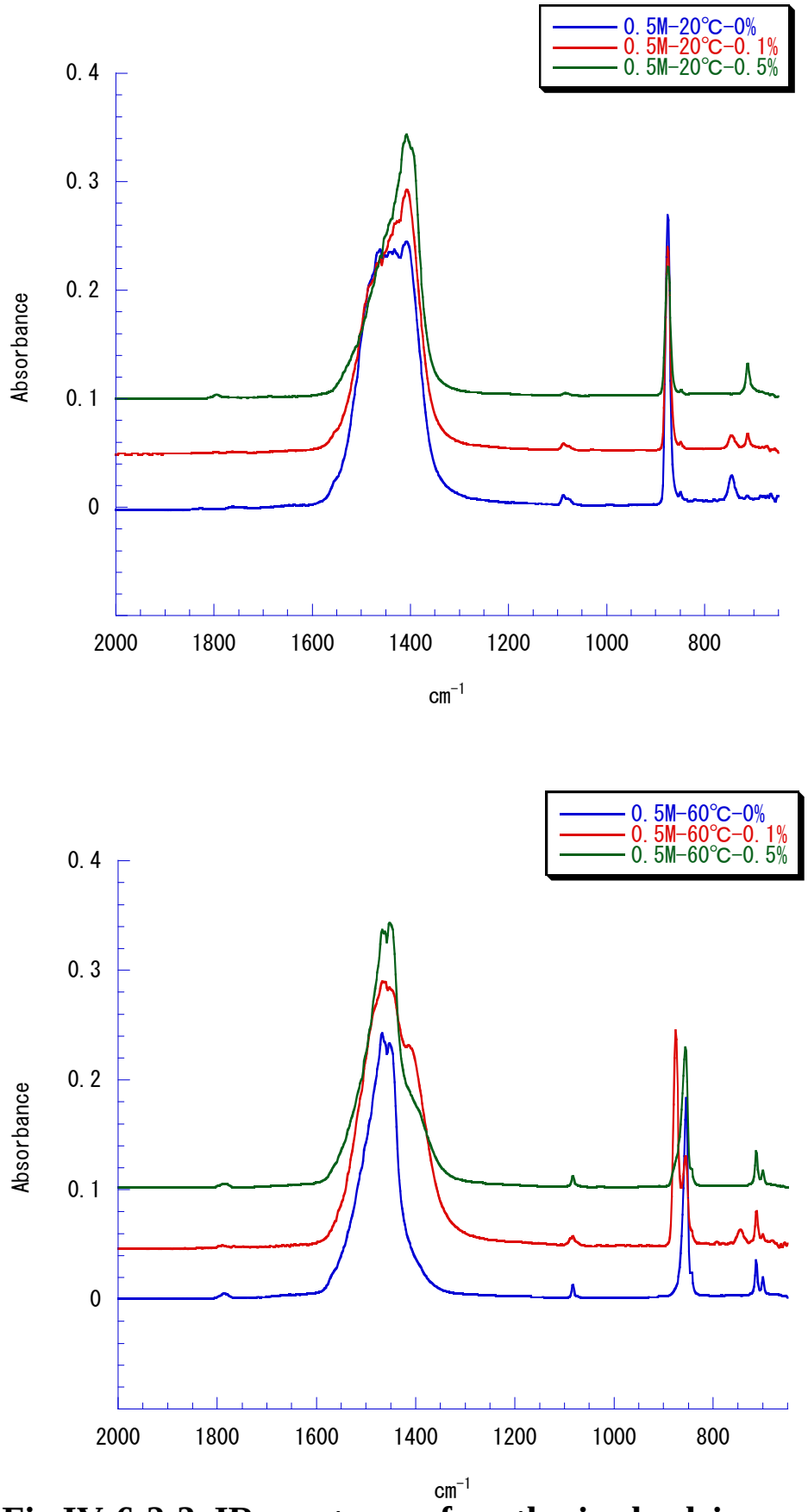

Fig.IV-6-2-3. IR spectrum of synthesized calcium carbonate

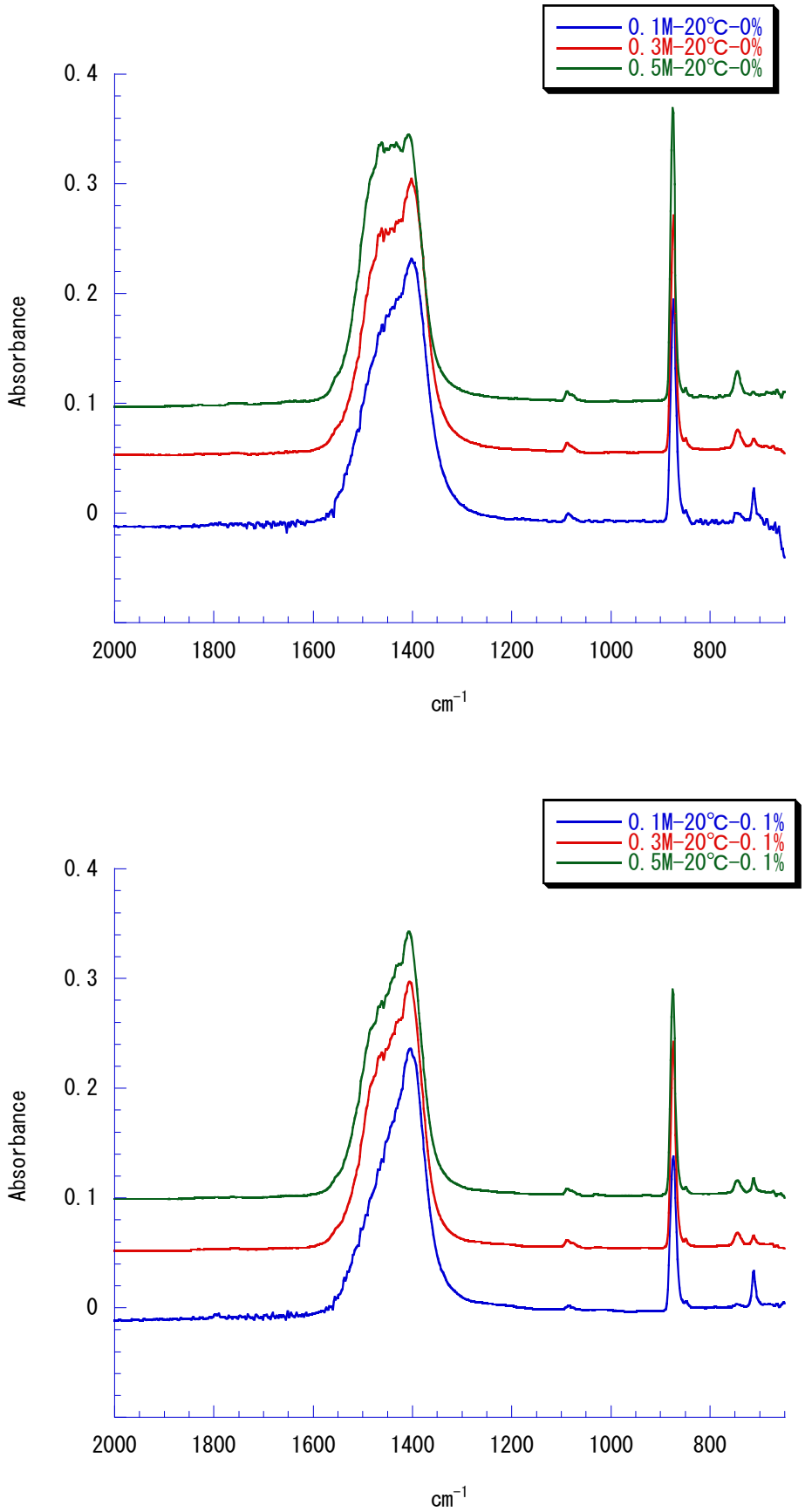

Fig.IV-6-2-4. IR spectrum of synthesized calcium carbonate

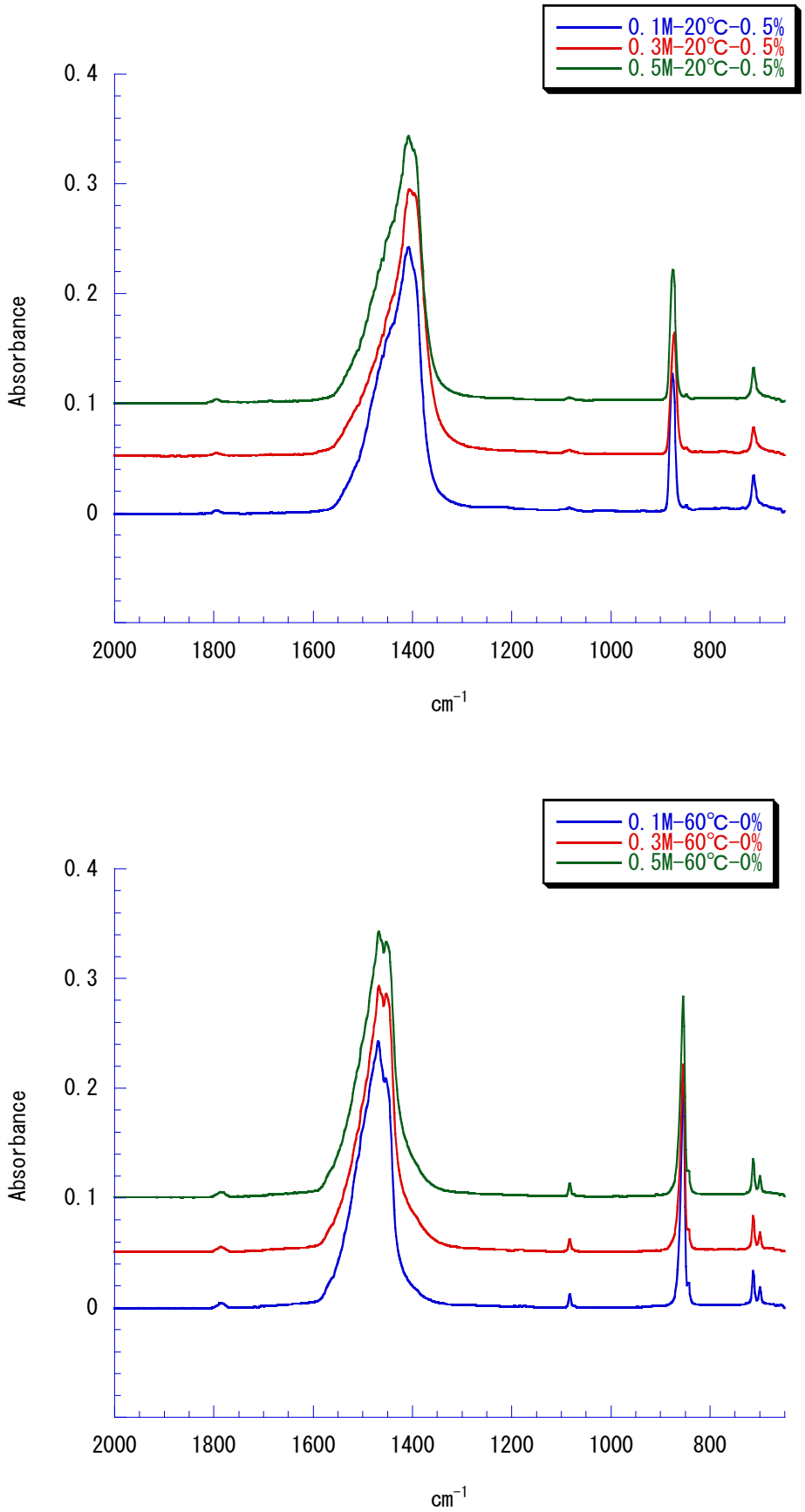

Fig.IV-6-2-5. IR spectrum of synthesized calcium carbonate

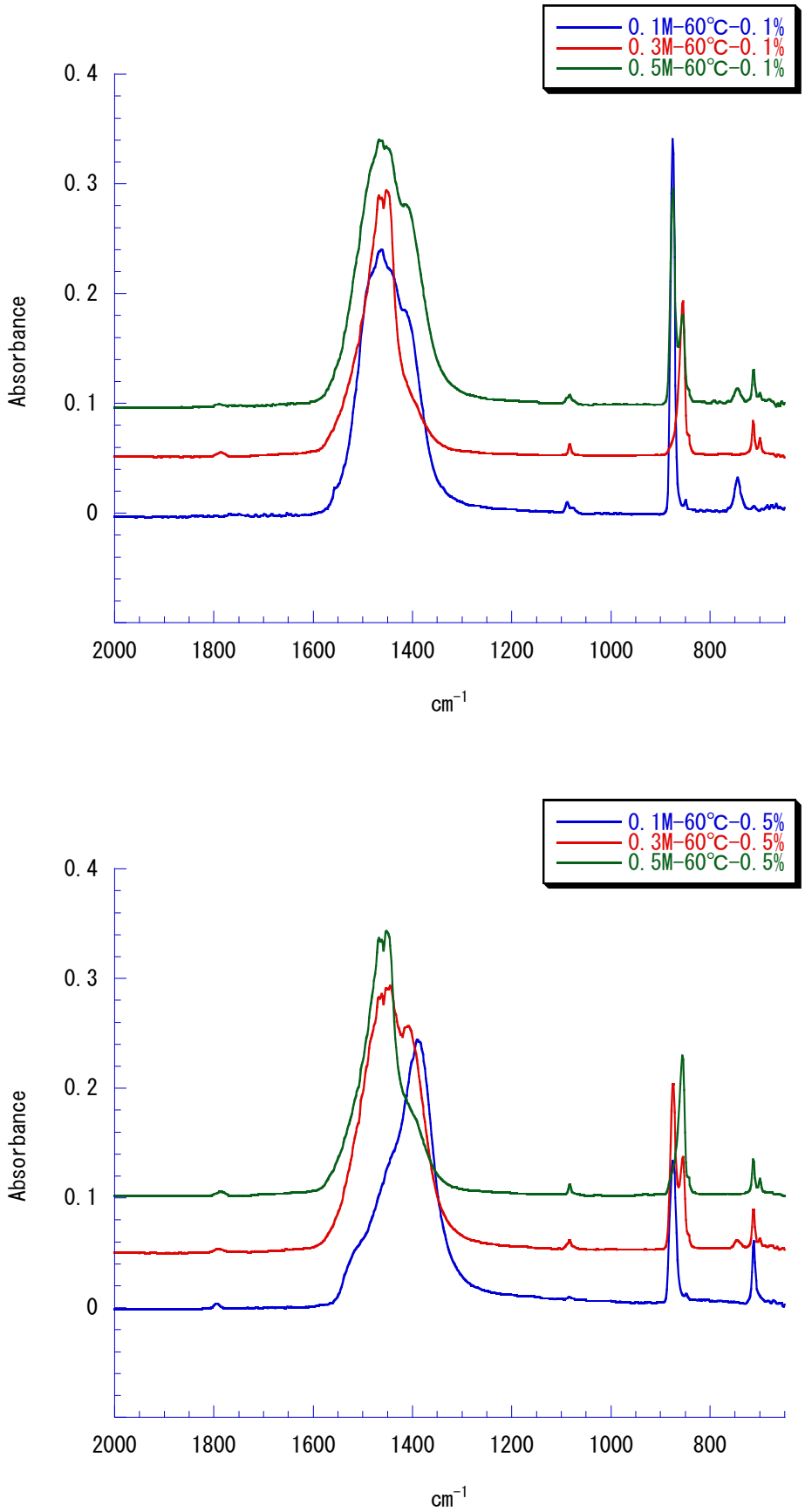

Fig.IV-6-2-6. IR spectrum of synthesized calcium carbonate

Chapter V

Synthesis of calcium carbonate vaterite crystals and effect of them on stabilization of suspension polymerization of MMA

V-1. Abstract

Spherical calcium carbonate vaterite crystals were synthesized and the effect of them on stabilization of suspension polymerization of methyl methacrylate was investigated. Suspension polymerization of methyl methacrylate could be stabilized with calcium carbonate vaterite crystals and sodium dodecyl benzene sulfonate of the concentrations from 25 ppm to 100 ppm. Poly (methyl methacrylate) beads coated with spherical calcium carbonate vaterite crystals were prepared. With increase in the concentration of sodium dodecyl benzene sulfonate from 25ppm to 100ppm, the amount of calcium carbonate vaterite crystals adhered on the surface of poly methyl methacrylate bead increased and the mean diameters of polymer beads decreased.

V-2. Introduction

In suspension polymerization, fine inorganic powders such as calcium carbonate, tricalcium phosphate, talc, magnetite, etc, have been used as a suspension stabilizer together with a surfactant [1, 2]. We have carried out suspension polymerization of styrene by adding various solid powders such as carbon black, magnetite, kaolin, sulfur and calcium carbonate, and reported that more hydrophobic solid powder made monomer droplets coalesce to agglomerate and hydrophilic solid powder stabilized suspension polymerization. Also, we have reported that needle-shaped aragonite of calcium carbonate stabilized suspension polymerization of styrene compared with cube-shaped calcite of calcium carbonate and resulted in polystyrene

beads with the smaller and more uniform size [3]. It is well known that the effect of solid powder on stabilization of emulsion is depending on the adhesion amount, the thickness of adhesion layer, the size and morphology of solid powder and so on. There are three types of calcium carbonate crystals, cube-shaped calcite, needle-like aragonite and spherical vaterite [5-15]. Recently we carried out suspension polymerization of MMA by adding spherical vaterite calcium carbonate as a stabilizer, and then prepared the hemispherical hollow silica microcapsules with different affinity surface by using spherical vaterite calcium carbonate as template [4]. In this work, it was found that the effect of vaterite calcium carbonate on stabilization of suspension polymerization of MMA strongly depended on the adhesion amount of vaterite calcium carbonate. To date, however, there are little investigations about the effect of spherical vaterite calcium carbonate crystals on stabilization of the liquid-liquid dispersion because of difficulty in synthesis and instability of vaterite crystals. The purpose of this work is to stably synthesize calcium carbonate vaterite crystals (CCVC) and to investigate in detail the effect of them on stabilization of suspension polymerization of methyl methacrylate (MMA).

V-3. Experimental

V-3-1. Materials

Calcium chloride and sodium carbonate, manufactured by Wako Pure Chemical Industries, Ltd., were used without purification. Methyl methacrylate (MMA), manufactured by Mitsubishi Rayon Co., Ltd.,

was used as received. Benzoyl per oxide (BPO) as an initiator was manufactured by Kawaguchi Chemical Co., Ltd. Sodium dodecylbenzenesulfonate (DBS) was manufactured by Nacalai Tesque, Inc. Ethanol, 1 N-hydrochloric acid, 1 N-sodium hydroxide and distillated water were all reagent-grade.

V-3-2. Measurement of surface tension and interfacial tension

The surface tension of DBS solution containing calcium carbonate ion of various concentrations and the interfacial tension between MMA containing 0.1mol/L of BPO and the DBS aqueous solution were measured by the Surface Tension Meter (Kyowa Interface Science Co., Ltd., KVBP-A3).

V-3-3. Measurement of ζ-potential

The ζ-potentials of MMA droplets and CCVC were measured by the Zeta potential analyzer (Otsuka Electronic Ltd., ELS-8000).

V-3-4. Determination of DBS concentration in the presence of calcium carbonate ion

The effect of calcium carbonate ion on the solubility of DBS was investigated. More specifically, the concentration of DBS in the presence of calcium carbonate ion was determined by HPLC.

V-3-5. Synthesis of calcium carbonate vaterite crystals

Calcium carbonate vaterite crystals (CCVC) were synthesized under the conditions specified in **Table V-1**. More specifically, 2.5 L

of 0.3 mol/L calcium chloride was put into a 5 L flange-type reaction flask kept at 293K, and the mixture was agitated at the impeller speed of 700 rpm with a 6-blade disk turbine under solution temperature of 293K. Then 2.5 L of 0.3 mol/L sodium carbonate solution kept at 293K was added into the flask at once, and the mixture was agitated at 700 rpm for 1 min. Thereafter the impeller speed was reduced to 500 rpm and agitation was continued for 19 min. On elapsing 20 min after addition of sodium carbonate, the impeller speed was further reduced to 300 rpm and the mixture was agitated for 40 min. After the completion of reaction, the mixture was filtrated under reduced pressure and then washed with 2 L of ion exchanged water. CCVC synthesized were then freeze-dried.

V-3-6. Suspension polymerization and preparation of PMMA beads coated with CCVC

Suspension polymerization of MMA was carried out under the conditions specified in **Table V-2**. More specifically, 250 ml of ion exchanged water containing the given amount of DBS was put into a 500 ml flange-type reaction flask with four baffles made of stainless plate. While the solution was agitated at the impeller speed of 150rpm with a 6-blade disk turbine under room temperature, nitrogen gas was introduced at 2 L/min for 30 min. After addition of a given amount of MMA and agitation at 150 rpm for 5 min, the given amount of CCVC slurry suspended in 20 ml of ion exchanged water was added into the flask and the mixture was agitated for 5 min. After this operation, the flask was heated to 343K and suspension polymerization was carried

out during 3 h. Then, the suspension was filtrated with a 200-mesh fabric filter to remove unadhered CCVC. Polymer beads coated with CCVC were then freeze-dried.

V-3-7. Characterization

V-3-7-1. IR and XRD analysis

Infrared absorption spectrum (IR) and X-ray diffraction (XRD) of the synthesized CCVC were analyzed to identify the crystal form and calculate the crystallinity.

V-3-7-2. Determination of amount of adhered $CaCO_3$

The amount of CCVC adhered onto the PMMA beads was determined by back titration with hydrochloric acid and sodium hydroxide according to the previous work [15]. More specifically, 10ml of 1 N-hydrochloric acid was added into 100 mg of polymer beads weighed to a precision of 0.1 mg, and the mixture was agitated by vibration for 3 h to dissolve the whole amount of CCVC adhered onto the PMMA beads. Then, after adding bromothymol blue indicator, back titration with 1N-sodium hydroxide was performed to determine the amount of CCVC adhered.

V-3-7-3. Observation of calcium carbonate vaterite crystals and polymer beads

CCVC and polymer beads were observed by using scanning electric microscope (model JSM-5800, JEOL Ltd).

V-4. Results and Discussion

V-4-1. Synthesis and characterization of calcium carbonate vaterite crystals

Figure V-1 shows the IR spectrum of CCVC synthesized at 293K, 313K and 333K. It is found that the absorbances of CCVC at 1400 and 2350 cm^{-1} disappear with increase in temperature from 293K to 333K because of transition from vaterite crystal to aragonite crystal.

Figure V-2 shows the XRD spectrum of CCVC synthesized at 293K, 313K and 333K. From this figure it is found that the signals of CCVC at 21°, 25° and 53° become weaker with increase in temperature because of the same reason as mentioned above. Further more, the proportion of crystal type from these XRD spectrum results was calculated. Namely, while the yield of vaterite crystal of ca. 92 % was obtained under the reaction temperature of 293K and 313K, the yield of aragonite crystal of ca. 92 % was obtained instead of vaterite crystal under the reaction temperature of 333K. The residue was calcite crystal of the yield of ca 7 % at every conditions.

Figure V-3 shows the SEM photographs of calcium carbonate synthesized at 293K, 313K and 333K. Calcium carbonate crystals synthesized at 293K and 313K are spherical, but needle at 333K. From these results, CCVC are found to be stably synthesized at the reaction temperature of 293K and 313K under the conditions adopted in this work.

V-4-2. Effect of CCVC on stabilization of suspension polymerization

In general, solid powder as particulate surfactant is known to stabilize the liquid-liquid dispersion by adhering on the surface of a droplet. And the degree of stabilizing effect is depending on the amount of solid powder adhered on a droplet, the thickness of adhesion layer, the zeta potential of solid powder adhered and so on.

In this work, suspension polymerization of MMA was not stabilized by addition of only CCVC. However, it is found that CCVC is able to stabilize suspension polymerization of MMA together with DBS of the concentrations from 20 ppm to 100 ppm. As the interfacial tension and the zeta potential may be affected by the DBS concentration, the amount of CCVC adhered may also be affected by the DBS concentration.

Figure V-4 shows the dependence of the amount (W_{ad}) of CCVC adhered on the DBS concentration (C_{DBS}). As the amount of CCVC adhered increases with the DBS concentration, the stabilizing effect becomes more effective. However, the stabilizing effect of CVCC may be insufficient at the DBS concentration less than 20 ppm because of lack of the amount of CVCC adhered. On the other hand, at the DBS concentration higher than 100 ppm, as the interfacial tension becomes very low (γ : 0) as shown in **Figure V-5**, the interface between monomer phase and the continuous water phase may become unstable and it may be hard for CCVC to adhere on the surface of a droplet. As a result, suspension polymerization may agglomerate.

V-4-3. Preparation of polymer beads coated with CCVC

Figure V-6 shows the SEM photographs of polymer beads prepared at each DBS concentration. From this figure, it is found that a PMMA bead is well coated with CCVC and these polymer beads are prepared under all the conditions with which suspension polymerization could be carried out. Furthermore, it is found that polymer beads are spherical and the adhesion amount of CCVC increases with the DBS concentration.

Figure V-7 shows the dependence of the mean diameters of polymer beads on the DBS concentration. The mean diameters are found to decrease with the DBS concentration and to be proportional to $C_{DBS}^{-0.11} \sim W_{ad}^{-0.42}$. In general, it is well known that there is a critical amount of solid powder required to stabilize the liquid-liquid dispersion. For example, the critical amount of tricalcium phosphate in suspension polymerization of styrene was 1.25×10^{-3} kg/m^2. From the results of **Figures V-4** and **V-7**, the critical amount of CCVC required to stabilize suspension polymerization of MMA is found to be 3.5 wt%-MMA monomer, namely 2.5×10^{-3} kg/ m^2.

Figure V-8 shows the dependence of the zeta potential of CCVC on the DBS concentration. The zeta potential is found to negatively increase with the DBS concentration. As with the DBS concentration, the adhesion amount of CCVC increase and the zeta potential of CCVC decrease, respectively, the mean diameters of polymer beads may decrease.

Figure V-9 shows the SEM photographs of the surface of polymer

beads after removing CCVC with the hydrochloric acid solution together with the results at 15 ml and 45 ml of MMA for comparison. From this figure, it is found that CCVC with the ca 5 μm diameter immersed about half into a PMMA bead. In general, when particulate surfactants adhere on the liquid-liquid interface, the depth of immersion of particulate into the interface depends on the contact angle and the interfacial tension. The relation between the depth of immersion (h) and the contact angle (θ) is shown as Eq. (1).

$$h = r\,(1+\cos\theta) \tag{1}$$

where r is the radius of particulate. If the contact angle is equal to 90°, the depth of immersion is equal to r. As the interfacial tension may change by the DBS concentration, the depth of immersion may change. Accordingly, as the thickness of the adhesion layer of CCVC is also changed by the DBS concentration, the stabilizing effect may be affected.

V-5. Conclusion

Calcium carbonate crystal was synthesized using calcium chloride and sodium carbonate at the temperature 293, 313 and 333K. Calcium carbonate vaterite crystals were found to be synthesized at the reaction temperature of 293K and 313K. Suspension polymerization of MMA was able to be stabilized with calcium carbonate vaterite crystals and DBS of the concentration from 20 ppm to 100 ppm. PMMA beads coated with calcium carbonate vaterite crystals ware prepared. The

amount of calcium carbonate vaterite crystals adhered increased with the DBS concentration and the diameters of polymer beads decreased with the adhesion amount.

REFERENCES

[1]M. Tanaka, K. Hayashi, Kagaku Kogaku Ronbunshu **15** (1989) 1144-1152

[2]Y. Taguchi, M. Tanaka, Kagaku Kogaku Ronbunshu **24** (1998) 603-608

[3]Y. Taguchi, K. Hosogai, M. Tanaka, Kagaku Kogaku Ronbunshu **25** (1999) 758-763

[4] K. Fuchigami, Y. Taguchi, M. Tanaka, Polym. Adv. Technol. **18** (2007) 1-7

[5]X. Zhang, Z. Zhang, Y. Yan, Journal of Crystal Growth **274** (2005) 550-554

[6]A.J. Xiea, Z.W. Yuana, Y.H. Shen, Journal of Crystal Growth **276** (2005) 265-274

[7]H. Tong, W. Ma, L. Wang, P. Wan, J. Hu, L. Cao, Biomaterials **25** (2004) 3923-3929

[8]J. Yua, X. Zhao, B. Cheng, Q. Zhang, Journal of Solid State Chemistry **178** (2005) 861-867

[9]A.J. Xie, Y.H. Shen, C.Y. Zhang, Z.W. Yuan, X.M. Zhu, Y.-M.

Yang, Journal of Crystal Growth **285** (2005) 436-443

[10]H. Wei, Q. Shen, Y. Zhao, D. Wang, D. Xu, Journal of Crystal Growth **260** (2004) 545-550

[11]H. Wei, Q. Shen, Y. Zhao, Y. Zhou, D. Wang, D. Xu, Journal of Crystal Growth **264** (2004) 424-429

[12]J. Yu, M. Lei, B. Cheng, X. Zhao, Journal of Solid State Chemistry **177** (2004) 681-689

[13]J. Yu, M. Lei, B. Cheng, Materials Chemistry and Physics **88** (2004) 1-4

[14]L. Xiang, Y. Xiang, Y. Wen, F. Wei, Materials Letters **58** (2004) 959-965

[15]J. Kawano, N. Shimobayashi, Mo Kitamura, K. Shinoda, N. Aikawa, J. Cryst. Growth **237** (2002) 419-423

Figure Captions

Fig. V-9-2. SEM photographs of composite particle surface after dissolving CCVC

Table Captions

Table V-1. Preparation of calcium carbonate vaterite crystal

Table V-2. Preparation of microparticles

Table V-1. Preparation of calcium carbonate vaterite crystal

Reaction solution	Volume
$CaCl_2$ 0.3mol/L	2.5L
Na_2CO_3 0.3mol/L	2.5L

Reaction condition ; 700rpm-1min at 293K, 500rpm-19min at 293K, 300rpm-40min at 293K

Table V-2. Preparation of microparticles

Ingredient	Quantity or concentration
DBS solution(ppm)	0, 25,50,75,100,200
MMA including 0.1mol/L of BPO(ml)	15, 30, 45
Vaterite crystal(g)	10

Reaction condition ; 3H at 343K with rotation speed at 150rpm

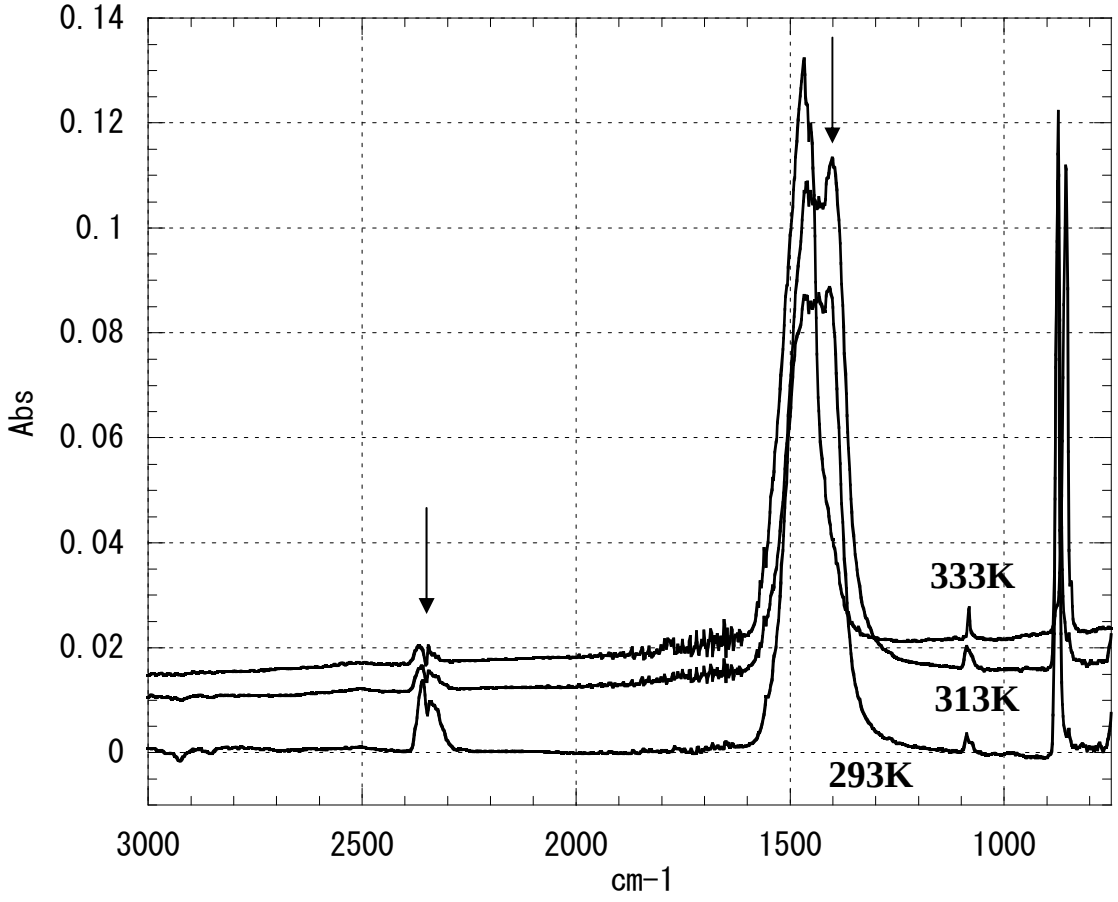

Fig. V-1. IR spectrum of CCVC synthesized at each temperature

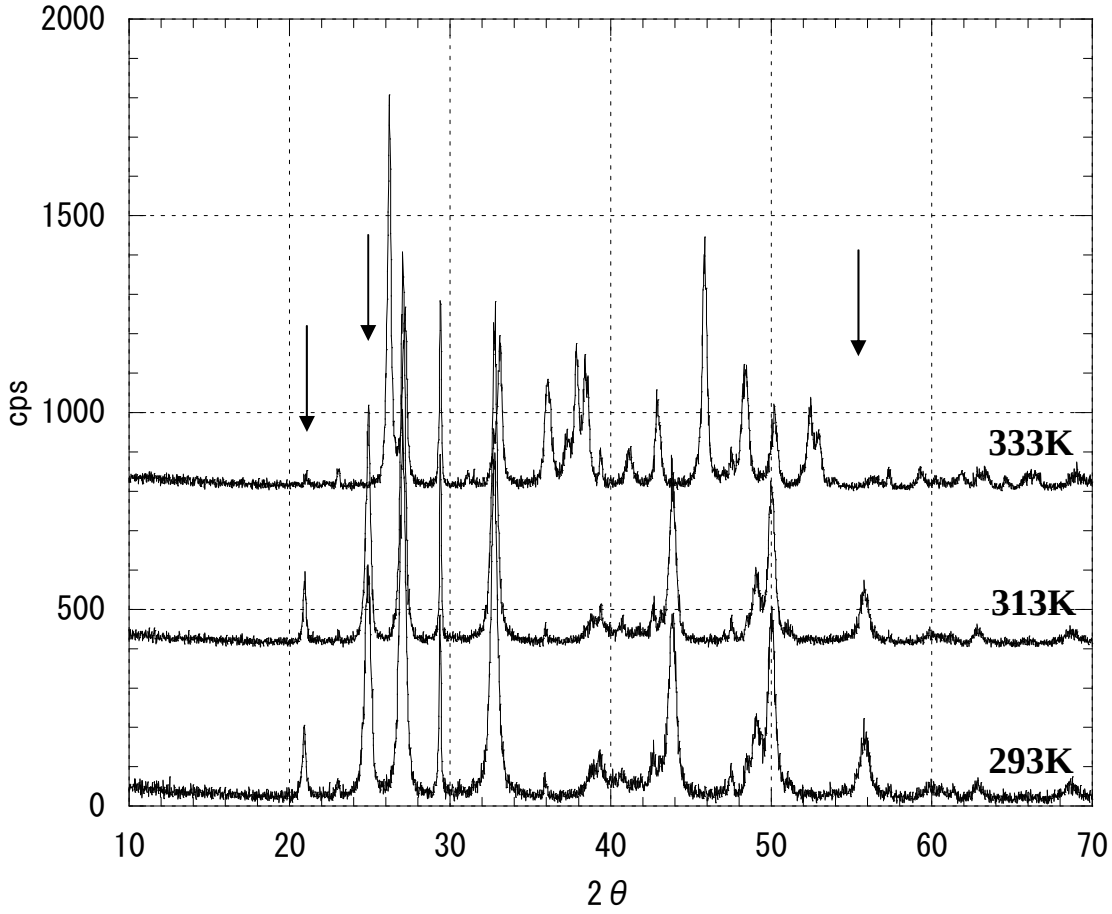

Fig. V-2. XRD spectrum of CCVC synthesized at each temperature

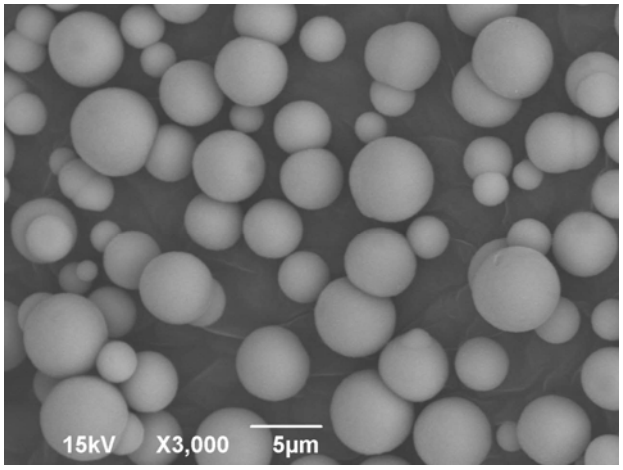

Reaction temp. at 293K

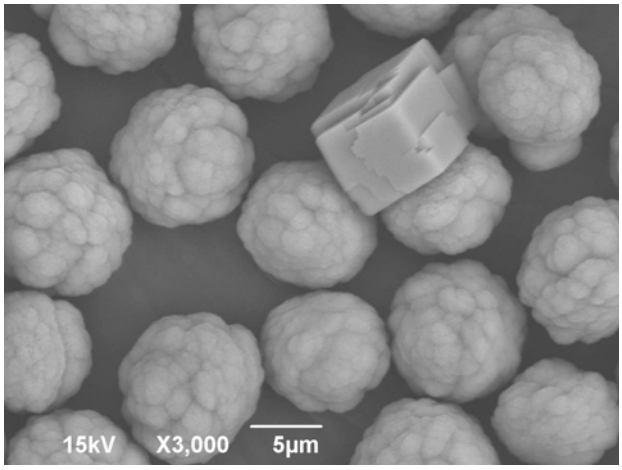

Reaction temp. at 313K

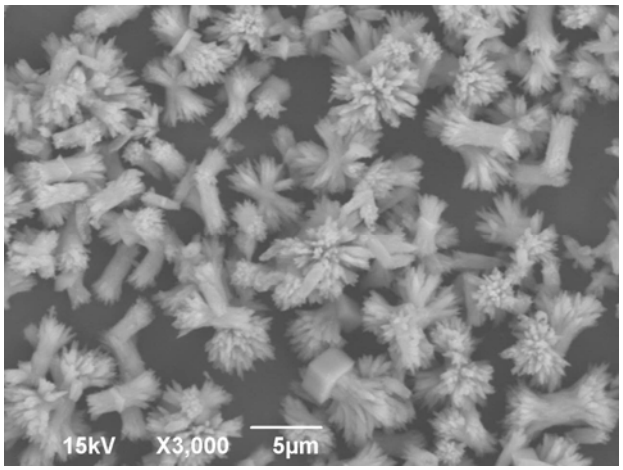

Reaction temp. at 333K

Fig. V-3. SEM photographs of CCVC synthesized at each temperature

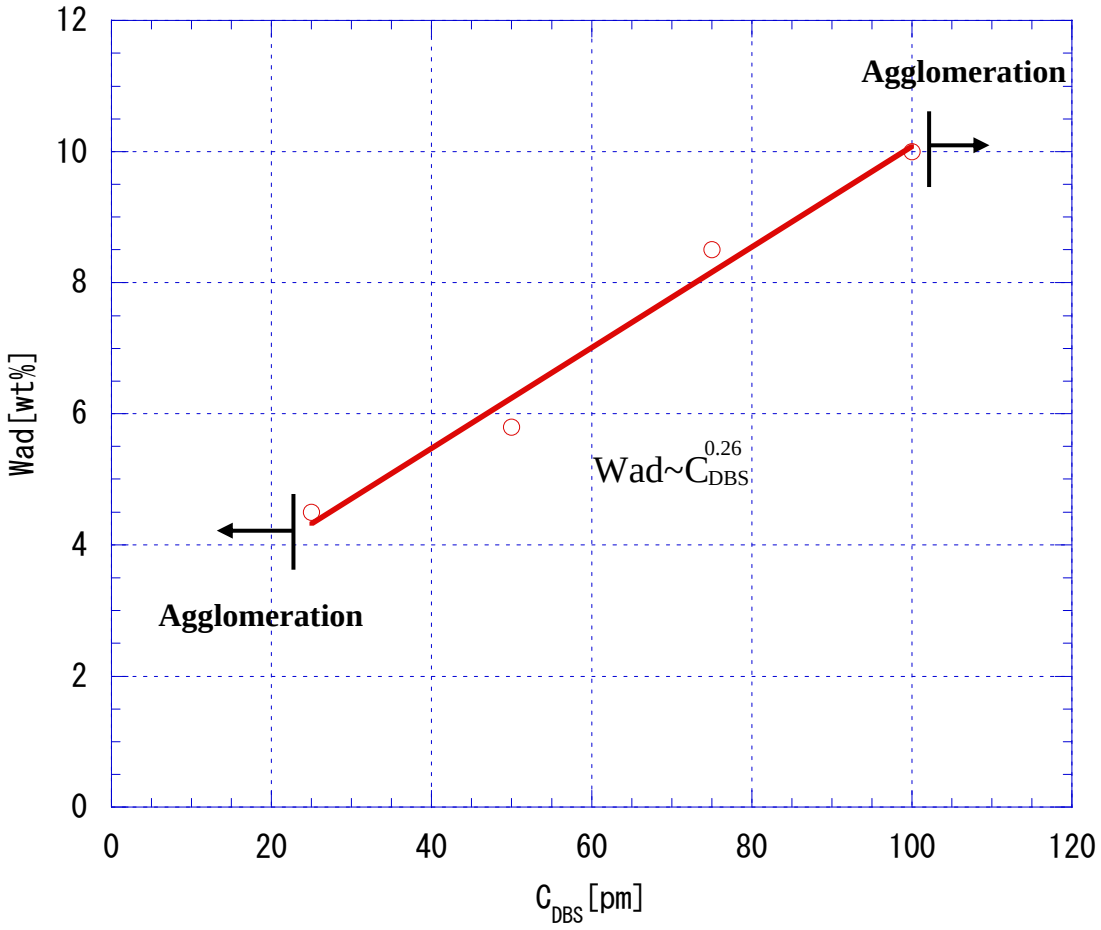

Fig. V-4. Dependence of adhesion amount of CCVC on DBS concentration

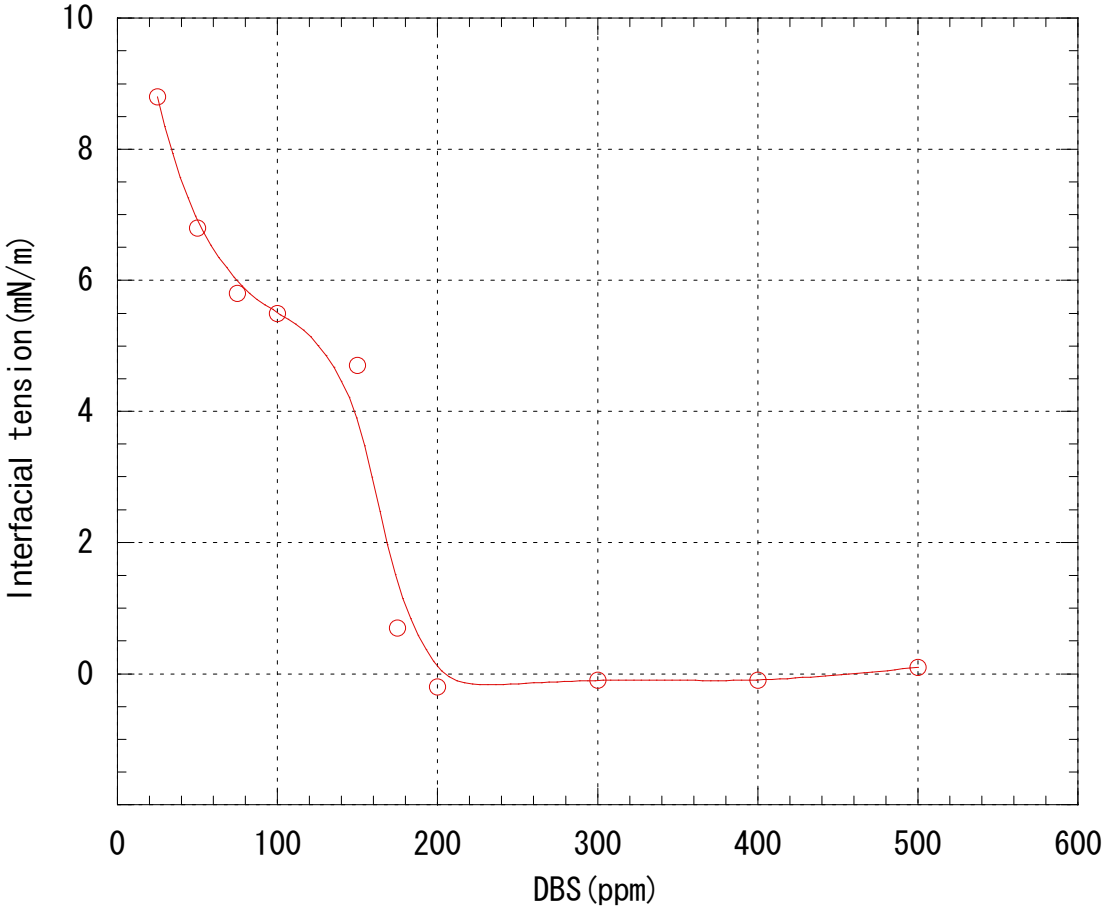

Fig. V-5. Dependence of interfacial tension between MMA and DBS solution

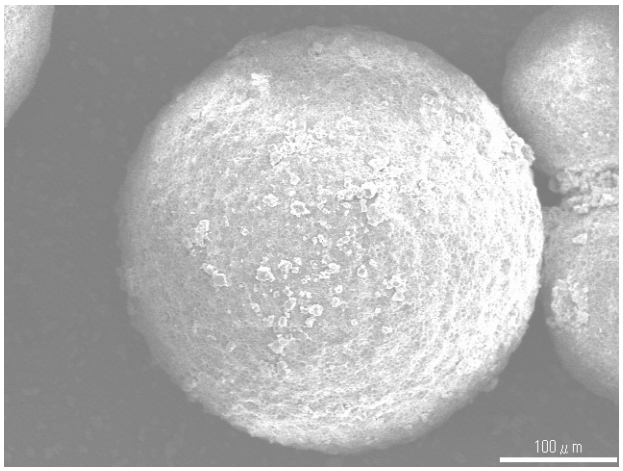

25ppm

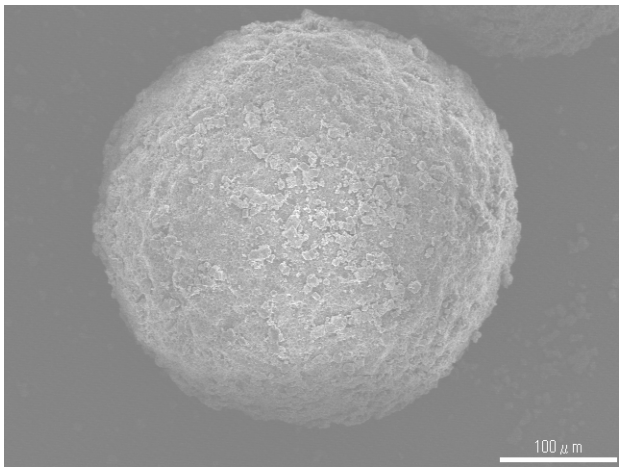

50ppm

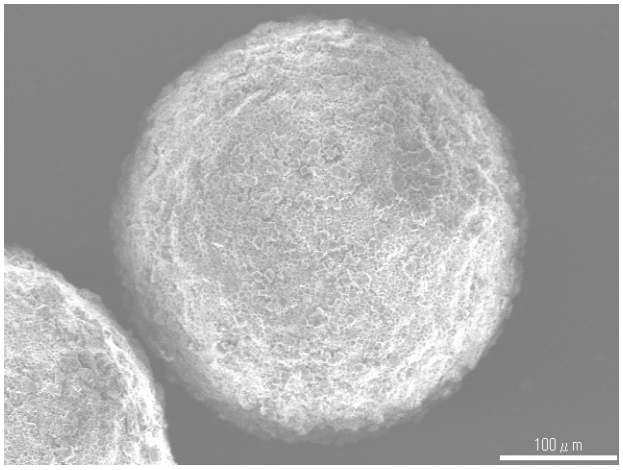

75ppm

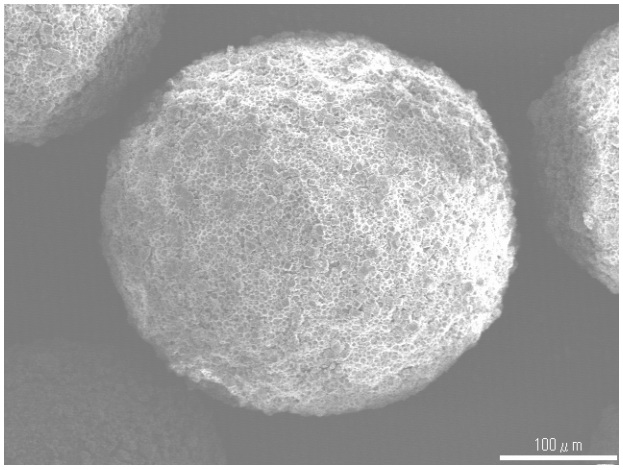

100ppm

Fig. V-6. SEM photographs of the composite particle

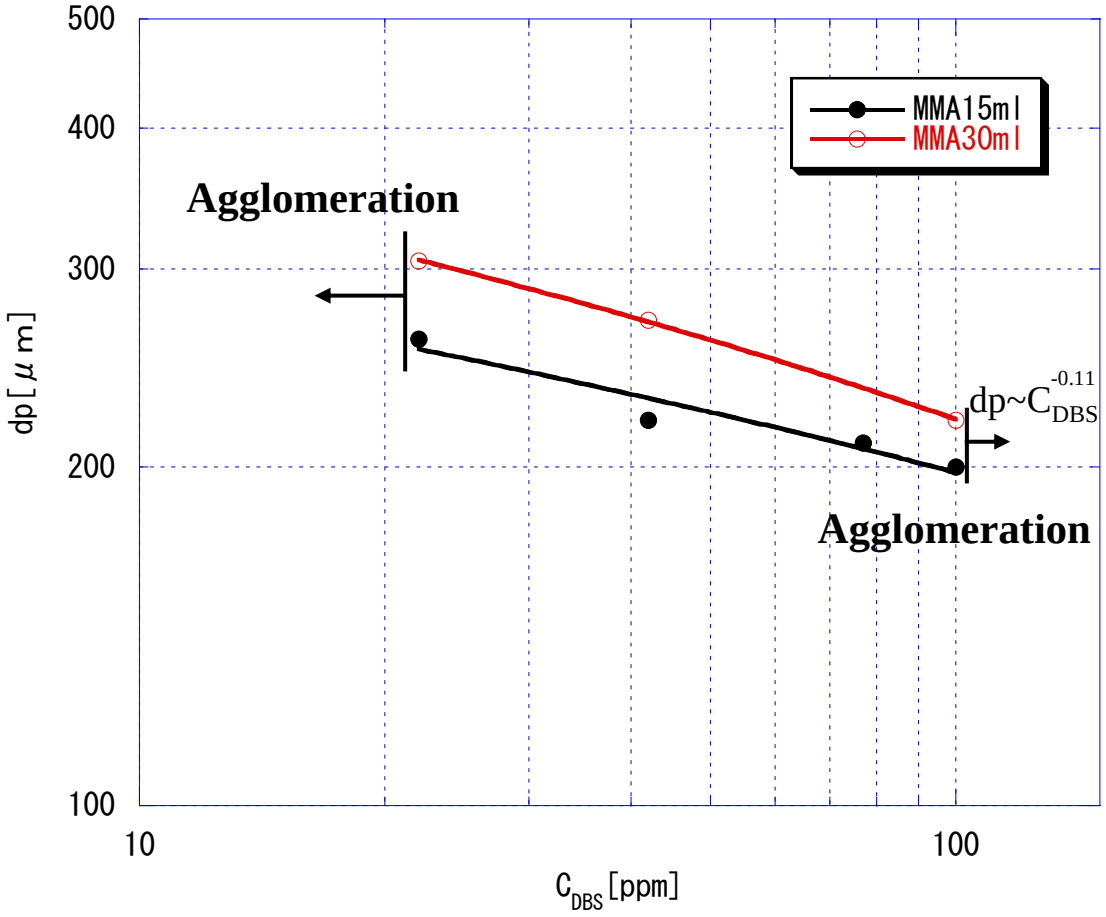

Fig. V-7. Dependence of mean diameters of composite particle on the DBS concentration

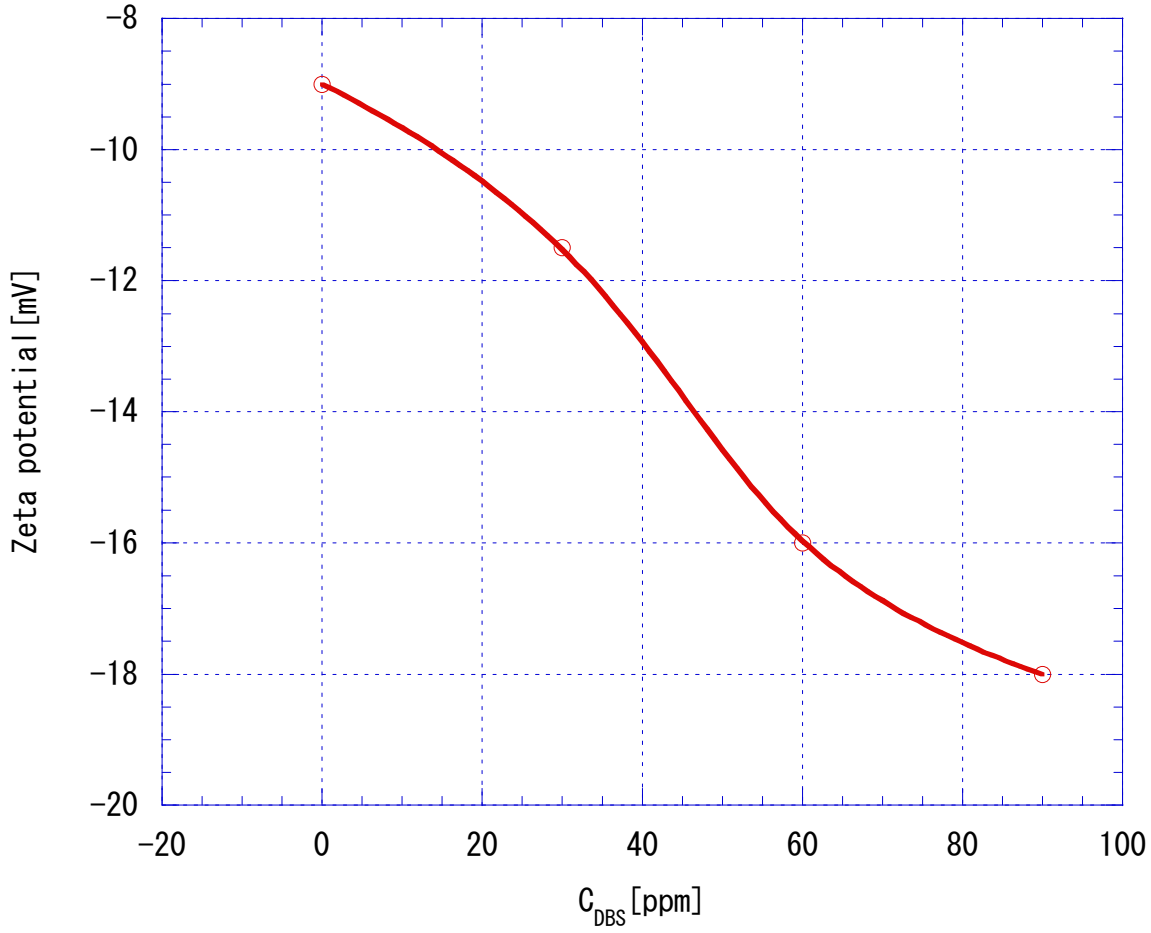

Fig. V-8. Dependence of ζ-potential of CCVC on the DBS concentration

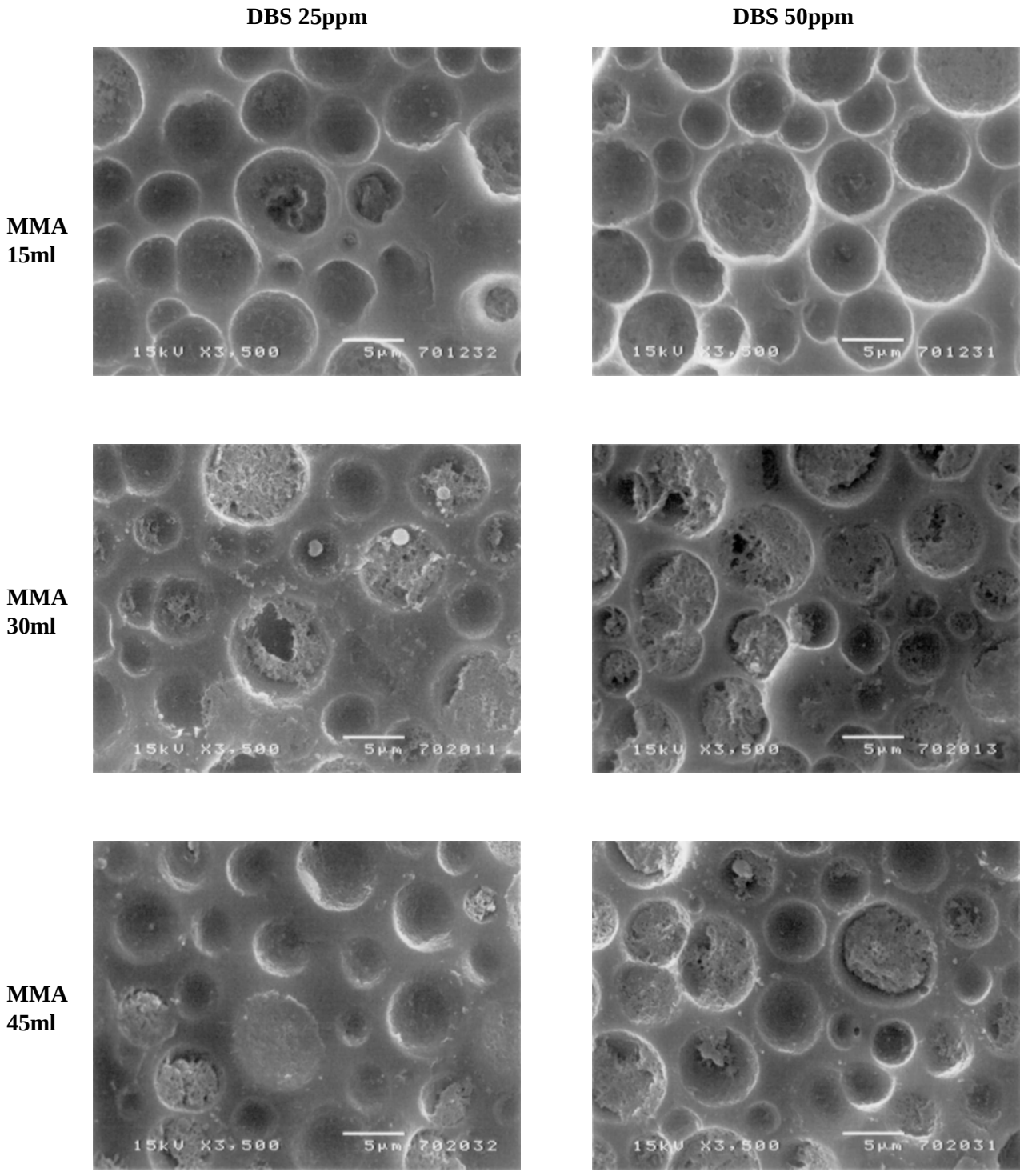

Fig. V-9-1. SEM photographs of composite particle surface after dissolving CCVC

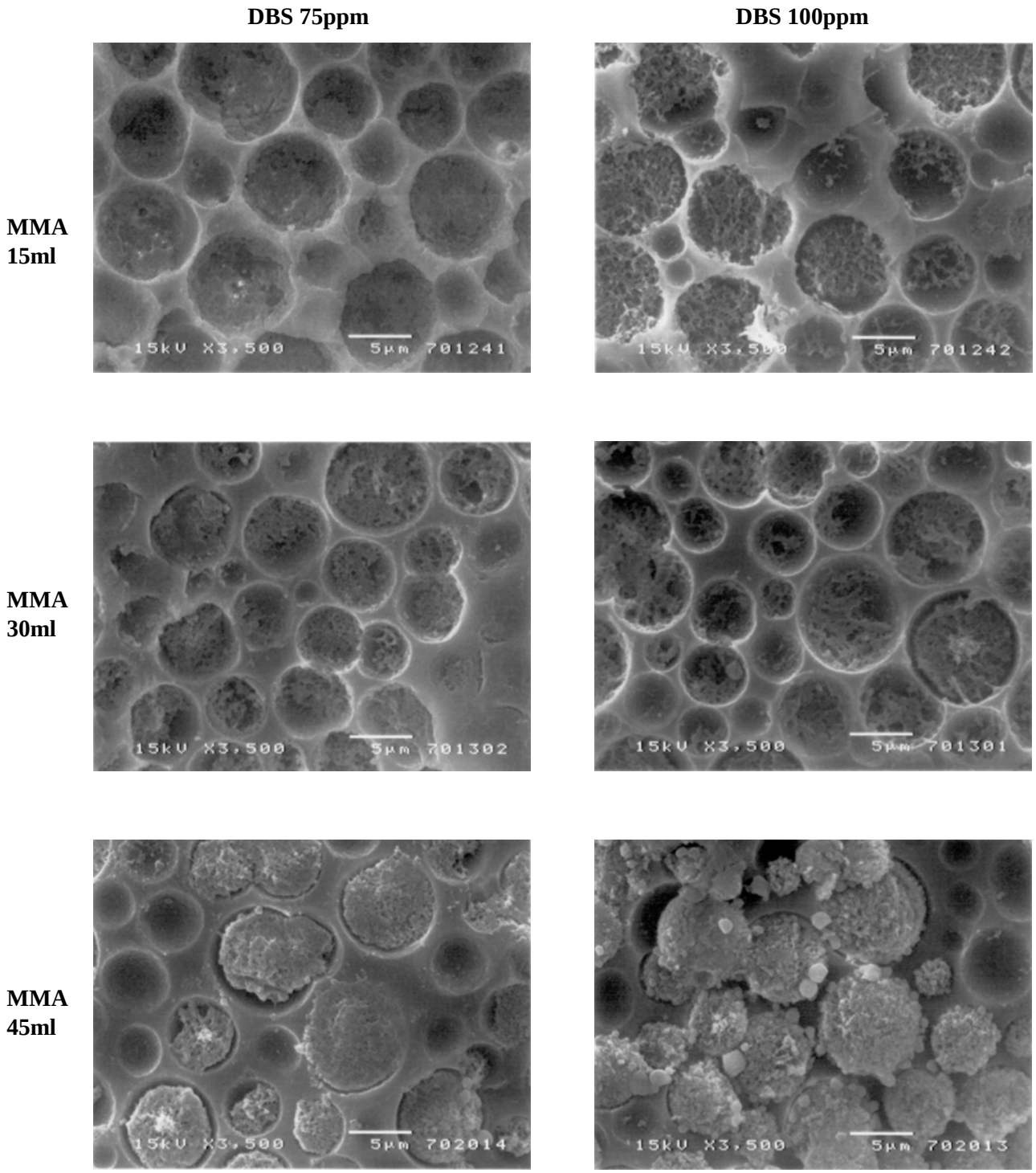

Fig. V-9-2. SEM photographs of composite particle surface after dissolving CCVC

Chapter VI

Synthesis of spherical silica particles by sol-gel method and application

VI-1. Abstract

Spherical silica was synthesized using the sol-gel method by hydrolyzing tetraethyl orthosilicate (TEOS) with an alkali catalyst, and its preparation conditions, i.e. the reaction temperature, concentration and dropping rate of the hydrolysis catalyst, were examined. Furthermore, the synthesized silica was doped with sodium fluoride to measure its ion release ability. The findings are as follows. There was a significant difference in the mean diameter of the synthesized silica particles in connection with the reaction temperature and dropping rate of the hydrolysis catalyst: the higher the reaction temperature was, the smaller the mean particle size was; and the slower the dropping rate was, the smaller mean particle size was obtained. The surface area of the synthesized silica particles was significantly different depending on the dropping rate of the hydrolysis catalyst: the faster the dropping rate was, the smaller the specific surface area became, which suggested that the dropping rate must be slower to obtain a porous particle structure. There were significant differences in the specific heat capacity and thermal reduction of the synthesized silica in association with the reaction temperature: the higher the reaction temperature was, the lower the specific heat capacity and thermal reduction were. When fluoride release was measured for two groups of fluoride-doped, synthesized silica particles of approximately equal diameter with different surface area, it was found that the fluoride retaining ability was proportional to the surface area of the particles. The fluoride ion release was

equilibrated at approx. 5 minutes for both groups. These results suggested that it was possible to control the particle porosity by manipulating the reaction conditions, such as the dropping rate of the catalyst and reaction temperature during the silica synthesis, providing spherical silica particles with various porosities and diameters. This can be applied to the release control of agents doped to silica.

VI-2. Introduction

It is known that metal alkoxides such as tetraethyl orthosilicate and aluminium isopropoxide are easily hydrolyzed into a polymer in the presence of acid or alkali: bulk gel is formed with an acid catalyst, while a spherical microparticle is formed with an alkali catalyst. Several previous studies reported the synthesis of the types of glass body, which had been difficult to prepare with the melting method: high-value added glass and ceramics were synthesized by hydrolyzing the combination of varied alkoxides [1-3]. Recently, more and more studies have introduced spherical microparticles synthesized with alkali hydrolysis catalysts and their application for liquid crystal spacers and so on [4-7]. In these studies, silanol groups are extremely unstable during the hydrolysis process and quickly polymerized with neighboring reaction groups such as silanol and thiol groups[18-48]. Focusing on such reactivity, the present study aimed to perform characterization of hollow silica synthesized with calcium carbonate used as a template [49]. As an example of its application, synthesized silica particles doped with fluoride were also

examined for their fluoride-releasing ability.

VI-3. Experimental

VI-3-1. Materials

Tetraethyl orthosilicate (TEOS), sodium hydroxide solution, and sodium fluoride, all manufactured by Nacalai Tesque, Inc., were used without refining. A buffer solution (TISAB-11, manufactured by TOA Denpa) was used for measuring fluoride ion release. Ethanol and distilled water used were reagent-grade.

VI-3-2. Preparation of silica particles by using sol-gel method

Silica particles were synthesized by the sol-gel method under the conditions specified in **TableVI-1**. More specifically, 180ml of ethanol and a given amount of TEOS were put into a 500ml flange-type reaction flask having a reflux cooling tube. While the flask content was being agitated with a 6-blade disk turbine at 150rpm, sodium hydroxide solution in multiple concentrations was delivered by drops into the flask. The dropping rates of the reactive catalyst employed were 10ml/h and 500ml/h, and the reaction temperature was set at 4 levels: 278, 298, 323 and 348K. The duration of reaction time was 10 hours from the completion of dripping of the reactive catalyst. After the reaction, the content was centrifuged at 5000rpm for 1 hour. The resultant silica particles were washed with 300ml each of ethanol and distilled water, and then freeze-dried.

VI-3-3. Preparation of silica particles containing sodium fluoride

Sodium fluoride was added to 2 groups of silica particles prepared according to the procedure described in 1-2 above, i.e. one group was obtained with 5 mmol of the reactive catalyst (NaOH) at the dropping rate of 10ml/h and the reaction temperature of 298K, while the other group was prepared with 3 mmol of NaOH at 500ml/h and 348K. One gram each from these two groups was dispersed into 100ml of 1wt% sodium fluoride solution, agitated for 24 hours at room temperature using a magnetic stirrer, and centrifuged at 5000rpm for 1 hour. The centrifuged silica particles, doped with sodium fluoride, were then freeze-dried.

VI-3-4. Characterization

VI-3-4-1. SEM observation of silica particles and measurement of particle size

Surface observation of the resultant spherical silica particles was performed using a scanning electron microscope (manufactured by JEOL). The particle diameter of approx. 500 particles was measured using an image processing software (WinROOF V5.0, Mitani Corporation) to obtain the mean diameter. For nano-order particles, which were beyond the limit of SEM observation, the measuring results provided by Photal PAR-III (Otsuka Electronics) were used.

VI-3-4-2. Measurement of surface area

The surface area of the synthesized silica particles was measured using Shimadzu Micromeritics Flow Sorb II 2300. More specifically,

the prepared silica particles placed in an adsorption tube were precisely weighed and flowed with the mixture of nitrogen and helium gas at a constant velocity while cooled with liquid nitrogen in order to obtain nitrogen adsorption in the surface and pores of silica particles. Then the tube was brought back to room temperature to measure the amount of nitrogen evaporated and calculate the surface area of silica particles per unit mass.

VI-3-4-3. Measurement of specific heat capacity

The specific heat capacity of the synthesized silica particles was measured using SEIKO DSC. More specifically, a precisely-weighed aluminium pan was heated up at a heating rate of 283K/min to measure its DSC. Likewise, the synthesized silica placed in the same pan was precisely weighed and heated up at a heating rate of 283K/min to measure its DSC. In both cases, sapphire was used as a reference material. The difference spectrum from the two DSC curves was determined to obtain the specific heat capacity of the silica particles.

VI-3-4-4. Measurement of thermal reduction (TG)

The thermal reduction of the synthesized silica particles up to 1123K was measured using SEIKO TG-DTA. More specifically, the synthesized silica particles in a platinum pan were precisely weighed and heated up at a heating rate of 283K/min to measure thermal reduction.

VI-3-4-5. Measurement of infrared ray absorption

The IR spectrum of the synthesized silica particles was measured using Shimadzu FT-IR.

VI-3-4-6. Measurement of sodium fluoride concentration

Fluoride release from the silica particles doped with sodium fluoride according to the procedures in 1-3 above was measured using TOA pH meter HM-30S. More specifically, 10ml of distilled water and 1.0ml of buffer solution TISAB-11 were added into 0.10g of sodium fluoride-doped silica, and fluoride ion strength was measured over time using a fluoride ion electrode F-125 and reference electrode HS-305DP (manufactured by TOA Denpa).

VI-4. Results and Discussion

VI-4-1. Results of morphological observation on silica particles

Mean particle size results are shown in **TableVI-2**. SEM images and mean diameter plots are shown in **Figures VI-1-1** to **VI-1-4** and **Figures VI-2-1** to **VI-2-3**, respectively. As indicated by these results, monodispersed silica particles were synthesized at the reaction temperature of 278K with the catalyst concentration of 1mmol regardless of the dropping rate, however, with 3 and 5mmol concentration of NaOH, the particles were broader at any dropping rate. At 298K, monodispersed particles were observed in all reaction systems except the 5mmol-500ml/h system, which showed the combination of large particles over 1.5μm and smaller 200nm particles. The 1mmol-10ml/h system exhibited finer particles

ranging from 100nm to 200nm, which were close to the observable limit with SEM. At 323K, all the 10ml/h systems showed submicron particles at any catalyst concentration, while the 500ml/h systems were relatively monodispersed particles. Finally at 348K, as in the case of 323K, the 10ml/h systems were also submicron particles at any catalyst concentration, and the 500ml/h systems showed even better monodispersity of the particles compared to those at 323K. Over all, the particle size was significantly different depending on the reaction temperature, catalyst concentration, and dropping rate. More specifically, the higher the reaction temperature was, the smaller the particle size became. Similarly, the slower the dropping rate was, the smaller the particle size became. As for the catalyst concentration, the higher the concentration was, the larger the particle diameter became, which was notable especially with the 500ml/h systems. These results suggested that the particle size was easily controllable by manipulating the reaction temperature, catalyst concentration, and dropping rate.

VI-4-2. Results of the surface area measurement

Surface area measurements are shown in **TableVI-3**, and these values are plotted in **Figures VI-3-1**, **VI-3-2**, and **VI-3-3**. As indicated by the results, there was a significant difference in the surface area in connection with the dropping rate of the catalyst, i.e. the reaction systems at the 10ml/h-dropping rate had a significantly larger surface area except when the reaction temperature was 278K. As for the systems at 278K, the surface area between the two dropping

rates was not significantly different, but unlike the systems at other temperature settings, the higher the reactive catalyst concentration was, the larger surface area was obtained. This phenomenon was significant, especially for the 10ml/h system, showing an increase of the surface area with an increase in the concentration of the reactive catalyst, despite the increase in the mean particle diameter. This clearly indicated the formation of porous particle structure. Additionally, two groups of silica particles, obtained under the two different reaction conditions (one at the 5mmol-10ml/h-298K setting, and the other at the 3mmol-500ml/h-348K setting) had an approximately equal mean diameter (820nm and 726nm), but obtained different surface area (59.6m^2/g and 11.3 m^2/g), which suggested substantially different porosity between the two.

VI-4-3. Results of the specific heat capacity measurement

Specific heat capacity measurements are shown in **TableVI-4**, and these values are plotted in **Figures VI-4-1**, **VI-4-2**, and **VI-4-3**. As apparent from the results, a significant difference in the specific heat capacity was observed in connection with the reaction temperature: the higher the reaction temperature was, the lower the specific heat capacity became. There was a positive correlation between the specific heat capacity and thermal reduction (TG) as described later. A positive correlation between the surface area and TG was also confirmed. Thus it can be considered that there is a positive correlation between the specific heat capacity and surface area. When air density is 1.024Kgm^{-3} (920hPa, 37ºC, relative humidity of

50%), the specific heat under constant pressure (CP) for air is 1.007 $\times 10^{-3}$J/(g・K) (920hPa, 310K), while that for silica glass is 0.815 $\times 10^{-3}$J/(g・K). It was considered that the high specific heat capacity observed in the synthesized silica with a large surface area was due to its porous structure, which enables more air to be trapped in the pores.

VI-4-4. Results of the thermal reduction (TG) measurement at 1123K

Thermal reduction (TG) measurements are shown in **TableVI-5**, and the values are plotted in **Figures VI-5-1**, **VI-5-2**, and **VI-5-3**. It was assumed from the results that there was a positive correlation between the surface area and TG as mentioned in 2-3 above: the thermal reduction measured here was the sum of the silanol groups withdrawn from both the silica surface and pores formed during the synthesis of silica.

VI-4-5. Results of the infrared ray absorption measurement

Infrared ray absorption measurements are plotted in **Figures VI-6-1**, **VI-6-2**, and **VI-6-3**. As indicated by these charts, infrared absorption was observed in virtually entire silica except for the slight absorption by tetraethyl orthosilicate, a starting material of silica synthesized. Thus it was confirmed that the thermal reduction described in 2-4 above was mainly from the silanol groups.

VI-4-6. Results of the sodium fluoride concentration measurement

Sodium fluoride concentration measurements are shown in

TableVI-6, and the values are plotted in **Figure VI-7**. The results showed that fluoride retaining ability of two groups of silica particles of approximately equal diameter was proportional to the surface area: the difference of retaining ability between the two groups was 5-fold. The fluoride ion release was equilibrated at approx. 5 minutes for both groups. These results suggested that it was possible to control the particle porosity by manipulating the reaction conditions, such as the dropping rate of the catalyst and reaction temperature during the silica synthesis.

VI-5. Conclusion

Spherical silica was synthesized using the sol-gel method by hydrolyzing tetraethyl orthosilicate (TEOS) with an alkali catalyst, and its preparation conditions, i.e. the reaction temperature, concentration and dropping rate of the hydrolysis catalyst, were examined. At this moment, The hydrolysis reaction of silicone alkoxide with alkaline catalyst is a nucleophilic substitution reaction where OH^- ions are involved. The alkoxyl group that is adjacent to the generated silanol group is easily subjected to a nucleophilic substitution by water, with the electrons attracted from silicon elements to the silanol group. Meanwhile, the dehydration polycondensation reaction is initiated by the proton abstraction from the silanol group by the OH^- ions. More specifically, the reaction proceeds as a result of the nucleophilic attack on the remaining silicon elements by the generated bare $Si\text{-}O^-$. In this study, it is conceivable that both the hydrolysis reaction resulting from the electrophilic

substitution reaction with protons and the polycondensation reaction initiated by OH^- ions proceed slowly under the reaction conditions at the low catalyst concentration and slow dropping rate, thereby resulting in the synthesis of almost the same sized particles without being greatly affected by the reaction temperature. Additionally, it is also conceivable that the particle size became large at the fast catalyst dropping rate because polycondensation proceeds slowly at the low reaction temperature due to the higher catalyst concentration resulting from the fast dropping rate. At the high reaction temperature, on the other hand, the particle size became small since the generated silanol group was considered to be rapidly polycondensed, with TEOS being consumed to complete the particle growth. Furthermore, the synthesized silica was doped with sodium fluoride to measure its ion release ability. The findings are as follows:

1. There was a significant difference in the mean diameter of the synthesized silica particles in connection with the reaction temperature and dropping rate of the hydrolysis catalyst: the higher the reaction temperature was, the smaller the mean particle size was; and the slower the dropping rate was, the smaller mean particle size was obtained.

2. The surface area of the synthesized silica particles was significantly different depending on the dropping rate of the hydrolysis catalyst: the faster the dropping rate was, the smaller the specific surface area became, which suggested that the dropping rate must be

slower to obtain a porous particle structure.

3. There was a significant difference in the specific heat capacity of the synthesized silica in association with the reaction temperature: the higher the reaction temperature was, the lower the specific heat capacity was.

4. There was a significant difference in the thermal reduction of the synthesized silica in association with the reaction temperature: the higher the reaction temperature was, the lower thermal reduction was.

5. When fluoride release was measured for two groups of fluoride-doped, synthesized silica particles of approximately equal diameter with different surface area, it was found that the fluoride retaining ability was proportional to the surface area of the particles, i.e. the difference of retaining ability between the two groups was 5-fold. The fluoride ion release was equilibrated at approx. 5 minutes for both groups. These results suggested that it was possible to control the particle porosity by manipulating the reaction conditions, such as the dropping rate of the catalyst and reaction temperature during the silica synthesis.

REFERENCES

[1] S. Sakka “Gel method for making glass”, in TREATISE ON MATERIALS SCIENCE AND TECHNOLOGY. VOL22 Glass Ⅲ, M. Tomozawa, R. H. Doremus ed, Academic Press, P,129 (1982)

[2] Z. Deng, E. Breval and C. G. Pantano “Colloidal sol/gel processing of ultra-1ow expansion TiO_2/SiO_2 glasses” J. Non-Cryst, Solids, **100**, 364 (1988)

[3] H. Dislich “New routes to multicomponent oxide glasses” Angew. Chem. Int. Ed., **10**, 363 (1971)

[4] M. Yamane, S. Inoue and A. Yasumori “Sol-gel trandition in the bydrolysis of siliconmethoxide” J. Non-Cryst. Solids, **63**, 13 (1984)

[5] B. E. Yoldas “Formation of titania-silica glasses by low temperature chemical polymerization” J. Non-Cryst. Solids, 38-39, **81** (1980)

[6] M. Yamane, S. Inoue and K. Nakazawa “Preparation of gels to obtain glasses of high homogeneity by low temperature synthesis” J. Non-Cryst. Solids, **48**, 153 (1982)

[7] M. Yamane, H. Kawazoe, A. Yasumori and T. Takahashi “Preparation of Pb-containing glass by sol-gel prosess” J. Non-Cryst. Solids, **99**, 160 (1988)

[8] I. Schwartz, P. Anderson, H. de Lambilly and L. C. Klein “Stability of lithium silicate gels” J. Non-Cryst. Solids., **83**, 391 (1986)

[9] A. Yasumori and M. Yamane “Preparation of Na_2O-SiO_2 glasses in the metastable immiscibility region” J. Non-Cryst. Solids, **82**, 177 (1986)

[10] M. Yamane and T. Kojima “Low temperature synthesis of Non-Crystalline Solids of the system SrO-SiO_2” J. Non-Cryst. Solids, **44**, 181 (1981)

[11] T. Hayashi and H. Saito “Preparation of CaO-SiO2 glasses by the gel-method” J. Mat. Sci., **15**, 1971 (1980)

[12] M. Yamane, H. Kawazoe, A. Yasumori and T. Takahashi :”Gradient-index glass rods of PbO-K_2O-B_2O_3-SiO_2 system prepared by the sol-gel process,” J. Non-Cryst. Solids, **100**, 506 (1988)

[13] B. Fegley, Jr. and E. A. Barringer “Synthesis, Characterization and Processing of Monosize Ceramic Powders” Better Ceramics Through Chemistry, (North Holland NY 1984) ppl87-197.

[14] Y. Oguri and E. Hattori “Preparation of Translucent SiO2 Glass from Monosized Particles” Ceramic Transaction. Vol 1, Part B, Ceramic Powder Science, American Ceramic Soc. (1988) pp701-708

[15] E. M. Tory, B. H. Church. M. K. Tam and M. Ranter “Simulated Random Paking of Equal Spheres” Can. J. Chem. Eng., **51** [8] 484-493 (1973)

[16] E. A. Barringer and H. K. Bowen “Formation, Packing and Sintering of Monodisperese TiO2 Powder” J. Am. Ceram. Soc., 65 (12) C119-21 (1982)

[17] Y. Oguri, R. E. Riman and H. K. Bowen “Processing of Anatase Prepared from Hydrothermally Treated Alkoxy-derived Hydrojus Titania” J. Mat. Sci., **23** 2897-2904 (1988)

[18] M. Yamane, S. Inoue and A. Yasumori “Sol-gel transition in the hydrolysis of silicon methoxide”, J. Non-Cryst. Solids, **63**, 13 (1984)

[19] C. J. Brinker, K. D. Keefer, D. W. Schaefer and C. S. Ashley “Sol-gel transition in simple silicates”, J. Non-Cryst. Solids, **48**, 47 (1982)

[20] C. J. Brinker, K. D. Keefer, D. W. Schaefer, R. A. Assink, B. D. Kay and C. S. Ashley “sol-gel transition in simple silicates Ⅱ”, J. Non-Cryst. Solids, **63**, 45 (1984)

[21] T. Kawaguchi, H. Hishikura, J. Iura and Y. Kokubu “Monolithic dried gels and silica glass prepared by the sol-gel process”, J. Non-Cryst. Solids, **63**, 61 (1984)

[22] S. Wallace and L. L. Hench “The prccessing and characterization of DCCA modified gel-derived silica”, Mater. Res. Soc. Symp. Proc., 32, 47 (1984)

[23] G. Orcel and L. L. Hench “Effects of formamide additive on the chemistry of silica sol-gels”, J. Non-Cryst. Solids, **79**, 177 (1986)

[24] G. Orcel, J. Phalippou and L. L. Hench “Structural changes of silica xerogels during low temperature dehydration”, J. Non-Cryst. Solids, **88**, 114 (1986)

[25] T. Adachi and S. Sakka “The role of N. N - dimethylformamide, a DCCA, in the formation of silica gel monoliths by sol-gel method”, J. Non-Cryst. Solids, **99**, 118 (1988)

[26] T. Adachi and S. Sakka “Sintering of silica gel derived from the alkoxysilane solution containing N, N – dimethylformamide”, J. Non-Cryst Solids, **100**, 250 (1988)

[27] K. D. Keefer : The effect of hydrolysis conditions on the structure and growth of silicate polyners, “Better ceramics through chemistry.” Edited by C. J. Brinker, D. E. Clark and D. R. Ulrich. North-Holland, New York, 15 (1984)

[28] H. Schmidt, H. Scholze and A. Kaiser “Principles of hydrolysis and condensation reaction of alkoxysilanes”, J. Non-Cryst. Solids, **63**,

1 (1984)

[29] A. Yasumori, M. Yamane and T. Kawaguchi “Effects of temperature and time on the structural evolution of alkoxy-derived silicagel” “Ultra structure processing of advanced ceramics”, Edited by J. D. Mackenzie and D. R. Ulirch. John Wiley, New York, Chapter 15 (1988)

[30] A. Yasumori, H. Kawazoe and M. Yamane “The structural evolution of alkoxy derived gel during drying”, J. Non-Cryst. Solids, **100**, 215 (1988)

[31] M. F. Lappert and G. J. Leigh : "Development in Inorganic Polymer Chemistry", Elsevier Publishing Company (1962) : H. R. Allcock : "Heteroatom Ring Systems and Polymers", Academic Press (1967)

[32] K. A. Andrianov : "Metalorganic Polymers", Interscience Publishers (1965)

[33] Y. Abe and T. Misono, “Preparation of Polysiloxanes from Silicic Acid. II. Esterification of Silicic Acid with Various Alcohols and Isolation of Esterification Products by Silylation” J. Polym. Sci. Polym. Lett. Ed., **20**, 205 (1982)

[34] Y. Abe and T. Misono, “Preparation and Properties of

Polysilicic Acid Butyl Esters", J. Polym. Sci. Polym. Chem. Ed., **21**, 41 (1983)

[35] Y. Abe, T. Sekiguchi and T. Misono "V. Condensation of Silicic Acid Butyl Esters and Formation of Silica Fiber from the Ester Solution", J. Polym.Chem. Ed. , **22**, 761 (1984)

[36] Y. Abe and T. Misono "VI. Formation of a Gel like Silica Glass from Silicic Acid", J. Polym. Sci. Polym. Lett. Ed., **22**, 565 (1984)

[37] Y. Abe, N. Shintani and T. Misono "VII. Effect of the Degree of Esterification and Alkyl Group on Condensation of Silicic Acid Esters and Formation of Fibrous Silica", J. Polym. Sci. Polym. Chem. Ed., **22**, 3759 (1984)

[38] Y. Abe, N. Shintani, T. Magome and T. Misono "VIII. A polysiloxanes with a Good Spinnability", J. Polym. Sci. Polym. Lett. Ed., **23**, 497 (1985)

[39] Y. Abe, A. Kaijou, N. Shintani, Y. Nagao and T. Misono "IX. Partially Silylatd Silicic Acid and its Spinnability", J. Polym. Sci. Polym. Chem. Ed., **25**, 1567 (1987)

[40] Y. Abe, A. Kaijou. Y. Nagao and T. Misono "X. Preparation and Properties of Allyldimethyl-silylated Silicic Acid", J. Polym. Sci. Polym. Chem. Ed.. **26**, 419 (1988)

[41] Y. Abe, T. Gunj, M. Hikita. Y. Nagao and T. Misono “Preparation of $Si0_2$-$Ti0_2$ Fibers from Polytitanosiloxanes”, Yogyo Kyokai-Shi, **94**, 1243 (1987)

[42] Y. Abe. N. Sugimoto, Y. Nagao and T. Misono “Preparation of A Gel-Like Silica Glass by the Condensation of Silicic Acid in Organic Solvents”, Yogyo Kyokai-Shi, **95**, 672 (1987)

[43] Y. Abe, N.Sugimoto, Y. Nagao and T. Misono “A New Method for Preparing Monolithic Gels as Precursor for MxOy and SiO_2-MxOy Glass (M=Al, Ti, Zr) of an Arbitrary Composition”, Yogyo Kyokai-Shi, **95**, 1l41 (1987)

[44] Y. Abe, T. Gunji, Y. Kimata, Y. Nagao and T. Misono “Preparation of SiO_2-Al_2O_3 and SiO_2-ZrO_2 Fibers from Polyaluminosiloxanes and Polyzirconosiloxanes”, Seramikku Ronbunshi, **96**, 221 (1988)

[45] Y. Abe, N. Sugimoto, Y. Nagao and T. Misono “Preparation of Monolithic SiO_2-TiO_2 Gels by Condensation Polymerization of Silicic Acid and Titanium Chelates”, J. Non-Crystal. Solids, **104**, 164 (1988)

[46] T. Gunji, Y. Nagao, T. Misono and Y. Abe “Preparation of $Si0_2$-$Ti0_2$ Fibers from Polytitanosiloxanes”, J. Non-Crystal. Solids, **107**, 149 (1989)

[47] Y. Abe, N. Sugimoto, Y. Nagao and T. Misono “Preparation of SiO_2-MxOy (M=Al, Zr) Monolithic Gels by Condensation Polymerization of Silicic Acid with Metal Chelate Compounds and Their Thermal Treatment”, J. Non-Crystal. Solids **108**, 150 (1989)

[48] Y. Abe, Y. Kimata, T. Gunji, Y. Nagao and T. Misono “Preparation of Polymethalloxanes as a Precursor for Oxide Fibers from Metal Chelate Compounds”, Serammic Ronbunshi, **97**, 596 (1989)

[49] Kiyomi Fuchigami, Yoshinari Taguchi, Masato Tanaka, “Preparation of hemispherical hollow silica microcapsules with different affinity surface by using spherical vaterite calcium carbonate as template” Polymers for advanced technologies **18**, 1-7(2007)

Figure Captions

Fig.VI-1. SEM photographs of silica synthesized at various temperatures, catalyst concentrations and dropping rates

Fig.VI-2. Dependence of mean diameter of silica particle on temperature, catalyst concentration and dropping rate

Fig.VI-3. Dependence of surface area of silica particle on temperature, catalyst concentration and dropping rate

Fig.VI-4. Dependence of specific heat capacity of silica particle on temperature, catalyst concentration and dropping rate

Fig.VI-5. Dependence of thermal reduction (TG) of silica particle on temperature, catalyst concentration and dropping rate

Fig.VI-6. Dependence of FT-IR spectrum of silica particle on temperature, catalyst concentration and dropping rate

Fig.VI-7. Fluoride release from sodium fluoride-doped silica

Table Captions

TableV-1. Reaction conditions

Reaction Temperature (K)	278	298	323	348
NaOH (mmol)	1.0	3.0	5.0	
Dropping rate (ml/h)	10		500	
TEOS ($moldm^{-3}$)	0.1			
D.W ($moldm^{-3}$)	10			
EtOH (dm^{-3})	0.18			

TableV-2. Results of mean particle size measurement Unit: μm

	10ml/h			500ml/h		
	1mmol	3mmol	5mmol	1mmol	3mmol	5mmol
278K	331	800	798	1013	900	891
298K	180	468	820	913	1497	1706
323K	195	289	388	863	1326	1400
348K	215	221	319	230	726	913

TableV-3. Results of surface area measurement Unit: m^2/g

	10ml/h			500ml/h		
	1mmol	3mmol	5mmol	1mmol	3mmol	5mmol
278K	55.8	95.6	191.7	70.5	93.0	168.0
298K	42.0	26.3	59.6	20.2	11.2	44.4
323K	92.0	70.8	93.2	11.6	9.1	30.7
348K	154.9	135.6	110.2	22.9	11.3	56.4

TableV-4. Results of specific heat capacity measurement at 323K

Unit: J/(g・K)

	10ml/h			500ml/h		
	1mmol	3mmol	5mmol	1mmol	3mmol	5mmol
278K	4.487	4.622	4.261	4.978	4.701	4.061
298K	2.805	2.542	2.862	3.675	3.164	2.580
323K	2.236	2.439	4.726	2.692	2.500	3.145
348K	2.117	2.926	3.354	1.906	2.512	3.139

TableV-5. Results of thermal reduction measurement (TG) at 1123K **Unit: %**

	10ml/h			500ml/h		
	1mmol	3mmol	5mmol	1mmol	3mmol	5mmol
278K	19.90	20.15	20.09	20.75	20.62	19.66
298K	14.82	16.88	18.61	18.14	17.89	17.68
323K	12.33	14.36	19.64	14.68	14.75	15.94
348K	11.64	15.43	16.41	12.01	14.03	16.20

TableV-6. Results of sodium fluoride concentration measurement **Unit: ppm, Mean(S.D)n**

	2min	5min	10min	30min
5mmol-10ml/h-298K	172.1(23.6)2	208.2(5.8)2	212.3(0)2	212.3(0)2
3mmol-500ml/h-348K	37.5(3.1)	47.3(1.3)2	46.4(0)2	46.4(0)2

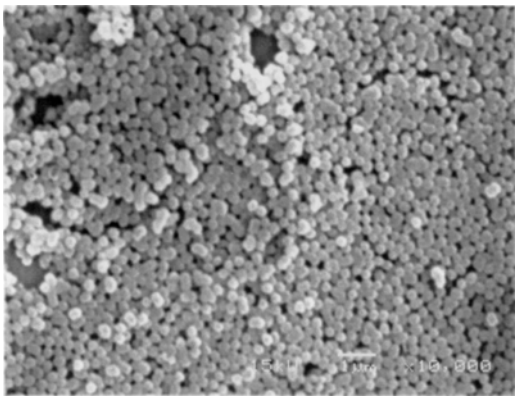

1mmol-10ml/h-5℃

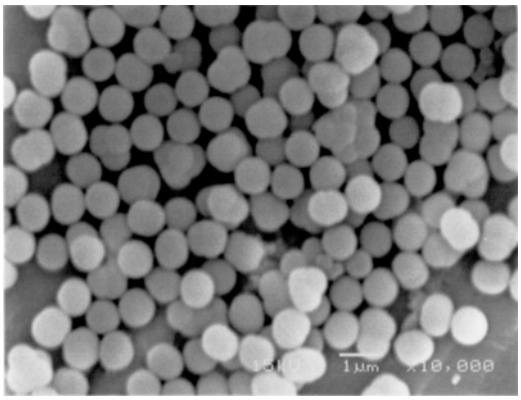

1mmol-500ml/h-5℃

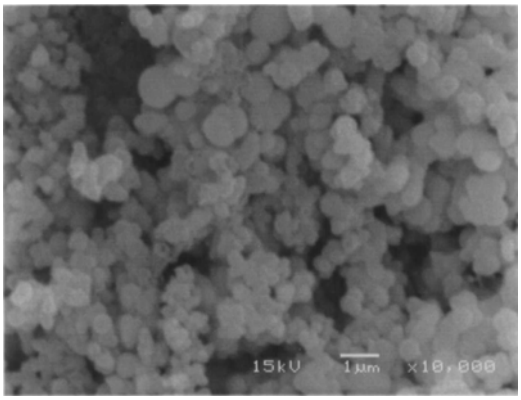

3mmol-10ml/h-5℃

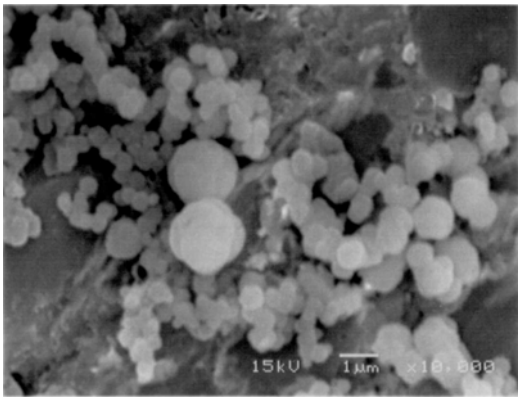

3mmol-500ml/h-5℃

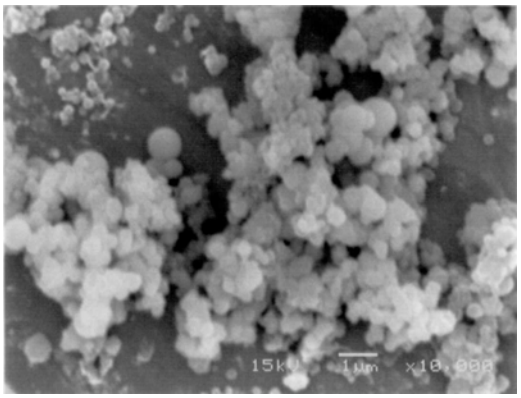

5mmol-10ml/h-5℃

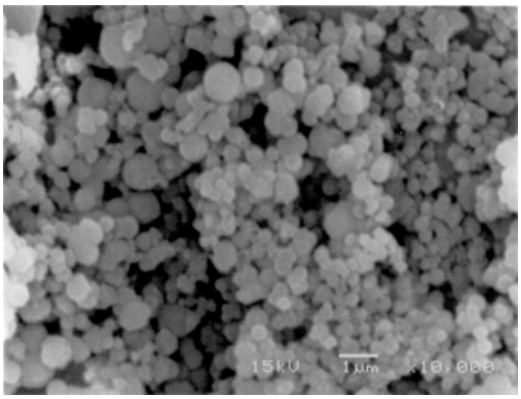

5mmol-500ml/h-5℃

Fig.VI-1-1. SEM photographs of prepared silica

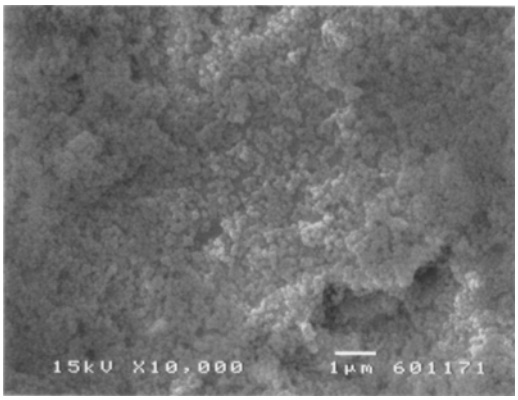

1mmol-10ml/h-25℃

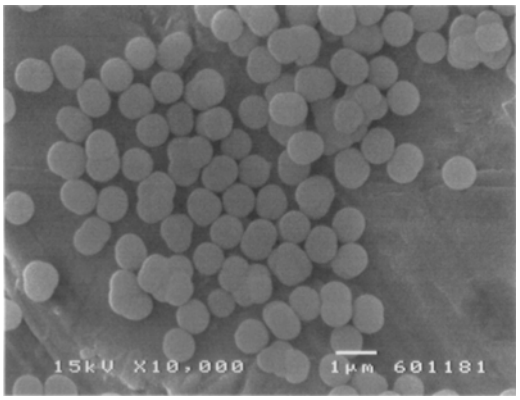

1mmol-500ml/h-25℃

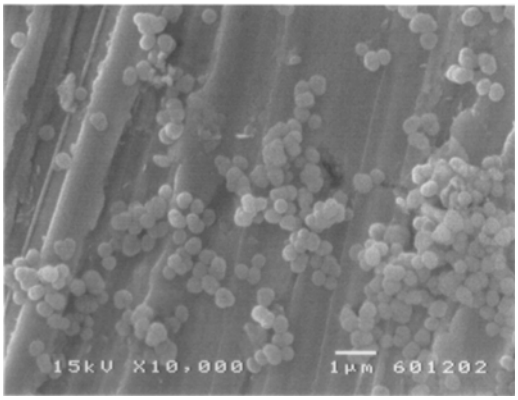

3mmol-10ml/h-25℃

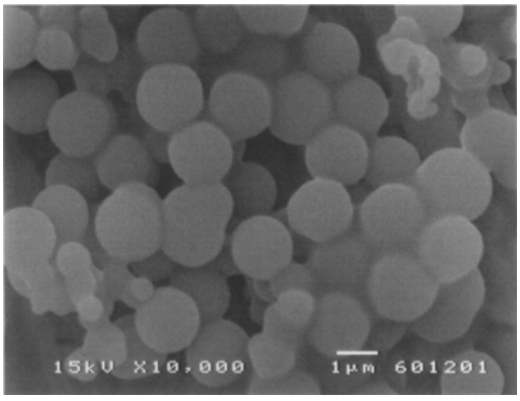

3mmol-500ml/h-25℃

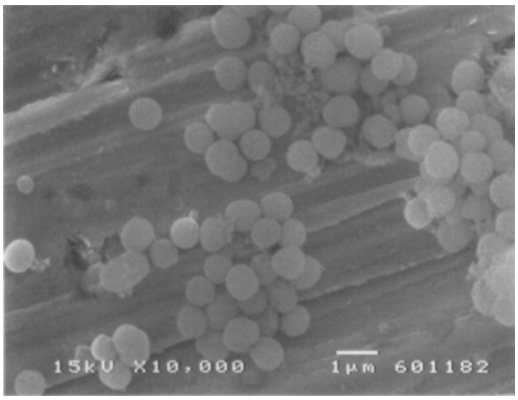

5mmol-10ml/h-25℃

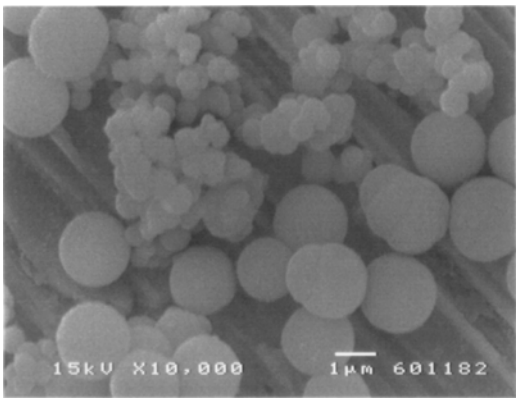

5mmol-500ml/h-25℃

Fig.VI-1-2. SEM photographs of prepared silica

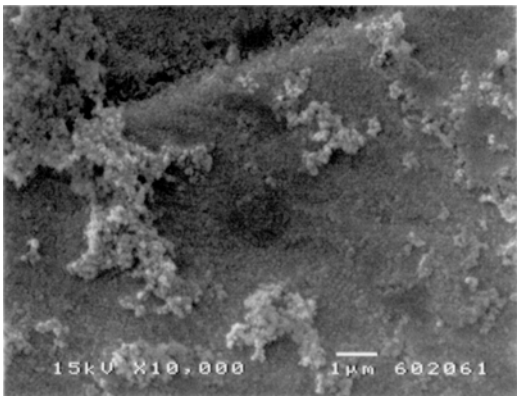

1mmol-10ml/h-50℃

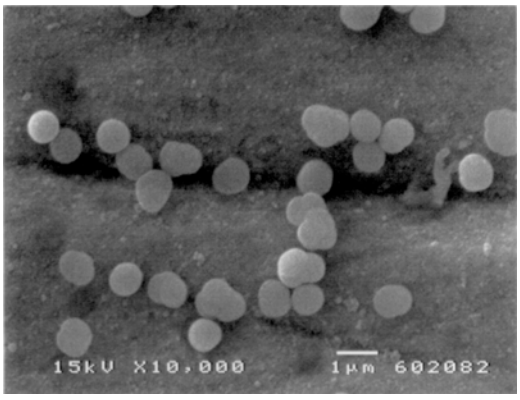

1mmol-500ml/h-50℃

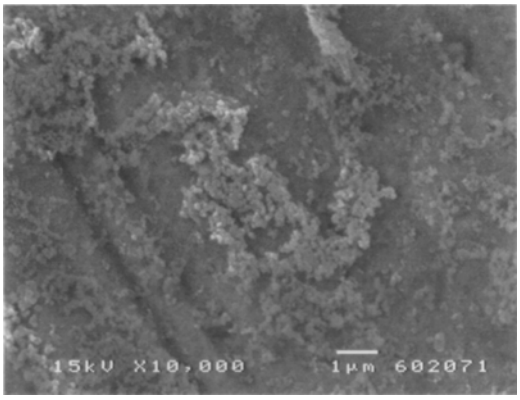

3mmol-10ml/h-50℃

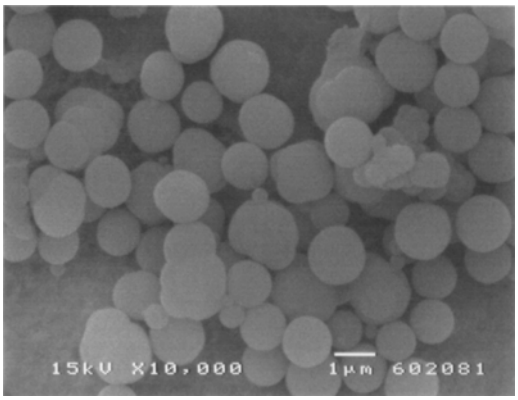

3mmol-500ml/h-50℃

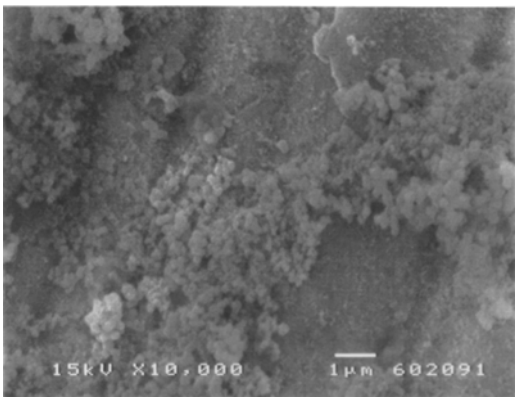

5mmol-10ml/h-50℃

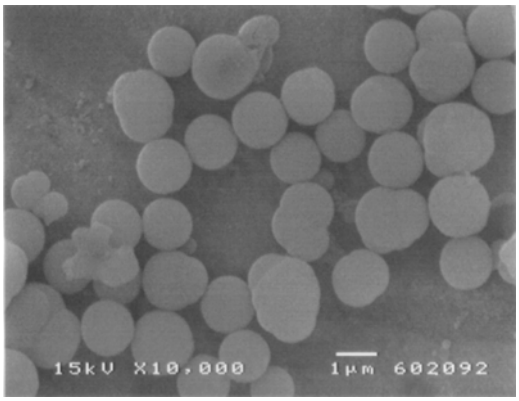

5mmol-500ml/h-50℃

Fig.VI-1-3. SEM photographs of prepared silica

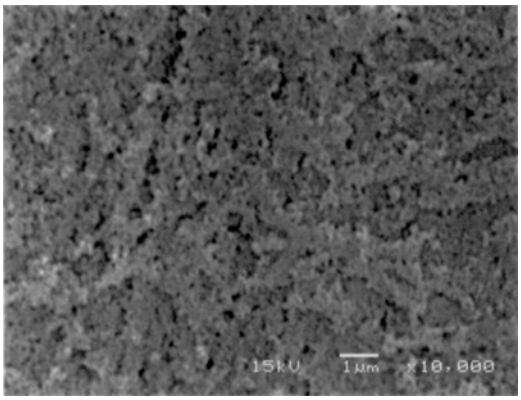

1mmol-10ml/h-75℃

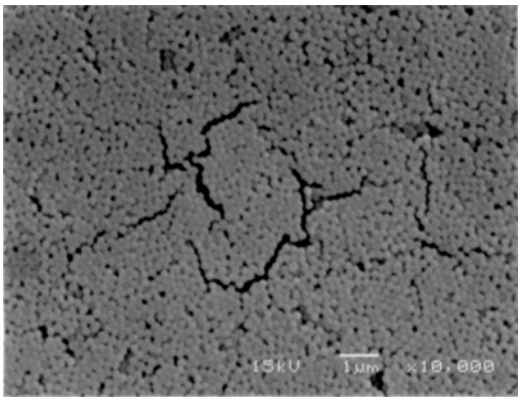

1mmol-500ml/h-75℃

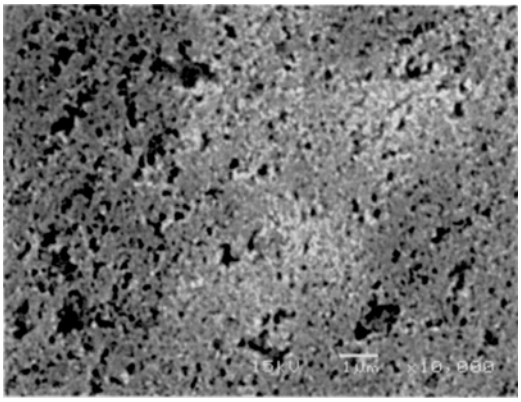

3mmol-10ml/h-75℃

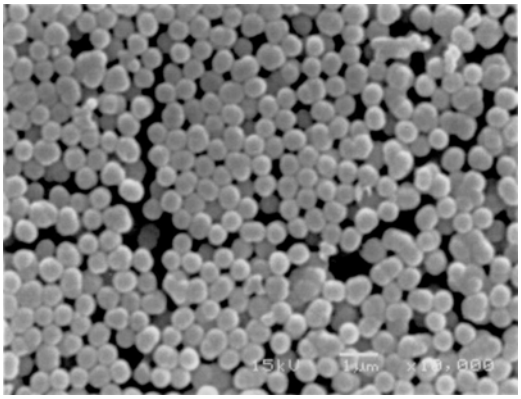

3mmol-500ml/h-75℃

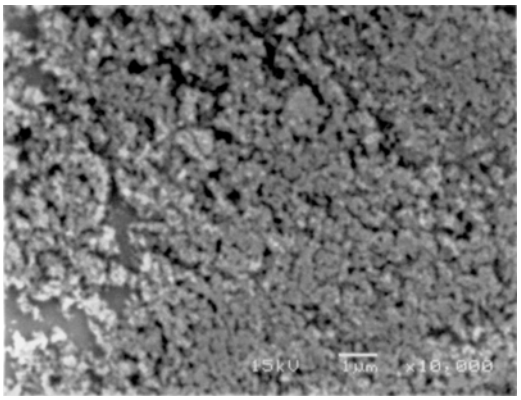

5mmol-10ml/h-75℃

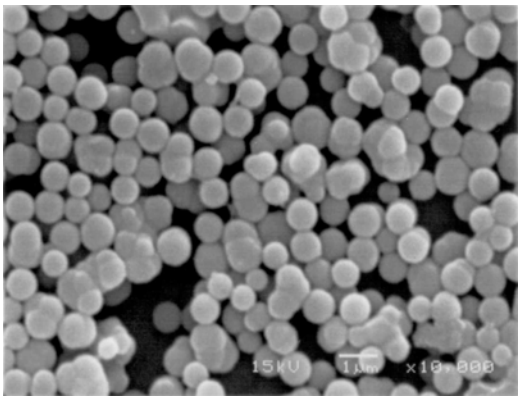

5mmol-500ml/h-75℃

Fig.VI-1-4. SEM photographs of prepared silica

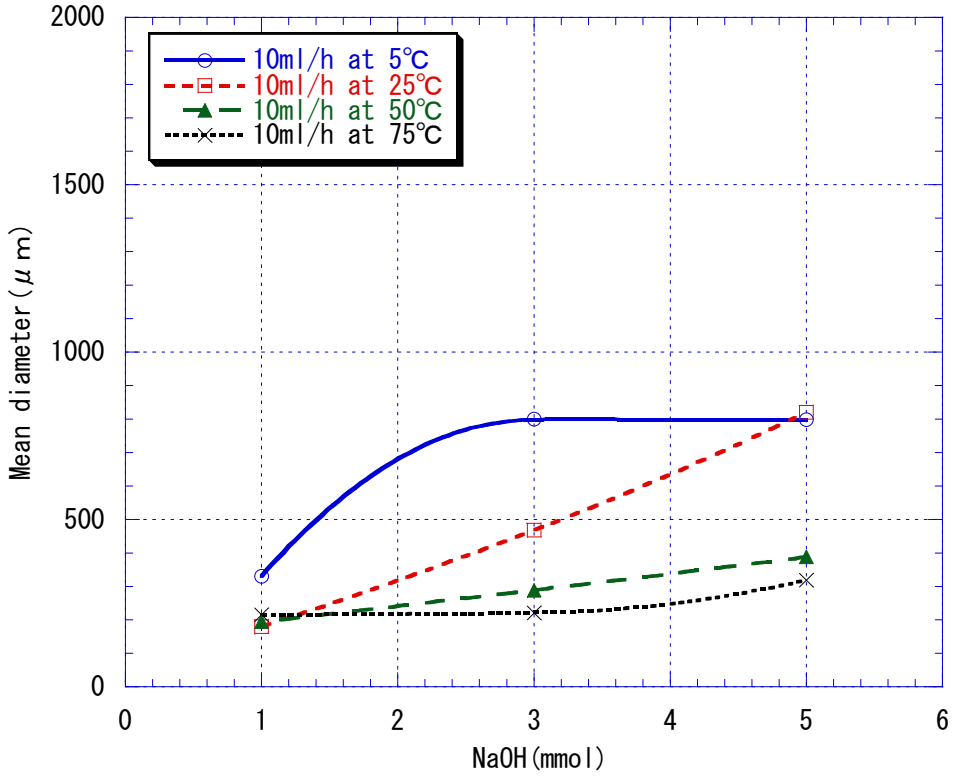

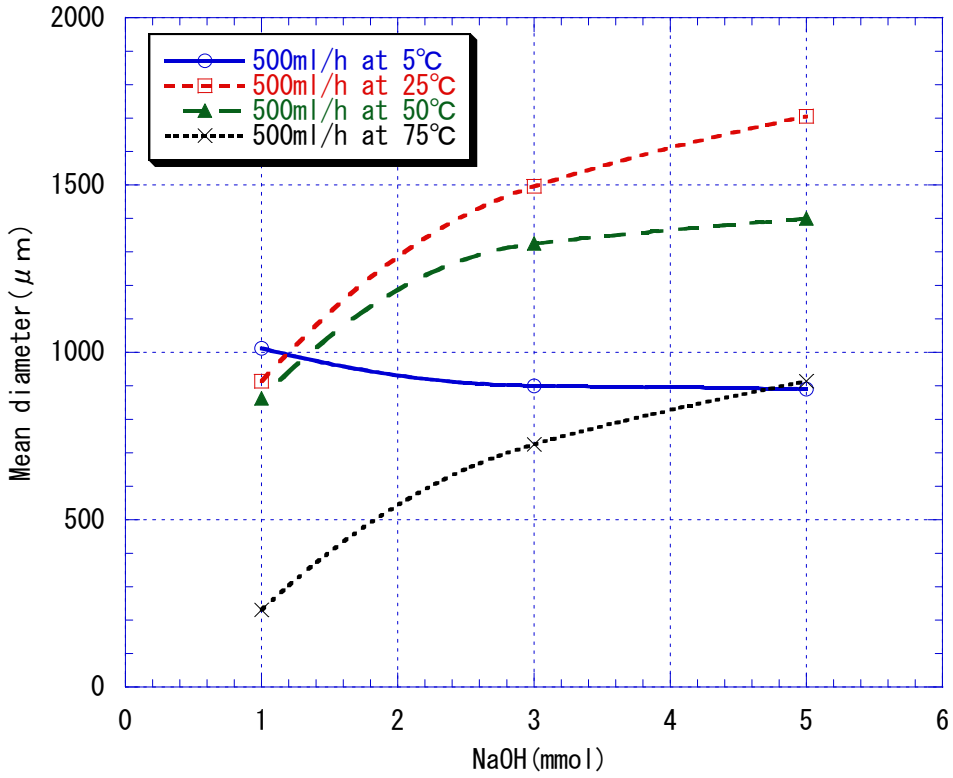

Fig.VI-2-1. Mean particle size of prepared silica

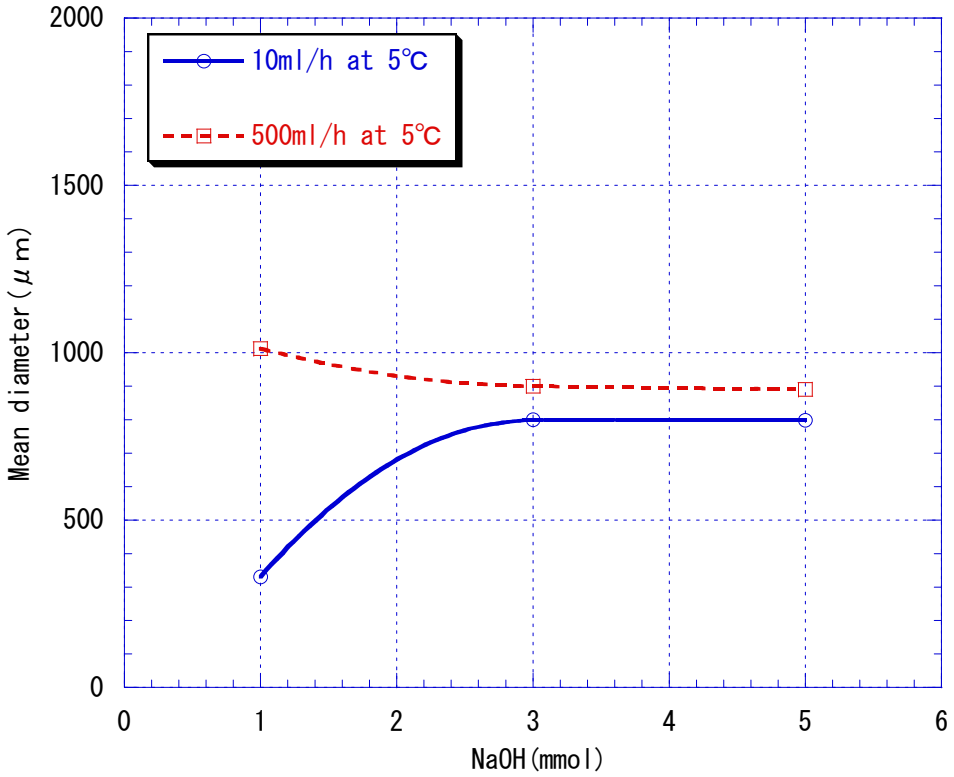

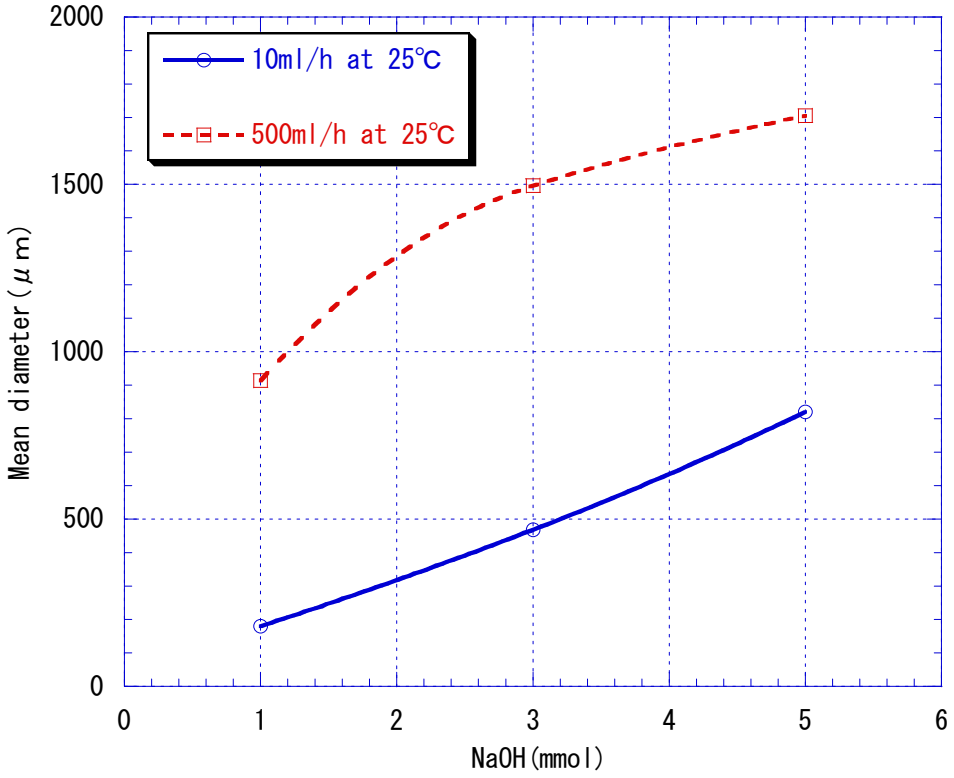

Fig.VI-2-2. Mean particle size of prepared silica

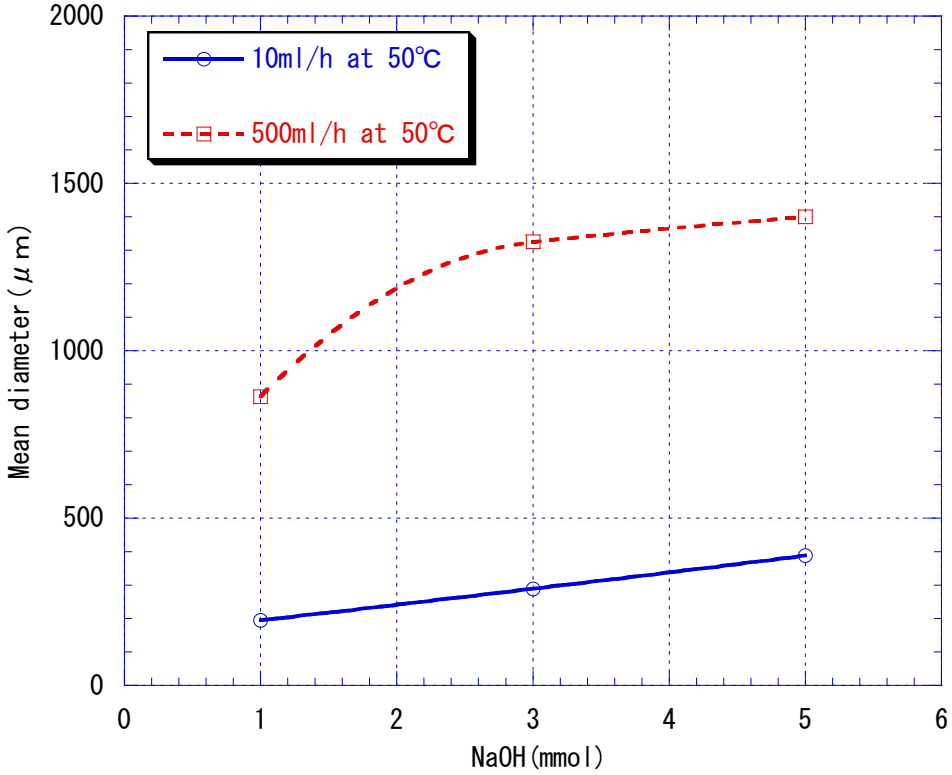

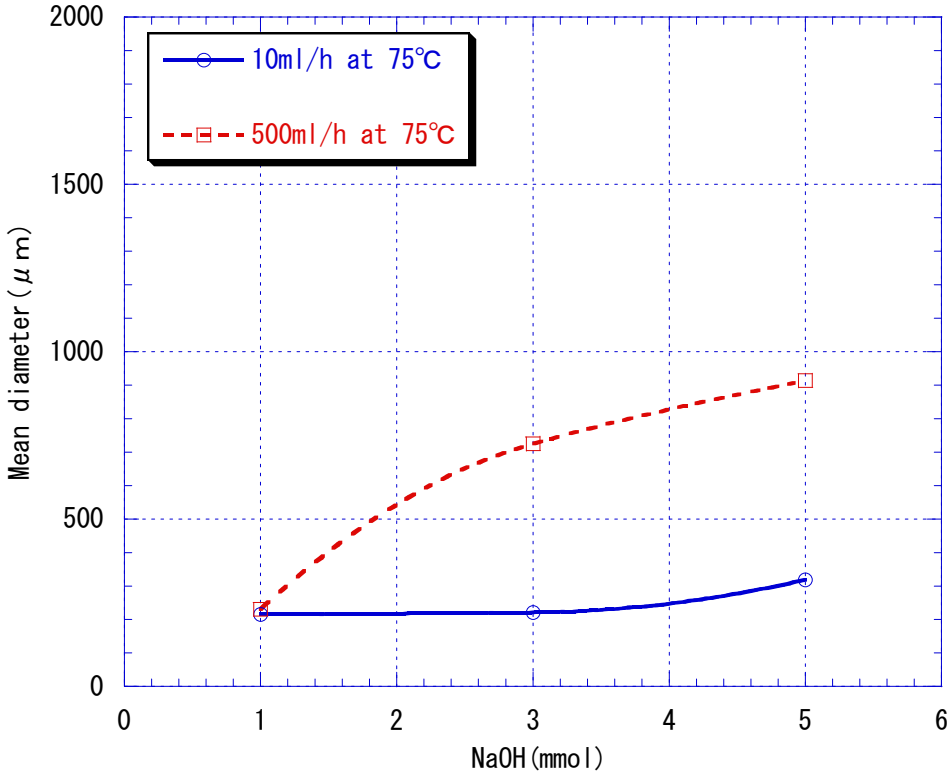

Fig.VI-2-3. Mean particle size of prepared silica

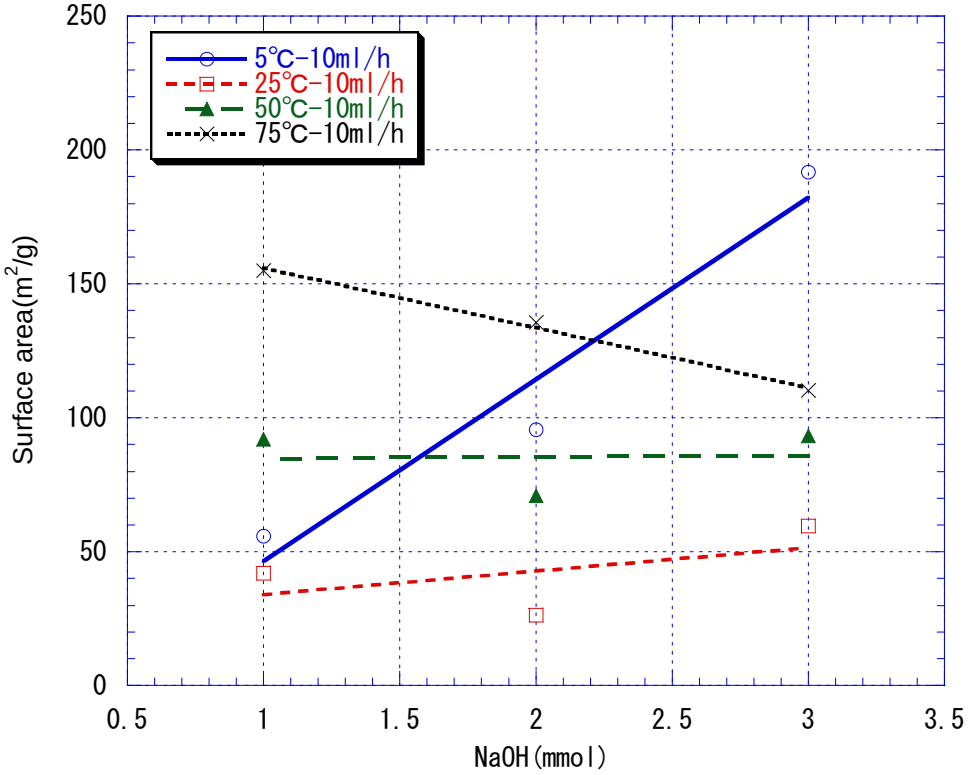

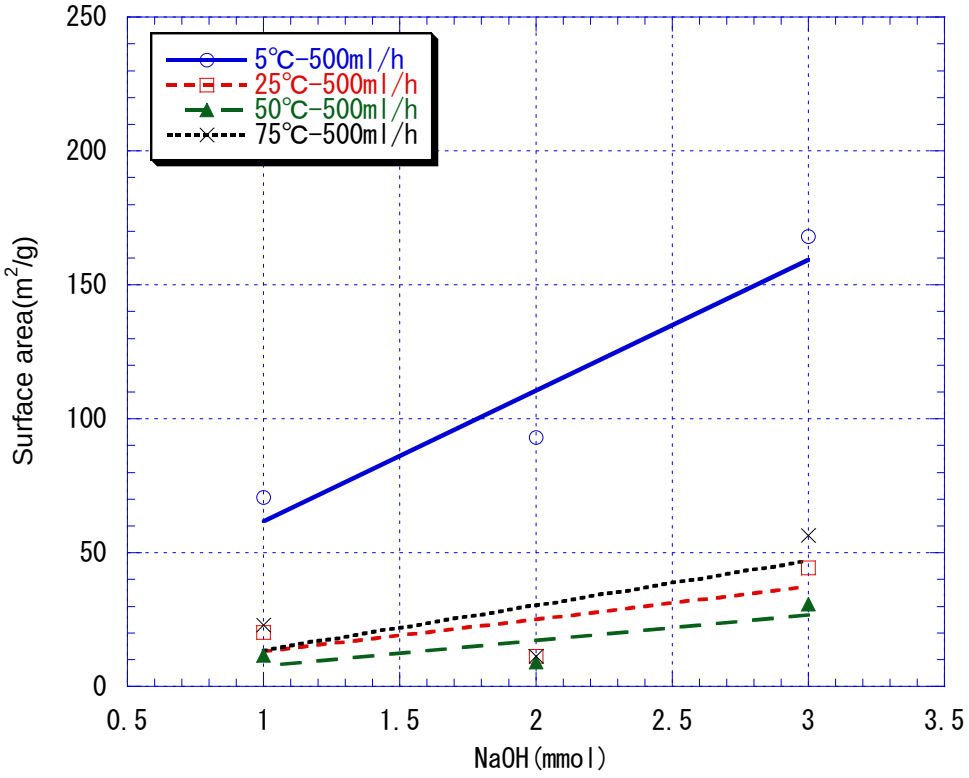

Fig.VI-3-1. Surface area of prepared silica

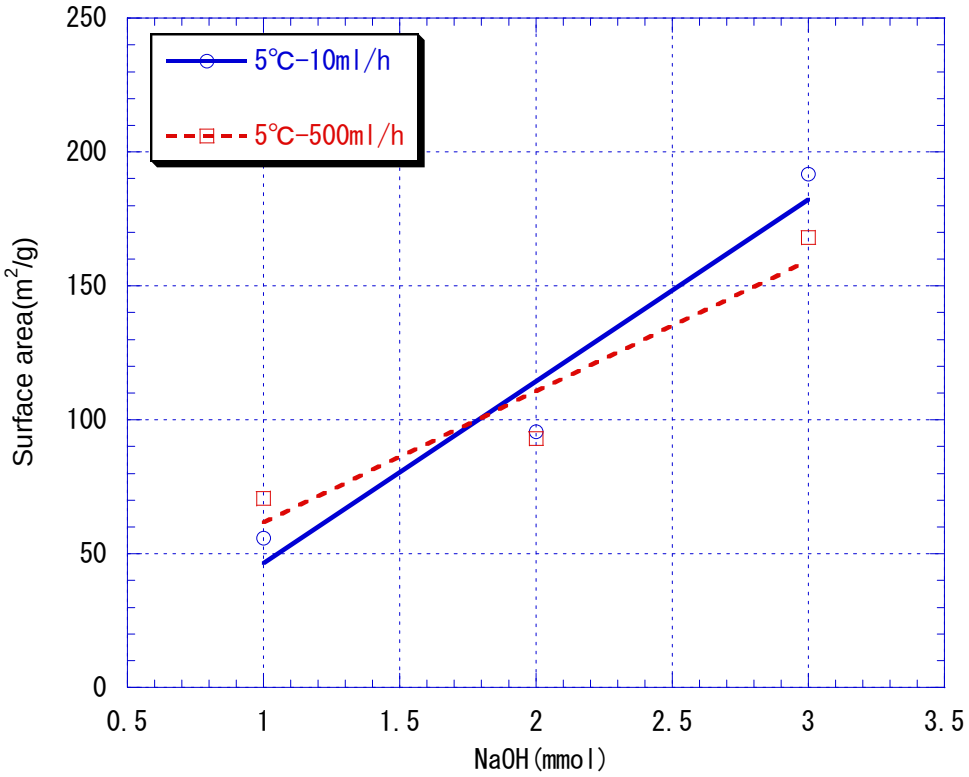

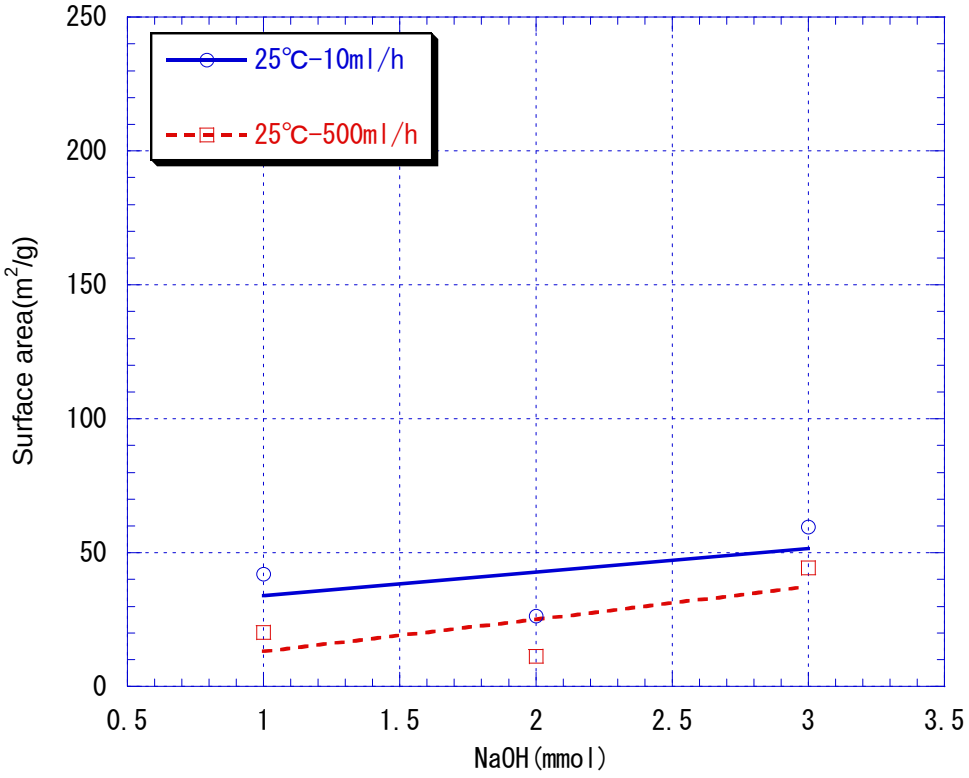

Fig.VI-3-2. Surface area of prepared silica

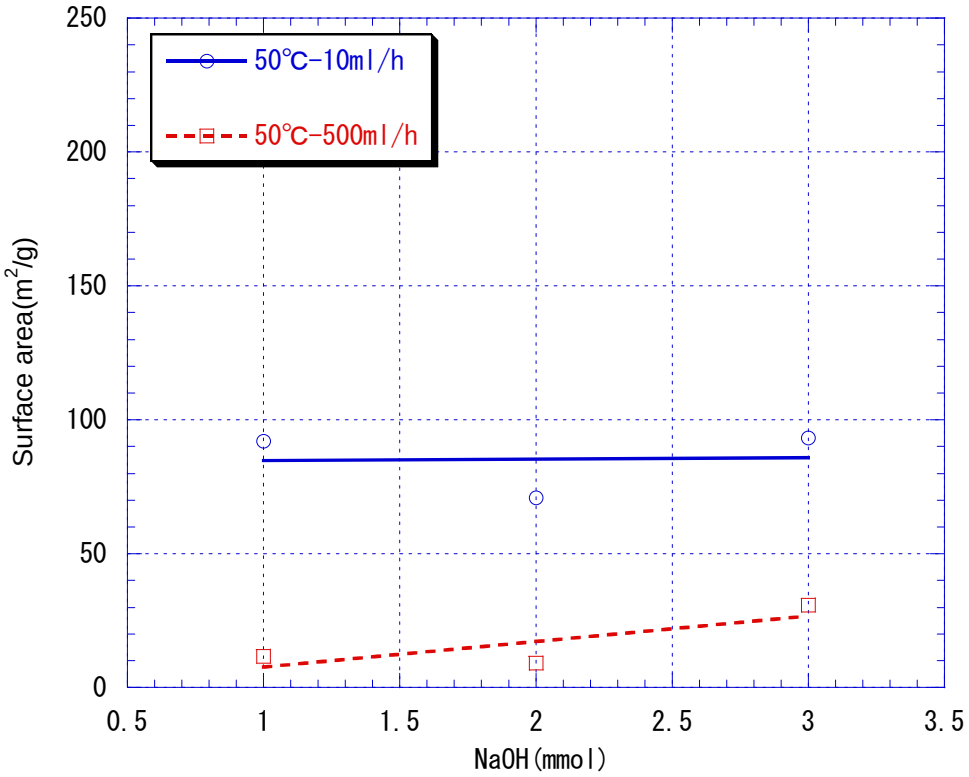

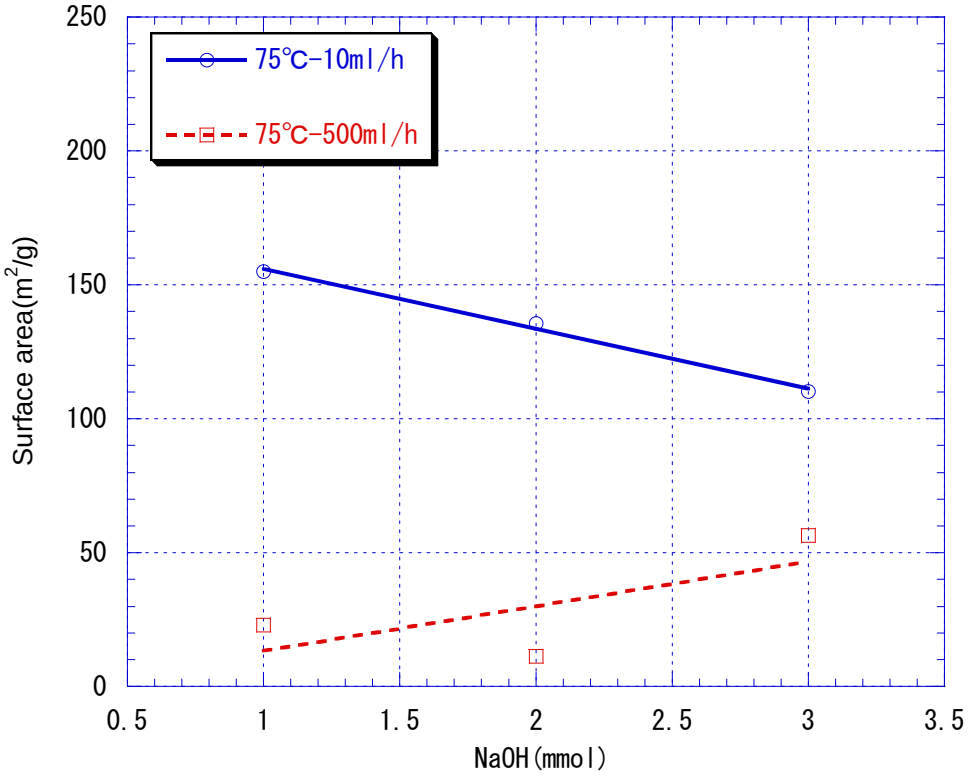

Fig.VI-3-3. Surface area of prepared silica

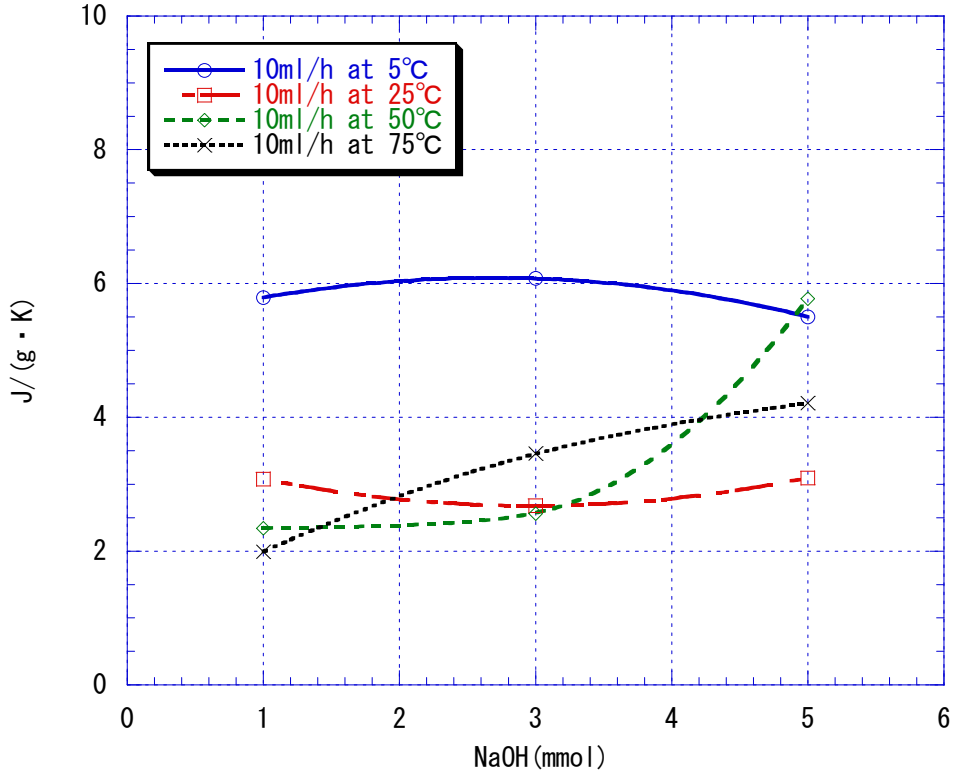

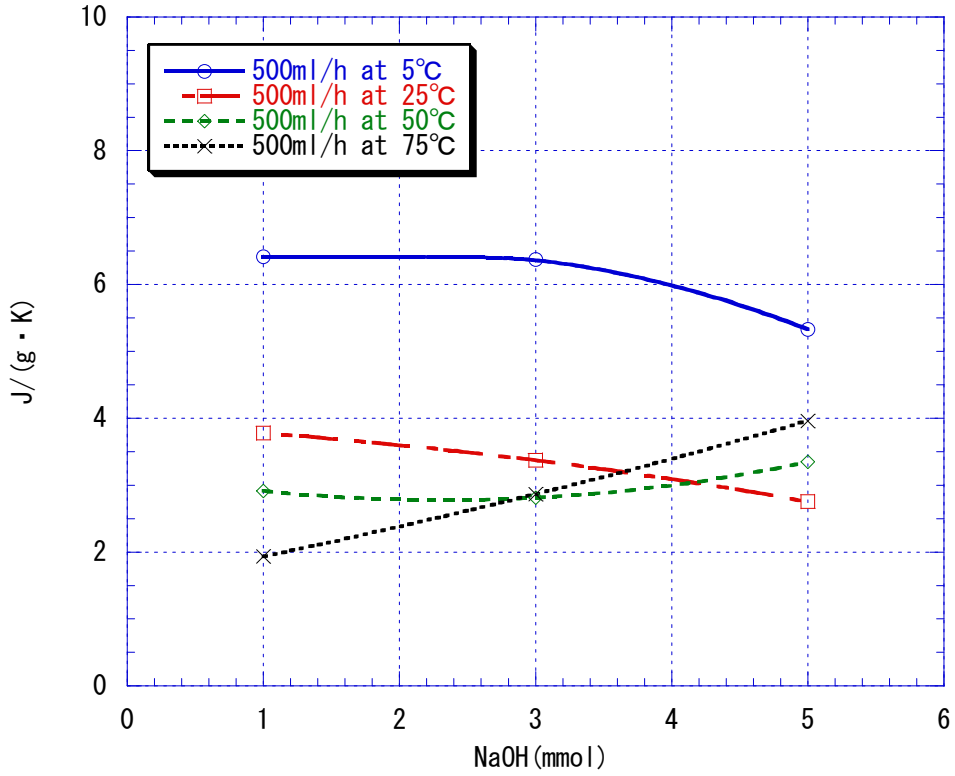

Fig.VI-4-1. Specific heat capacity of prepared silica

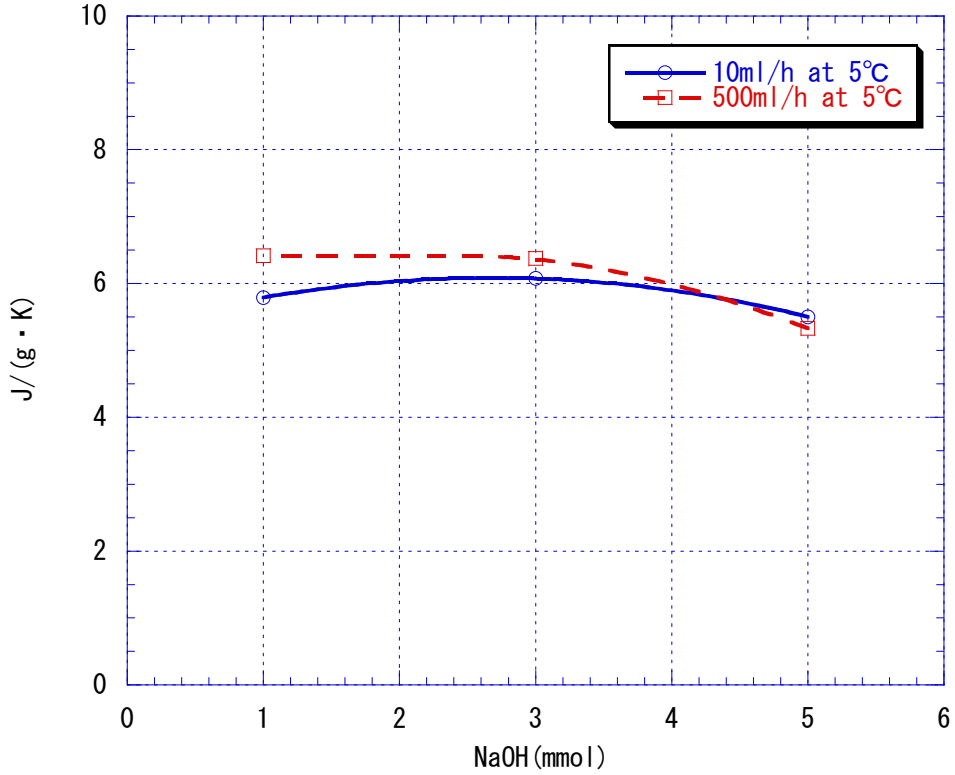

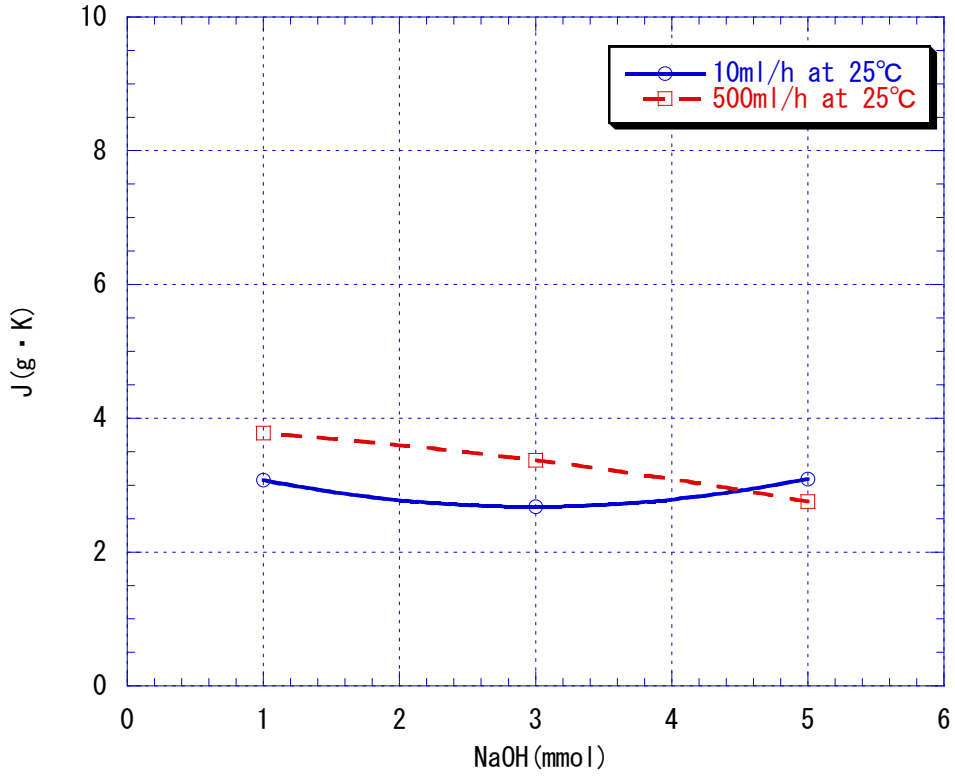

Fig.VI-4-2. Specific heat capacity of prepared silica

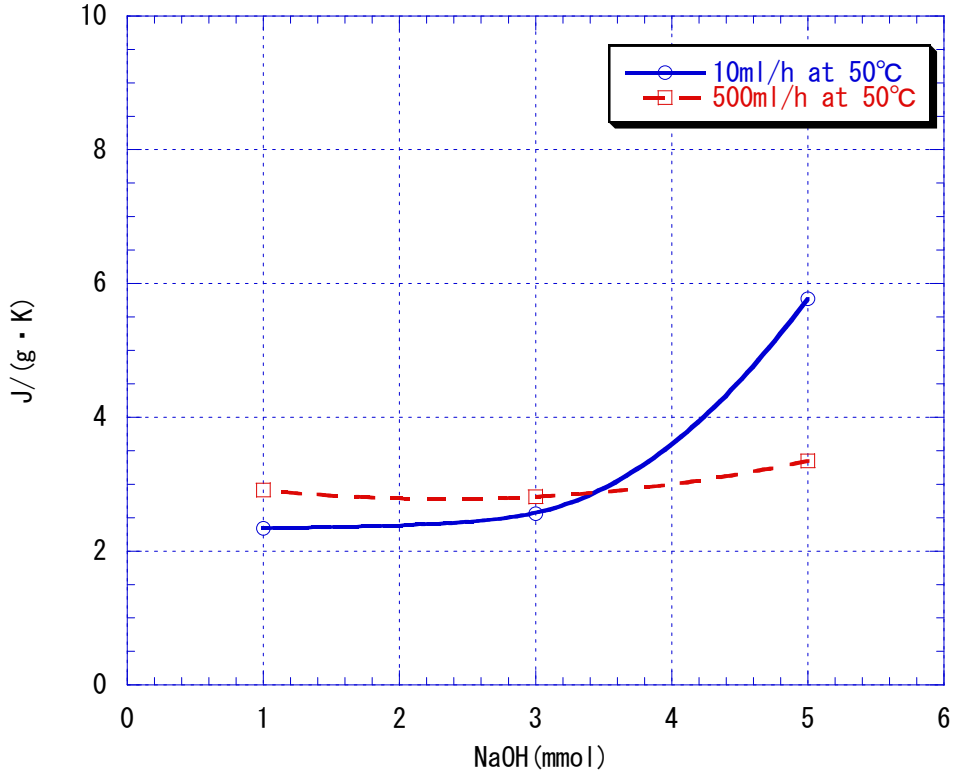

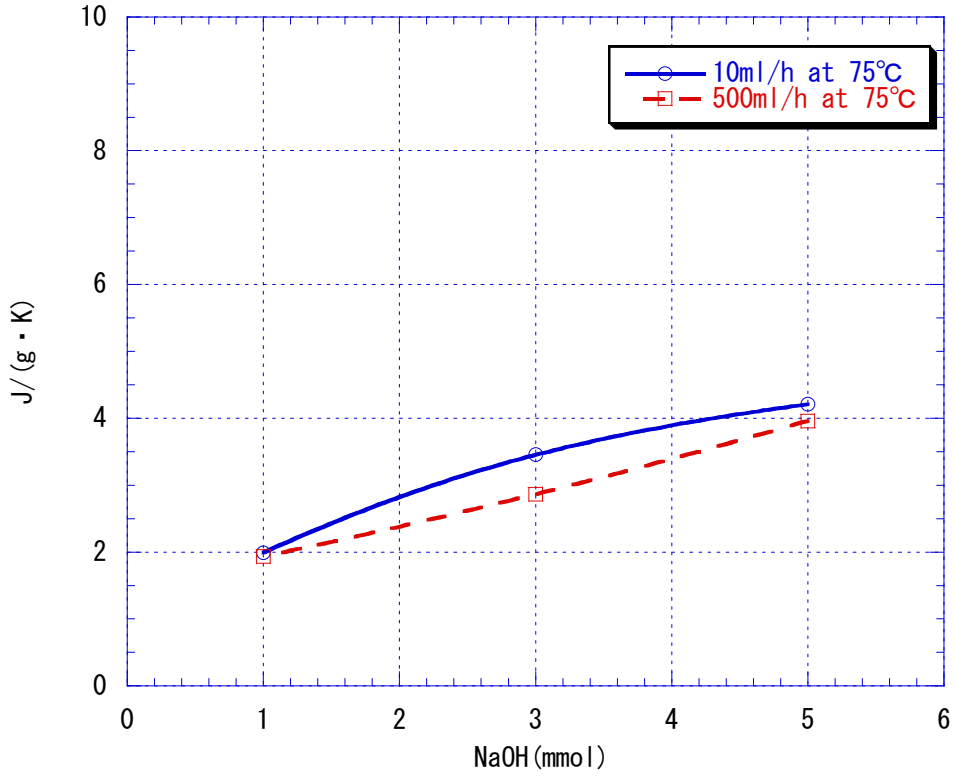

Fig.VI-4-3. Specific heat capacity of prepared silica

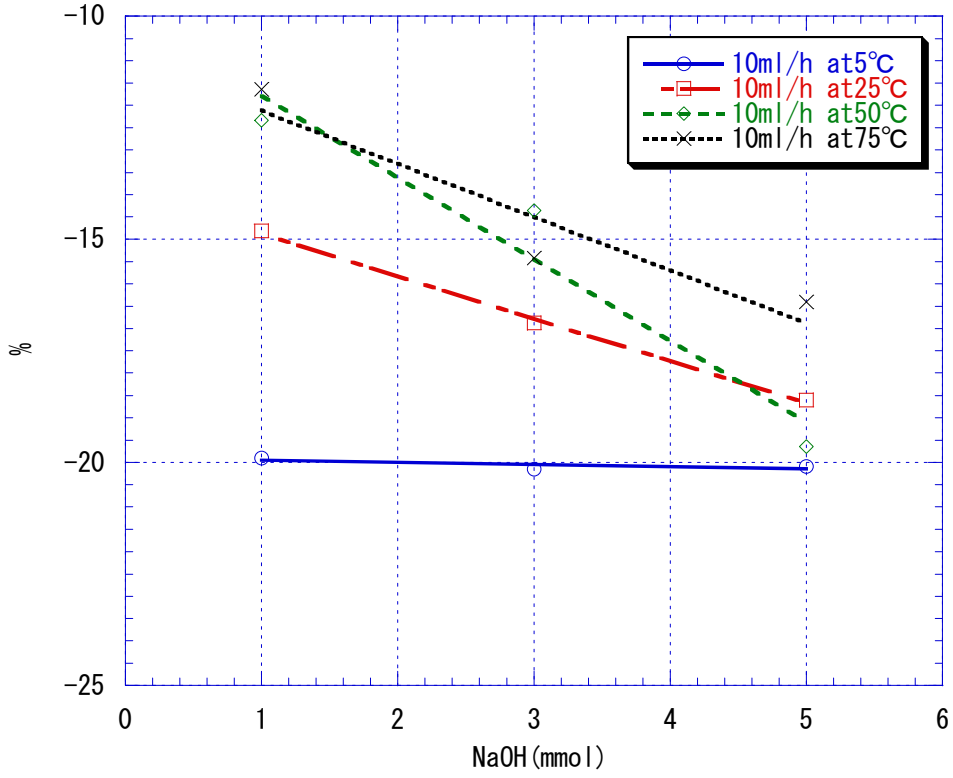

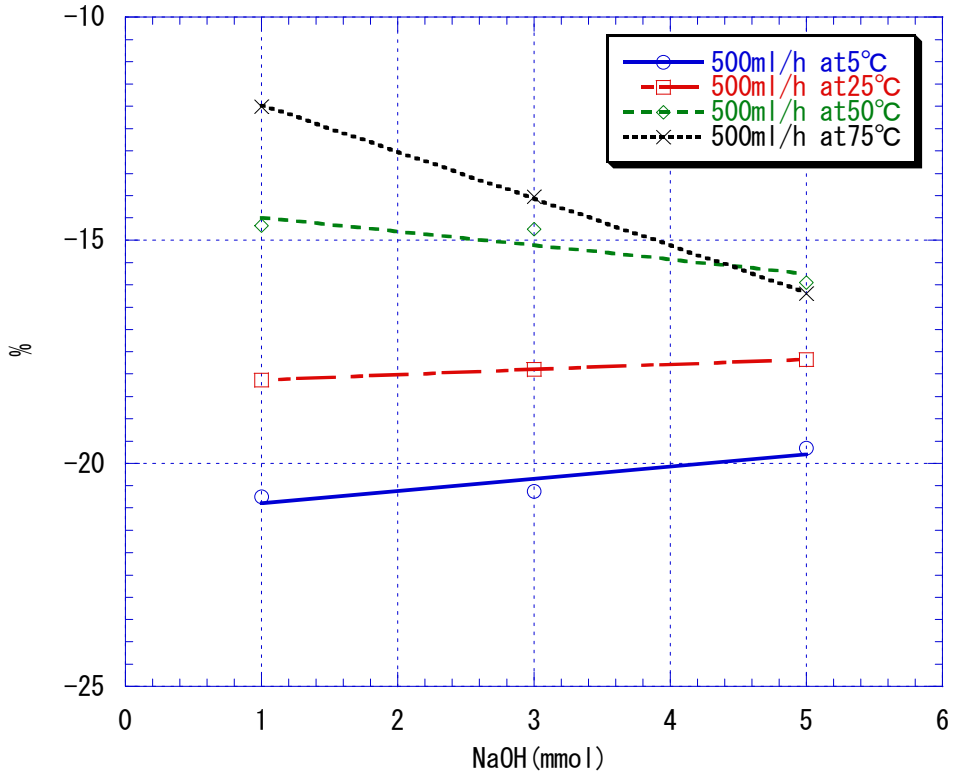

Fig.VI-5-1. Thermal reduction (TG) at 850℃ of prepared silica

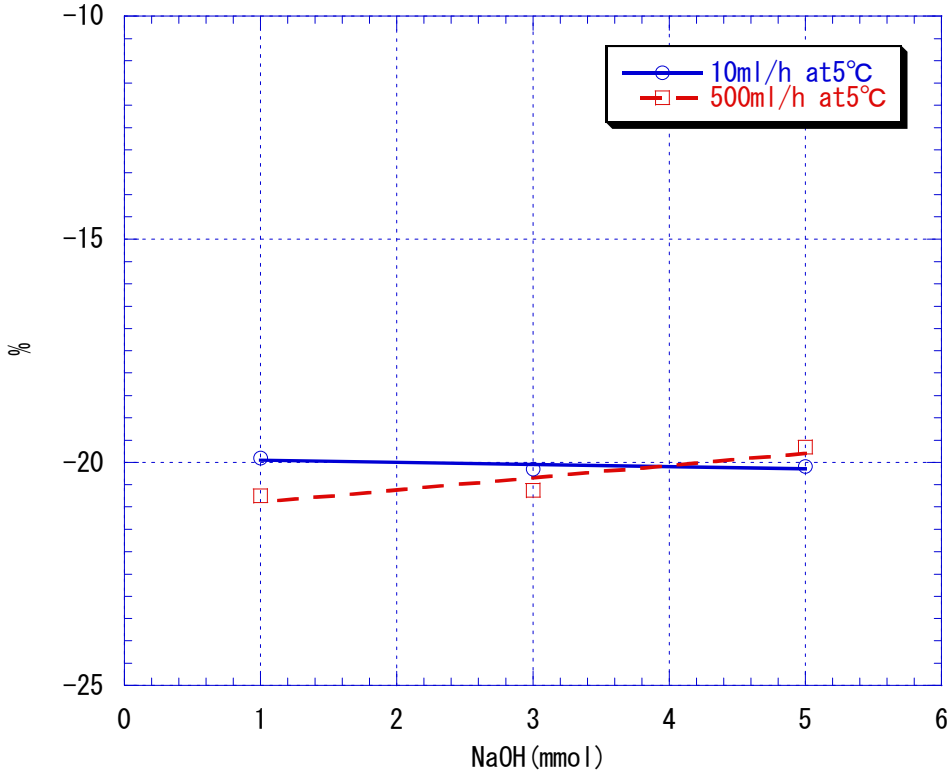

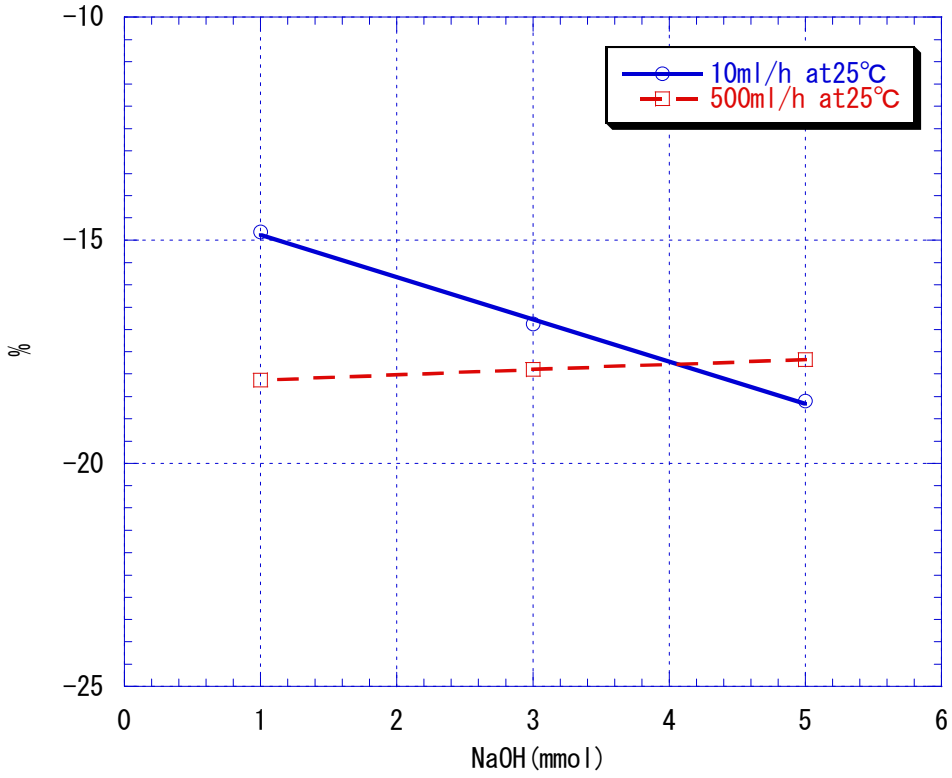

Fig.VI-5-2. Thermal reduction (TG) at 850℃ of prepared silica

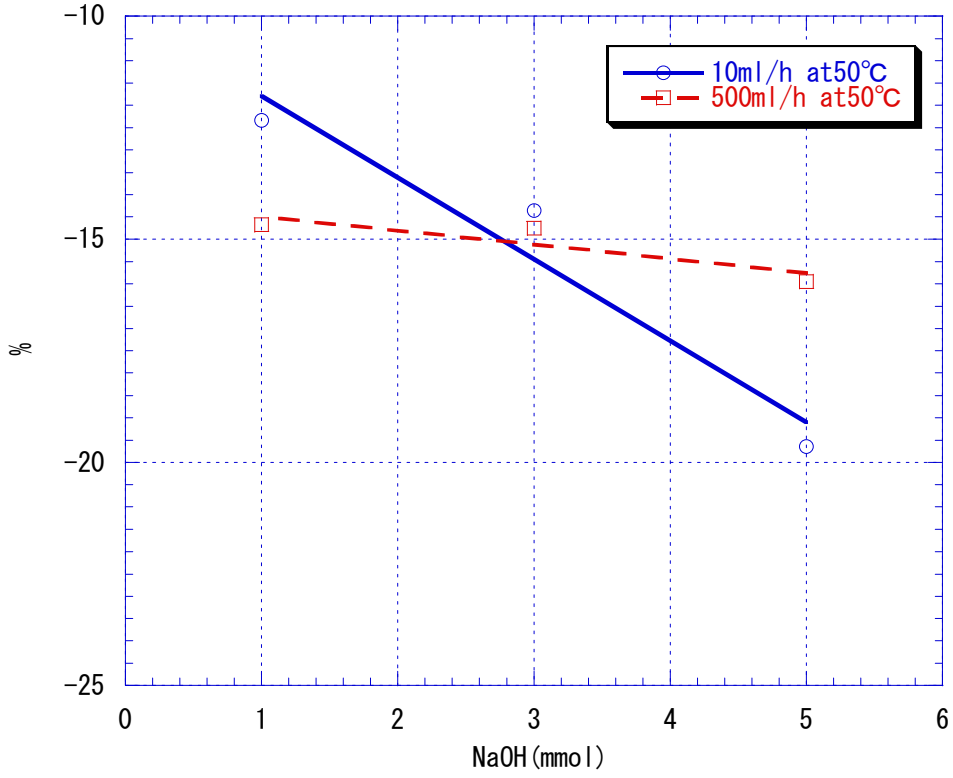

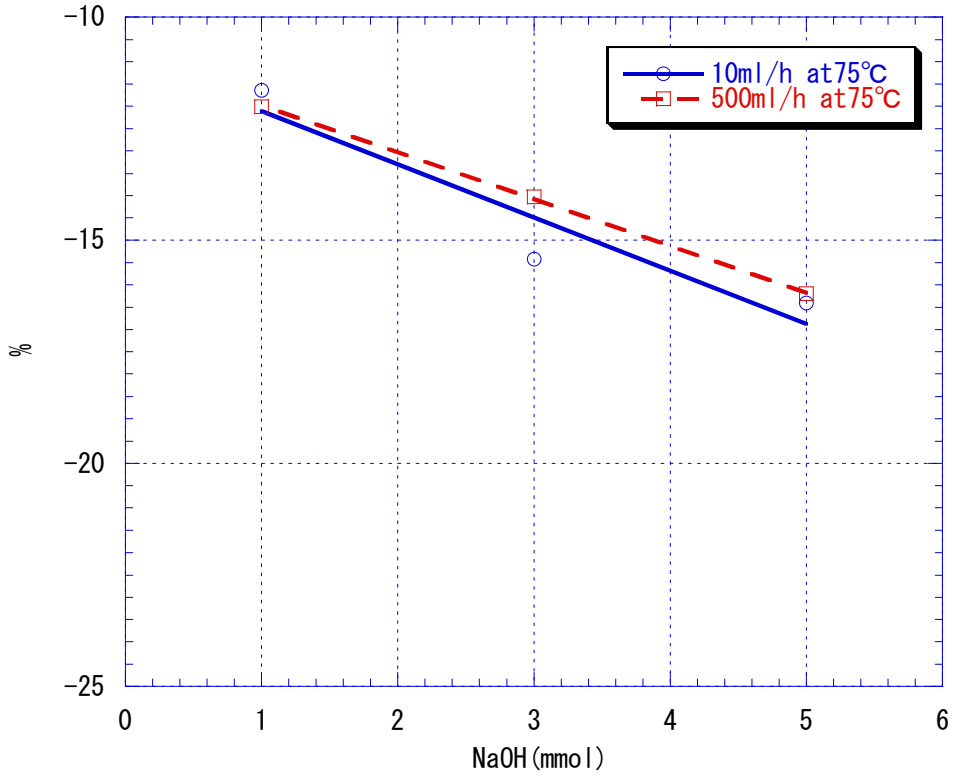

Fig.VI-5-3. Thermal reduction (TG) at 850℃ of prepared silica

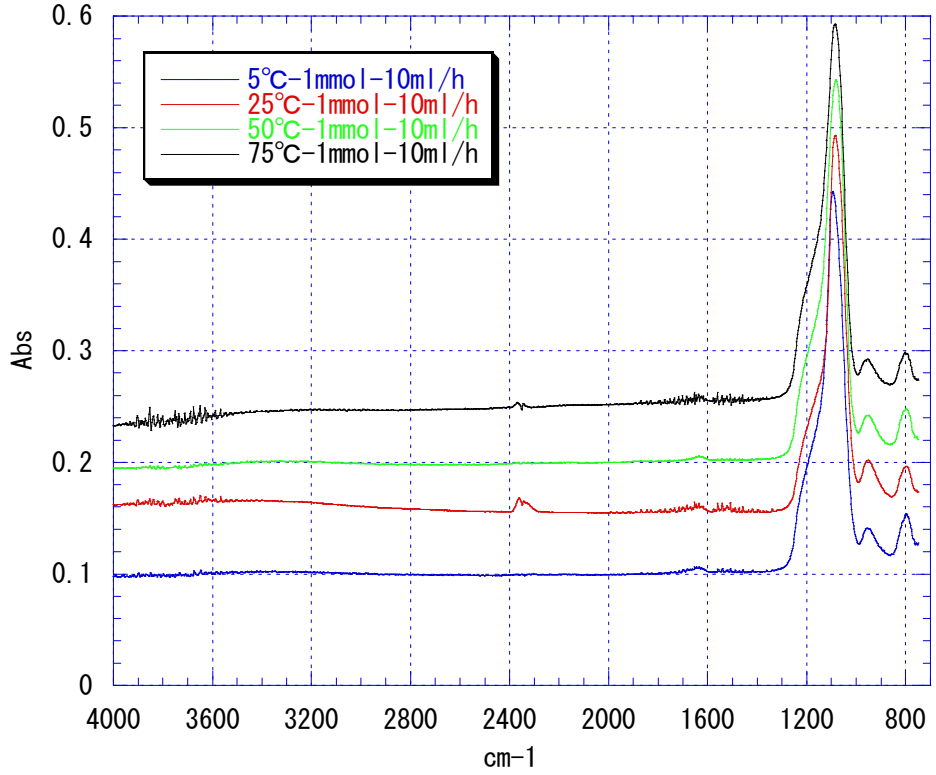

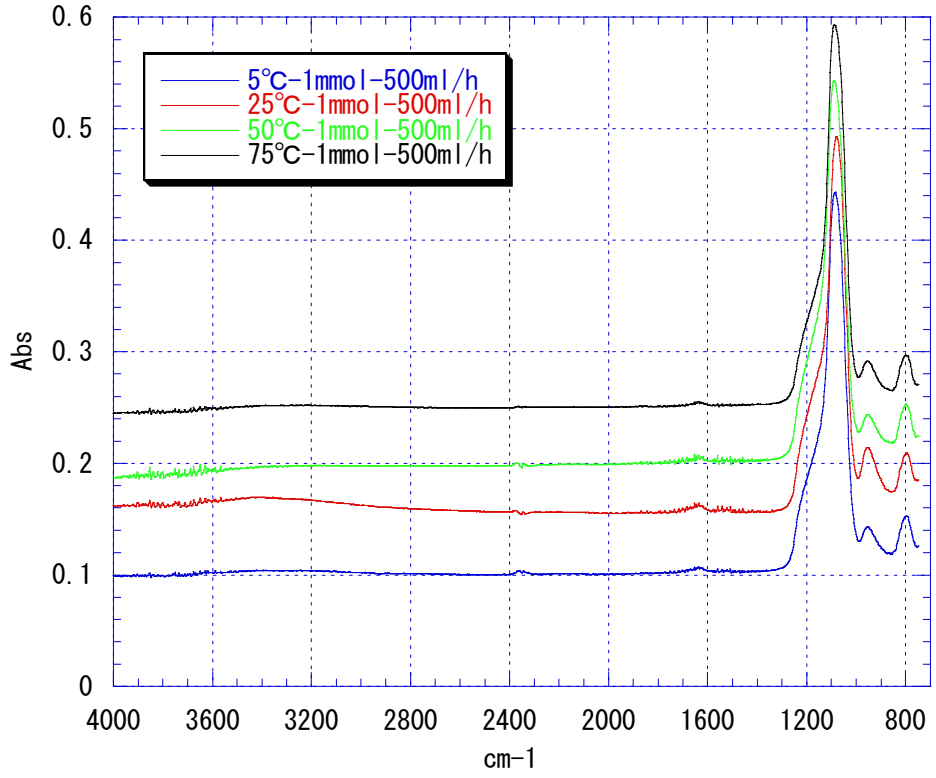

Fig.VI-6-1. FT-IR spectrum of prepared silica

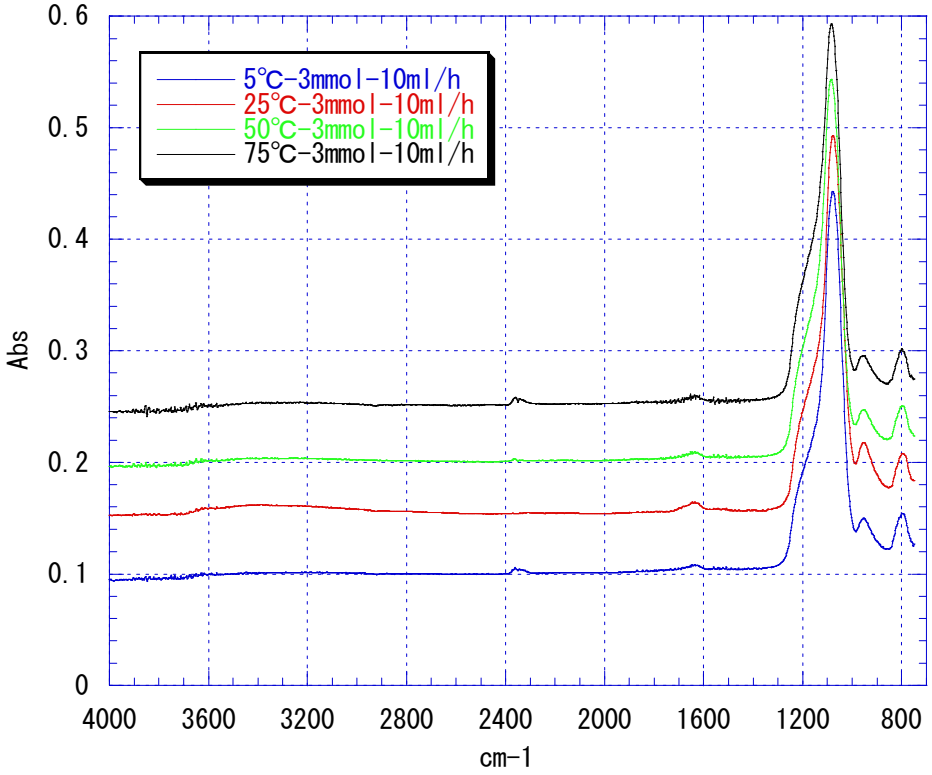

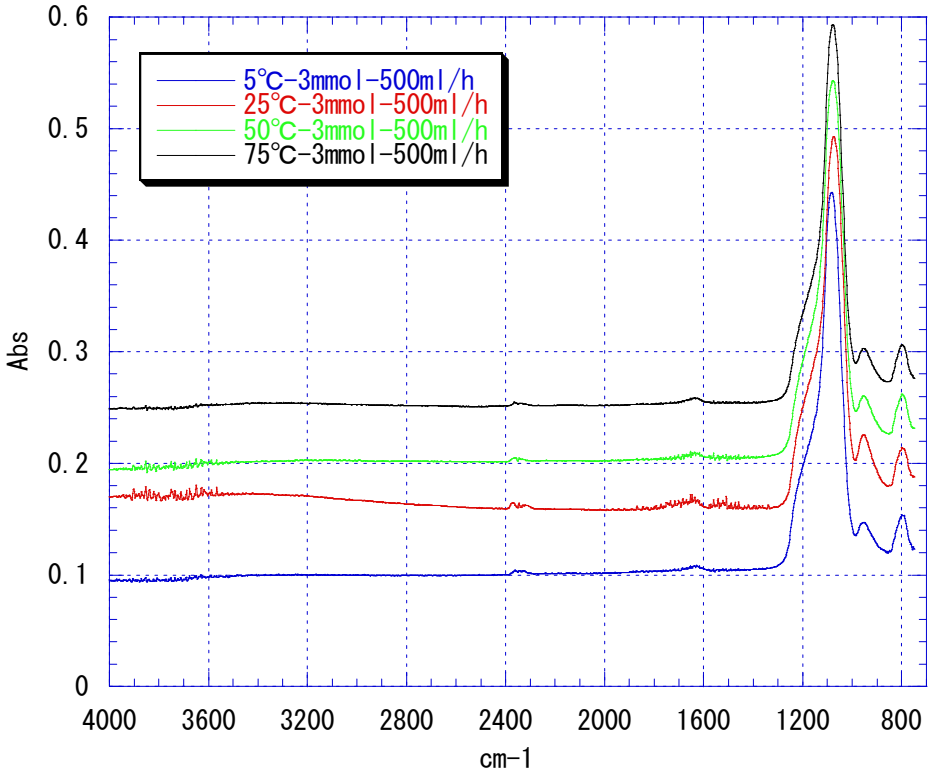

Fig.VI-6-2. FT-IR spectrum of prepared silica

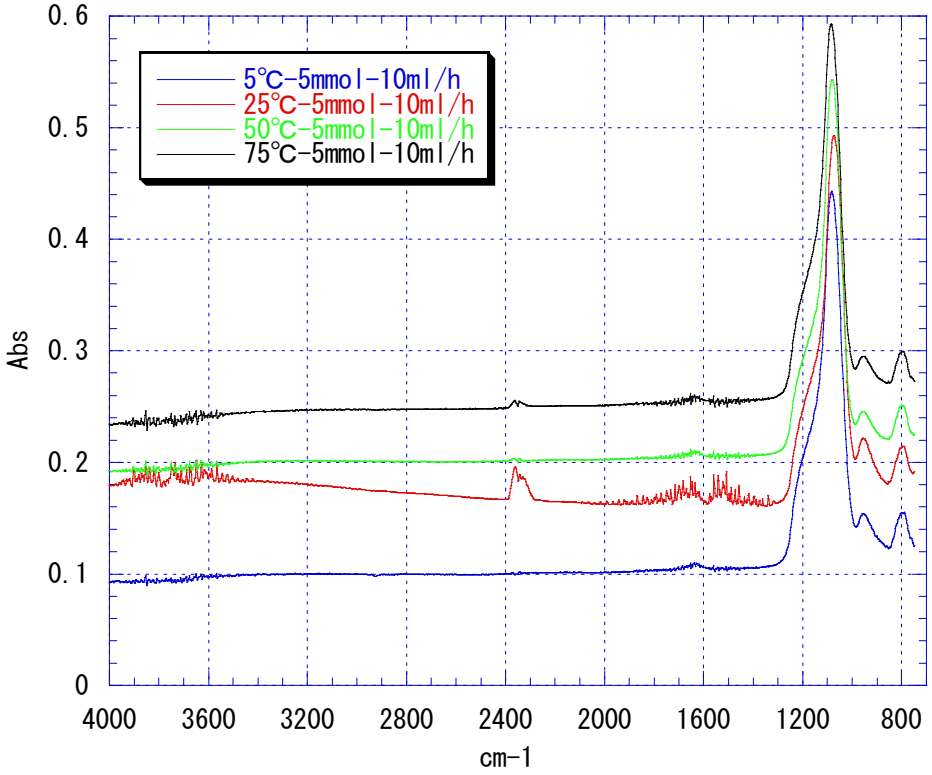

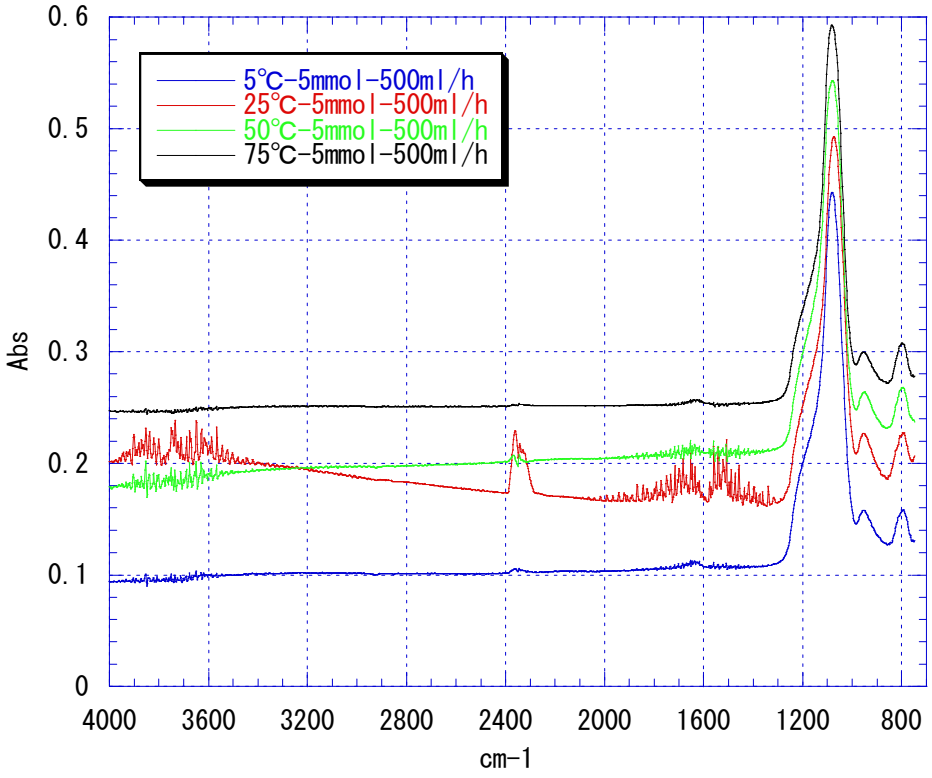

Fig.VI-6-3. FT-IR spectrum of prepared silica

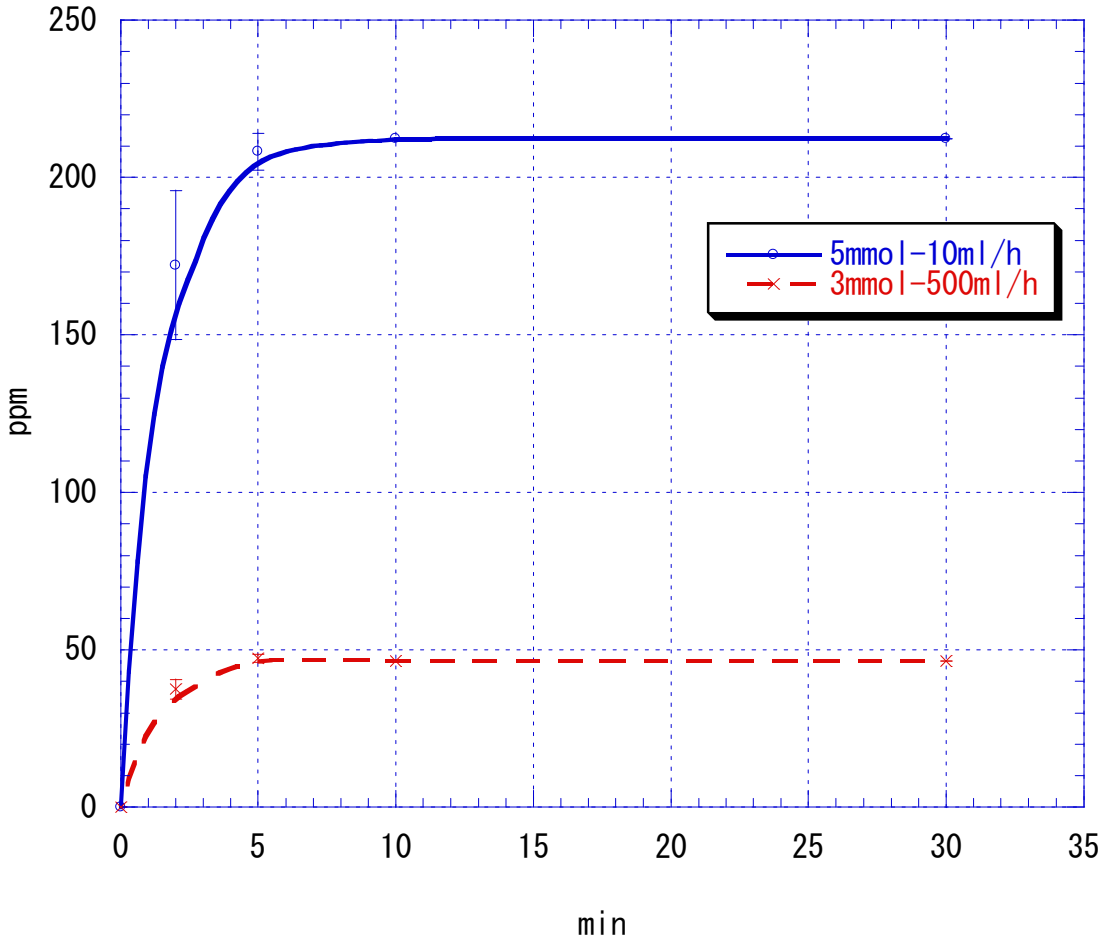

Fig.VI-7. Fluoride release results of prepared silica containing sodium fluoride

Chapter VII

Preparation of hemispherical hollow silica microcapsules with different affinity surface by using spherical vaterite calcium carbonate as template

VII-1. Abstract

We developed the method to prepare hemispherical hollow silica microcapsules with different affinity surfaces by using spherical vaterite calcium carbonate as template. The preparing process was composed of the adhesion of calcium carbonate onto the surface of methyl methacrylate droplets followed by suspension polymerization, the partial etching of calcium carbonate on the poly methyl methacrylate mother particle, the formation of silicon dioxide powder by sol-gel reaction and their deposition onto the etched flat surface of calcium carbonate, the surface modification of deposited silicon dioxide with silane coupling agent, the remove of the mother particle with acetone, the formation of silicon dioxide powder by sol-gel reaction and deposition onto the exposed hemispherical surface of calcium carbonate and the surface modification of deposited silicon dioxide with silane coupling agent. The synthesized microcapsules had complete hemispherical structure and both the more hydrophilic and the more hydrophobic surface.

VII-2. Introduction

Microcapsules have been applied in various fields such as information recording, cosmetics, paintings, medicine, agriculture, food and so on [1-8]. Moreover, active researches and developments have been performed to prepare microcapsules with various functions. Among them, the drug delivery system by use of micro/nano-capsules has attracted much attention because of the ability of delivering effectively and concentratedly the drug to the affected lesions such as organs, cells and pathogens as targets [9-19]. By microencapsulating the drug to protect from environment, it will be able to enhance the curative effect by releasing the drug to the affected lesion without any undesired absorbing or degradation. Moreover, the drug delivery system has such an advantage that not only enhance the curative effect but also reduce the side effects and the dose. For an example, the drug delivery system of anticancer agent is composed of the following process, (1) injection of microcapsules with the surface combining specific molecule which can detect the cancer cell, (2) passing of microcapsules through the blood vessel, (3) reaching and adhering of microcapsules on the cancer cell, (4) selective releasing of anticancer agent from microcapsules to the cancer cell.

In this instance, if the shape of microcapsule is spherical, the area of contact between microcapsule and affected lesion may be restricted. Further more, it was very difficult to introduce the different type of functional groups on the spherical microcapsule at the same time and to make the partial area of microcapsule hydrophobic or hydrophilic [20-23].

When microcapsules are prepared by using the dispersion, in general, the shape of microcapsules may be spherical because of the thermodynamic stability of the dispersion [24-29]. Recently, an interesting method has reported for the drug delivery system as gastrointestinal muco-adhesive system named GI-MAPS® [33, 34]. This GI-MAPS® has the hemispherical shape to adhere the mucous membrane to release the drug. However, this drug delivery system has been designed for oral administration and prepared by machinery process. Thus, it will be difficult to apply to the injection administration system owing to microcapsules with the size lager than millimeter.

In this study, we tried to develop the method of preparing hemispherical hollow silica microcapsules (HHSM) with both the more hydrophilic and the more hydrophobic surface, where spherical vaterite calcium carbonate (SVCC) was used as template.

VII-3. Experimental

VII-3-1. Materials

Spherical vaterite calcium carbonate (SVCC) used was manufactured (ED-SX) by Komesho Sekkai Kogyo Co. Ltd., having an average particle diameter of 8 μm. Methyl methacrylate monomer (MMA: Mitsubishi Rayon Co. Ltd.) was used as received. Tetra-ethoxy silane (TEOS: Wako Pure Chemical Industries, Ltd) was used as received. Benzoyl peroxide as initiator (BPO: Kawaguchi Chemical Co., Ltd.) and sodium dodecylbenzenesulfonate as an auxiliary stabilizer (DBS: Nacalai Tesque, Inc.) were used as received. Silane coupling agents

(KBM503, KBM903) were manufactured by Toshiba Silicones co. Ethanol and 1 N-hydrochloric acid were all reagent-grade. 1N-Sodium hydroxide(Wako Pure Chemical Industries, LTD) was used as received

VII-3-2. Preparation of microcapsules

To help understand the preparation method, the scheme of preparing hemispherical hollow silica microcapsules (HHSM) is shown in **FigureVII-1** and explained in the order of the preparation as follows.

Scheme VII-I

Suspension polymerization of methyl methacrylate (MMA) was conducted by using the same apparatus as the previous one[30-31]. In brief, 15.0 g of SVCC was added to 270 ml of distilled water dissolving a given amount of DBS. This continuous water phase was irradiated by ultrasonic at 150W-28kHz for 5 min to uniformly disperse SVCC and transferred to a 500ml flanged type reaction flask with four baffles (the width of 1.2×10^{-2} m, the length of 7.5×10^{-2} m). While the continuous water phase was agitated at the impeller speed of 200 rpm with a six blade disk turbine of the impeller diameter of 5.0cm, which was located at one third the liquid depth. Bubbling by N_2 gas was conducted at room temperature for 30 min before suspension polymerization. After this operation, 30 ml of MMA as the dispersed phase containing 0.73g(0.1mol/L-MMA) of BPO was added. After agitation for 5 min at room temperature to form the O/W dispersion, suspension polymerization of MMA was conducted at

343K for 7 hr. Fundamental experiments were performed by changing the concentration of DBS from 0 to 75ppm.

This scheme shows SVCC adhering onto the surface of MMA droplets. In this dispersion, SVCC acts as suspension stabilizer in the continuous water phase.

Scheme VII-II

After suspension polymerization of MMA, the PMMA particles covered with SVCC were filtered and dried. About a half portion of each SVCC was embedded into a PMMA mother particle due to the affinity to the interface between MMA monomer and the water phase [30-32].

Scheme VII-III

The hemispherical surface of SVCC exposed on the surface of the PMMA mother particle was etched by adding them into the hydrochloric acid aqueous solution of 1 mol/l. By this operation, SVCC had both the flat surface exposed on the surface of PMMA mother particle and the hemispherical surface embedded in the PMMA mother particle.

Scheme VII-IV

The sol-gel hydrolysis and polycondensation of TEOS were conducted by adding catalyst into the suspension under the conditions in **Table VII-1**. By this reaction, hydrophilic silicon dioxide powder with the silanol group was formed in the water phase and deposited

selectively due to the hydrophilic-hydrophobic interaction on the hydrophilic flat surfaces of SVCC to form the deposition layer of silicon dioxide. Then, silicon dioxide was modified with 3-methacryloxy propyltrimethoxy silane (MPTS) with the methacryloyl group terminus under the conditions in Table II to result in the more hydrophobic flat surface of deposition layer of silicon dioxide.

Scheme VII-V

After separation by filtration, the PMMA mother particles were dissolved with acetone in order to separate off the hemispherical SVCC embedded into the PMMA mother particle.

SchemeVII-VI

As in Scheme VII-IV, the sol-gel hydrolysis and polycondensation of TEOS were conducted under the conditions in **Table VII-3** to form silicon dioxide. As the flat surface of SVCC modified in Scheme VII-IV was hydrophobic, silicon dioxide powder selectively deposited only on the hydrophilic hemispherical surface of SVCC to form the deposition layer of silicon dioxide.

SchemeVII-VII

As in Scheme VII-IV, after separation by filtration, silicon dioxide was modified with 3-aminoprophyl-trimethoxy silane (APMS) with the amino group terminus under the conditions in **Table VII-4** to result in the more hydrophilic hemispherical surface of SVCC.

Scheme VII-VIII

Hemispherical SVCC as template was dissolved by 1N-hydrochloric acid to finally result in hemispherical hollow silica microcapsules (HHSM). HHSM may have both the more hydrophobic flat surface and the more hydrophilic hemispherical surface.

VII-3-3. Measurement of amount of SVCC adhered

The PMMA mother particles were washed by deionized water, filtered and freeze-dried. Then, the amount of SVCC adhered was determined by means of back titration with 1 N-hydrochloric acid and 1 N-sodium hydroxide as follows. Namely, after 100 mg of the PMMA mother particles was added into 20 ml of 0.5 N-hydrochloric acid, the mixture was agitated by magnetic stirrer for 3 h so as to dissolve the whole amount of SVCC adhered. Then, after adding bromothymol blue indicator, back titration with 1 N-sodium hydroxide was performed to determine the amount of SVCC adhered.

VII-3-4. Etching hemispherical surface of SVCC

By reacting SVCC adhered on the PMMA mother particles with half the amount of 1 N-hydrochloric acid obtained just above, the surface of SVCC was partially etched to expose the flat surface of SVCC **(Scheme VII-III)**.

VII-3-5. Preparation of monodispersed gold particle

A colloidal gold-trapping test with an amino group was conducted in order to determine whether HHSM has the more hydrophilic surface

or not. Colloidal gold was prepared according to the procedure by G. Frens and S. Ikeda [20, 35]. In brief, 50ml of 0.01wt% solution of ($HAuCl_4$ Hydrogen tetrachloro aurate (III) tetrahydrate) was boiled for 5 min after adding 0.6 ml of trisodium citrate dihydrate solution (Na-Ca solution) containing 0.23 mmol of Na-Ca solution. Finally 30 μmol of Na-Ca solution was added to stabilize the colloidal gold. The solution prepared thus showed a vivid dark red color, indicating the presence of colloidal gold with the size from 20 to 50 nm.

VII-4. Characterization

VII-4-1. Observation of PMMA mother particles and hemispherical hollow silica microcapsules

SEM observation(SEM, JEOL Ltd., model;JSM-5800) was performed to examine the situation of adhesion of SVCC on the PMMA mother particles, the surface of the PMMA mother particles after partial etching and the deposition layer of silicon dioxide on the flat surface of SVCC.

VII-4-2. Demonstration of more hydrophilic surface

The affinity between colloidal gold and the more hydrophilic surface of HHSM was determined by the following method. Namely, 10 mg of HHSM was added to 10 ml of monodispersed gold particle solution under magnetic agitation to observe color change.

VII-4-3. Demonstration of more hydrophobic and more hydrophilic surfaces

If HHSM has both the more hydrophobic flat and the more hydrophilic hemispherical surface, they must behave as a kind of

particulate surfactant and adsorb on the liquid-liquid interface. To evaluate this, 10 mg of HHSM was added to the O/W dispersion, where 0.1 ml of MMA monomer was dispersed in 4.9 ml of distilled water. After agitation, the dispersion system was observed under optical microscope.

VII-4-4. Measurement of zeta potential of droplets and particles

Zeta potential of particles was measured by a particle size and zeta potential analyzer (OTSUKA ELECTRONICS Ltd., ELS-8000)

VII-5. Results and Discussion

VII-5-1. Observation of PMMA mother particles and determination of amount of adhered SVCC

Figure VII-2 shows the SEM images of the surface of PMMA mother particles. The PMMA mother particles could not be prepared without DBS, because suspension polymerization system was unstable. As the concentration of DBS increases, the amount of SVCC adhered may increases due to the change of zeta potential and the affinity. Furthermore, as the contact angle of SVCC to the liquid-liquid interface changed according to the interfacial tension, it could be expected that SVCC is embedded more deeply into the PMMA mother particle.(30,31)

Figure VII-3 shows the dependence of the amount of SVCC adhered on the concentration of DBS. The amount of SVCC adhered is found to linearly increase with the concentration of DBS. As MMA droplets have the negative charge of -10 mV and SVCC has the negative

charge of -12 mV, SVCC may adhere on the surface of a MMA droplet due to wettability between them.

Figure VII-4 shows the surface of PMMA mother particles, which were prepared at 75ppm of DBS, before and after etching. Only the exposed portion of SVCC adhered onto the PMMA mother particles was found to be etched.

Figure VII-5 shows the SEM images of the flat surface of SVCC. As compared to the surface of SVCC without modification, it is found that the surfaces modified with the dripping rate(slow) of 0.39 ml/min of sodium hydroxide solution exhibit deposition of silicon dioxide nanoparticles with the size of approx. 100 nm and those with the dripping rate(fast) of 0.79 ml/sec do deposition of larger silicon dioxide particles with the size of approx. 1 μm. This suggests that the slow dripping(0.39ml/min) of sodium hydroxide produces the large amount of nano sized core of SiO_2. On the other hand, the fast dripping(0.79ml/sec) of sodium hydroxide produces less amount of nano sized core of SiO_2 than slow dripping and then grows them.From these results, it is found that the surface of SVCC is able to cover with different sized SiO_2.

Figure VII-6 shows the SEM images of the direct front of the hemispherical surface of SVCC, which were separated off from the PMMA mother particles by dissolution with acetone, before and after deposition of silicon dioxide. The images on the left-hand side look very smooth, whereas the images on the right-hand side show deposition of silicon dioxide nanoparticles. The driving force that the silicone dioxide nanoparticles deposit selectively on to the round

surface may be affinity. Namely, the flat surface has already modified by hydrophobic silane coupling agent, so it may hard to deposit the hydrophilic silicone dioxide nanoparticles on to it

Figure VII-7 shows the photographs of the solution before and after adding HHSM into the colloidal gold solution. Before addition of HHSM, the color of solution was vivid, transparent red, and after addition of HHSM, it turned navy blue instantly. Furthermore, immediately after addition of HHSM, the suspension started separating into a clear, colorless supernatant liquid part and a black sediment part, indicating that gold nanoparticles were trapped with amino group introduced on the hemispherical surface of HHSM. This phenomenon may demonstrate that the amino group which has good affinity with gold nanoparticles was introduced onto the round surface, if not, this gold solution does not changes its color. In order to verify the trappment of gold nano-particles, TEM observation should be performed in future.

VII-5-2. Demonstration of particulate surfactant

An optical micrograph of a MMA droplet in the O/W emulsion is shown on the left-hand side in **Figure VII-8**. It is found that HHSM adheres on the surface of MMA droplet. As HHSM has the more hydrophobic flat surface, it may be supposed that HHSM adhered on the surface of MMA droplets.

Figure VII-9 shows an optical micrograph of HHSM. This reveals that hemispherical hollow silica microcapsules are able to be prepared. Although we tried to take SEM photographs of the particles instead of

optical micrographs, we couldn’t do because the samples were broken down during the drying process. We believe that the hollow microcapsule has been synthesized by the developed procedure, in which the silicone dioxide nanoparticles selectively deposit onto the surface of SVCC and SVCC as template is dissolved easily by penetrating hydrochloric acid.

VII-6. Conclusion

Hemispherical hollow silica microcapsules with both the more hydrophilic and the more hydrophobic surface were synthesized by the sol-gel method using spherical vaterite calcium carbonate as template. The flat and hemispherical surfaces of hollow silica microcapsules can be modified with various functional groups, which can be anticipated to be applied to drug delivery systems. Findings obtained from this study are as follows.

1) Adhesion of spherical vaterite calcium carbonate on the MMA droplets largely depended on the concentration of DBS.

2) Suspension polymerization was unstable without DBS.

3) An amino group introduced was easily identified by the color change caused by trapping nano-gold particles with amino group.

4) Hemispherical hollow silica microcapsules adhered on the liquid-liquid interface as particulate surfactant.

REFERENCES

[1] Y. Taguchi and M. Tanaka, J. Appl. Polym. Sci., **80** (2001) 2662

[2] I. Kimura, S. Ikarashi, N. Saito and M. Tanaka, Adv. Powder Technol., **8** (1997) 1

[3] R. Bondmeier and J. W. McGinity, Int. J. Pharm., **51** (1987) 1

[4] J. W. Fong, J. P. Nazanero, J. Pearson and H. V. Maulding, *J.* Control. Release., **3** (1986) 119

[5] J. T. Kenney et al., J. Colloid Interface Sci., **42** (1973) 589

[6] P. W. Morgan et al., J. Polym. Sci., **40** (1959) 289

[7] T. Kondo, in “Surface and Colloid Science” (Plenum Press, New York, 1978) p1

[8] A. Imhof, Langmuir, **17** (2001) 3579

[9] P. B. O’donnell, J. W. McGinity, Adv. Drug Deliver Rev., **28** (1997) 25

[10] M. D. Dhanaraju, K. V. R. Jayakumar and C. Vamsadhara, Int. J. Pharm., **268** (2003) 23

[11] L. Mu, S. S. Feng, J. Control. Release, **86** (2003) 33

[12] X. Shi and T. Tan, Biomaterials, **23** (2002) 4469

[13] L. Wang, G. Ma and Z. Su, J. Control. Release, **106** (2005) 62

[14] S. Pamujula, R. A. Graves, V. Kishore and T. K. Mandal, Eur. J. Pharm. Biopharm., **57** (2004) 213

[15] M. J. D'Souza and P. DeSouza, Adv. Drug. Deliver Rev., **17** (1995) 247

[16] S. Freiberg and X. X. Zhu, Int. J. Pharm., **282** (2004) 1

[17] H. Ichikawa, K. Fujioka, M. C. Adeyeye and Y. Fukumori, Int. J. Pharm., **216** (2001) 67

[18] T. Gorner, R. Gref, D. Michenot, F. Sommer, M. N. Tran and E. Dellacherie, J. Control. Release, **57** (1999) 259

[19] N. A. Peppas, P. Bures, W. Leobandung and H. Ichikawa, Eur. J. Pharm. Biopharm., **50** (2000) 27

[20] Y. K. Takahara, S. Ikeda, S. Ishino, K. Tachi, K. Ikeue, T. Sakata, T. Hasegawa, H. Mori, M. Matsumura and B. Ohtani, J. Am. Chem. Soc., **127** (2005) 6271

[21] H. Takei, Langmuir, **13** (1997) 1865

[22] K. Fujimoto, K. Nakahama, M. Shidara, H. Kawaguchi, Langmuir, **15** (1999) 4630

[23] L. Petit, J. P. Manaud, C. Mingotaud, S. Ravaine and E. Duguet, Mater. Lett., **51** (2001) 478

[24] T. Kawakatsu, G. Tragardh and C. Tragarudh, Colloids Surf., **189** (2001) 257

[25] K. Kato and N. Yamasaki, Chem. Eng. Jpn., **24** (1991) 709

[26] T. Hirai, N. Okamato and I. Komasawa, Am. Inst. Chem. Eng. J., **44** (1998) 197

[27] T. Kawakatu, Y. Kikuchi and M. Nakajima, J. Am. Oil Chem. Soc., **74** (1997) 317

[28] T. Kawakatu, H. Komori, M. Nakajima, Y. Kikuchi and T. Yonemoto, J. Chem. Eng. Jpn., **32** (1999) 241

[29] T. Kawakatsu, G. Tragardh, C. Tragarudh, M. Nakajima, N. Oda and T. Yonemoto, J. Colloid Surf. A, **179** (2001) 29

[30] M. Tanaka and K.Hayashi, Kagaku Kogaku Ronbunshu, **15**(6)

(1989) 1144

[31] M. Tanaka, A Saito and K. Hosogai and N, Saito, Kagaku Kogaku Ronbunshu, **18**(4) (1992) 528

[32] Y. Taguchi and M. Tanaka, Kagaku Kogaku Ronbunshu, **24**(4) (1998) 633

[33] S. Eiamtrakarn, Y. Itoh, J. Kishimoto, Y. Yoshikawa, N. Shibata, M. Murakami and K. Takada, Biomaterials, **23** (2002) 145

[34] S. Eaimtrakarn, Y. Itoh, J. Kishimoto, Y. Yoshikawa, N. Shibata and K. Takada, Int. J. Pharm., **224** (2001) 61

[35] G. Frens, Nature Phys. Sci., **241** (1973) 20

Figure Captions

Table Captions

Table VII-1. Reaction conditions of TEOS on the flat surface of SVCC

EtOH	180ml
TEOS	3.75g(0.1mol/l)
D.Water	22.3g(6.9mol/l)
1N-NaOH soln.	1.35ml(TEOS/NaOH=13.3mol ratio)
Mother particles	2.00g

Reaction condition : 293K-2H

Table VII-2. Conditions for surface modification with silane coupling agent (introducing a methacryloyl group)

MPTS	0.06 g
EtOH	1.00 g
D.Water	1.00 g
↓ 0.5 ml	
Mother particles after TEOS reacted	0.70 g
Reaction condition	383K-30 min

Table VII-3. Reaction conditions of TEOS on the hemispherical surface of SVCC

EtOH	10ml
TEOS	0.63g(0.3mol/l)
D.Water	1.31g(7.3mol/l)
1N-NaOH soln.	0.15ml(TEOS/NaOH=20mol ratio)
Mother particles	100mg

Table VII-4. Conditions for surface modification with silane coupling agent (introducing an amino group)

APMS	0.10 g	
EtOH	1.00 g	
D.Water	1.00 g	
↓ 50 μl		
Hemiparticles after TEOS reacted		0.05 g
Reaction condition		383K-30 min

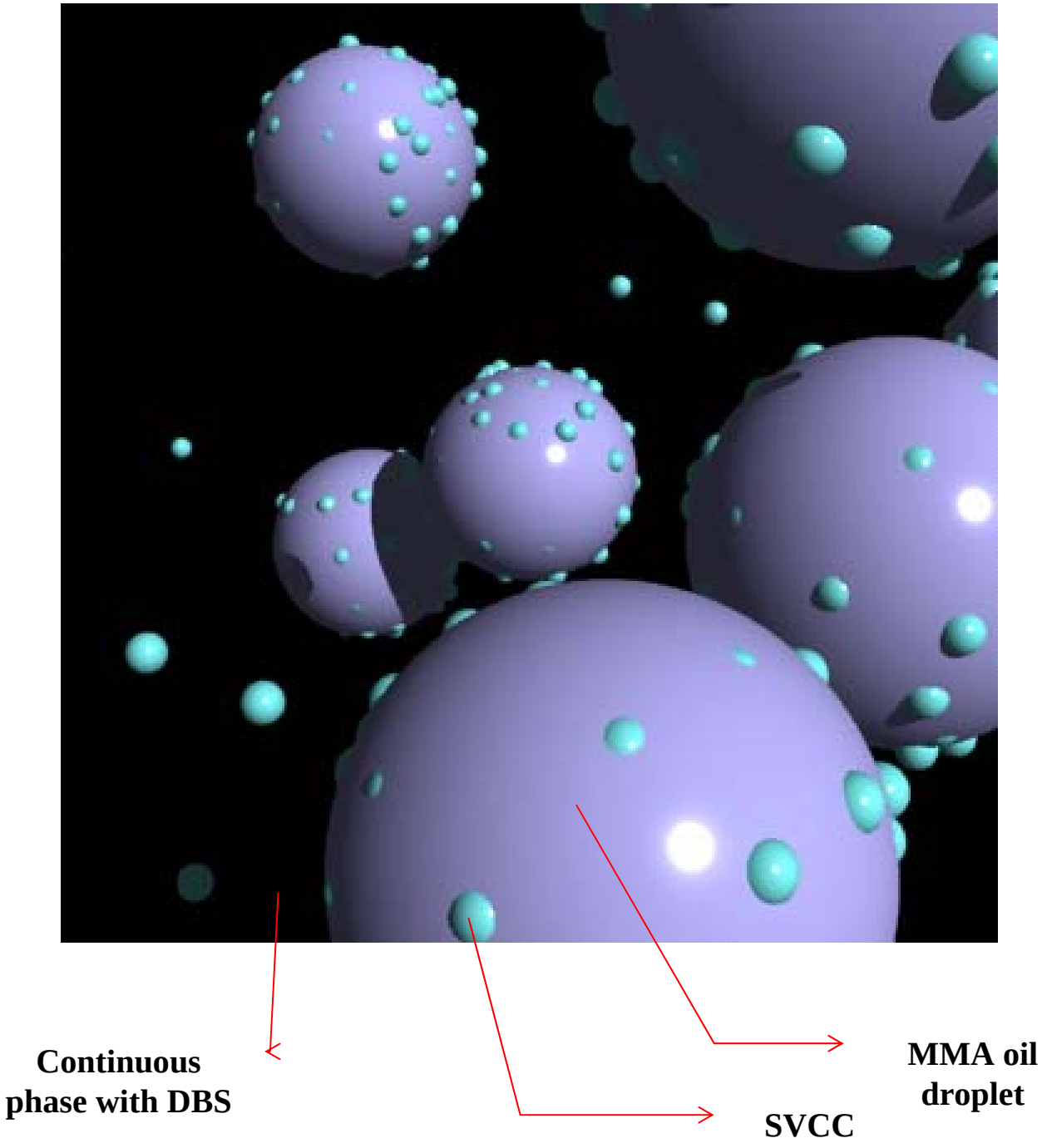

Scheme VII-I (Whole image)

Figure VII-1. Scheme for preparing HHSM

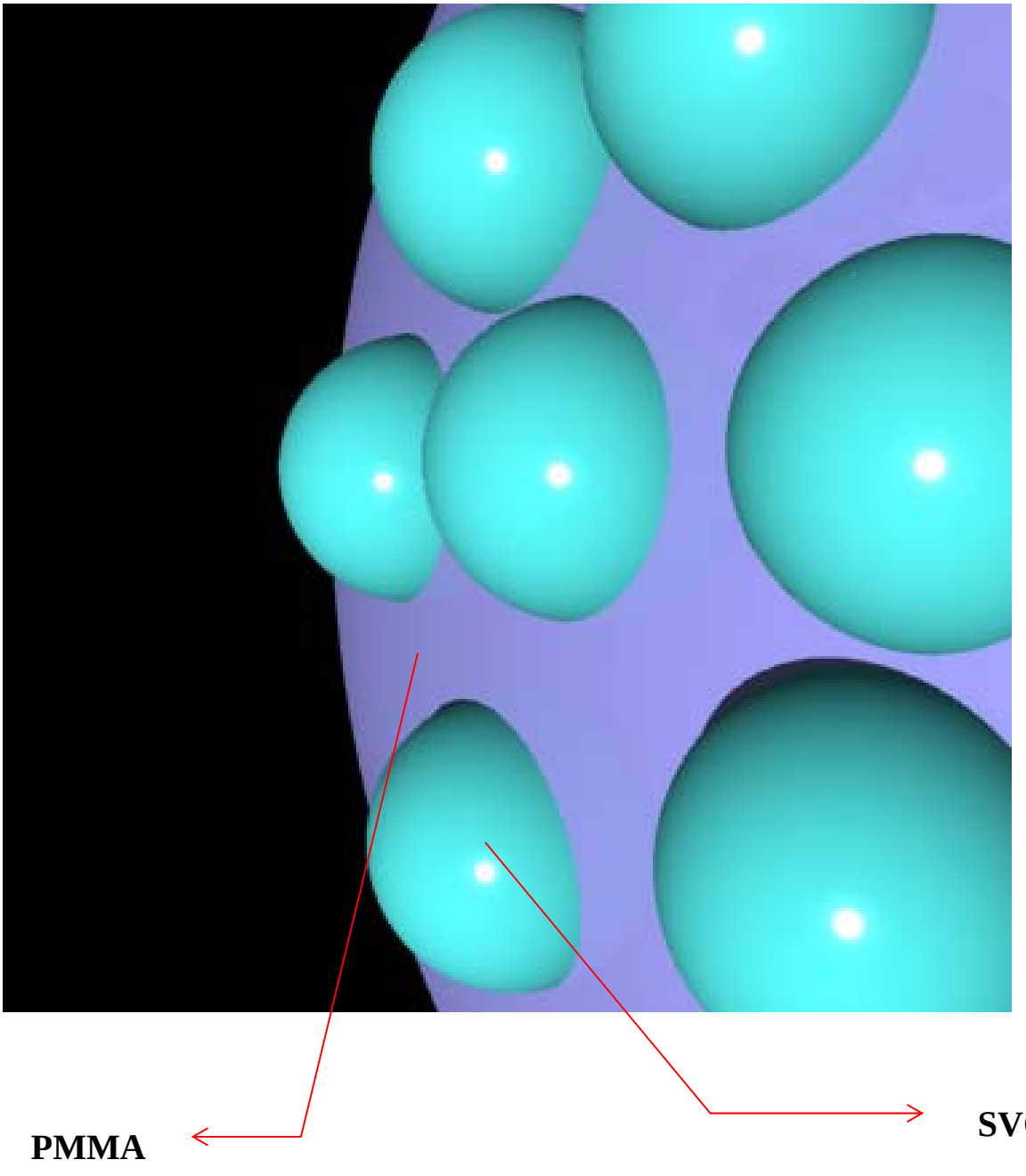

Scheme VII-II (Magnified image after polymerization)

Figure VII-1. Scheme for preparing HHSM

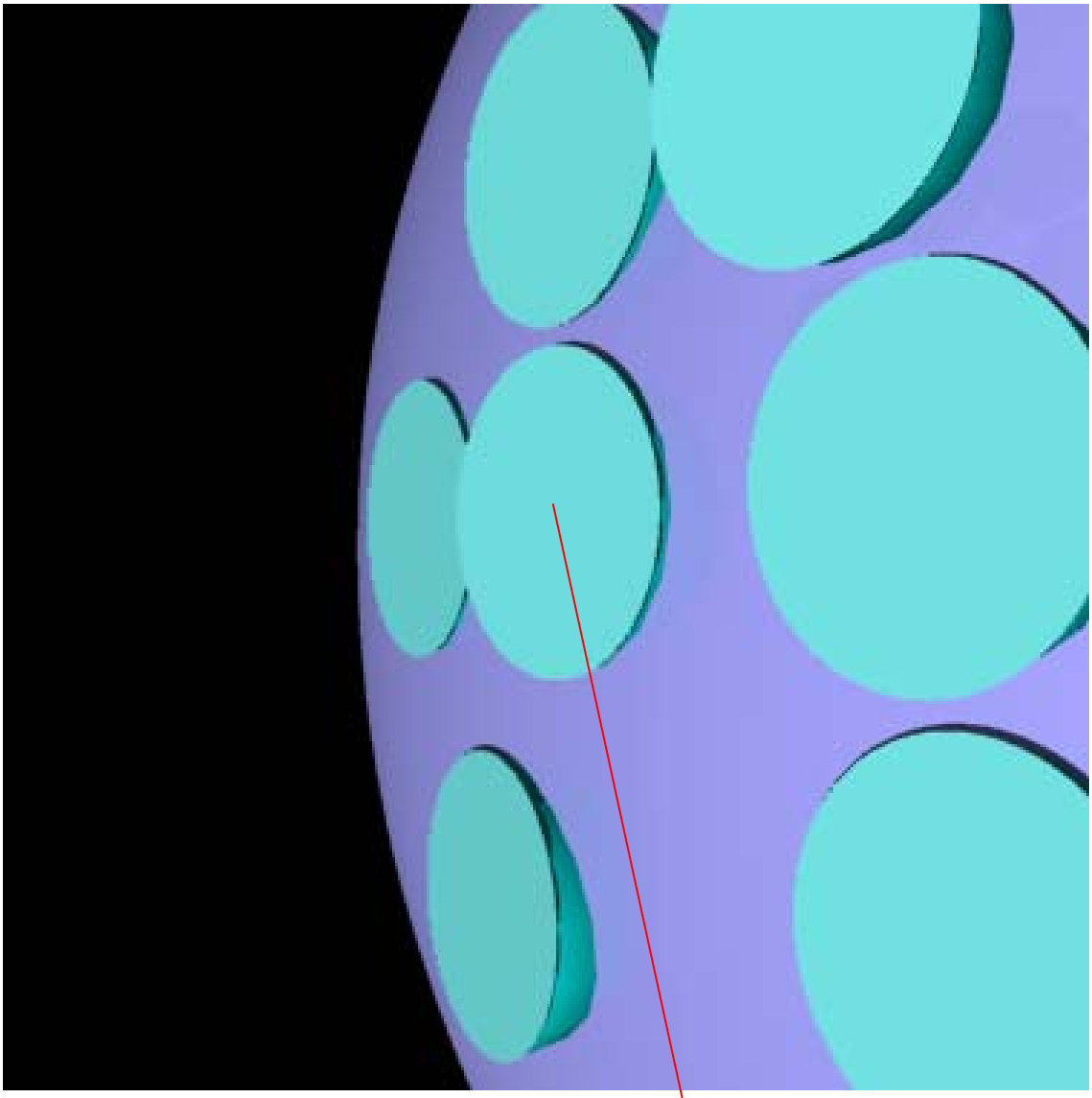

Scheme VII-III(Magnified image after etching)

Figure VII-1. Scheme for preparing HHSM

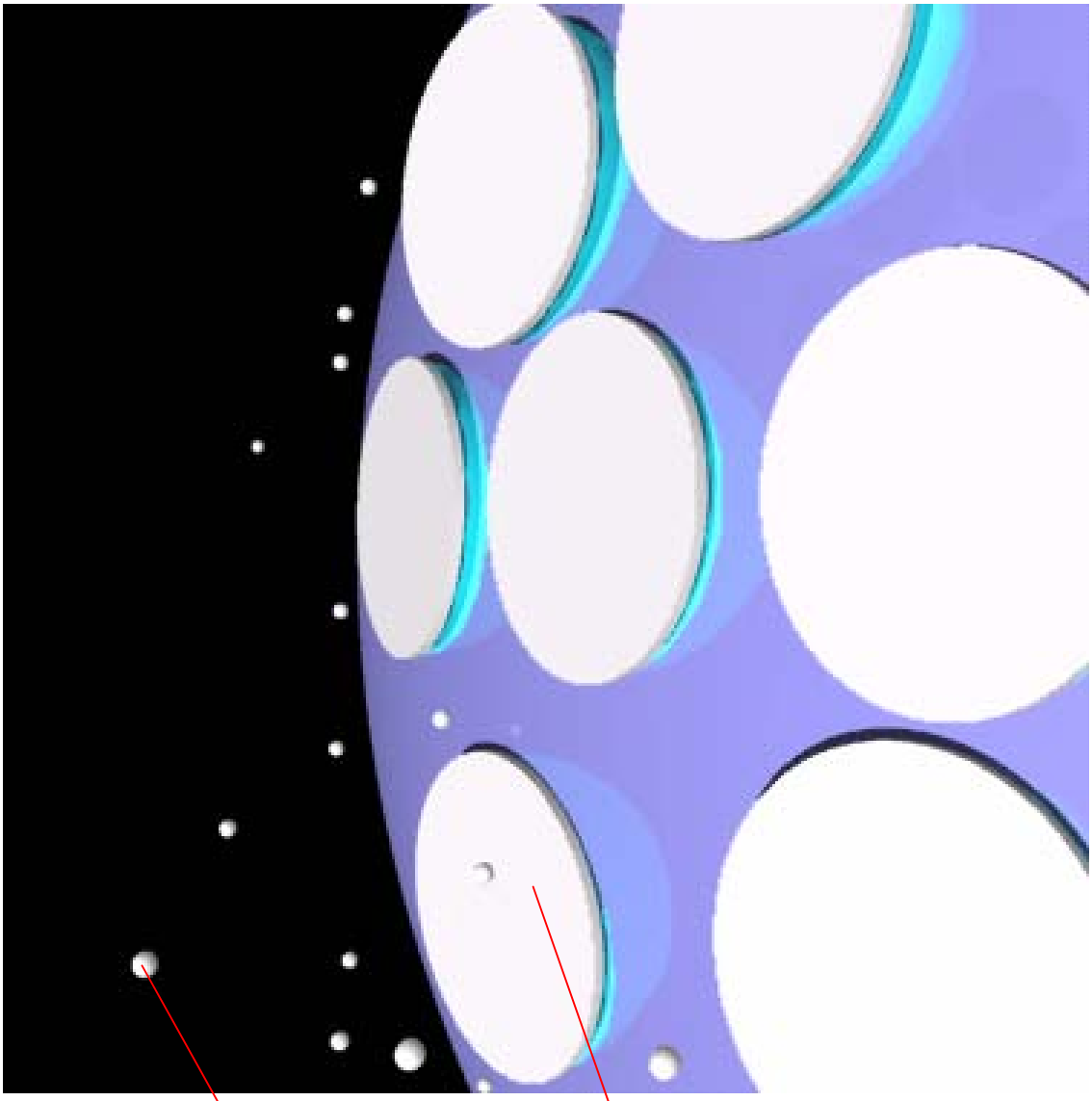

Scheme VII-IV-1(Magnified image)

Figure VII-1. Scheme for preparing HHSM

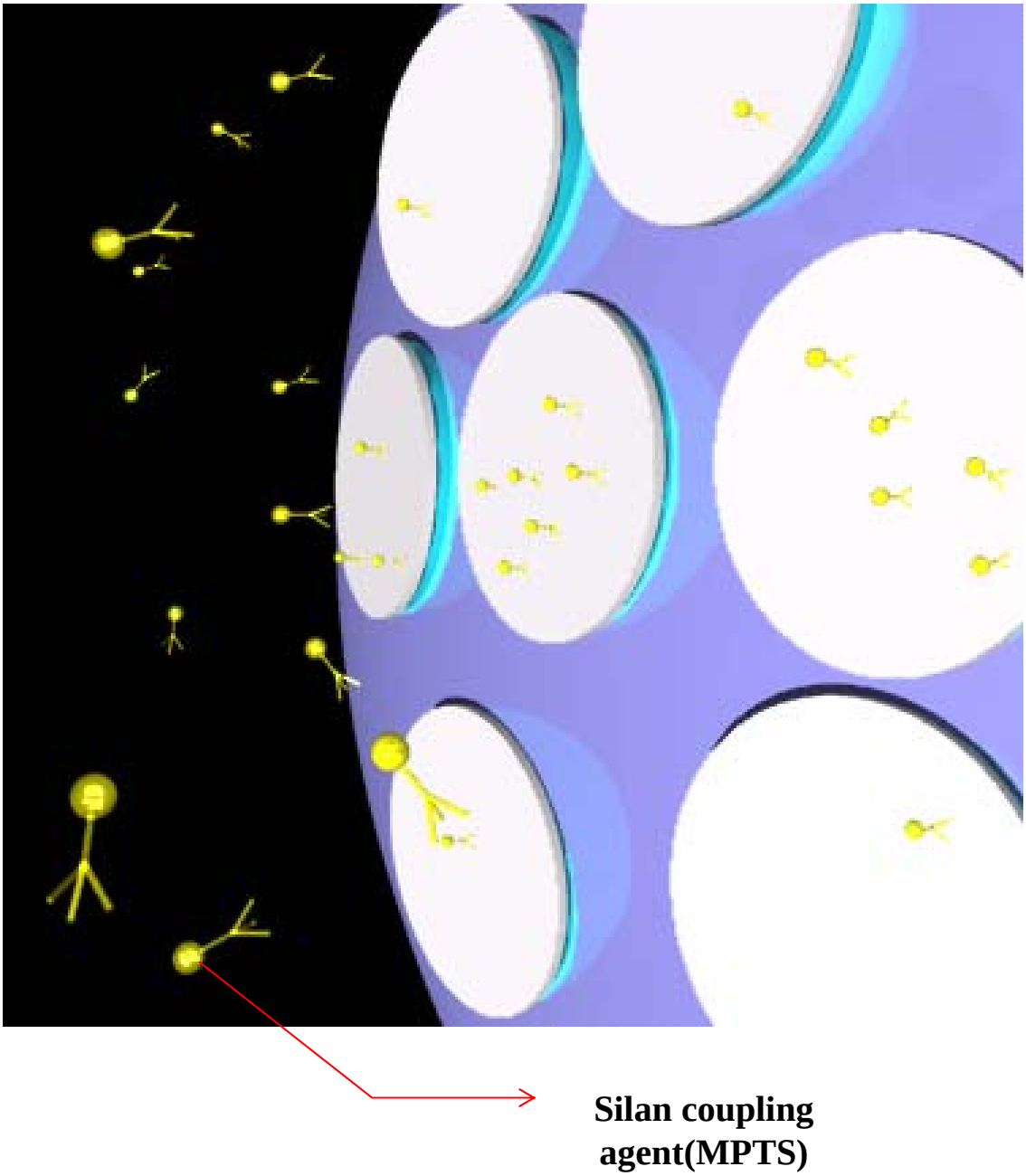

Scheme VII-IV-2(Magnified image)

Figure VII-1. Scheme for preparing HHSM

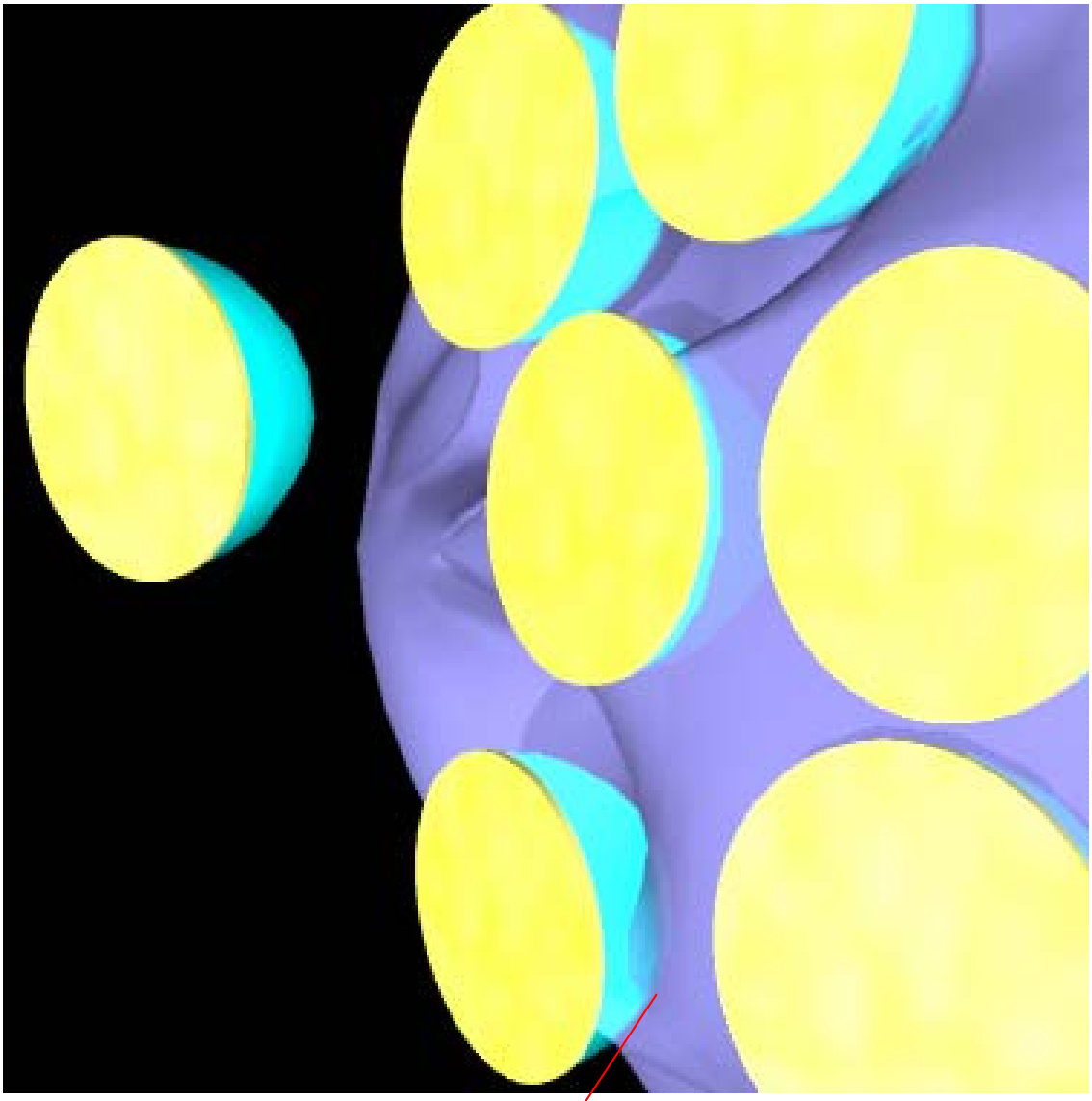

Scheme VII-V(Magnified image)

Figure VII-1. Scheme for preparing HHSM

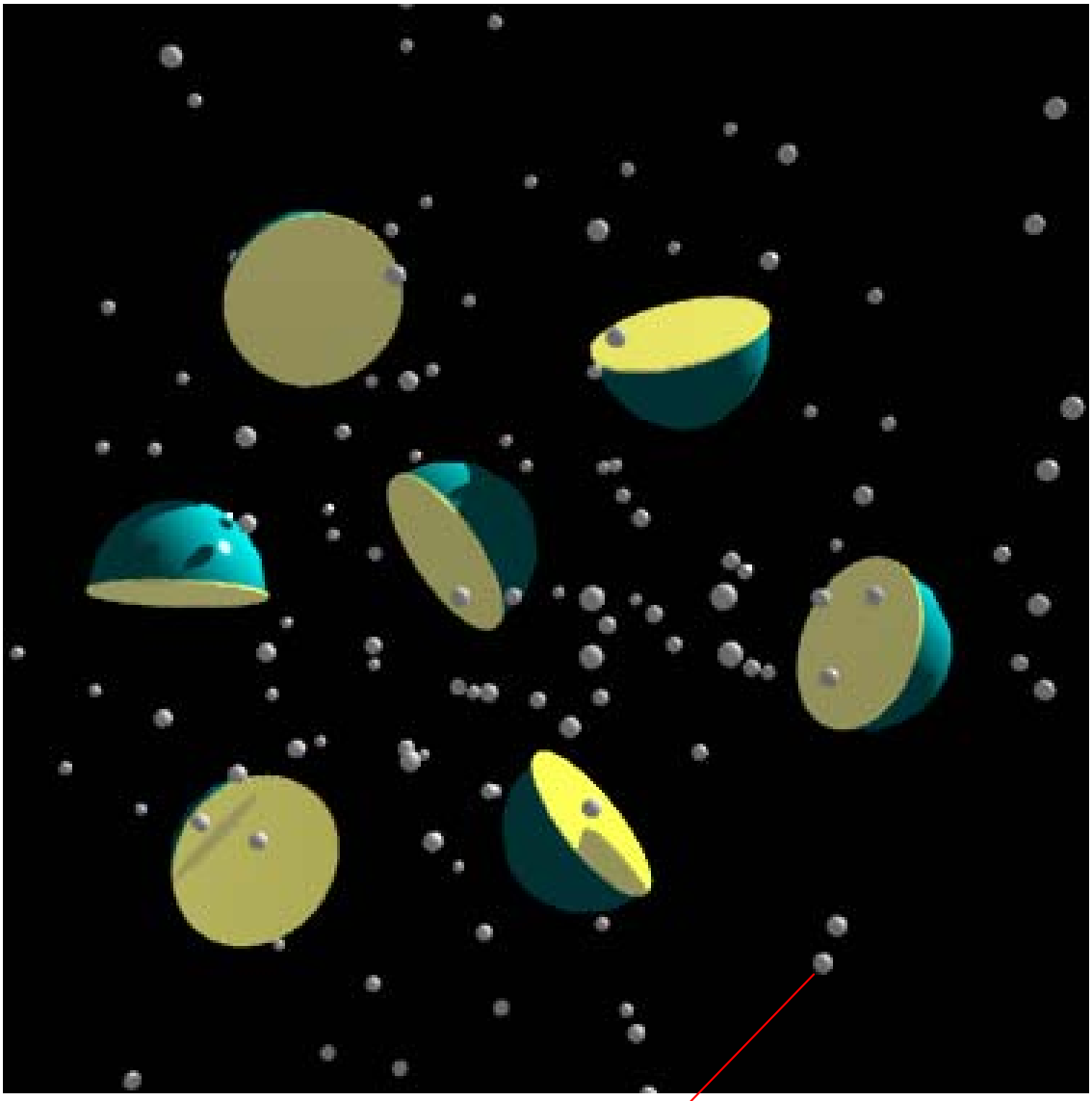

Silicon dioxide nano particles

Scheme VII-VI-1(Whole image)

Figure VII-1. Scheme for preparing HHSM

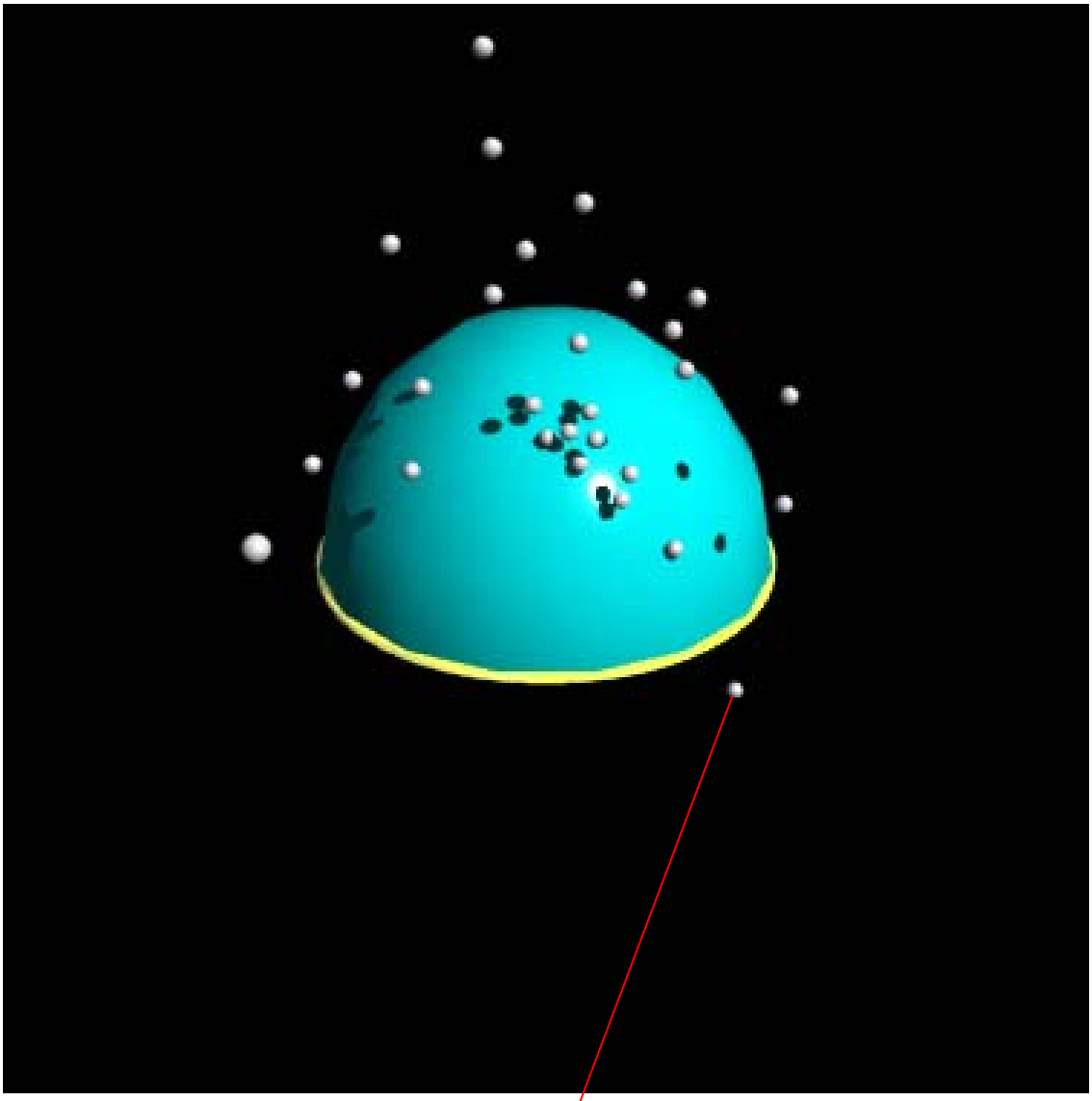

Scheme VII-VI-2(Magnified image)

Figure VII-1. Scheme for preparing HHSM

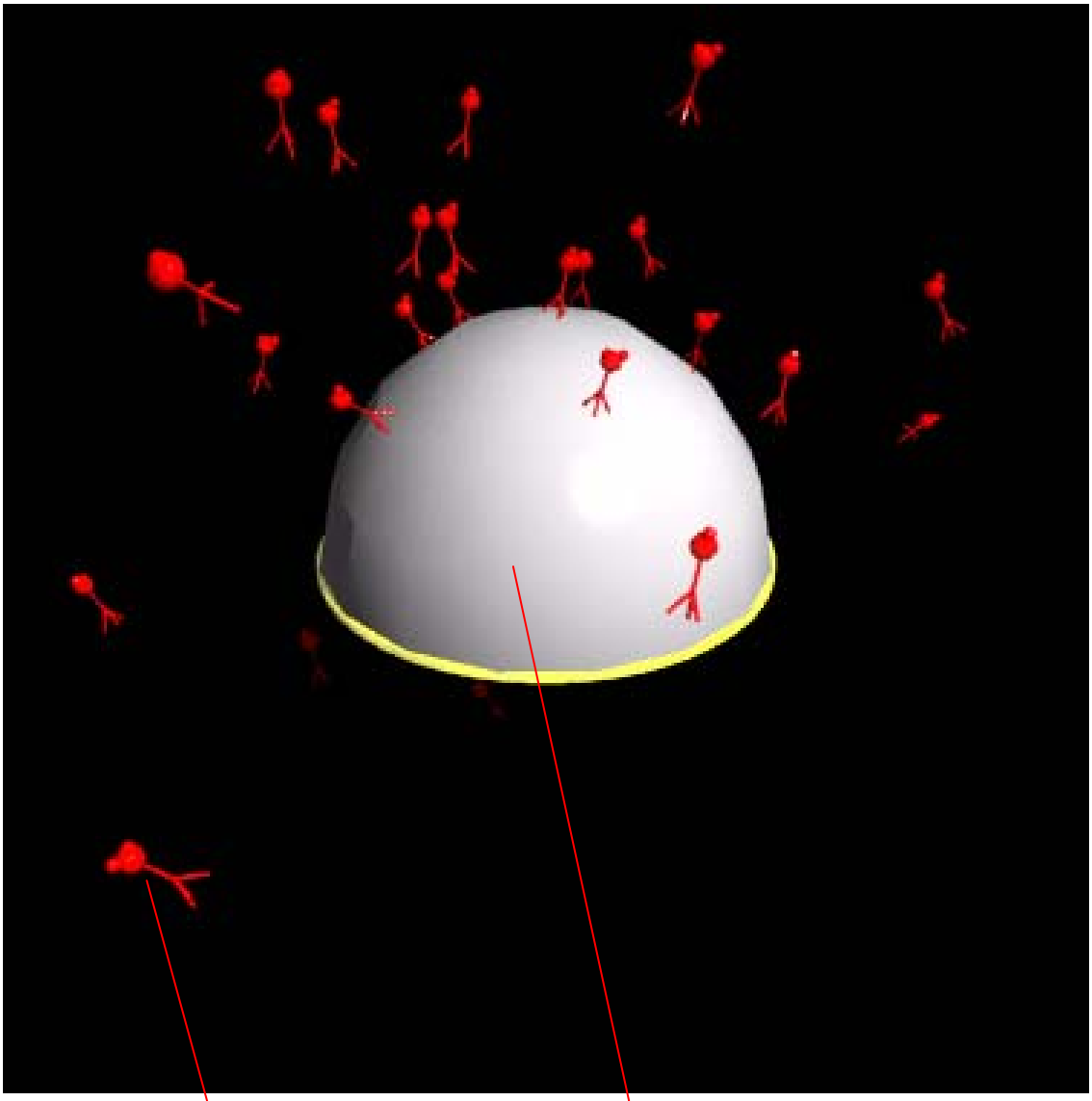

Scheme VII-VII(Magnified image)

Figure VII-1. Scheme for preparing HHSM

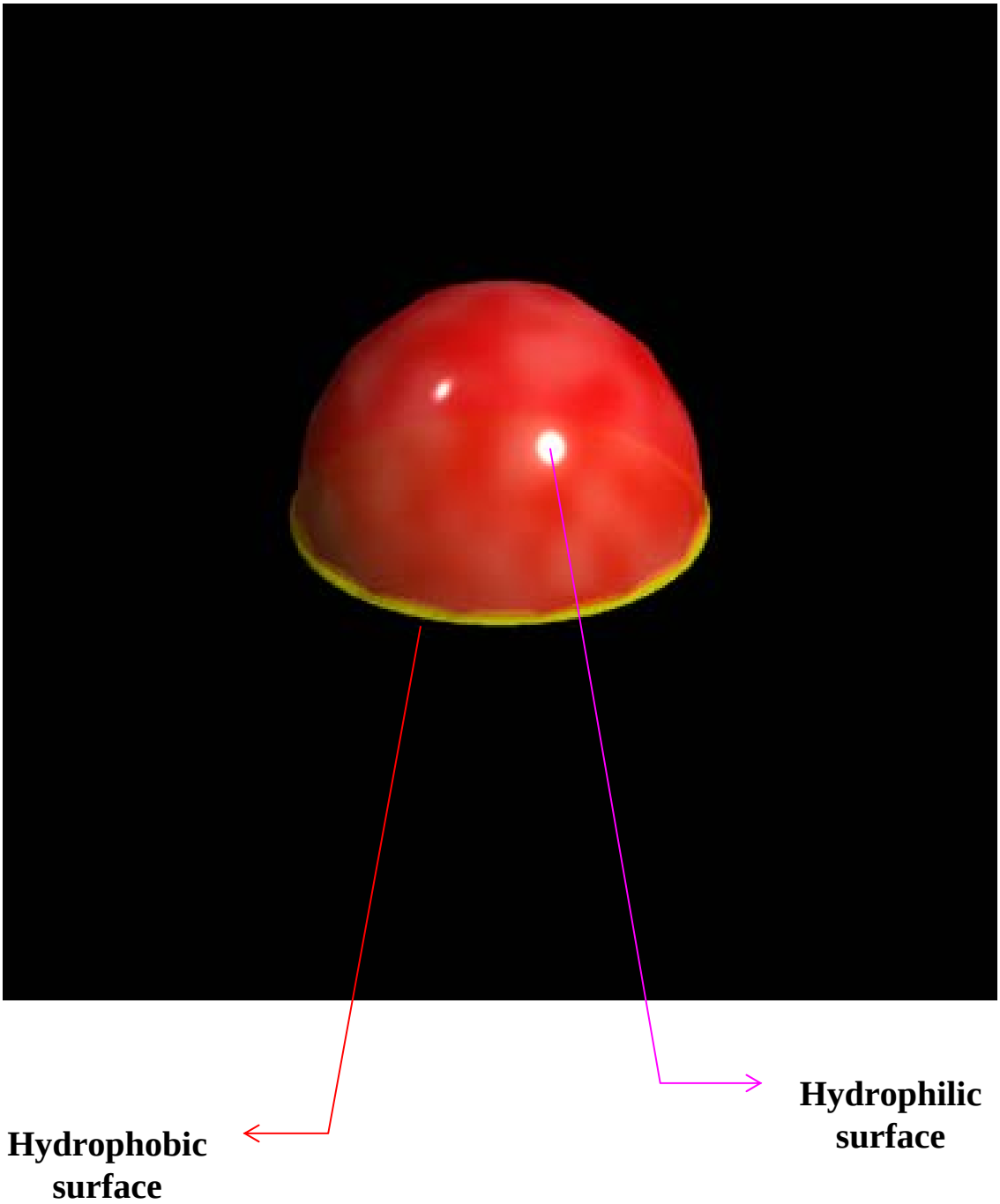

Scheme VII-VIII(Magnified image)

Figure VII-1. Scheme for preparing HHSM

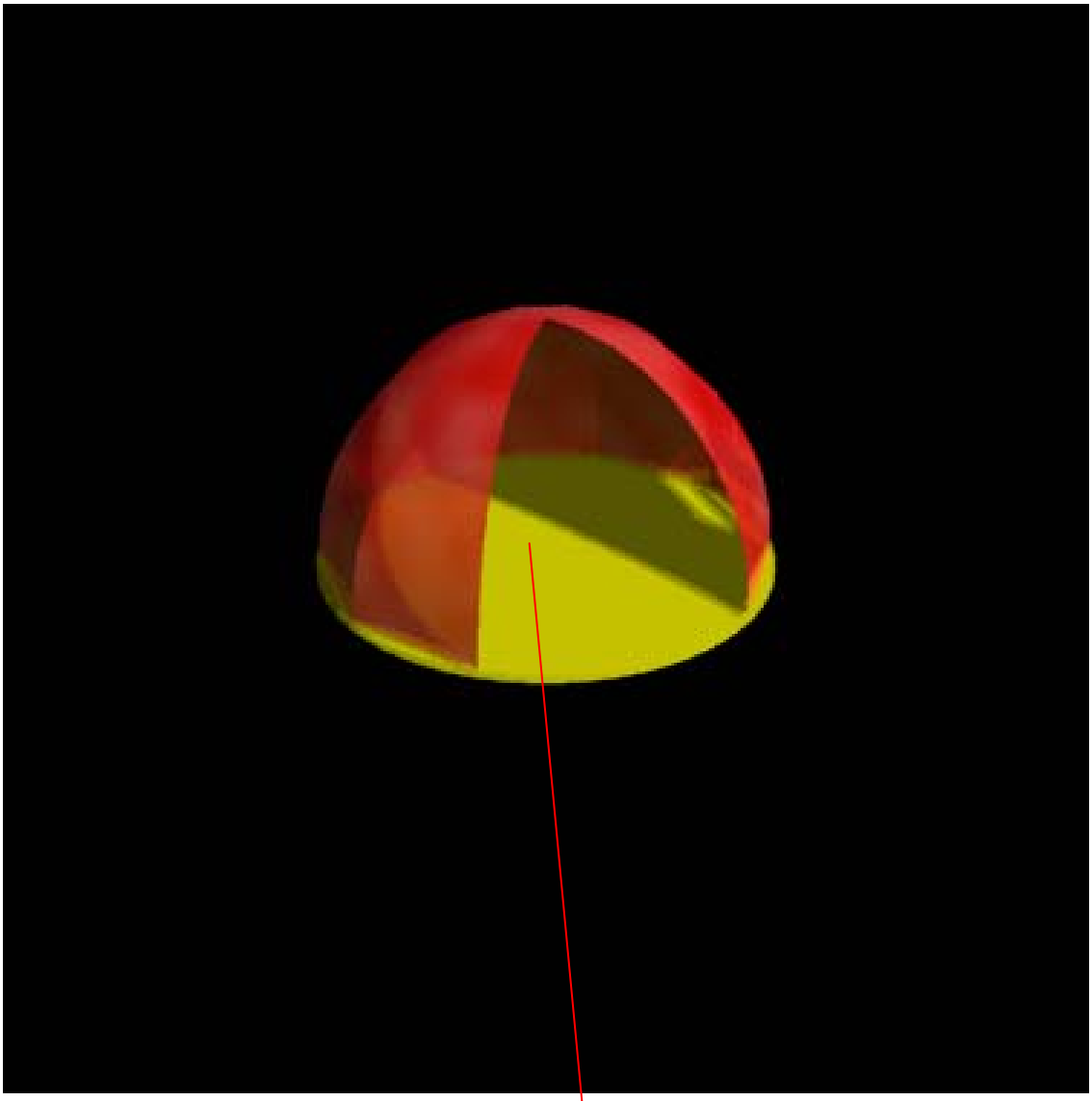

Scheme VII-VIII-2

(Partiality cross section magnified image)

Figure VII-1. Scheme for preparing HHSM

DBS
25 ppm

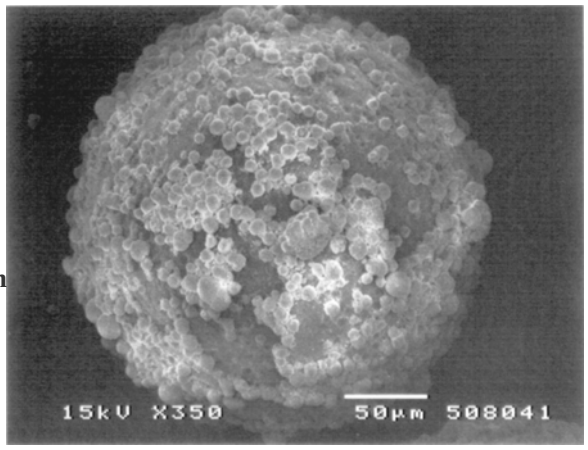

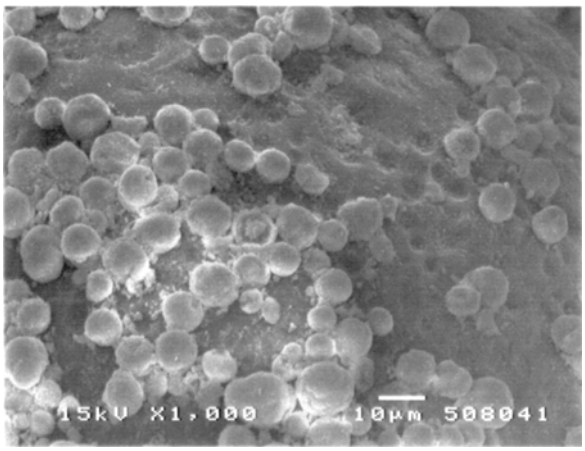

DBS
50 ppm

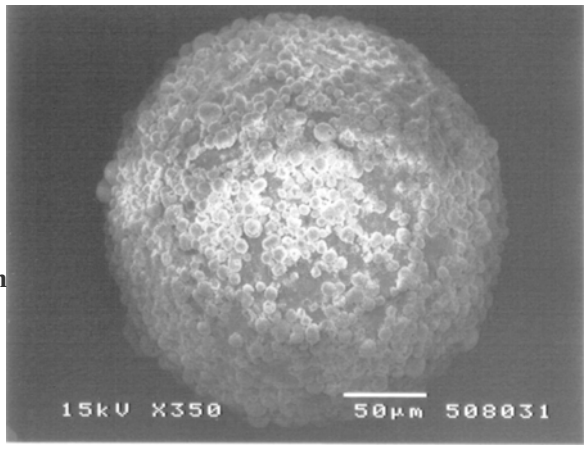

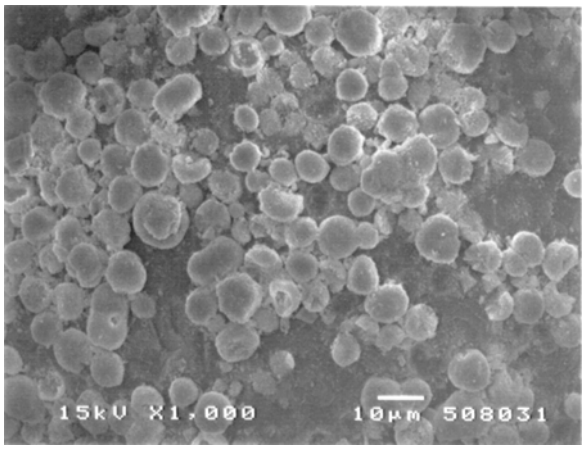

DBS
75 ppm

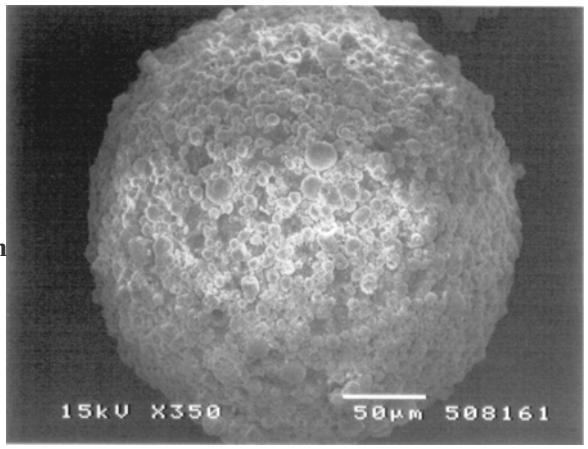

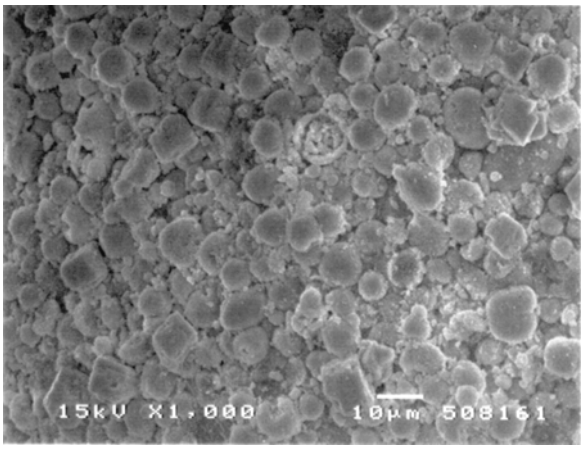

Figure VII-2. SEM images showing the relationship between the concentration of DBS and the amount of SVCC adhered

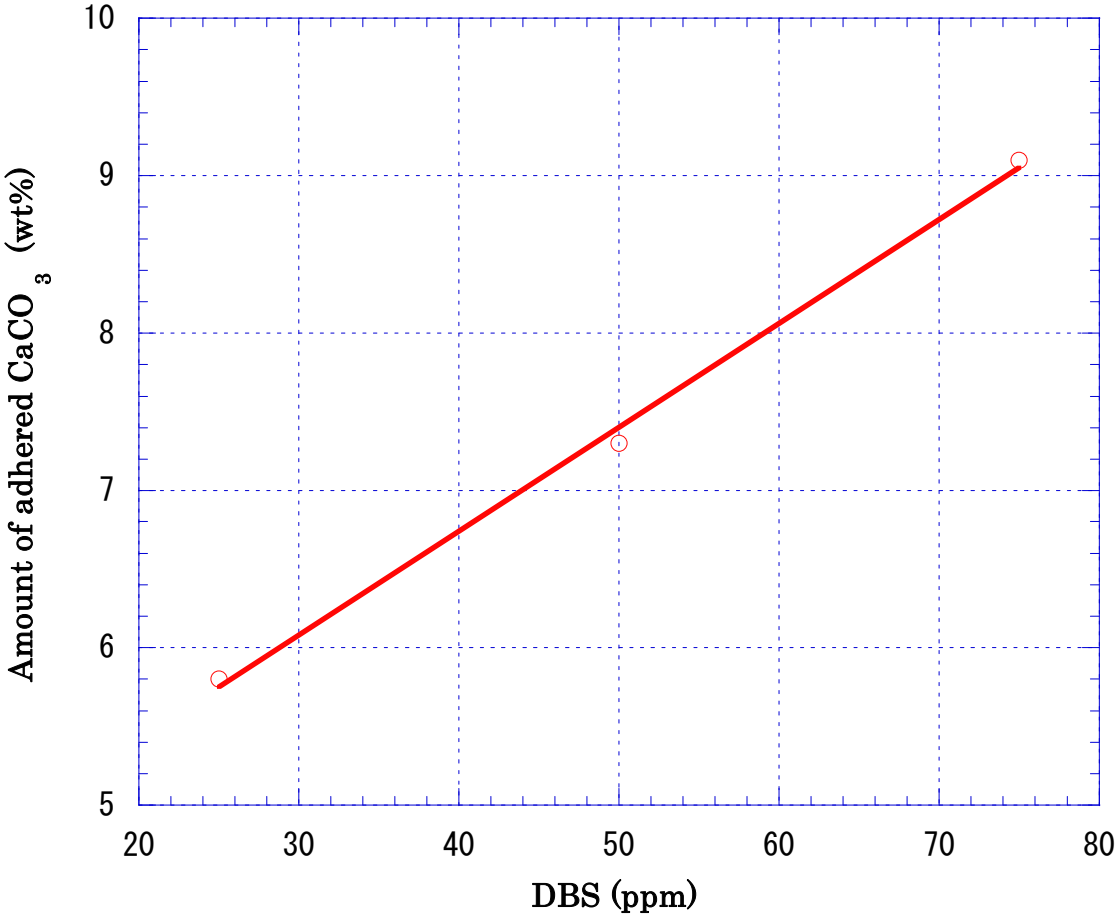

Figure VII-3. The relationship between the concentration of DBS and the amount of SVCC adhered

Mother particle (before etching)

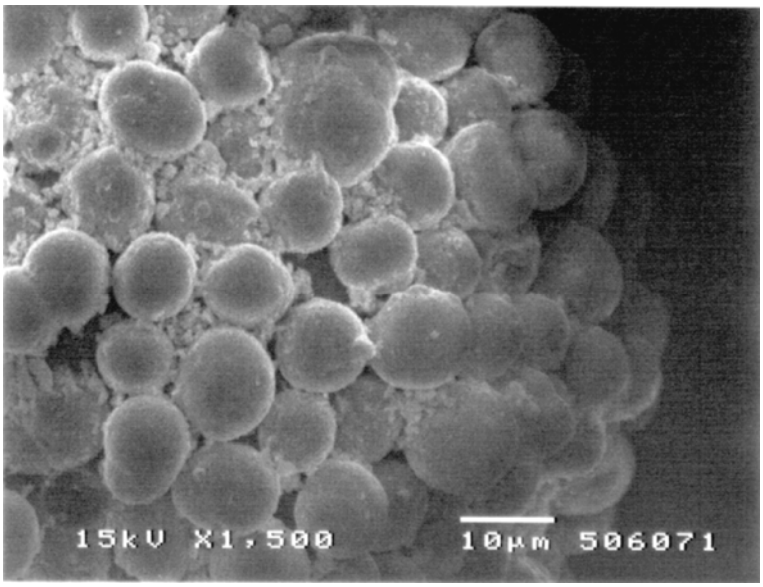

Mother particle (after etching)

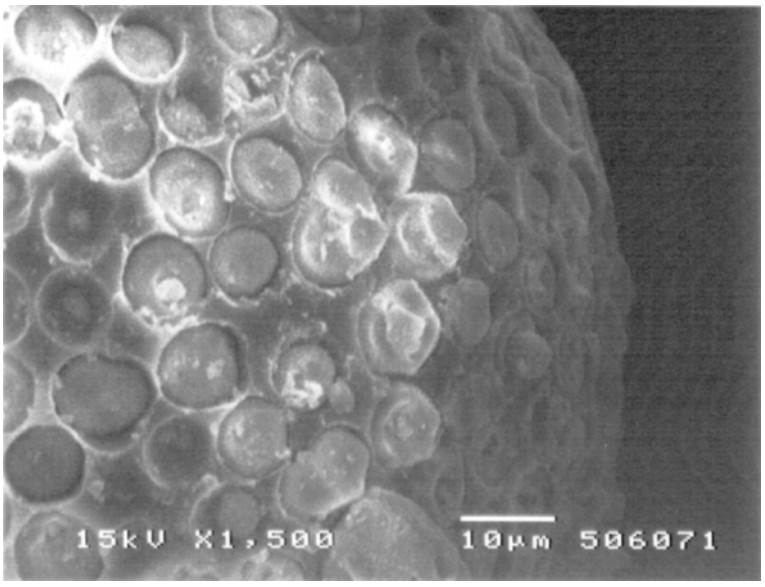

Figure VII-4. SEM images before and after etching

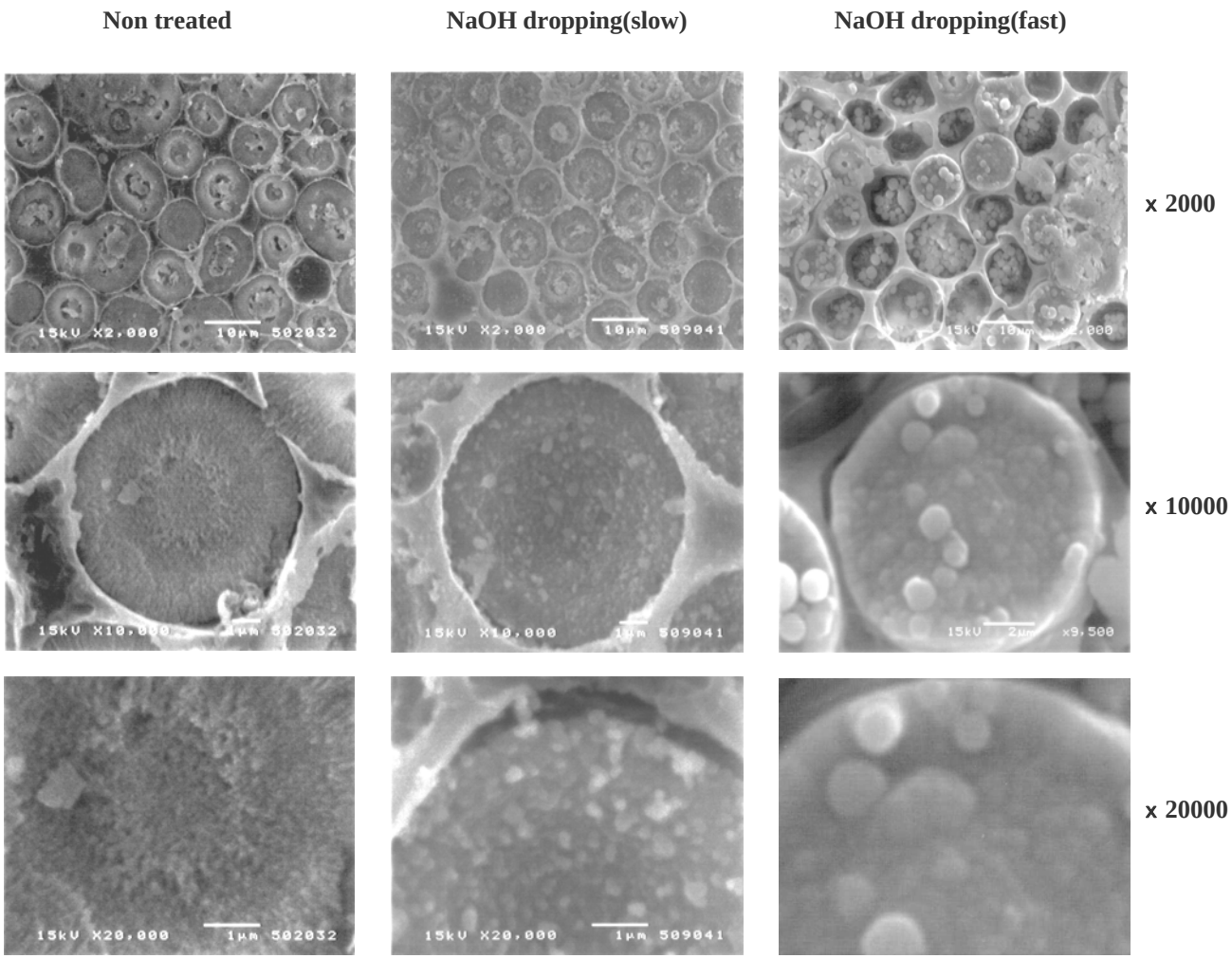

Figure VII-5. SEM images after condensation of TEOS onto the flat surface of SVCC

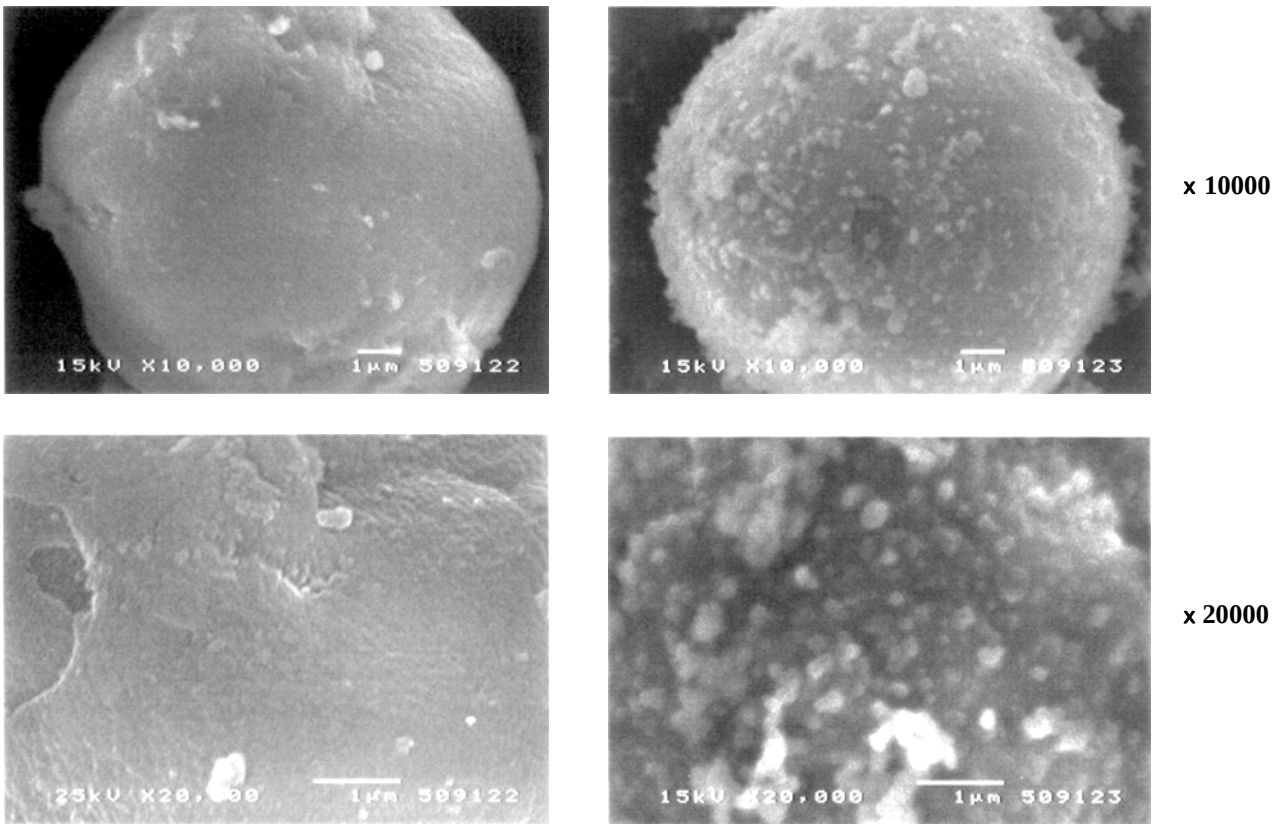

FigureVII-6. SEM images after condensation of TEOS onto the hemispherical surface of SVCC

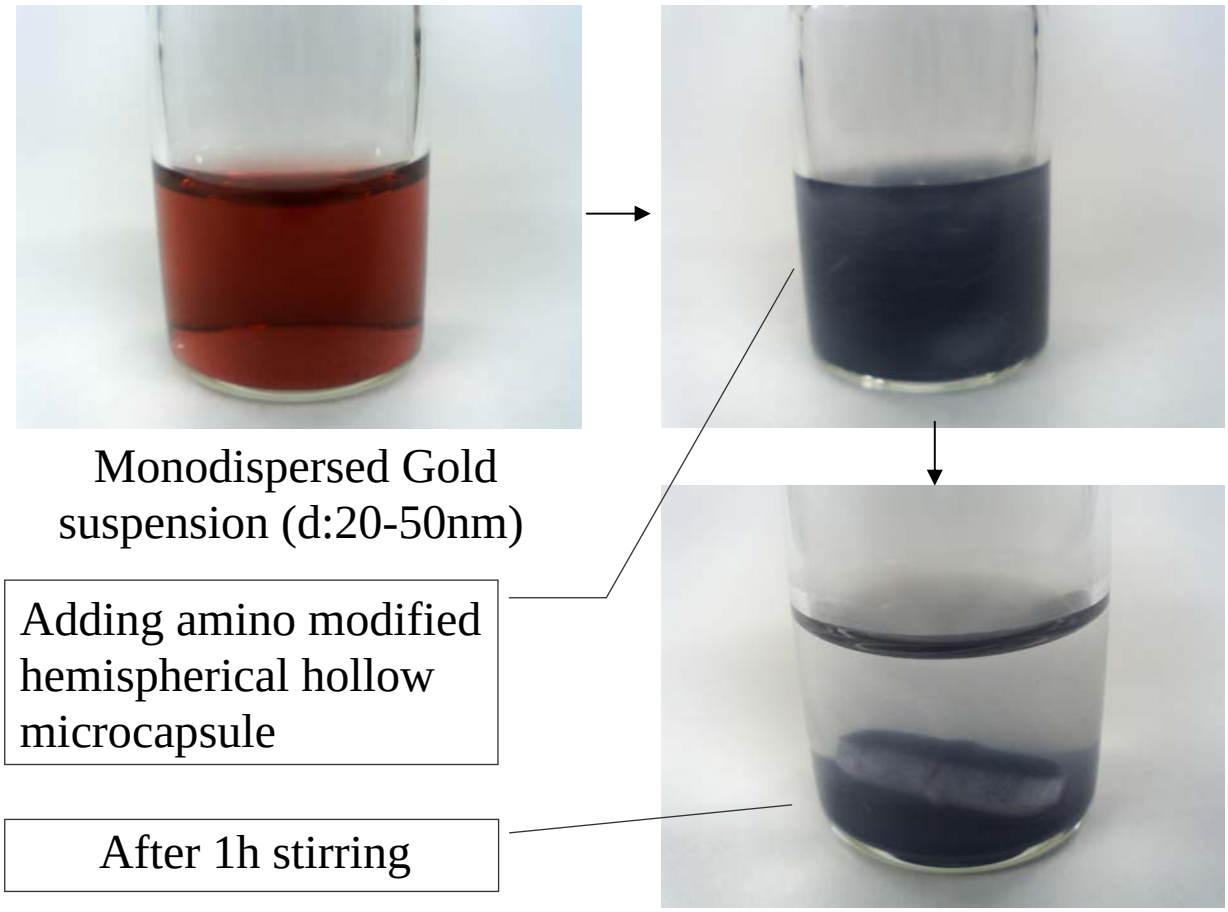

FigureVII-7. Photos before and after colloidal gold adheres to hemispherical microcapsules

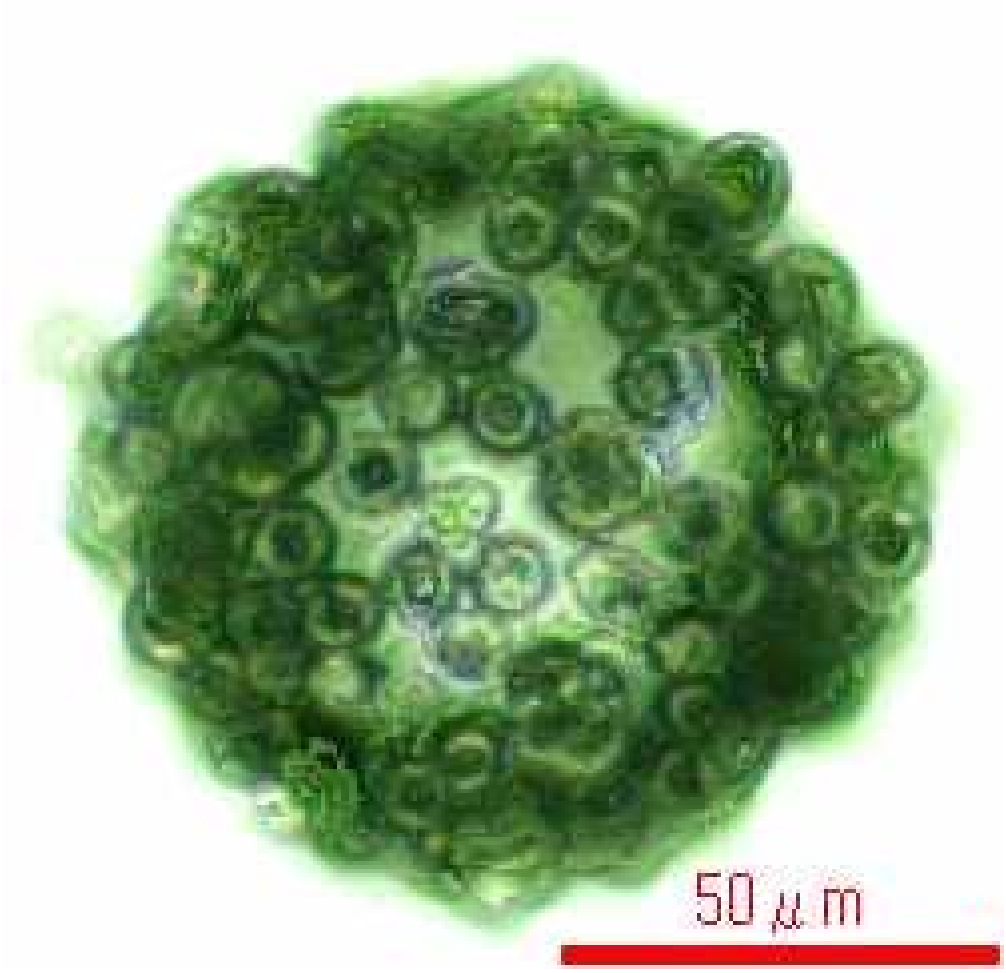

D.Water 4.9ml / MMA 0.1ml / Sample 10mg

FigureVII-8. An Optical micrograph showing hemispherical microparticles adsorbed onto an oil droplet of the MMA/W dispersion system, indicating surfactant potency

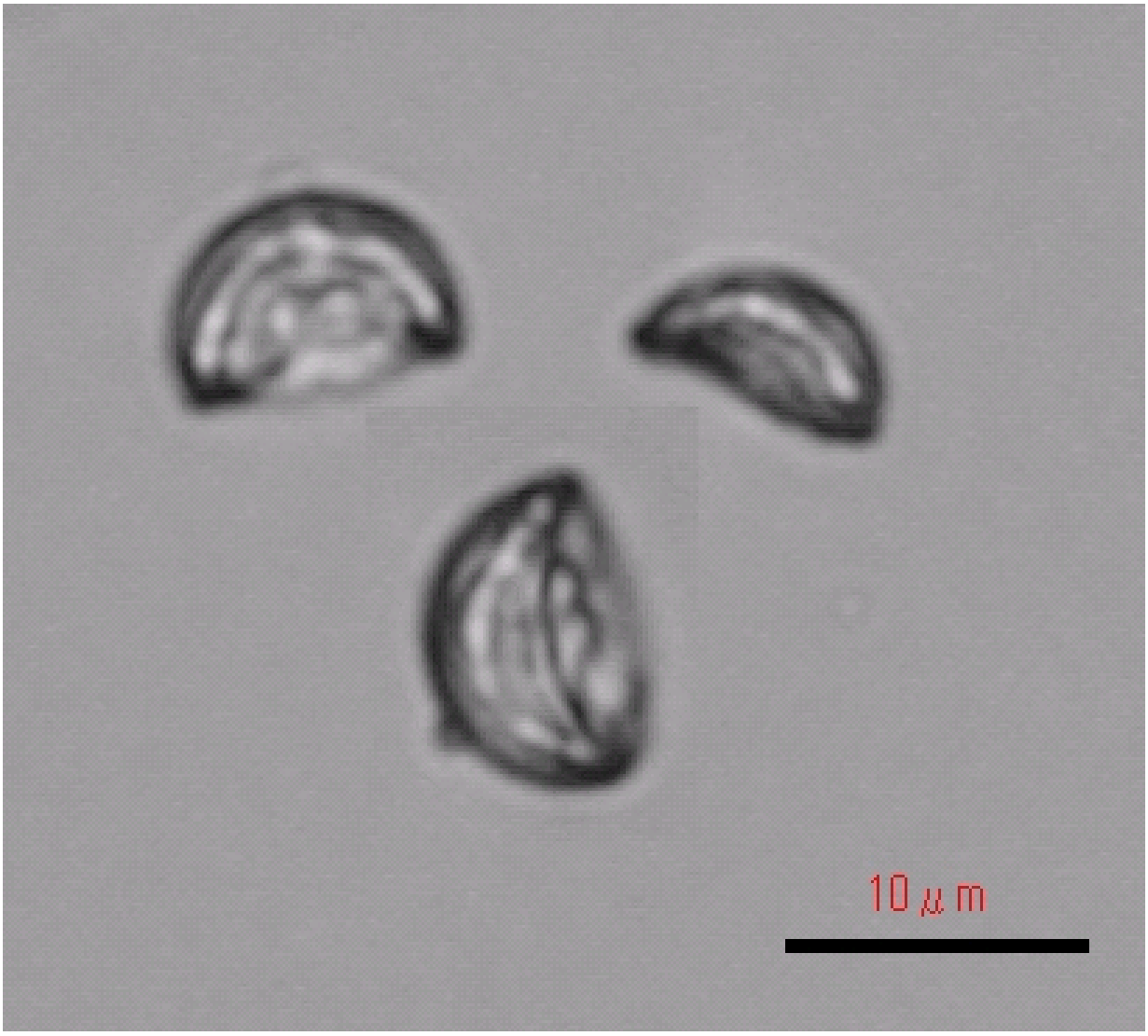

FigureVII-9. An Optical micrograph of HHSM

Chapter VIII

Concluding remarks

This thesis dealt with the both of microencapsulation of radical polymerization initiator applied in the field of adhesive biomaterials and preparation of hemispherical hollow silica microcapsules with different affinity surface for drug delivery system. In order to procure the eruditions of microencapsulation technologies of radical polymerization initiator and the synthesis of hemispherical hollow silica microcapsules with different affinity surface, several experiments were performed. More specifically, in ***Chapter II***, Benzoyl peroxide (BPO) was microencapsulated with polyethyl methacrylate (PEMA) by the drying-in-liquid method using calcium carbonate as stabilizer. Methyl methacrylate (MMA) was used as solvent for PEMA in consideration of biosafety. Microcapsules prepared were characterized for medical applications. It was found that adhesive biomaterials prepared using microcapsules had sufficient ability for initiating radical polymerization even after one and two month storage at 313K and relative humidity of 75 %. In ***Chapter III***, experimented on microencapsulation of TMBA (1,3,5-trimethylbarbituric acid), a polymerization coinitiator heavily used in the fields of orthopedics and dentistry for polymerizing polymethyl methacrylate (PMMA)/methyl methacrylate (MMA), using the drying-in-liquid method. Additionally, the obtained TMBA microcapsules were used for preparing a biological hard tissue-adhesive material and validated for the microencapsulation effects. The results showed that the microencapsulated systems had excellent bonding properties and high storing stability regardless of storing conditions which were at 2-months at 278K, 296K and 313K

in a relative humidity of 75 %. In ***Chapter IV***, the several calcium carbonate crystals were synthesized by changing the reaction conditions. Namely, as reaction factors, the number of reaction moles, reaction temperature for the sodium carbonate/calcium chloride solutions, and the concentration of anionic surfactant may influence the resultant crystal system were chosen. As the results of that, the high-yield synthesis conditions of spherical vaterite-type calcium carbonate crystals with a particle size of less than 3μm could be procured by an addition of anionic surfactant (0.1%) at a high reaction temperature (333K). In ***Chapter V***, Spherical calcium carbonate vaterite crystals were synthesized and the effect of them on stabilization of suspension polymerization of methyl methacrylate was investigated. Suspension polymerization of methyl methacrylate could be stabilized with calcium carbonate vaterite crystals and sodium dodecyl benzene sulfonate of the concentrations from 25 ppm to 100 ppm. Poly (methyl methacrylate) beads coated with spherical calcium carbonate vaterite crystals were prepared. With increase in the concentration of sodium dodecyl benzene sulfonate from 25ppm to 100ppm, the amount of calcium carbonate vaterite crystals adhered on the surface of poly methyl methacrylate bead increased and the mean diameters of polymer beads decreased. In ***Chapter VI***, Spherical silica was synthesized using the sol-gel method by hydrolyzing tetraethyl orthosilicate (TEOS) with an alkali catalyst, and its preparation conditions, i.e. the reaction temperature, concentration and dropping rate of the hydrolysis catalyst, were examined. Furthermore, the synthesized silica was doped with sodium fluoride to measure its ion

release ability. The findings are as follows. There was a significant difference in the mean diameter of the synthesized silica particles in connection with the reaction temperature and dropping rate of the hydrolysis catalyst: the higher the reaction temperature was, the smaller the mean particle size was; and the slower the dropping rate was, the smaller mean particle size was obtained. The surface area of the synthesized silica particles was significantly different depending on the dropping rate of the hydrolysis catalyst: the faster the dropping rate was, the smaller the specific surface area became, which suggested that the dropping rate must be slower to obtain a porous particle structure. There were significant differences in the specific heat capacity and thermal reduction of the synthesized silica in association with the reaction temperature: the higher the reaction temperature was, the lower the specific heat capacity and thermal reduction were. When fluoride release was measured for two groups of fluoride-doped, synthesized silica particles of approximately equal diameter with different surface area, it was found that the fluoride retaining ability was proportional to the surface area of the particles. The fluoride ion release was equilibrated at approx. 5 minutes for both groups. These results suggested that it was possible to control the particle porosity by manipulating the reaction conditions, such as the dropping rate of the catalyst and reaction temperature during the silica synthesis, providing spherical silica particles with various porosities and diameters. This can be applied to the release control of agents doped to silica. In ***Chapter VII***, We developed the method to prepare hemispherical hollow silica microcapsules with different affinity

surfaces by using spherical vaterite calcium carbonate as template. The preparing process was composed of the adhesion of calcium carbonate onto the surface of methyl methacrylate droplets followed by suspension polymerization, the partial etching of calcium carbonate on the poly methyl methacrylate mother particle, the formation of silicon dioxide powder by sol-gel reaction and their deposition onto the etched flat surface of calcium carbonate, the surface modification of deposited silicon dioxide with silane coupling agent, the remove of the mother particle with acetone, the formation of silicon dioxide powder by sol-gel reaction and deposition onto the exposed hemispherical surface of calcium carbonate and the surface modification of deposited silicon dioxide with silane coupling agent. The synthesized microcapsules had complete hemispherical structure and both the more hydrophilic and the more hydrophobic surface.

According to the above mentioned experiments, the following eruditions were procured,

In ***Chapter I***, general introduction, the background of this thesis, reviews of the previous studies and scope of this thesis were described.

In ***Chapter II***, BPO was microencapsulated with polyethyl methacrylate(PMMA) by the drying-in-liquid method using calcium carbonate with different crystal shape and size as an inorganic stabilizer. We evaluated the surface morphology, the particle diameter distributions, the microencapsulation efficiency together with their

possibility for use in adhesive biomaterials. The results obtained are as follows,

(1) Microcapsules containing BPO were able to be prepared by using polyethyl methacrylate as shell material, calcium carbonate powder as stabilizer and MMA monomer as volatile solvent.

(2) The mean diameters of microcapsules strongly depended on the amount of calcium carbonate adhered on the surface of microcapsule.

(3) The surface of microcapsule became smoother with decrease in the size of calcium carbonate.

(4) Microencapsulation efficiencies of BPO were above 0.90 under all the experimental conditions adopted here.

(5) Microcapsules had the ability for initiating polymerization after two month storage at 313K and relative humidity of 70%

In ***Chapter III***, Microencapsulation was carried out on 1,3,5-trimethylbarbituric acid (TMBA), a hydrosoluble material used widely for redox catalysts such as organic peroxide, aromatic tertiary amine, and anhydride, by the drying-in-liquid method with the use of PEMA as a wall material. Experimental conditions were made by setting 4 levels of the amount of TMBA added for preventing

osmotically-induced leakage of the core material into the continuous phase (PVA solution), and also 3 levels of the disperse phase/continuous phase ratio (hold-up). The results indicated that the microencapsulation efficiency increased with the increase of the amount of TMBA added to the continuous phase, although the efficiency remained 36% at the highest even with the saturated level of TMBA (7wt% TMBA-PMA soln.). No effect was observed on the particle size. As for the systems with different levels of hold-up, the microencapsulation efficiency decreased with the increase of the disperse phase/continuous phase ratio, and no effect on the mean particle diameter was observed in any levels of hold-up. It is generally considered here that as the hold-up level increases, it takes longer for droplets in the disperse phase to reach an equilibrium state following several cycles of breakup and coalescence. It was thus suggested that the systems which went through droplet breakup more frequently, i.e. the systems with a higher level of hold-up, were more likely to have the core material of TMBA leaked in a crystalline state without dissolution. Additionally, the obtained TMBA microcapsules were used for preparing a biological hard tissue-adhesive material and validated for the microencapsulation effects. The results showed that the microencapsulated systems had excellent bonding properties and high storing stability. The results obtained are as follows,

(1) Microcapsules containing TMBA were able to be prepared by using polyethyl methacrylate as shell material, PVA as an organic surfactant and MMA monomer as volatile solvent.

(2)The maximum microencapsulation efficiency of TMBA was around 0.36 under the experimental conditions adopted ***Chapter III***.

(3)The higher hold up conditions gave the lower microencapsulation efficiencies.

(4) Microcapsules had the ability for initiating polymerization after two months storage at 313K and relative humidity of 70%

In ***Chapter IV***, The present study conducted a systematic experiment to evaluate how the number of reaction moles, reaction temperature for the sodium carbonate/calcium chloride solutions, and the concentration of anionic surfactant influence the resultant crystal system, and the following findings are obtained,

(1) At the reaction temperature of 293K, the systems, regardless of any mol concentrations, showed a decrease in mean diameter of the resultant calcium carbonate crystals with the surfactant concentration. The effect of surfactant was especially remarkable in the 0.1 mol reaction system. As for the systems without surfactant, the particle size became smaller with the number of reaction moles. This tendency, however, became less prominent as the surfactant concentration became higher. As for the systems prepared at 333K, it was observed that the influence of the surfactant was not as significant as in the case of the 293K systems, and that the number of

reaction moles did not affect the particle size for the systems without surfactant.

(2) With any systems prepared at 293K, only vaterite and calcite crystals were produced, and the addition of surfactant tended to inhibit vaterite synthesis, whereas at 333K, the resultant crystals were greatly influenced by the addition of surfactant, which means that synthesis of metastable vaterite-type calcium carbonate crystals is achievable under the conditions of the present study.

(3) It was found that a high-yield synthesis of vaterite-type calcium carbonate crystals with a particle size of less than 3μm could be obtained by an addition of anionic surfactant (0.1%) at a high reaction temperature (333K).

In ***Chapter V***, Calcium carbonate crystal was synthesized using calcium chloride and sodium carbonate at the temperature 293, 313 and 333K. Calcium carbonate vaterite crystals were found to be synthesized at the reaction temperature of 293K and 313K. Suspension polymerization of MMA was able to be stabilized with calcium carbonate vaterite crystals and DBS of the concentration from 20 ppm to 100 ppm. PMMA beads coated with calcium carbonate vaterite crystals ware prepared. The amount of calcium carbonate vaterite crystals adhered increased with the DBS concentration and the diameters of polymer beads decreased with the adhesion amount.

In ***Chapter VI***, Spherical silica was synthesized using the sol-gel method by hydrolyzing tetraethyl orthosilicate (TEOS) with an alkali catalyst, and its preparation conditions, i.e. the reaction temperature, concentration and dropping rate of the hydrolysis catalyst, were examined. At this moment, The hydrolysis reaction of silicone alkoxide with alkaline catalyst is a nucleophilic substitution reaction where OH^- ions are involved. The alkoxyl group that is adjacent to the generated silanol group is easily subjected to a nucleophilic substitution by water, with the electrons attracted from silicon elements to the silanol group. Meanwhile, the dehydration polycondensation reaction is initiated by the proton abstraction from the silanol group by the OH^- ions. More specifically, the reaction proceeds as a result of the nucleophilic attack on the remaining silicon elements by the generated bare $Si\text{-}O^-$. In this study, it is conceivable that both the hydrolysis reaction resulting from the electrophilic substitution reaction with protons and the polycondensation reaction initiated by OH^- ions proceed slowly under the reaction conditions at the low catalyst concentration and slow dropping rate, thereby resulting in the synthesis of almost the same sized particles without being greatly affected by the reaction temperature. Additionally, it is also conceivable that the particle size became large at the fast catalyst dropping rate because polycondensation proceeds slowly at the low reaction temperature due to the higher catalyst concentration resulting from the fast dropping rate. At the high reaction temperature, on the other hand, the particle size became small since the generated silanol group was considered to be rapidly polycondensed, with TEOS being

consumed to complete the particle growth. Furthermore, the synthesized silica was doped with sodium fluoride to measure its ion release ability. The findings are as follows,

(1) There was a significant difference in the mean diameter of the synthesized silica particles in connection with the reaction temperature and dropping rate of the hydrolysis catalyst: the higher the reaction temperature was, the smaller the mean particle size was; and the slower the dropping rate was, the smaller mean particle size was obtained.

(2) The surface area of the synthesized silica particles was significantly different depending on the dropping rate of the hydrolysis catalyst: the faster the dropping rate was, the smaller the specific surface area became, which suggested that the dropping rate must be slower to obtain a porous particle structure.

(3) There was a significant difference in the specific heat capacity of the synthesized silica in association with the reaction temperature: the higher the reaction temperature was, the lower the specific heat capacity was.

(4) There was a significant difference in the thermal reduction of the synthesized silica in association with the reaction temperature: the higher the reaction temperature was, the lower thermal reduction was.

(5) When fluoride release was measured for two groups of fluoride-doped, synthesized silica particles of approximately equal diameter with different surface area, it was found that the fluoride retaining ability was proportional to the surface area of the particles, i.e. the difference of retaining ability between the two groups was 5-fold. The fluoride ion release was equilibrated at approx. 5 minutes for both groups. These results suggested that it was possible to control the particle porosity by manipulating the reaction conditions, such as the dropping rate of the catalyst and reaction temperature during the silica synthesis.

In ***Chapter VII***, Hemispherical hollow silica microcapsules with both the more hydrophilic and the more hydrophobic surface were synthesized by the sol-gel method using spherical vaterite calcium carbonate as template. The flat and hemispherical surfaces of hollow silica microcapsules can be modified with various functional groups, which can be anticipated to be applied to drug delivery systems. Findings obtained from this study are as follows,

(1) Adhesion of spherical vaterite calcium carbonate on the MMA droplets largely depended on the concentration of DBS.

(2) Suspension polymerization was unstable without DBS.

(3) An amino group introduced was easily identified by the color change caused by trapping nano-gold particles with amino group.

(4) Hemispherical hollow silica microcapsules adhered on the liquid-liquid interface as particulate surfactant.

List of publications

[1] **"Preparation of Microcapsules Containing Reactive Compound by the Drying-in-liquid Method using Calcium Carbonate as Stabilizer"** Kiyomi Fuchigami, Yoshinari Taguchi, Masato Tanaka, J.Chemical Engineering of Japan, **39**(9),994-999(2006) [***Chapter II***]

[2] **"Preparation of hemispherical hollow silica microcapsules with different affinity surface by using spherical vaterite calcium carbonate as template"** Kiyomi Fuchigami, Yoshinari Taguchi, Masato Tanaka, Polymers for advanced Technologies **18**,1-7 (2007) [***Chapter VII***]

[3] **"Synthesis of sphrical silica particles by sol-gel method and application"** Kiyomi Fuchigami, Yoshinari Taguchi, Masato Tanaka, Polymers for advanced Technologies in press [***Chapter VI***]

[4] **"New Material Design of Multi-purpose PMMA-type Adhesive Resin with Newly Synthesized Microcapsule of Radical Polymerization Initiators"** Kiyomi Fuchigami, Kunio Ikemura, Kensuke Ichizawa, Dental material Journal in press [***Chapter II and III***]

[5] **“Synthesis of calcium carbonate vaterite crystals and effect of them on stabilization of suspension polymerization of MMA”** Kiyomi Fuchigami, Yoshinari Taguchi, Masato Tanaka, Advanced powder technology in press [***Chapter V***]

Acknowledgment

This dissertation has been carried out during 2004-2008 as a doctorate thesis under the direction of Professor Dr. Masato Tanaka at the Graduate School of Science and Technology, Department of Chemistry and Chemical Engineering, Niigata University.

I wish to express my deepest gratitude to Professor Dr. Masato Tanaka at the Graduate School of Science and Technology, Department of Chemistry and Chemical Engineering, Niigata University, for his constant guidance and kind suggestions throughout this study.

I would like to express my grateful gratitude to Professor Dr. Yoji Taguchi, Department of Chemistry and Chemical Engineering, Niigata University, Professor Dr. Norio Tsubokawa, Department of Chemistry and Chemical Engineering, Niigata University, Associate Professor Dr. Noriyasu Hotta, Department of Chemistry and Chemical Engineering, Niigata University, Associate Professor Dr. Isao Kimura, Graduate School of Science and Technology, Niigata University, Assistant Professor Dr. Yoshinari Taguchi, Department of Chemistry and Chemical Engineering, Niigata University, Mr Natsukaze Saito, Department of Chemistry and Chemical Engineering, Niigata University for reviewing this thesis.

I wish to express my grateful acknowledgement to Messrs Ryou Morita, Hiroki Abe, Tadashi Kasahara, and other members of Tanaka

Laboratory for their helps and useful suggestions.

I would like to express my grateful gratitude to Messrs Katsuya Ota, Yoshikazu Wakino, Hiroyuki Kaji, Noriyuki Negoro, Dr. Toshiyuki Nanbu, SusumuTokuda, Ryuichi Yoshimoto, Dr. Kunio Ikemura, Dr. Masaki Nishino, Dr. Takuya Kawakami, Dr. Tom A. Roberts and other members of Shofu inc. for their helps and supports.

I would like to express my grateful gratitude to my familiar, Mr Hirokazu Yaginuma and Mrs Tomoko Matsubara for their encouragements and supports during this study.

Finally, I wish to express my grateful thanks to my family, Mrs Miyako Fuchigami, Miss Keiko Fuchigami, Miss Shiho Fuchigami, Mrs Keiko Okajima and my deceased mother Kiyoko Sakaguchi for their encouragement and supports during this study.

Kiyomi Fuchigami

Doctoral Program in Advanced Materials Science and Technology
Science and Technology for Materials
Graduate school of Science and Technology
Niigata University
March, 2008.